SWIRLING FLOW GENERATORS AND SWIRLING FLOW SEPARATORS

A MASTER'S THESIS

in

Mechanical Engineering

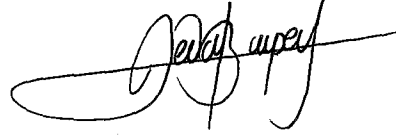University of Gaziantep

By

M. Yaşar GÜNDOĞDU

September 1995

Approval of the Graduate School of Natural and Applied Sciences.

Prof.Dr. Mazhar Ünsal
Director

I certify that this thesis satisfies all the requirements as a thesis for the degree of Master of Science.

Assoc. Prof. Dr. Sedat Bayseç
Chairman of the Department

I certify that I have read this thesis and that in my opinion it is fully adequate in scope and quality. as a thesis for the degree of Master of Science.
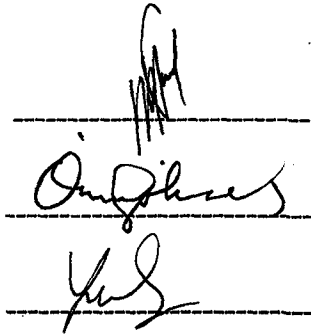
Prof. Dr. Ömer T.Göksel
Supervisor

Examining Committee in Charge

Prof. Dr. Mazhar Ünsal

Prof. Dr. Ömer T. Göksel

Assist. Prof. Dr. Yusuf A. Uskaner

ii

ABSTRACT

SWIRLING FLOW GENERATORS AND SWIRLING FLOW SEPARATORS

GÜNDOĞDU, Mehmet Yaşar
M. S. in Mechanical Engineering
Supervisor: Prof. Dr. Ömer T. GÖKSEL
September 1995, 200 pages

In the work presented in this thesis, a survey of the available literature on swirl generators and particle separators are given. A cyclone particle separator whose tangential inlet height and width, fluid discharge pipe diameter and depth, dust discharge diameter and cone height may be changed independently from each other, was designed and constructed.

A particle feeder with celled-wheels was designed and constructed for the calibration of fluid-particle concentration at the inlet of cyclone separator. A five-tube probe was constructed and calibrated to measure the distribution of tangential, radial and axial velocity, and static pressure throughout the cyclone cross-section in swirling flow. A calibration mechanism which enables the rotation of the five-tube probe in yaw and pitch directions independently, was designed and constructed.

The effects of the Re number based on the cyclone inlet velocity and the characteristic cyclone dimensions on the static pressure loss between the inlet and outlet of the cyclone are determined.

The effects of Re number and the characteristic cyclone dimensions on the radial distributions of the tangential, radial and axial velocity and the static pressure throughout the cyclone body cross-section at different vertical stations, are determined.

Key Words: Swirl, Swirl Generators, Swirling Flow, Particle Separators, Cyclone, Particle Feeders, Five-tube Probe

ÖZET

DÖNEL AKIM ÜRETECLERİ VE DÖNEL AKIM AYIRICILAR

GÜNDOĞDU, Mehmet Yaşar
Yüksek lisans tezi, Mak. Müh. Böl.
Tez yöneticisi: Prof. Dr. Ömer T. Göksel
Eylül 1995, 200 sayfa

Bu tezde sunulan çalışmada, dönü üretecleri ve parçacık ayırıcıları üzerine bir literatür araştırması yapıldı. Teğetsel giriş yüksekliği ve genişligi, akışkan çıkış borusu çapı ve derinliği, artık parçacık çıkış çapı, ve koni yüksekliği biri birinden bağımsızca değiştirilebilen bir siklon parçacık ayırıcısı tasarlanıp imal edilmiştir.

Siklon ayırıcı girişinde akışkan-parçacık sıklığının ayarlanması için hücre tekerli bir parçacık besleyicisi tasarlanıp imal edilmiştir. Dönel akım içerisinde, siklon kesit alanı boyunca teğetsel, radyal ve eksenel hızın, ve statik basıncın dağılımını ölçmek için bir adet beş-tüp'lü sonda üretilip kalibre edilmiştir. Beş tüp'lü sondanın yatay ve dikey eksenler etrafında bağımsızca dönmesini mümkün kılan bir kalibre mekanizması tasarlanıp imal edilmiştir.

Siklon giriş hızı üzerine dayandırılmış Re sayısının ve tipik siklon boyutlarının siklon giriş ve çıkışı arasındaki statik basınç kaybı üzerine etkileri belirlenmiştir.

Re sayısının ve tipik siklon boyutlarının, farklı dikey ölçüm mevkilerinde, siklon kesit alanı boyunca teğetsel, radyal ve eksenel hızın, ve statik basıncın radyal dagılımları üzerine etkileri belirlenmiştir.

Anahtar Kelimeler: Dönü, Dönü üretecleri, Dönel akım, Parçacık ayırıcıları, Siklon, Parçacık besleyiciler, Beş tüplü sondalar.

ACKNOWLEDGEMENTS

TABLE OF CONTENTS

LIST OF TABLES

LIST OF FIGURES

NOMENCLATURE

Symbol	Description
a	Cyclone tangential inlet height, m
A_{in}	Total inlet area of the cyclone, $\pi D_{in}^2/4$, m^2
A_{out}	Total outlet area of the cyclone, $\pi/4(D_{out}^2+D_{in}^2)$, m^2
A_r	Outlet-to-inlet area ratio of the cyclone, A_{out}/A_{in}
AC	Alternating current
b	Cyclone tangential inlet width, m
C	Dimensionless strength of the free vortex
C_p	Experimentally determined pressure loss coefficient, $\Delta P_{st}/1/2\rho V^2$
C_s	Dimensionless static pressure coefficient, $P_{st}/1/2\rho V_{in}^2$
D	Cyclone cylindrical body diameter, m
D_d	Cyclone fluid discharge pipe diameter, m
D_{in}	Cyclone tangential inlet pipe diameter, m
D_u	Cyclone dust discharge diameter or under flow diameter, m
$f(\alpha)$	5-tube pressure probe calibration factor, $(P_3-P_1)/(P_5-P_m)$
$f(\varphi)$	5-tube pressure probe calibration factor, $(P_2-P_4)/(P_5-P_m)$
g	Gravitational acceleration, m/s^2
H	Total height of the cyclone configuration, m
h	Height of the cyclone cylindrical body, m
h_{av}	Radial position of the average fluid velocity within the inlet pipe of the cyclone from the pipe wall, m
h_c	Height of the cyclone cone, m
h(r)	Dynamic head of the air flow in the inlet pipe of the cyclone at any radial position
LDA	Laser Doppler Anemometer
LDV	Laser Doppler Velocitimeter
n	Free vortex exponent
P_{in}	Wetted perimeter of the cyclone tangential inlet, m
P_{ki}	Dynamic pressure o f the air flow at the inlet of the cyclone, Pa
P_m	Arithmetic mean of the pressures sensed from the side tubes of the 5-tube pressure probe, $(P_1+P_2+P_3+P_4)/4$
P_T	Total pressure of the fluid flow, Pa
P_{st}	Static pressure of the fluid flow, Pa

$P_{st}(r)$	Static pressure of the air flow at any radial position, r in the cyclone body, Pa
P_w	Static pressure at the cyclone wall, Pa
$P_1...P_5$	Pressures sensed at individual orifices of the 5-tube pressure probe, Pa
q	Dynamic pressure of the air flow, $1/2 \rho V^2$, Pa
Q_p	5-tube pressure probe calibration factor, $(P_5-P_m)/1/2 \rho V^2$
R	Radius of the cyclone cylindrical body, m
r_c	Common radius between the free and forced vortex flow regimes in the cylindrical body, m
Re	Reynolds number, $(V_{in} D_{in}/v)$
R_d	Radius of the fluid discharge pipe, m
R_{in}	Radius of the fluid inlet pipe, m
r_m	Radial position in the cyclone body at which the value of dimensionless tangential velocity becomes maximum, m
R_u	Radius of the dust discharge opening, m
r_u	Radial position in the cyclone body at which the value of the axial fluid velocity becomes maximum, m
r_0	Radial position in the cyclone body at which the magnitude of the fluid velocity becomes zero, m
r_1	Radial position in the cyclone body at which the forced vortex character of the flow ends and the compound vortex character of the flow starts, m
r_2	Radial position in the cyclone body at which the compound vortex character of the flow ends and the free vortex character of the flow starts, m
S	Depth of the fluid discharge pipe of the cyclone from the top of the cyclone cylindrical body, m
S_p	5-tube pressure probe calibration factor, $(P_T-P_5)/P_5-P_m$
V	Free stream velocity, m/s
V_{in}	Average air velocity at inlet to the cyclone, m/s
V_a	Axial component of the air velocity in the cyclone (i.e, in z-direction), m/s
V_t	Tangential component of the air velocity in the cyclone, m
V_r	Radial component of the air velocity in the cyclone, m
$V(r)$	Local air velocity in the inlet pipe of the cyclone at any radial position, m
V_a^+	Dimensionless axial velocity of the air in the cyclone body, V_a/V_{in}

$V_t{}^+$	Dimensionless tangential velocity of the air in the cyclone body, V_t/V_{in}
$V_r{}^+$	Dimensionless radial velocity of the air in the cyclone body, V_r/V_{in}
$V_{au}{}^+$	Maximum value of the upward directed dimensionless axial air velocity
$V_{ad}{}^+$	Maximum value of the downward directed dimensionless axial air velocity
$V_{tm}{}^+$	Maximum value of the dimensionless tangential velocity of the air obtained at dimensionless radius, r_m/R
$V_{tc}{}^+$	Value of the dimensionless tangential velocity of the air at a common radius, r_c/R between the free and forced vortex flow regions
Z/h	Dimensionless height of the measurement stations measured from the top of the cyclone cylindrical body
ΔP_{st}	Static pressure loss between the inlet and outlet of the cyclone, Pa
ω	Dimensionless angular velocity of the forced vortex
ρ	Air density, kg/m^3
υ	Kinematics viscosity of air, m^2/s
α	Pitch angle, °
ψ	Yaw angle, °
θ	Chamfer angle of the probe tip, °

subscripts

t	Tangential compenent
r	Radial component
a	Axial component
av	Average
m	Maximum
in	Conditions at inlet
w	Cyclone wall
+	Dimensionless
c	Conditions at common radius
u	Upwards
d	Downwards
st	Kinetic
T	Total

CHAPTER 1

INTRODUCTION

Swirling flow is a three-dimensional turbulent flow that can be created by means of swirl generators to use in engineering applications. The swirling flow has been applied to particle separation from a suspended fluid flow by means of cyclone separators for more than a hundred years. Cyclone is a funnel-shaped, industrial device for separating solid, liquid and/or gaseous phases from a dispersed suspension. Its operation is chiefly based on the density difference and high rotational velocities that are imparted as the suspension is injected tangentially into the upper part of the cyclone.

Chapter 2 gives a complete survey of the available literature on swirl generators, particle separators and on the cyclone particle separators that use only the swirling flow structure for the separation of particles.

In chapter 3, the test set-up used in the experimental investigations of the swirling flow in the cyclone separator is described. The measurement techniques used to measure the flowrate through the cyclone, static pressure loss across the cyclone, static pressure and velocity distributions in the cyclone and the calibration of the measuring instruments are also given in this chapter.

The results of experimental works directed on the static pressure loss and the swirling flow field of the cyclone separators are presented in chapter 4. The effects of volume throughput and characteristic cyclone dimensions on the static pressure loss and swirling flow field of cyclone are determined. The conclusions that are drawn from the experimental work on cyclone pressure loss and swirling flow structure of cyclone are also presented in this chapter.

The conclusions that are obtained from this study on the use of swirling flow field to separate granular particles from a dispersed suspension by means of cyclone separators and the recommendations for further work are presented in chapter 5.

CHAPTER 2

LITERATURE SURVEY

2.1 INTRODUCTION

Swirling flow is a highly turbulent three-dimensional flow. It has a wide spread use for many purposes in many engineering applications, such as in burners, heat exchangers, diffusers, particle separators, etc. It is also seen as naturally generated in some types of fluid machinery, such as in pumps, fans, turbines, etc.

Swirling flow is used together with the gravitational and inertial effects as a tool of particle separation from a particle suspended fluid flow in some types of particle separators, such as in settling chambers, scrubbers, centrifugal separators, etc. Cyclone separators which are also named as centrifugal separators, use only swirling flow structure as a primary tool of the separation of solid, liquid and /or gaseous phases from a dispersed suspension. Swirling flow field within a cyclone separator may be characterised by the free and forced type vortex flows superimposed on a sink flow. The flow field within a cyclone separator may be related mainly to the dimensions of the cyclone, swirl generation method used in cyclone, fluid properties, and the properties of suspended particles. The effects of these factors on the swirling flow structure in the cyclone separators are not completely known and are very difficult to determine due to the complexity of flow.

Over many years a great deal of effort has been devoted to obtaining a better operating knowledge for the industrial cyclones by many researchers. Experimental investigations on the cyclone separators were mainly composed of three important fields as;

1. The increase of collection efficiency
2. The decrease of pressure loss
3. The determination of swirling flow structure

The collection efficiency and pressure loss of the cyclone separators have been investigated due to the to the swirl generating methods used in cyclones, the type of cyclone fluids, the properties of suspended particles, and the dimensions of the cyclone separators by many investigators. However these investigations are not generally supported by the experimental works directed on the swirling flow structure of the cyclones. The reason for that, the measurement of swirling flow field in different cyclone configurations with different operational constructions is hard and expensive.

Furthermore, the experimental investigations directed to determine the swirling flow structure in the cyclone separators are only performed on the limited cyclone configurations. These are the most efficient cyclone configurations designed according to the results of experimental works directed on the collection efficiency and pressure loss of the cyclones. Therefore, the effects of cyclone geometry and dimensions on the swirling flow generated in the cyclones are not completely known.

In front of the investigations focused on the cyclone separators in the available literature, present work must be undertaken to include the experimental works directed on the static pressure loss and the swirling flow structure of the cyclones. This is required for obtaining adequate information about the use of swirling flow structure for particle size and mass classification.

2.2 SWIRL GENERATION METHODS

Swirling flow has many engineering applications. Different methods have been used in order to generate swirl for different purposes. In the available literature, the swirling flow generation is accomplished commonly by;

4

1. Rotation of a pipe section
2. Rotating perforated plates and vanes
3. Rotation of a roughened disk
4. Non-rotating guide vanes
5. Twisted tapes
6. Coiled wires
7. Bell mouth and Center body with entry vanes
8. A swirl generator together with axial and tangential fluid inlets
9. A swirl generator with only tangential fluid inlets

In references [1, 2], it was stated that the swirling flows generated by the rotation of a pipe section have a relatively weak degree of swirl. In reference [1], it was also stated that, imparting rotation to an axial pipe flow by means of a rotating perforated plate in which holes were drilled either parallel or 45 deg. to the pipe axis, was possible. However, a continuous variation in angular velocity and axial asymmetry within the flow field was seen.

Riahi and Hill [3] used a rotating roughened disk inside a closed cylindrical chamber with different length-to-diameter ratios, L/D to generate swirling flow. They studied the effects of swirl on the rate of heat transfer to the wall of constant-volume cylindrical chambers, such as in the cylinders of a spark ignition engine. They stated that, the strength of swirl and the turbulence field were found to be strongly dependent on the rotational speed and roughness size of the rotating roughened disk, and on the cylindrical chamber length-to-diameter ratio, L/D.

Swirling flows generated by non-rotating guide vanes were discussed in references [2, 4, 5, 6, 7]. In references [4, 5], the hydraulic drag of the non-rotating sequential swirling contact vanes which were used as swirler for a concurrent cyclone separator, was studied. It was found that, the hydraulic drag of sequential swirling contact vanes was affected by the vane angle from axial direction, active crossectional area of the vanes, profile of the vanes, and the number of vanes. In references [5, 6, 7], it was also stated that the rotational asymmetry and unsteadiness in the central core region of the swirling pipe flow generated by non-rotating vanes may be reduced by

increasing the number of vanes and choosing optimal guide vane angles for the reduction of flow separation over the vanes.

Swirling flows generated by twisted tapes and coiled wires [1, 2, 8, 9, 10] mainly affected by the tape helix angle and the pitch-to-diameter ratio, H/D of the wire coils. It was found that the swirl strength was increased by increasing the tape helix angle and decreasing the pitch-to-diameter ratio of coils at the same flowrate. The actual flow field behind the coiled wires and twisted tapes was further complicated by weak secondary circulation patterns. It was also stated that, it was impossible to generate strong swirling flows by these methods of swirl generation.

Swirling flows generated by bell mouth and center body with adjustable entry vanes were studied in references [11, 12, 13, 14]. It was found that, secondary flows were not created by this type of swirl generating equipment. Rotational asymmetry can be reduced by increasing the number of entry vanes, but unsteadiness was observed in the central region of the pipe, particularly near the entry section, probably owing to unsteady separation on the end disk of the entry section. Continuous control of the swirl provided by the adjustable entry vanes may be useful in experiments. A cone with a cubic profile was used to stabilize the flow and to provide a gradual reduction in crossectional area. Unsteadiness was markedly diminished after the installation of the cone as center body.

Swirling flows generated by a swirl device together with axial and tangential fluid inlets were discussed in reference [1, 15, 16, 17]. Hallett [15] produced swirl by admitting air through four tangential entries, whose inlet areas may be varied by means of a sliding sleeve, thus he controlled the angular momentum imported to the flow. A second, non-swirling axial flow stream entered through a central tube, reducing the swirl intensity of the resulting flow. Chigier and Beer [16] used a similar swirl device for creating swirling air jets. However, they introduced the air in axial direction through a settling chamber so as to provide a uniform distribution of velocity while the remainder of the air was introduced tangentially through four nozzles which were placed in the same crossectional plane. Chigier and Chervinsky [1] used a swirl generator with an axial fluid inlet through a central tube and tangential fluid inlets through tangential slots for producing swirling pipe flow. Their swirl device had eight tangential slots. The annular distance

between the tangential slots and the casing of swirl generator was kept constant, therefore slight asymmetry of flow was observed downstream of their swirl generator. This was due to the uneven distribution of tangential air stream between the tangential slots. To avoid the asymmetry of the swirling flow, Uskaner, Y.A.[17] improved the design of Chiggier and Chervinsky. The velocity and pressure of the air stream entering the tangential slots of the swirl generator was kept constant by decreasing the annular crossection area in proportion to the decrease in flowrate after each tangential slot in the improved swirl device of Uskaner [17]. This resulted in an annulus geometry similar to a volute casing of pumps or centrifugal fans. At the exit of the Uskaner's swirl generator, the swirling flow was found to be steady and axisymmetric [17].

Swirling flows generated by a swirl device with only tangential fluid inlet(s) were discussed in references [1, 17, 18, 19, 20]. It was found that, the swirl strength could be varied by changing the flowrate through the swirler and by changing the angle and geometry of the tangential inlets. Swirling flows which were produced by this type of swirl device, were found to be axially asymmetric which tends to become more axi-symmetrical as the swirl gradually decayed. The centre of the swirling flow was found to be offset from the pipe centreline and was helical about the pipe centre line. This was caused by the single tangential inlet of the swirler. Hay and West [20] used this type of swirl generator with various tangential inlet duct angles (30, 60, and 90 deg.) to produce swirling flows. They found that, the degree of asymmetry of the swirl shows strong dependence on the inlet duct angles. The 90 deg. inlet could be used to produce a tighter flow helix and a more rapid convergence to a symmetrical swirl.

Many researchers [21, 27, 28, 29, 30] used the swirl generator with only tangential fluid inlets to produce swirling flows within the cyclone separators. The swirl generating section of the cyclones have tangential inlet(s) with 90 deg. angle to the cylindrical cyclone body, (i.e., 90 deg. angle to axial direction). It was found that, slight asymmetry of the swirling flows within the cyclone separators had no acceptable effect on the separation efficiency. However, this type of swirl generators was found preferable to use with respect to the simplicity of production and simplicity of swirl strength control.

2.3 PARTICLE SEPARATORS

Particle separators may generally be classified as;

1. Filters
2. Electrostatic precipitators
3. Scrubbers
4. Settling chambers
5. Inertial separators
6. Centrifugal separators

As indicated in references [21, 22], it was stated that, the filter collection mechanisms were direct interception and inertial impact for the larger particles and diffusion impact for the smaller particles. The main advantages were stated as high efficiency, low capital cost, fine for very small particles and ability to handle a wide range of operating conditions. However, disadvantages to filtering were stated as the high-pressure drop and the clogging of the filters.

The separation mechanism of electrostatic precipitators was stated in references [21, 22, 23, 24] as that, the particulate matter was separated from a gas stream by first charging the particles to a negative voltage, and then precipitated it onto grounded collecting electrodes, finally the agglomerated particles neutralized and dropped into a hopper. Electrostatic precipitators have the advantages of the operation with the high efficiency, wide range of flowrate and very low pressure drops, while their main disadvantage was that the continuous cleaning was necessary.

As stated in references[22, 23], the principle of the scrubbers was to remove the particles, or gas, by absorbing the material into liquid droplets directly by contact. The contact mechanism may be inertial impingement or gravitational settling. The advantages of the scrubber systems were that, it can remove simultaneously particles and gases. It has high efficiencies for the particle size range of 0.2 to 10 μm. Some disadvantages of the wet scrubbers were the high energy cost, high material cost was related to chemical corrosion within the scrubber, the handling of dirty liquid and

removal of the entrained material was difficult and may cause a water pollution problem.

In references [24, 25], it was stated that, the settling chambers utilize gravity to separate particulate matters from an effluent gas stream. They were constructed with a large crossectional area perpendicular to gas flow so that the gas velocity was reduced to a minimum in an effort to prevent re-entrainment of the settled particles. They were used to collect large particles above approximately 50 μm. The pressure drop was small, less than 1 inch of water column, but the efficiency was low for particles below 50 μm.

The inertial separators caused the particles to be separated with a combination of the inertia of the dust particle, impaction on a target, and centrifugal forces by causing sudden changes in the direction of the fluid stream [25, 26]. Even though inertial separators were extremely important particle separation devices, very little information was available concerning the mechanism of particle collection other than the fact that collection was by inertial deposition. Therefore, centrifugal separators, scrubbers and filters can be considered as inertial separators.

Centrifugal separators commonly called as cyclone separators were discussed by many researchers [21, 22, 23, 24, 25, 26, 27, 28, 29, 30, 31]. It was stated that, the centrifugal force was the primary mechanism of particle collection in the cyclone separators. Cyclone separators have fluid entrance(s) designed to cause the fluid to swirl inside a cylindrical body. The fluid and particles had essentially the same tangential velocity but the particles had a much greater normal velocity due to centrifugal force and high particle density. This forced the particles to move toward the cyclone wall and those that reached the wall were separated from the fluid stream.

The cyclone separators have a tangential fluid inlet section designed to cause the fluid to attain a swirling motion, an outlet section for cleaned fluid and a dust discharge section. The various configurations of these sections are possible as considered in references [21, 24, 26];

a- The common cyclone; tangential fluid inlet with axial dust discharge.

b- Tangential fluid inlet with peripheral dust discharge

c- Axial fluid inlet through swirl vanes, with axial dust discharge

d- Axial fluid inlet through swirl vanes, with peripheral dust discharge.

Above mentioned cyclone configurations are shown in Figure 2.1. The common cyclone arrangement that was used by many investigators, stated in references [23, 24, 26, 27, 28, 29, 30, 31], was the cyclone arrangement with tangential fluid inlet and axial dust discharge which is shown in Figure 2.1.a. This was due to it's swirl generation advantages and it's dust discharge capacity. In reference [23], the different types of tangential fluid inlets that could be used on the common cyclone arrangement, were discussed to be standard inlet, helical inlet, and involute inlet which are shown in Figure 2.2.a, b and c, respectively. It was stated that, the most preferable inlet type was the rectangular shaped tangential inlet with 90 deg. angle from the cyclone body. The reason for that, is the simplicity of flow control by it and simplicity of it's construction. Helical and involute type inlet designs have been developed to minimize the interference between the incoming fluid and the mass of fluid already rotating within the annulus region between the fluid discharge pipe and the cylindrical body wall of the cyclone separator. However, existing test data were conflicting as to whether or not these designs actually provided a lower pressure drop and there was some indications that a lower efficiency was obtained. Therefore, most commercial cyclones did not have the helical and involute type fluid inlets.

Cyclone separators are economical pre-cleaners. Their efficiency is comparably higher than the settling chambers and lower than the filters, scrubbers and electric precipitators, but they are inexpensive, economical to operate devices which also have the advantages of being able to handle high temperature fluids. As indicated in references [21, 22, 23, 26, 27, 28, 29, 30, 33, 34, 35, 36, 41, 42, 44], it was found that; the flow pattern, collection efficiency and pressure drop of the cyclone separators were affected by many parameters such as the type and geometry of tangential fluid inlet, the dimensions of the cyclone configuration, the properties of cyclone fluid, the dust particle properties, capacity of fluid flow, etc. Therefore the efficient cyclone operations requires a more detailed investigation on these effective parameters.

2.4 MEASUREMENT METHODS

The velocity measurements within the swirling flow fields were made by using optical flow meters or different types of yaw meters by many researchers [1, 2, 14, 15, 16, 17, 27, 28, 29, 30, 31]. The velocity measurements within the cyclone separators were made by using LDV [27, 29, 30, 31] unfortunately could not be extended to stations near the cyclone wall, because it included experimental errors arising from the refractive index difference between the feeding materials and the Plexiglas cyclone wall. However, the LDV measurements have an important advantage as that the measuring system did not disturb the swirling flow field in the cyclone, as in the yaw meter measurements.

Knowles at all [28], used tracer particles and a cine camera for measuring velocity profiles in a cyclone separator. This type of measurement was also included with errors arising from the refractive index differences and errors arising from the time period of the cine camera. Riahi and Hill [3] used LDA for measuring swirling flow field within a short closed cylindrical chamber with the same advantages and disadvantages of LDV measurements.

Hallett [15] made measurements on the magnitude and direction of fluid velocities in a swirling flow field by means of a five-tube pressure probe. Chigier and Beer [16] made similar type measurements by a five-hole hemispherical impact tube in a swirl generator. They stated that, disadvantages of using the five-hole yaw meters were the calibration difficulty and the small disturbance of the flow field. However, the five-hole yaw meters had several important advantages as that; all of velocity magnitude and direction measurements, and static pressure measurements could be done by only one traverse at any crossection. The calibration of five-hole yaw meters was shown to be independent of the Reynolds number and intensity of turbulence in the range of cyclone measurements and it has low cost.

Static and total pressure distributions at any cyclone crossection were measured with the aid of static pressure taps at the wall and different types of pitot pressure probes by the investigators [27, 29, 30, 31]. They used

optical flow meters ,such as LDV and LDA for flow field measurements. The researchers who used five-hole type yaw meters [15, 16], determined directly the static and total pressures from the calibration charts of these yaw meters.

The internal head loss between the fluid inlet and outlet of a cyclone separator was measured by using U-tube gauges or other types of pressure gauges in references [29, 30, 33, 34]. It was assumed that, the effect of the swirling flow in the exit tube of the cyclone on the static head loss measurement was negligible level in comparison to the total of internal head loss. The internal head loss of a cyclone is mainly caused by the surface roughness and geometry of the cyclone and the energy consumption within the center vortex region.

Experimental determination of the collection efficiency of cyclone separators was performed simply by weighing the suspended and collected particles or by using an optical particle counter by many investigator [34, 35, 36, 37, 38, 39, 41, 42, 44].

2.5 VELOCITY PROFILES IN CYCLONES

Swirling flow structure in cyclone separators was reported by many investigators [21, 22, 24, 27, 28, 29, 30, 32]. As the fluid flow enters tangentially near the top of the cylindrical body of the cyclone, it moves towards the cyclone wall, forming an outer downward vortex flow between the walls of the fluid discharge pipe and the cylindrical body of the cyclone due to the strong action of the centrifugal force. This outer downward flow is characterized by a free vortex type velocity distribution except the near wall region. In the near wall region, the flow affected by the cyclone wall friction, therefore the velocity distribution in the near wall region were characterized by conventional log law as shown in references [17, 29, 30]. After the outer downward vortex flow reaches a region near the bottom of the cyclone cone, the vortex reverses its direction of axial flow but maintains its direction of rotation, so that an inner upward vortex flow is formed travelling up to the fluid discharge pipe of the cyclone. This inner upward flow is characterized by a forced vortex type velocity distribution.

2.5.1 Tangential Velocity Profile in Cyclones

Zhou and Soo [27], Knowles at al [28], and Hwang at al [29] made measurements on the swirling flow field in the cyclone separators and they stated that:

1. The tangential fluid velocity profile in the cyclones is consisted by mainly two parts, a near axis core of forced vortex (i.e., solid body rotation) where V_t increased with increasing r, and an outer free vortex (i.e., irrotational vortex) where V_t decreased with increasing r. Thus, the tangential fluid velocity was related to radial distance r from the cyclone centerline by the equation;

$$V_t \cdot r^n = constant \qquad\qquad 2.1$$

where , n was called as the vortex exponent.

2. The forced vortex velocity profile was correlated by the equation;

$$V_t/r = constant \qquad\qquad 2.2$$

or by the Equation (2.1) with n= -1.

3. The free vortex velocity profile followed the term $V_t \, r^n = constant$, where $0<n\leq1$. Exact values of the exponent 'n' was affected by the cyclone dimensions and the operating conditions.

Knowles at al [28] stated that, the value of the exponent 'n' in the outer free vortex region varied from 0.2 to 0.4 instead of 0.7 to 0.8, as was proposed by Kelsall, Ohasi and Maeda in a hydrocyclone. The reason for this discrepancy was that, Knowles et al [28] used a hydrocyclone operating without an air core in their experimental work, whereas Kelsall, Ohasi and Maeda used a hydrocyclone with an air core. If the under flow is open to the atmosphere, a cylindrical core of air develops along the centreline of the hydrocyclone. However, if a hydrocyclone was used when the under flow at the bottom of the cyclone had been closed, an air core does not develop in the hydrocyclone. Knowles et al. also stated that , the value of free vortex

13

exponent 'n' slightly increases from top to a region near the bottom of the cone in the same hydrocyclone.

Zhou and Soo [27] made measurements directed on the swirling flow field in an air cyclone. They stated that, all experimental measurements in the same cyclone for the same inlet Reynolds number which based on the hydraulic diameter of the tangential fluid inlet and the average fluid velocity in the tangential inlet, showed that the value of maximum tangential velocity and it's radial position at different axial distances except in the near-bottom region did not change. This was the result of conservation of angular momentum. The value of the maximum tangential fluid velocity was found as approximately 1.86 times of the tangential fluid velocity near the cyclone wall and the radial position of it was found to be approximately 0.74 times the radius of fluid discharge pipe measured from the centre of cyclone. As indicated in reference[28], the radial position of the maximum tangential velocity was found as approximately 0.4 , 0.68 and 0.8 times the radius of fluid discharge outlet by the investigators Knowles et al, Kelsall, Ohasi and Maeda, respectively. The reason for this inconsistency on the radial position of the maximum tangential fluid velocity was discussed in references [28, 29, 30] as that ; the radial position of the maximum tangential velocity had been affected by some geometrical constructions of the cyclone equipment, that were used in flow field experimentation, such as the fluid inlet to outlet area ratio, the fluid overflow to under flow area ratio, etc. However there is no specific investigation reported on the above mentioned discrepancy in the available literature.

2.5.2 Axial Velocity Profile in Cyclones

As stated in references [21, 22, 26, 27, 28, 29, 30], the axial fluid velocity profile is consisted of mainly two parts in the cyclone cylindrical body. An outer free vortex region where the axial fluid velocity is directed downwards, and an inner forced vortex region where it is directed upwards.

Zhou and Soo [27] stated that the magnitude of the maximum upward fluid velocity was much larger than the magnitude of maximum downward fluid velocity in the axial fluid velocity profile at all vertical distances of cyclone cylindrical body. The forced vortex motion caused very low pressures in the region near the vertical axis of cyclone cylindrical body,

therefore the maximum upward fluid velocity was not right at the center line of the cyclone cylindrical body. It was located at some radial distance measured from the axis of the cyclone cylindrical body. Experiments had shown that in case of a strong swirl, the direction of axial fluid velocity in the near axis region could be downwards. Thus, forming two recirculating flow regions in the vertical (z-r) plane of the cyclone cylindrical body, and the axial velocity profile takes the from of S-shaped curves in radial direction of the cyclone cylindrical body.

In reference [30], it was stated that, there was a stationary layer approximately under the wall of fluid discharge pipe through the all vertical heights of cyclone cylindrical body where the axial and radial velocities were found to be zero. The existence of this layer had already been reported by Knowles et al.[28] and Hwang et al.[29].

2.5.3 Radial Velocity Profile in Cyclones

Knowles, Woods and Fuerstein [28] found that, the radial velocity were relatively small and constant with the radial motion is slightly outward near the central axis of the cyclone cylindrical body and is inward toward the wall of cylindrical cyclone body at all vertical locations in a hydrocyclone operating without an air core. Whereas, Ohasi and Maeda's results reported in reference [28] also suggested relatively small radial velocities, although the direction of radial velocity tends to be inward near the central axis and the wall of the cyclone cylindrical body, and is outward in a small annular region between the central axis and the wall of the hydrocyclone. Kellsal's results reported in reference [28] suggested a radial velocity profile decrease linearly from outer to inner of the cylindrical body of the hydrocyclone and the direction of radial velocities is inward along the all radial distances in the cylindrical cyclone body.

In reference [27, 28, 30], it was stated that, there was a stationary layer approximately under the wall of fluid discharge pipe through the all vertical heights of cyclone cylindrical body where the radial velocities were found to be zero.

References [27, 28, 30], showed that there was an inconsistency between the measured radial velocity distributions in a cyclone. The reason

15

for that, the radial velocity distributions were estimated from the axial fluid velocity distributions by using continuum concept between the two successive test section of the cyclone with assuming axially symmetric flow by the researchers Kelsall, Ohasi and Maeda, whereas Knowles et al [28] directly measured the radial fluid velocities at each test section of the cyclone.

2.6 STATIC PRESSURE DISTRIBUTION IN CYCLONES

As indicated in references[21, 29, 30, 31, 33], the vortex motion caused very low pressure in the region near the axis of the cyclone cylindrical body, where the solid body rotation was in effect, and the lowest static pressure was located at the vertical axis of the cyclone cylindrical body. Static pressure first raised rapidly in the radial direction within the forced vortex region and then levelled off, reached it's maximum value at the wall of cyclone body. The static pressure gradient in radial direction in the forced vortex region was much higher than the pressure gradient in the free vortex region. Axial variation of the static pressure through the vertical heights of the cyclone body was very small compared to it's radial variation.

In references [16, 17, 28, 29, 30, 31, 32], It was stated that the radial distribution of the static pressure in a cyclone could be estimated from the radial distribution of the tangential fluid velocity with the elimination of radial velocities, fluctuating velocities and pressures in radial direction, and by integrating the tangential velocity profile from the wall of cyclone to a series of radial distances by means of the following equation;

$$dP_{st}/dr = \rho \, V_t^2/r \qquad\qquad 2.3$$

or by the integrated form of it ;

$$P_{st} = P_w - \rho \int V_t^2/r \, dr \qquad\qquad 2.4$$

where, P_w is the static pressure at the cyclone wall, V_t is the tangential fluid velocity at any specified radial position and P_{st} is the static pressure corresponding to the specified radial position. For higher degrees of swirl,

suitable agreement was obtained between the calculated and measured values of the static pressures, but for lower degrees of swirl where the effects of friction may be expected to become relatively of greater importance, the agreement was not good. Calculated static pressure values have a singular point at the centre of the cyclone and it has no meaning.

2.7 STATIC PRESSURE LOSS OF CYCLONES

As indicated in references [27, 29, 30, 31, 33, 34], a number of factors contribute to the static pressure loss between the fluid inlet and outlet of the cyclone separators. These had been reported as;

1. Loss due to expansion of the fluid when it enters the cyclone
2. Loss as kinetic energy of rotation in the cyclone chamber
3. Losses due to wall friction in the cyclone chamber
4. Any additional frictional losses in the exit duct, resulting from the swirling flow above and beyond those incurred by straight flow

In references [30, 33, 34], the experimental results showed that, the static pressure drop was mainly related to the inlet dynamic pressures and the dimensions of the cyclone separators, by the equation;

$$\Delta P_{st} = C_p \; 1/2 \, \rho \, V_{in}^2 \qquad\qquad 2.5$$

where, V_{in} is the average fluid velocity at the inlet to the cyclone, ρ is the fluid density, C_p is the experimentally determined static pressure loss coefficient which is related to the dimensions and operation conditions of the cyclone equipment, and ΔP_{st} is the corresponding static pressure loss between the inlet and outlet of the cyclone separator. The dimensions of the conventional cyclones were specified in terms of the cyclone cylindrical body diameter, D and seven dimensionless ratios a/D, b/D, D_d/D, S/D, h/D, H/D and D_u/D, where a, b, D_d, S, h, H and D_u were the characteristic cyclone dimensions which are shown in Figure 2.3.

Zhou and Soo [27] found that the pressure drop of a conventional air cyclone is proportional to the inlet fluid velocity of the cyclone, but they showed that ;

$$\Delta P_{st} = C_p \, \rho \, V_{in}^{\ m} \qquad\qquad 2.5$$

where the value of exponent 'm' should be somewhat higher than 2, possibly $2<m<3$. This means that vorticity was not constant within the cyclone. They found the value of static pressure loss coefficient, C_p as 8.18 for V_{in}=21 m/s for their cyclone geometry. Zhou and Soo [27] also made measurements for determining the effect of a central body which was placed at the vertical axis of the cyclone, to reduce the pressure drop of the cyclone. They found that the pressure drop remarkably reduced up to 1/3 of the original pressure drop of the cyclone without a central body.

In references [31, 33, 34], the effects of some cyclone dimensions on the pressure loss were investigated and it was found that; the static pressure loss coefficient, C_p was a function of the inlet to total outlet area ratio(i.e. C_p was related to the cyclone dimensions a/D, b/D, D_d/D and D_u/D). Rietema [31] made experiments on the cyclone with inlet to outlet area ratios 3.2, 0.8 and 0.2 and he found that, the pressure loss was decreased by decreasing the inlet to outlet area ratios of the cyclones. Xu et al [33] also made experiments for determining the effects of the cyclone dimensions a/D, b/D, D_d/D and D_u/D on the cyclone pressure loss, and they showed the effects of these cyclone dimensions on the pressure loss as was done in the references [31, 32, 34]. The retention time of the suspended particles within the cyclone could be shortened and the efficiency might be cut down with the enlarging of the outlets, therefore a moderate inlet to outlet area ratio must be selected for an efficient cyclone operation. In available literature, the effects of cyclone dimensions on the cyclone pressure loss were not complete. The effects of S/D, h_c/D, a/b on the cyclone pressure loss should be investigated.

2.8 COLLECTION EFFICIENCY OF CYCLONES

Collection efficiency of the cyclone separators is defined as the weight of collected particles by the cyclone, divided by the total weight of particles fed into the cyclone separator by means of fluid flow. The complex way in which solid particles move in cyclone separators with a swirled fluid flow makes it difficult to determine the efficiency of their separation by theoretical means. Theoretical methods of calculating the separation efficiency of a cyclone separator which were reported in references [35, 37, 39, 43, 44], are not accurate.

Experimental investigations dealing with the collection efficiency of cyclone separators[31, 34, 36, 38, 40, 41, 42] had shown that, the collection efficiency was significantly increased with;

1- Increasing particle size and density.
2- Increasing speed of rotation in the cyclone vortex
3- Decreasing cyclone diameter.
4- Increasing cyclone length.
5- Drawing some of the fluid from the cyclone through the dust exit outlet.
6- Wetting the cyclone's wall

As indicated in references [34, 36, 38, 40, 42], the collection efficiency was increased continuously with increasing the particle size, and approached 100 percent asymptotically for sufficiently large particles. It also increased with increasing tangential fluid inlet velocity. However with the rising tangential fluid inlet velocity some other factors which decreased the collection efficiency and increased the pressure loss, became active. Therefore in practice , the tangential fluid inlet velocity was limited to 15-20 m/s in cyclone operations. The collection efficiency improved with decreasing dimensionless widths of tangential inlet, b/D, owing to higher tangential velocities. However, the pressure loss was increased with decreasing the width of inlet, owing to the sudden contraction. Therefore, the width of inlet, b was approximately equal to $1/2(D-D_d)$ in standard designs. The dimensionless height of tangential entry, a/D was chosen smaller than the dimensionless depth of fluid discharge pipe ,S/D, in order to prevent the

short-circuiting of flow. The collection efficiency increased with increasing the dimensionless height of the cyclone cylindrical body, h/D, due to increase in separation length and longer residence time of the particles in the cyclone. However, due to the increase in wall friction losses, the static pressure loss across the cyclone increased with increasing h/D. Therefore, the optimum height of the cyclone cylindrical body (h) ranged from 1.5 to 3 times of the cyclone diameter, D in standard designs [40, 42], (i.e., $1.5D \leq h \leq 3D$). The collection efficiency of the cyclone increased with decreasing the diameters of the clean fluid discharge, D_d and the dust discharge, D_u, but this increased the static pressure loss of the cyclone. Therefore, the clean fluid discharge diameter, D_d and the dust discharge diameter, D_u were selected as approximately 0.5 and 0.25 times of the cyclone diameter, D, respectively. As is shown in references [40, 41, 43, 44], the effect of the solid loading on the collection efficiency of the cyclone was found to be very small within the acceptable range of 1 to 6 particle weight to fluid weight ratios.

2.9 CONCLUSIONS

Literature survey showed that;

1. Swirling flow structure was used only by the cyclone separators as a tool of the particle separation from a particle suspended fluid flow.

2. Most common cyclone separators have a swirl generating section with only one tangential fluid inlet which has a rectangular-shaped crossection.

3. Swirling flow field within the cyclone separators is mainly affected by the inlet pipe Reynolds number and the structure of the cyclone.

4. Five-tube probes can successfully be used to measure the velocity and static pressure distributions of the swirling flow field in the cyclone separators.

5. The swirling flow structure in a cyclone may be divided into three regions namely a region near the wall where logarithmic velocity distribution prevail, an outer region between the projection of the clean fluid discharge pipe and

the wall of the cyclone cylindrical body where the tangential fluid velocity distribution may be represented by a free vortex type velocity distribution and a central core region where the tangential fluid velocity distribution can be represented by a forced vortex type velocity distribution.

6. Axial velocity distribution in the radial direction of the cyclone cylindrical body can be successfully represented by the s-shaped curves. Axial velocity is directed downwards at the outer region and directed upwards at the central core region of the cyclone cylindrical body at all vertical heights. The magnitude of the maximum upward fluid velocity is much greater than the magnitude of the maximum downward fluid velocity.

7. There is inconsistency between the measured radial velocity profiles in the cyclone cylindrical body. Knowles et al [28] found that, the radial fluid velocity is slightly outward near the central axis of the cyclone cylindrical body and is inward toward the wall of cyclone cylindrical body at all vertical locations. Whereas, Ohasi and Maeda's results reported in [28] suggested that, the direction of radial fluid velocity tend to be inward near the central axis and the wall of the cyclone cylindrical body, and tend to be outward in a small annular region between the central core region and the near wall region of the cyclone cylindrical body at all heights. Kellsal's results reported in [28] suggested a radial velocity profile decreases linearly from outer to the center in the cylindrical body of a hydrocyclone at all vertical locations. The direction of the radial fluid velocity tend to be outward through the all radial positions measured from the central axis of the cyclone cylindrical body.

8. The effects of the dimensionless parameters of the cyclone separator geometry on the swirling flow field was not fully investigated in the available literature.

9. The lowest static pressure was located at the central axis of the cyclone cylindrical body. It first raised rapidly in the radial direction within the forced vortex region and then levelled off, reached its maximum value at the cyclone wall

10. The static pressure loss of the cyclone separators was mainly related to the inlet dynamic pressure and the physical dimensions of the cyclone geometry. The complete investigation directed to determine the effects of the

physical dimensions of the cyclone on the static pressure loss was not available in the literature.

11. The effects of the dust properties, cyclone fluid properties, fluid-dust concentration, fluid flowrate and physical dimensions of the cyclone on the collection efficiency of the cyclone separators were investigated in the available literature.

12. There is no available investigation on the use of swirling flow structure as a tool for particle size or particle mass classification in the available literature.

CHAPTER 3

DESIGN AND PRODUCTION OF EXPERIMENTAL SET-UP

3.1. INTRODUCTION

The experimental set-up used for this study was designed and constructed under the light of the available literature. The experimental set-up is mainly composed of the following sections;

1. Fan unit
2. Settling tank
3. Pitot tubes and traverse mechanisms
4. Particle feeder
5. Five-tube yaw meter probe and its traverse mechanism
6. Yaw meter calibration mechanism
7. Cyclone arrangements with different principal dimensions
8. Bag filter
9. Inclined tube alcohol micro manometers

A general view of the experimental set-up is shown in Figure 3.1. It is seen from Fig. 3.1 that, the fluid flow supplied by a centrifugal fan is firstly transferred into the settling tank by means of a flexible duct, and then it continues to flow through plastic PVC pipes into the particle feeding unit. The fluid flowrate was measured by means of a pitot tube and wall static tapping placed just before the particle feeding unit. After the particle feeding unit, flow is fed into the cyclone with a small length PVC pipe section. The fluid flow from the top of the cyclone is transferred into a bag filter by means of a pipe section and a 90°-elbow. Suspended particles are collected in a hopper which is quick mounted under the cyclone. The flow field in the cyclone was measured by means of a five-tube yaw meter probe and static tapping placed

on the cyclone wall which are connected to the inclined tube alcohol micro manometers. The pressure loss across the cyclone separator was measured by means of static pressure tapping located on the inlet and exit pipe sections of the cyclone.

3.2 FAN UNIT

Under the light of the available literature, total head and flowrate requirements of the experimental set-up were determined. The required maximum flow rate and head of present experimental investigation were estimated as the 0.16 m³/sec of air flowrate under a head of 135 mAC.

A vertical shaft centrifugal fan which is capable of providing 0.175 m³/sec of air under a head of 150 mAC when running at 2835 rpm, was used to supply air to the cyclone test set-up. It had an impeller with 420 mm outer and 320 mm inner diameters, having 12 backward curved blades. The exit cross-section of the volute casing of fan was a 250×300 mm rectangle. The fan was driven by a 2.95 HP/2.2 kW, 2835 rpm electric motor. This motor was controlled by an AC motor variable speed control unit which controls the motor speed by controlling the frequency of the mains. The specifications of the motor and speed controller are given in Appendix 1. The speed of motor could be changed safely from 0 to 5000 rpm via the variable speed control unit. Thus the amount of flow rate through the set-up was controlled by controlling the rotational speed of the fan.

3.3 SETTLING TANK

The non-uniformity of air flow supplied by the fan unit was removed by means of a settling tank which was placed at the exit of fan unit. It has a size of 800×800×800 mm. The settling chamber provided a steady and axis symmetric flow in the exit pipe.

3.4 DETERMINATION AND ADJUSTMENT OF THE AVERAGE FLUID INLET VELOCITY OF CYCLONE UNIT

A pitot tube together with wall static pressure tapping were used to measure the radial velocity distributions within the inlet pipe of cyclone test set-up. Six static pressure holes were drilled in accordance with reference [46]. These holes are drilled on the wall in the plane passing through the tip of pitot tube. The holes were surrounded by a pressure chamber. A L-shaped copper tube with 2.2 mm outside and 1.1 mm inside diameters was used as the pitot tube. The pitot tube was traversed across the pipe crossection with an accuracy of ±0.025 mm by means of a traverse mechanism. The pitot tube and traverse mechanism which were placed on the PVC pipe at a distance 4000 mm downstream of the settling tank, are shown in Figure 3.2.

The velocity profiles within the inlet pipe were measured for ten different motor speeds of fan unit from 567 to 2835 rpm by changing the nominal frequency of the mains from 10 Hz to 50 Hz. The velocity at any radial position within the pipe was determined by the equation;

$$V(r) = \sqrt{2gh(r)} \qquad\qquad 3.1$$

Where $V(r)$ is the local fluid velocity at any radial position, g is the gravitational acceleration and $h(r)$ is the dynamic head of the air at any radial position which was measured by using an inclined tube alcohol micro manometer. One end of the micro manometer was connected to the outlet of the pitot tube and the other end of it was connected to the static pressure chamber.

The velocity profiles corresponding to the ten different motor speeds of the fan unit which were found as in the turbulent axis symmetric pipe flow, were integrated across the pipe cross-section, and thus the flow rates corresponding to the different motor speeds of the fan unit were estimated. Then, these flow rates were divided by the cross sectional area of the pipe for determining the average fluid velocities within the pipe corresponding to the different motor speeds of fan unit. After the determination of the average fluid velocities, the radial distances from the pipe wall corresponding to

these average fluid velocities were determined from the previously measured velocity profiles.

The values of radial distances of the average fluid velocities from the pipe wall was found as constant between the 3.6×10^4 to 1.5×10^5 of Reynolds numbers which were based on the average fluid velocity within the pipe and the pipe diameter. This is shown in Figure 3.3. It is seen that, the relation between the radial positions of the average fluid velocities and the pipe radius would be given by the equation;

$$h_{av} = 0.206\,R_{in} \qquad\qquad 3.2$$

where h_{av} is the radial positions of the average fluid velocities within the pipe from the pipe wall (i.e., R_{in}-r) and R_{in} is the pipe radius.

The above mentioned calibration is used to simplify the experiments and the pitot tube was fixed at a radial position where the center of the tip of pitot tube was placed at a radial distance 10.9 mm from the pipe wall corresponding to a pipe radius of 53 mm. Thus, required average fluid velocity within the inlet pipe would be directly calibrated by means of an AC motor variable speed control unit and an inclined tube micro manometer without changing the radial position of pitot tube with an accuracy of $\pm 0.5\%$ of it.

3.5 PARTICLE FEEDER

A celled-wheel particle feeder was designed and constructed for the calibration of particle concentration in the fluid flow of cyclone unit. The feeding unit is mainly consisted of the following parts;

1. A short cylindrical casing
2. Celled-wheels
3. A particle storage tank
4. An electric motor driven with direct and/or belt
5. An AC motor speed controller

The crossectional views of the particle feeder are shown in Figure 3.4 and 3.5. The operation procedure of the particle feeder may be summarized as that; A definite amount of the particle is filled into the particle storage tank and then the top cover of storage tank is closed, when the particle exit mouth of the storage tank which is placed at the bottom of the storage tank cone, is closed. After that the required rotational speed of the celled-wheel which was determined experimentally from the testing of celled-wheel for the different rotational speeds with different particulate matters, is set by means of the AC motor speed controller. Then, the particle exit mouth of the storage tank is opened. Thus, the particles were taken with a definite mass flow rate from the particle storage tank and are transferred into the fluid flow through the inlet pipe of cyclone unit.

The desired fluid-particle concentrations were obtained by means of controlling fluid mass flow rates in the pipe by an AC motor variable speed controller which was linked on the electric motor of the fan unit and the particle mass flow rate was by an another AC motor variable speed controller which was linked on the electric motor of the particle feeder. The specifications of the motor and speed controller of the particle feeder unit are given in Appendix 2.

The calibration of the particle feeder with different types of celled-wheels and with the different types of particulate matters at different rotational speeds of wheels showed a problem as that; the low-density particulate matters such as, cereal scurf and semolina were repulsed back into the storage tank, when the surface level of the particulate matters was reduced to the bottom of storage tank. This was due to the high pressure within the pipe of fluid flow which was placed under the feeding unit. This type of problem was also seen in reference [48] in some other types of the particle feeders such as, the particle feeders with disk brush and the particle feeders with vibration feeding. Therefore, a feeding unit with band scale-vibration gutter-injector was suggested to feed the particulate matters in spite of the high capital cost of this unit mentioned in reference [48]. The mentioned problem of celled-wheel particle feeder was solved by the addition of a short-circuit flow linkage between the pipe of fluid flow just upstream of the feeding unit and the top cover of the particle storage tank in our experimental set-up. Thus, the repulsion of the low-density particles was prevented by means of balancing the pressures under and top of the

particulate matter which were contained in the storage tank. Addition of a pressure balance line avoided the repulsion of particles during the feeding.

The three types of celled-wheel rotors were designed and constructed to give the required mass flowrates of the different particulate matters. The end shapes and sizes of the three celled-wheel rotors are given in Figure 3.6. The calibration of the three celled-wheels was done with the different types of particulate matter for the different rotational speeds of the wheels. The results of the calibration are given in Figures 3.7 which shows the plot of particle mass flowrate versus the rotational speed of the celled-wheels for different types of the particulate matters. It was shown that, the designed celled-wheel particle feeder with three types of celled-wheels could be used to vary the mass flow rates of the particulate matters from 5 to 85 gr./s. The reproducibility of the mass flow rates was possible with experimental errors of ±1 to ±3 percent from lower mass flowrates to higher mass flowrates, respectively. It was also shown that, the upper limits of the particle mass flow rates of the feeder could be increased up to 150-200 gr./s by means of the new wheel designs with high rotational volumes.

3.6 FIVE-TUBE YAWMETER

As is seen in references [27, 28, 29, 30, 31] that, the measured radial velocity distributions in the cyclones were inconsistent with each other. there was an inconsistency on the distribution of radial fluid velocity in radial direction within the cyclone separators. This was due to the calculation of radial fluid velocity from the measured axial and tangential fluid velocities by using the continuum concept. The application of continuum concept was possible by making some assumptions for the simplifying the calculations. These assumptions were the axially symmetricity of the flow, unimportance of the short-circuiting flows, etc. The experimental measurement of the radial fluid velocity in the cyclones was required for the prevention of errors on radial velocity profile data. The measurement of the radial fluid velocity must be done by the experimental determination of the flow angles in two perpendicular planes of the flow (i.e., the pitch and yaw angles of the flow must be measured).

Bryer and Punkhurst [47] have described the details of determining wind speed and flow direction by using pressure probes. It was stated that, the five-tube probes consisting of a forward facing pitot-tube, two inclined side-tubes in horizontal plane and two inclined side-tubes in vertical plane could be used to determine the wind speed and the flow direction at two perpendicular planes. The five-tube pobes was used by two different methods for the measurements of velocities in the test sections.

The first method that was used, the nulling method in which the probe is rotated only in yaw about its apex within the test section until the horizontal side-tubes register the same pressure, then the yaw angle is read directly from the orientation gear of the probe, but the pitch angle, the dynamic pressure and the total pressure are obtained from the calibration of probe at the different pitch angles under the different wind speeds by using the nulling method [47].

The second method of using a five-tube probe, a five-tube probe could be used without any rotation in yaw and pitch directions within the test section by means of the calibration of it for use without rotation. The calibration of a five-tube probe for use without rotation in the angle ranges of $-40°<\psi<+40°$ and $-35°<\alpha<+35°$ has shown that, the wind speed measurements within these limits can be carried out with an accuracy of about ±3 percent up to speeds of 135 m/s [47].

As a result of the above discussion, it was decided to use a five-tube yaw meter probe without rotation to measure the velocity distribution, variation of the yaw and pitch angles and static pressure distribution within the swirling flow field of the cyclone arrangements. For this purpose a five-tube yaw meter probe was constructed from copper tubes having 1.2 mm outside and 0.7 mm inside diameters. The tip angles of the horizontal and vertical side-tubes were constructed to 45°. The traverse mechanism of the five-tube probe which was mounted horizontally on the vertically placed cyclone cylindrical body, was contained with a vernier scale in the radial direction. The traverse mechanism was capable of radial traversing of the cyclone crossection with an accuracy of ±0.025 mm. The traverse mechanism was also designed to enable the rotation of yaw meter probe through 360° in yaw direction. The yaw angle of the probe can be read from a protractor which was scaled to one degree intervals. Thus, the yaw angle could be read

with an accuracy of ±0.5°. The five-tube yawmeter and its traverse mechanism are shown in Figure 3.8.

The calibration of five-tube yawmeter for use without rotation required a calibration mechanism which enabled rotation of the five-tube probe about its tip and in two planes normal to each other (i.e., in its pitch (α) and yaw (ψ) directions). For this purpose a calibration mechanism which allowed a 360-degree rotation in yaw and a ±60° rotation from vertical in pitch with an accuracy of ±0.5° in both direction, was designed and constructed for calibrating the five-tube probe for use without rotation.

The five-tube calibration mechanism is shown in Figure 3.9. It mainly consisted from two orientation gear, an L-shaped arm to give orientations in pitch, a four-groove collate type coupling ring placed on the L-shaped arm to give angles in yaw, and a wind tunnel test section with a 140×210 mm crossection which carried the all other parts of the calibration mechanism. The five-tube calibration mechanism with a wind tunnel test section mounted on a blower type wind tunnel which was designed and constructed by Uskaner, F. [45]. The wind speed within the test section of the blower type wind tunnel can be varied by means of an AC variable speed controller which is linked on the driving motor of the wind tunnel propeller. The specifications of the blower type wind tunnel and its drive unit are given in Appendix 3.

As stated in reference[47], the calibration of five-tube probe for use without rotation was made in the ranges of -45° $\leq \psi \leq$ +45 and -35° $\leq \alpha \leq$ +35° with a 5-degree increments in both pitch and yaw angles at 5 m/s and 10 m/s of the test section wind speed. The following relationships are obtained from the calibration of the five-tube probe;

$$f(a) = \frac{P_3 - P_1}{P_5 - P_m} \qquad 3.3$$

$$f(\psi) = \frac{P_2 - P_4}{P_5 - P_m} \qquad 3.4$$

$$Q_p = \frac{P_5 - P_m}{\frac{1}{2}\rho V^2} = \frac{P_5 - P_m}{q} \qquad 3.5$$

$$S_p = \frac{P_T - P_5}{P_5 - P_m} \qquad 3.6$$

where, P_1 and P_3 are the pressures sensed from the side-tubes at vertical plane, P_2 and P_4 are the pressures sensed from the side-tubes at horizontal plane, P_5 is the pressure sensed from the central tube, and P_m is the arithmetic mean of the pressures sensed from the side-tubes at horizontal and vertical planes, i.e.;

$$P_m = \frac{P_1 + P_2 + P_3 + P_4}{4}$$

3.7

q and P_T are the dynamic and total pressures (i.e., $1/2\ \rho V^2$) of the air flow, respectively. Results of the five-tube probe calibration for use without rotation are shown in Figures 3.10. a, b and c. The calibration data obtained at 5 m/s and 10 m/s of the wind speed were found essentially the same. A similar effect of wind speed on the calibration of the five-tube probe was also stated in references [16, 47]

In order to determine the swirling flow structure in the cyclone, the previously mentioned five-tube probe is used without rotation. Measurements are made at many radial stations by traversing the five-tube probe between the center of the cylindrical cyclone body and the wall of the cylindrical body. The static pressures on the wall of cylindrical cyclone body are measured by means of the wall static pressure tapping. Five inclined tube alcohol micro manometers were used to measure the pressures which are sensed by the tubes of the probe (i.e., P_1, P_2, P_3, P_4 and P_5).

To determine velocities, static and total pressures from the readings of manometers, the measured pressures are first used to calculate the values of the f(α) and f(ψ) from the equations (3.3) and (3.4), then the values of pitch angle (α) and yaw angle (ψ) could be read from the calibration curves shown in Figure 3.10.a. Then the values of S_p and Q_p was read from the calibration curves shown in Figures 3.10.b and 3.10.c. Consequently, the value of the fluid velocity at the considered point is estimated by the equation;

$$V = (\frac{2\,(P_5 - P_m)}{\rho\,Q_p})^{1/2}$$

3.8

and the components of the fluid velocity in the three principle directions of the cylindrical co-ordinates which is used for the representation of the swirling flow field in the cyclone, as shown in Figure 3.11., can be calculated by the equations;

$$V_t = V\cos\psi\cos\alpha \qquad \text{in tangential direction} \qquad 3.9$$

$$V_r = V\cos\psi\sin\alpha \qquad \text{in radial direction} \qquad 3.10$$

and

$$V_a = V\sin\alpha \qquad \text{in axial direction} \qquad 3.11$$

The total pressure P_T is obtained from Equation (3.6) as;

$$P_T = S_p\,(\,P_s - P_m\,) + P_s \qquad\qquad 3.12$$

and then the static pressure P_{st} can be calculated from the expression as;

$$P_{st} = P_T - q \qquad\qquad 3.13$$

or

$$P_{st} = P_T - \frac{1}{2}\rho V^2$$

$$3.14$$

The atmospheric and the ambient temperature were measured during each experiment by using a mercury barometer and a mercury thermometer. All measured experimental data which were taken under varying atmospheric conditions, were reduced to STP conditions.

3.7 CYCLONE CONFIGURATIONS

Early experimental works directed on the increase of cyclone performance were mainly consisted of the collection efficiency experiments with powders and the pressure loss experiments. The dimensions of the cyclone separators affected the collection efficiency and pressure loss of the cyclones. The effects of cyclone dimensions on the swirling flow structure were not completely studied. The present work is undertaken to fulfil this gap.

The necessary elements of a conventional cyclone separator consists of a tangential fluid inlet which generates the swirling flow structure; an axial

32

outlet for the cleaned fluid; a dust discharge outlet for the collected particles and a cylindrical body to support all other cyclone elements. In the experimental research of the cyclone, conventional cyclone geometry has been selected as the starting point in present work. The principle dimensions of the conventional cyclone geometry are then specified by the cyclone body diameter, D and seven dimensionless ratios a/D, b/D, D_d/D, S/D, h/D, H/D and D_u/D which are shown in Figure 2.3. This permits a comparison of the geometric similarity of several cyclones through a consideration of their non dimensional ratios of their physical dimensions.

A number of cyclone "standard designs" or sets of non dimensional ratios have been suggested in the available literature. Several are listed in Table 3.1. Comparing these designs showed that, the non dimensional ratios differ according to the purpose which the cyclone is to be used. High efficiency cyclones have smaller inlet area (i.e., small a/D and b/D) and exit area (i.e. small D_d/D) than the high throughput designs. The fluid exit duct length (S/D) is small in high efficiency designs, because tangential inlet height (a/D) is small. Exit duct length is always greater than inlet height in order to avoid the fluid short-circuiting the cyclone by passing directly from the inlet to the outlet without forming a swirl. The general purpose designs appear to be a compromise between the high efficiency and high throughput designs. The variability in design shows that there is no single optimum cyclone. That is, there is no single cyclone design which will perform best for all dust collection problems.

Under the light of the above discussion and available literature a cylindrical cyclone body was constructed from sheet steel having 2 mm thickness. It had a 240 mm internal diameter and 480 mm height (i.e. D=240 mm and h/D=2). The cylindrical cyclone body was equipped with the mounting sections of the tangential fluid inlet nozzles, fluid exit ducts, cyclone cones with dust outlets, and five-tube probe traverse mechanism. A detailed section view of the cylindrical cyclone body with all of mounting sections is shown in Figure 3.11. Thus, the infinite numbers of cyclone configurations can be obtained by means of the changing the principle dimensions of the cyclone, however the swirling flow field experimentation must be restricted to few cyclone configurations with respect to the difficulties of the flow field measurement. Therefore, it was decided to perform experiments for the determination of the effects of primary cyclone

dimensions a/D, b/D, D_d/D, S/D, D_u/D , and h_c/D on the swirling flow structure.

Four types of the tangential inlet nozzles were constructed with four different a/D and b/D ratios. The total inlet area of the nozzles were kept constant (i.e., a×b = constant for all tangential inlet nozzles). Thus, effects of the tangential inlet height and width on the flow field could be tested with the elimination of the effects of total inlet area by mounting it on the same cyclone configuration with respect to the other principle dimensions with the exception of the S/D ratios. In the available literature the S/D ratios were related to the a/D ratios as a/D≤S/D≤a/D+1/8 in order to avoid the short circuiting of fluid flow. Therefore the S/D ratios of the configurations were changed with respect to the a/D ratios of the tangential inlet nozzles. The produced tangential inlet nozzles and their cyclone configurations are shown in Table 3.2.

The effect of the non-dimensional fluid discharge pipe depth, S/D on the flow field is tested by changing S/D ratios on the same cyclone configuration with using the flexible supporting mechanism of the fluid discharge pipe which is previously shown on Figure 3.11. It was decided to perform experiments on the cyclone configurations with five different S/D ratios which are shown in Table 3.3 with their principle dimensions.

The effect of the non-dimensional fluid discharge pipe diameter, D_d/D on the swirling flow field is tested by means of mounting the four different types of plastic PVC pipes with 50, 75, 106 and 120 mm internal diameters, respectively on the top of cylindrical cyclone body. For this purpose the top of cyclone body was designed to enable the mounting of different diameter discharge pipes with the use of adequate exit duct supporting rings. The exit duct mounting section is also previously shown on Figure 3.11. The used configurations for the experimentation of cyclone exit duct diameter are shown in Table 3.4 with their principle dimensions.

The effect of the non-dimensional dust discharge opening diameter, D_u/D which is the apex diameter of cyclone cone, is tested by means of four cyclone cones with different apex diameters. Four cyclone cones were constructed for this purpose. The apex angle of the cones were kept constant

34

14° from vertical as in large variety of available literature. The constructed cyclone cones and their cyclone configurations are shown in Table 3.5.

The effect of non-dimensional cyclone cone heights, h_c/D is tested by means of four cyclone cones which were constructed at four different cone heights with constant non-dimensional apex diameter (i.e., the apex angles of the cones from vertical were different). The constructed cyclone cones having different heights and their cyclone configurations are shown in Table 3.6.

All of the cyclone components such as tangential inlet nozzles, cyclone cones, exit duct supporting rings and cylindrical cyclone body were constructed from sheet steel with 2 mm thickness despite the corrosive property of sheet steel with respect to the easy forming and low cost advantages of it. The parts which were used mounting of the five-tube probe traverse mechanism on the cyclone cylindrical body at fluid inlet and impact sides, were constructed from aluminium sheets due the lightness of aluminium.

3.8 BAG FILTER

Early works on the collection efficiency of cyclone separators with particulate matter showed that the collection efficiency of cyclone separators could be varied between 60 percent to 99.9 percent depending on the operating and design conditions. This required a second filtering unit at the exit of the cyclone configuration in the experimental set-up to avoid the pollution of laboratory. For this purpose, a polyester bag filter with a vertically movable roof was constructed and connected to the fluid exit duct of the cyclone by means of a 90°-elbow with square crosssection. The polyester bag filter had total surface area of 4 m^2 with open area ratio of 3.21. The pressure loss of filter was measured to be between 3 to 10 Pa for the cyclone fluid inlet velocity ranges of 5 to 18 m/s corresponding to the fluid volume flowrates of 0.044 to 0.16 m^3/s.

CHAPTER 4

EXPERIMENTAL STUDY

4.1 INTRODUCTION

The experimental work is mainly consisted of the cyclone static pressure loss measurements, the cyclone collection efficiency measurements and the measurement of swirling flow field for different cyclone configurations. The cyclone configurations which were used in experimental work, were obtained by changing the characteristic cyclone dimensions, D_d, D_u, h_c, S, a and b, of the basic cyclone configuration which is given in Table 3.1.

The static pressure loss measurements were directed to determine the effects of characteristic cyclone dimensionless ratios, D_d/D, D_u/D, h_c/D, S/D, a/D and b/D, and the cyclone inlet Reynolds number on the static pressure loss of the cyclone particle separator. For this purpose, the static pressure loss measurements were conducted at least at four different values of each characteristic cyclone dimensionless ratio, for seven cyclone inlet Reynolds numbers. Re was varied between 15000 and 125000. The experimentally investigated values of each characteristic cyclone dimensionless ratio were selected such that they corresponded to the cited ranges in the available literature [31,32, 33, 35, 37, 40, 42, 43]. The cyclone inlet Reynolds number, Re was based on the average fluid inlet velocity, V_{in} and the hydraulic diameter, D_{in} of the rectangular shaped tangential inlet of the cyclones. It can be defined by the relation;

$$Re = \frac{V_{in} \, D_{in}}{\upsilon}$$

4.1

where, D_{in} is defined as;

$$D_{in} = \frac{4 A_{in}}{P_{in}}$$

4.2

where, A_{in} is the crossectional area of the tangential inlet of the cyclone (i.e., $A_{in}=a.b$) and P_{in} is the crossectional wetted perimeter of the inlet (i.e., $P_{in}=2a+2b$)

For each cyclone configuration, the swirling flow field measurements were conducted at four different vertical measurement stations on the cylindrical cyclone body for different values of Re. The velocity, yaw and pitch angle, and the static pressure variations in radial direction were measured within the cyclone body by using a five-tube yaw meter. The vertical locations of the measurement stations, Z were 0.412, 0.667, 0.813 and 0.979 cyclone body heights, h measured from the top of cyclone cylindrical body. The locations of measurement stations are shown in Figure 3.11.

4.2 STATIC PRESSURE LOSS MEASUREMENTS

The static pressure losses across the cyclone configurations were measured by means of two static pressure chambers. The pressure chambers were mounted on the fluid inlet and discharge pipe of the cyclone at distances 1000 mm measured from the inlet and exit, respectively. Ends of an inclined tube alcohol micro manometer were connected to the static pressure chambers. Each static pressure chamber encloses the multiple numbers of 1 mm diameter holes drilled on the pipe in accordance with the reference [46].

The effects of the characteristic cyclone dimensions, a, b, S, D_d, D_u and h_c, and Re number on the static pressure loss of the cyclone separators were experimentally investigated. Results of the measurements directed on the above parameters, are discussed separately in the following sections.

4.2.1 Effect of the Cyclone Inlet Reynolds Number on the Static Pressure Loss

The static pressure loss of the cyclone separators was related to the inlet dynamic pressure of the cyclone by many investigators [21, 27, 31, 33, 34]. They stated that , there was a linear relationship between the static pressure loss, ΔP_{st} and the square of the average fluid inlet velocity, V_{in} as given by the equation;

$$\Delta P_{st} = C_P \frac{1}{2} \rho \ V_{in}^2$$

4.3

where the static pressure loss coefficient, C_p was related to the dimensions of the cyclones.

Based on the knowledge cited in the available literature on the static pressure loss of the cyclones, experiments were conducted to determine the effect of Re on the static pressure loss of the cyclone separators in our basic cyclone configuration which is given in Table 3.1. Re was varied between 15000 and 125000, were applied. The results of the static pressure loss measurements were plotted firstly as a function of Re number. Figure 4.1 shows the variation of the static pressure loss of our basic cyclone configuration together with data of [27] and [34] as a function of Re. It can be seen that, when Re increases the static pressure losses of the cyclones increase as a second degree function of Re. We know that Re based on the independent variable, V_{in}. Therefore, the static pressure loss of the cyclone can be plotted as a function of the inlet dynamic pressure to obtain a linear relationship between ΔP_{st} and the inlet dynamic pressure. The inlet dynamic pressure depends on the square of average fluid inlet velocity, as shown below;

$$P_{ki} = \frac{1}{2} \rho \ V_{in}^2$$

4.4

Figure 4.2 shows the static pressure loss of our basic cyclone configuration and the results of investigators [27, 34] as a function of the inlet dynamic pressure. It can be observed from Fig. 4.2 that, there is a linear relationship between the static pressure loss and the inlet dynamic pressure. However the rate of change of static pressure loss is found to be

38

different by different investigators; indicating the effect of different geometry of the cyclones on pressure loss. A dimensionless static pressure loss coefficient, C_p can be defined as was done in references [21, 27, 34];

$$C_p = \frac{\Delta P_{st}}{\frac{1}{2}\rho \, V_{in}^2}$$

4.5

Figure 4.3 shows the variation of the C_p of the cyclone studied in the present work and of those used by the investigators in references [27, 34] as a function of Re. It is seen that, the C_p of the each cyclone have almost a constant value over the range of Re between 15000 and 125000. The C_p value of our basic cyclone configuration is determined as 5.862 from Fig. 4.3, whereas the C_p values determined by the investigators [27, 34] are 6.36 and 12.56, respectively. The difference in the values of the C_p coefficients indicate the difference in the geometrical configuration of the cyclones. Therefore, the effects of the cyclone dimensions on the static pressure loss of cyclones must be determined in order to design an efficient cyclone.

As a result of the above discussion, we may conclude that the effect of Re on the static pressure loss, ΔP_{st} of the cyclone is quite high. On the other hand the effect of Re on the C_p coefficient of the cyclone separators is negligibly small. So that the C_p of the cyclones depends on the geometrical construction of the cyclone. However the exact determination of the C_p value of a cyclone requires measurements for a wide range of Re number to find the average value of C_p at the same cyclone configuration.

4.2.2 Effects of Tangential Inlet Height and Width on the Static Pressure Loss

Effects of tangential inlet height, a and width, b on the static pressure loss of the cyclone were investigated by measuring the static pressure losses of the cyclone configurations with four different types of rectangular-shaped tangential inlets for Re numbers varied between 17500 and 125000.

The constructed tangential fluid inlets for this purpose have the same crossectional area, A_{in} with different dimensionless height, a/D and width, b/D ratios. The magnitudes of the dimensionless a/D and b/D ratios were

selected in accordance with the magnitudes of these parameters in standard cyclone configurations are given in Table 3.1 together with our basic cyclone configuration. When the constructed tangential inlets mounted on our basic cyclone configuration, four different types of cyclone configurations have been obtained. These cyclone configurations are given in Table 3.2 with their characteristic dimensionless ratios.

Figures 4.4 and 4.5 show the Cp coefficients of the cyclone configurations with different dimensionless a/D and b/D ratios as a function of Re. It can be seen from Fig. 4.4 and 4.5 that, the Cp coefficients of the cyclone configurations with different dimensionless inlet heights, a/D and widths, b/D are constant over the range of Re between 17500 and 125000. Therefore, Cp of the cyclone configurations could be plotted as a function of the dimensionless height, a/D and width, b/D ratios, independent of Re.

Figure 4.6 shows the variation of the Cp of the cyclone configurations which have different dimensionless inlet heights, a/D as a function of a/D. It is seen that the Cp curve is nearly flat for a/D>0.6. Cp slightly increases when a/D decreases for a/D<0.6. For a/D<0.6, the friction losses between the rotating stream bands and on the wall of cyclone body increase. This increase in friction losses are caused by the high numbers of turns of the gas stream in the cyclone body. We can say that, the decrease of inlet height, a below a critical value decreases the band width of the inlet gas stream, thus the inlet fluid stream has a high number of turns in the cyclone body. The preferred value of the dimensionless inlet height ratio a/D for high efficiency cyclones was given between 0.5 and 0.6 in references [31, 34, 35, 36, 38, 40, 41, 42]. The value of dimensionless a/D ratio was not preferred to be greater than 0.6 for high efficiency cyclones. This may be related to the effects of decrease in the separation length of the cyclone cylindrical body.

Figure 4.7 shows the variation of the Cp coefficients of the cyclone configurations which have different dimensionless inlet widths, b/D, as a function of b/D ratio. It can be seen from Fig. 4.7 that, the Cp curve is nearly flat for b/D<0.25, it slightly increases when b/D increases for b/D>0.25. For b/D>0.25, the increase of Cp indicate that, the static pressure losses caused by the sudden contraction at the cyclone inlet and the friction losses over the wall of fluid discharge pipe increase. Since the dimensionless ratio of the annular width between the walls of the fluid discharge pipe and the cyclone

cylindrical body of our basic cyclone configuration is 0.268 (i.e., 1/2 (D-D_d)/D=0.268). So that for b/D≥0.268, a sudden contraction region at the cyclone inlet is being formed. As a result of the above discussion, the proper dimensionless inlet width, b/D for a low pressure loss cyclone design may be specified by the relation;

$$b/D \le 1/2 (1 - D_d/D) \qquad\qquad 4.6$$

Fig. 4.6 and 4.7 also shows that, the effects of tangential inlet height, a and width, b on the static pressure loss depend on each other. Therefore C_p coefficients of the investigated tangential inlets plotted as a function of the height-to-width ratios, a/b of the tangential inlets. Figure 4.8 shows that, the C_p curve does not vary for a/b>2.4 and C_p slightly increases when a/b decreases for a/b<2.4. The preferred value of a/b ratio for high efficiency cyclones was given between 2.0 and 2.5 in references [40, 42].

As a result of the static pressure loss measurements, we may conclude that the dimensionless width of the tangential inlet, b/D can be firstly specified by the eq. (4.6), and then the dimensionless height of the tangential inlet, a/D can be related to b/D by the relation as that;

$$2.4 \, b/D \le a/D \le 0.6 \qquad\qquad 4.7$$

for the high performance cyclone designs.

4.2.3 Effect of the Fluid Discharge Pipe Depth on the Static Pressure Loss

Effect of fluid discharge pipe depth, S on the static pressure loss of the cyclone separator was investigated by measuring the pressure losses of the cyclone configurations which have different depths of fluid discharge pipe. Experiments were conducted at seven different Re numbers with a range of 17500≤Re≤125000.

The cyclone configurations used for the measurements to determine the effect of fluid discharge pipe depth, S on static pressure loss are obtained by changing the depth of fluid discharge pipe of our basic cyclone

configuration which is given in Table 3.1. The depth of fluid discharge pipe was changed by means of the flexible discharge pipe mounting section of the basic cyclone configuration shown in Figure 3.11. The magnitude of the dimensionless S/D ratios of the cyclone configurations was varied between 0.0 and 1.583. Types of cyclone configurations with different S/D ratios are given in Table 3.3.

The results of the measurements firstly plotted in Fig. 4.9 and 4.10 which show the variation of C_p of the cyclone configurations with different S/D ratios as a function of the Re number. It can be seen from Fig. 4.9 and 4.10 that, C_p coefficient of each cyclone configuration has a constant value over the Re number range of $17500 \leq Re \leq 125000$. Therefore, C_p coefficients of the cyclone configurations can be plotted independently from Re number, as a function of the dimensionless S/D ratios.

Figure 4.11 shows the variation of C_p coefficients of the cyclone configurations as a function of the dimensionless S/D ratio. It can be seen that, C_p increases slightly from its minimum value of 5.4 to its maximum value 6.05, when S/D increases for $0 \leq S/D \leq 0.583$. It decreases slightly for $0.583 < S/D < 1.25$ and it is nearly constant for $S/D > 1.25$. Careful investigation of the C_p curve show that, the maximum value of C_p occur when $S/D = a/D = 0.583$.

The static pressure loss coefficient, C_p decreases as S/D decreases for $S/D < a/D$ indicating the effect of the short-circuiting of fluid flow between the tangential fluid inlet and the fluid discharge pipe. The short-circuiting flow which can be considered for $S/D < a/D$, prevents the formation of a strong swirling flow in the cyclone. Therefore, the static pressure loss caused by the kinetic energy of rotation of the fluid, and the wall friction in the cyclone cylindrical body and in the fluid discharge pipe decreases.

The C_p coefficient and effective height of cyclone decrease as S/D increases for $a/D < S/D < 1.25$. This indicates the effect of the fluid discharge pipe depth when S is below the bottom level of the tangential fluid inlet (i.e., effect of the (S - a)).

Under the view of above discussion, we may conclude that the proper dimensionless depth of fluid discharge pipe, S/D for a low pressure loss cyclone design can be specified by the relation;

$$a/D < S/D \leq 1.25 \quad \text{or} \quad a/D < S/D \leq (a/D+2/3) \qquad 4.8$$

The upper limit of the above relation was given as $(a/D+1/8)$ by the investigators [34, 35, 36, 40, 42] due to the results of their collection efficiency measurements. This was due to the quite important effect of the effective height of the cyclone cylindrical body, (i.e., effect of $(h-S)/D$).

4.2.4 Effect of the Fluid Discharge Pipe Diameter on the Static Pressure Loss

Effect of the diameter of the fluid discharge pipe, D_d on the static pressure loss of cyclone separator was investigated by measuring the pressure losses of the cyclone configurations which have different dimensionless D_d/D ratios. The experiments were run at seven different Re numbers having a range of $17500 \leq Re \leq 125000$.

The used cyclone configurations were obtained by changing the fluid discharge pipe of the basic cyclone configuration with five different types of PVC pipes which have different internal diameters. These cyclone configurations are given in Table 3.4 with their dimensionless ratios.

The results of the measurements firstly plotted as a function of the Re number in Fig. 4.12 which shows that, the C_p coefficients of the cyclone configurations have almost constant values over the Re number range of $17500 \leq Re \leq 125000$. The magnitudes of C_p of cyclone configurations with D_d/D ratios of 0.196, 0.296, 0.400, 0.442 and 0.504 can be determined from this plot as 10.96, 9.33, 7.16, 5.95 and 4.30, respectively. After that, we can plot these C_p coefficients as a function of the dimensionless D_d/D ratios of the configurations, as being independent from the Re number.

Fig. 4.13 and 4.14 show the variation of the C_p coefficients of the cyclones as a function of the dimensionless D_d/D and $(D_d/D)^2$ ratios, respectively. It can be seen from Fig. 4.13 that, the C_p coefficient decreases

with a rate greater than observed at previous D_d/D ratio as D_d/D increases. Therefore, the C_p coefficient can be plotted as a function of the $(D_d/D)^2$ as in Fig. 4.14. Figure 4.14 shows a linear relationship between the C_p coefficient and $(D_d/D)^2$ as that, the C_p coefficient decreases linearly with a rather high rate when the $(D_d/D)^2$ increases. This indicates that the enlarging of the fluid discharge outlet decreases the static pressure loss. This fact may be caused by the decrease in the blockage of the fluid discharge outlet and the decrease in the retention time of the cyclone.

As a result of the above discussion, we can conclude that the enlarging of the fluid discharge outlet decreases the static pressure loss of the cyclone, continuously. Therefore, the magnitude range of the fluid discharge pipe diameter, D_d for an efficient cyclone design should be specified by the comparison of the collection efficiency measurements, the flow field measurements and the static pressure loss measurements. The preferred value of the dimensionless D_d/D ratio was found to be between $0.4 \leq D_d/D \leq 0.5$ for an efficient cyclone [27, 28, 34, 36].

4.2.5 Effect of the Dust Discharge Diameter of the Cyclone Cone on the Static Pressure Loss

Effect of the dust discharge diameter of the cyclone cone, D_u on the static pressure loss of the cyclones was investigated by measuring the static pressure losses of the cyclone configurations which were obtained by mounting the constructed cyclone cones with different dust discharge (i.e., apex) diameters on our basic cyclone configuration. The measurements were conducted at seven different Re numbers varied between Re values of 17500 and 125000.

The D_u was varied while keeping the apex angle constant. The apex angle of the cone was selected arbitrarily as 28° for all constructed cyclone cones with different values of D_u. As a result of this restriction, the constructed cyclone cones have slightly different heights for each different apex diameter, D_u. The constructed cyclone cones are given in Table 3.5 together with a diagrammatic explanation of their design criteria.

44

The result of static pressure loss measurements to determine the effect of D_u is firstly plotted in Fig. 4.15 which shows the variation of the C_p coefficients of the cyclone configurations with different dimensionless D_u/D ratios as a function of the Re numbers. The same trend of the C_p curve over the Re number range is seen from Fig. 4.15. As is seen from this figure C_p values are independent of Re number. The C_p values for the cyclone configurations with D_u/D ratios of 0.125, 0.250, 0.313, 0.375 and 0.500 are obtained to be 6.94, 5.90, 5.22, 4.75 and 4.45, respectively.

Figures 4.16 and 4.17 shows the variation of the C_p coefficient as a function of the dimensionless D_u/D and $(D_u/D)^2$ ratios, respectively. It can be seen from Fig. 4.16 and 4.17 that, the C_p coefficient decreases linearly when the dust discharge area of the cyclone cone increases indicating the effect which is also observed when the fluid discharge pipe area increases. This is caused by the short-path of fluid flow between the inlet and dust discharge outlet of the cyclone due to the decrease in the blockage of dust discharge outlet. The preferred value of the dimensionless D_u/D ratio were found to vary between 0.25 and 0.5 depending on the purpose for which the cyclone was used [35, 40, 42]. This moderate range of preferred values of D_u/D ratio had been obtained as a result of the collection efficiency measurements on the cyclone configurations with different D_u/D ratios.

4.2.6. Effect of the Outlet-to-Inlet Area Ratio of the Cyclone on the Static Pressure Loss

The results of the measurements to determine the effects of the fluid discharge pipe outlet, D_e and the dust discharge outlet, D_u on the static pressure loss of the cyclones which are shown in Figures 4.12, 4.13, 4.14, 4.15, 4.16 and 4.17 showed that; the effects of D_d/D and D_u/D on the static pressure loss of the cyclone separators are comparably more greater than the other cyclone dimensionless ratios a/D, b/D, h_c/D and S/D. Therefore, we may conclude that, the effect of the total outlet area, A_{out} of the cyclone on the static pressure loss is significant. The total outlet area of the cyclone is formed by the fluid discharge pipe area and the dust discharge area, as shown by the following equation;

$$A_{out} = \pi/4 \left(D_d^2 + D_u^2 \right) \qquad\qquad 4.9$$

The ratio of outlet-to-inlet area, A_r of the cyclone may be expressed as;

$$A_r = A_{out}/A_{in} = (\pi/4(D_d^2 + D_u^2))/ (a.b) \qquad\qquad 4.10$$

The C_p coefficients of the cyclone configurations with different D_d/D and D_u/D ratios plotted as a function of the cyclone outlet-to-inlet area ratio, A_r and are shown in Fig. 4.18. It can be seen from Fig. 4.18 that, the C_p coefficient increases rapidly when A_r decreases under a threshold value which is obtained as 1.5. We may conclude that ,the low pressure loss installation of the cyclone separators requires an outlet-to-inlet area ratio that must be greater than 1.5.

As a result of the above discussion, we may conclude that the outlet-to-inlet area ratio must be;

$$A_{out}/A_{in} \geq 1.5 \qquad\qquad 4.11$$

then,

$$(D_d^2 + D_u^2)/ (a.b) = 6/\pi \qquad\qquad 4.12$$

and thus,

$$D_u = (6/\pi \, (a.b) - D_d^2)^{1/2} \qquad\qquad 4.13$$

4.2.7 <u>Effect of cyclone cone height on the Static Pressure Loss</u>

Effect of cyclone cone height, h_c on the static pressure loss of the cyclones was investigated by measuring the static pressure losses of the cyclone configurations which have different heights of cyclone cone, at seven inlet Re numbers ranging between $17500 \leq Re \leq 125000$.

The required cyclone configurations are obtained by mounting the cyclone cones which have four different heights with the same apex diameter, on the basic cyclone configuration. The design of cones for this purpose required a restriction on the cone apex diameter, D_u. Under the view of the available literature on the geometry of cyclone cones [34, 39, 40, 41, 42, 43, 44], the magnitude of D_u/D ratio of the cones was selected as 0.25. The manufactured cyclone cones are given in Table 3.6 together with other dimensionless ratios of the cyclone configurations.

The results of the static pressure loss measurements for different h_c/D values of the cyclone cones are shown in Fig. 4.19. It shows the variations of the C_p coefficients of the configurations as a function of the Re number. For different h_c/D ratios, each cyclone configuration approximately have a constant C_p value over the range of Re numbers used in the investigation.

Figure 4.20 shows that, the C_p coefficients of the cyclones decrease linearly, when the dimensionless h_c/D ratio increases indicating the decrease in the blockage effect of the cyclone cone due to the increase in the volume of the cones. In other words, the decrease of the cone apex angle decreased slightly the value of C_p coefficient. The different heights of cyclone cones with the same apex and top diameter corresponds to different values of cone apex angles. The preferred value of the dimensionless h_c/D ratio in the available literature [39, 40, 42] varied between 1.5 and 2.5. Therefore, the specification of the dimensionless h_c/D ratio for a low pressure loss cyclone is selected as;

$$1.5 \leq h_c/D \leq 2.5 \qquad\qquad 4.14$$

4.2.8 Conclusions

The results of the experimental work to determine the effects of the dimensionless ratios , a/D, b/D, S/D, D_d/D, D_u/D and h_c/D of the cyclone configuration and Re number on the static pressure loss of the cyclone particle separators may be summarized as ;

1. The static pressure loss of the cyclone can be linearly related to the inlet dynamic pressures of the cyclone by the equation;

$$\Delta P_{st} = C_p \frac{1}{2} \rho \, V_{in}^2$$

4.15

2. The static pressure loss coefficient, C_p for the all of cyclone configurations is almost independent from the Re number.

3. The static pressure loss coefficient, C_p for a cyclone separator is a function of the characteristic cyclone dimensions a, b, S, D_d, D_u, h_c, and D.

$$C_p = f (a, b, S, D_d, D_u, h_c, D)\qquad\qquad 4.16$$

The effects of these cyclone dimensions on the static pressure loss across the cyclone are determined. Under the light of results, the cyclone dimensions can be limited within the moderate ranges for a proper cyclone operation. The moderate range of each cyclone dimension may be given as;

4. $0.4 \leq D_d/D \leq 0.5$ for D_d

5. $b/D \leq 1/2 \, (1 - D_d/D)$ for b

6. $2.4 \, b/D \leq a/D \leq 0.6$ for a

7. $a/D < S/D \leq a/D + (2/3)$ for S

8. $A_{out} / A_{in} \geq 1.5$ for a, b, D_d, D_u

9. $(6/\pi \, (a.b) - D_d^2)^{1/2} \leq D_u \leq 0.5 \, D$ for D_u

10. $1.5 \leq h_c/D \leq 2.5$ for h_c/D

4.3 SWIRLING FLOW FIELD MEASUREMENTS IN CYCLONES

The swirling flow field measurements were done in radial direction of the cyclone cylindrical body at four different vertical (i.e., axial) stations for the Re number range of 35000≤Re≤125000. The components of fluid velocity in three perpendicular direction of the cylindrical polar co-ordinate, yaw and pitch angles, and static pressure distribution were measured in the radial direction using a five-tube yawmeter without any rotation in the cyclone.

The measurements were done for different Re numbers which correspond to different inlet swirl strengths. The dimensionless vertical

positions of the measurement stations, Z/h were 0.412, 0.667, 0.813 and 0.979. In order to investigate the effects of the characteristic cyclone dimensionless ratios D_d/D, D_u/D, h_c/D, S/D, a/D and b/D on the swirling flow, the measurements were repeated on different cyclone configurations which have different values of the characteristic cyclone dimesionless ratios.

4.3.1 Axisymmetry of the swirling flow in cyclone

The axisymmetry of the swirling flow in the cyclone was checked by measuring the diametrical distribution of axial and tangential velocity, and static pressure at two vertical stations for two different Re numbers. Figures 4.21 and 4.22 show the diametrical distribution of the dimensionless axial and tangential velocity, and the dimensionless static pressure for the basic cyclone configuration which is given in Table 3.1. Measurements were made at vertical stations of Z/h=0.412 and 0.979 for Re=53000 and 124000, respectively. These figures showed that the flow is slightly asymmetric at the vertical measurement station of Z/h=0.412, whereas flow is axisymmetric at the vertical measurement station of Z/h=0.979. This indicates that the flow is slightly asymmetric at the region near the tangential inlet of the cyclone, but it tends to become more axisymmetric as the swirl gradually decayed. Therefore, the flow in the cyclone can be regarded as steady and axisymmetric except the region near the tangential inlet of the cyclone. Thus, only one half of the cyclone crossection is traversed for the swirling flow field measurements.

4.3.2 Effects of Re and the Characteristic Cyclone Dimensions on the Radial Distribution of Tangential Velocity in the Cyclone

The flow field measurements showed that, the dimensionless tangential velocity distribution in radial direction of the cyclone body can be described by means of the Figure 4.23. The characteristic variation of the dimensionless tangential velocity, V_t^+ as a function of the dimensionless radius, r/R are shown in Fig. 4.23. It can be seen from this figure that, the tangential velocity profile may be divided into three parts. Namely, part belonging to a near axis core of forced vortex for $0.0 \leq r/R \leq r_1/R$, part belonging to an intermediate region of compound vortex for $r_1/R < r/R < r_2/R$

and part belonging to an outer free vortex region for $r_2/R \leq r/R < 1.0$. The dimensionless tangential velocity increases linearly in the forced vortex region as the radius increases and it decreases as the radius increases in the free vortex region. The dimensionless tangential velocity, V_t^+ may be expressed by the following equations;

$$V_t^+ / (r/R)^n = \omega \quad \text{for} \quad 0.0 \leq r/R \leq r_1/R \qquad 4.17$$

and

$$V_t^+ \cdot (r/R)^n = C \quad \text{for} \quad r_2/R \leq r/R < 1.0 \qquad 4.18$$

where ω is the dimensionless angular velocity for forced vortex region, n is the vortex exponent and C is a dimensionless strength of the free vortex region.

A maximum ideal value of the dimensionless tangential velocity, V_{tc}^+ at a dimensionless common radius, r_c/R between the free and forced vortex regions is defined as shown in Fig. 4.23. However, a compound vortex character is seen for $r_1/R < r/R < r_2/R$; owing to the high friction losses caused by the viscosity and turbulence between two regions. Therefore, the actual value of the maximum tangential velocity, V_{tm}^+ is defined at a dimensionless radius, r_m/R. The values of the V_{tc}^+, V_{tm}^+, r_c/R and r_m/R can be affected by the interaction of the free and forced vortex regions on each other.

As a result of above discussion, we can report the effects of Re number and the characteristic cyclone dimensions on the dimensionless tangential velocity distribution by means of equations (4.17) and (4.18) referring to the values of ω, n, C, V_{tm}^+, r_m/R, V_{tc}^+ and r_c/R.

The distributions of the dimensionless tangential velocity corresponding to five different Re numbers at four different vertical stations on the cylindrical body of our basic cyclone configuration are shown in Figures 4.24, 4.25, 4.26 and 4.27. These figures show the effect of changing swirl strength on the dimensionless tangential velocity distribution at four different vertical stations of the cyclone body. As is seen from these figures that, forced, compound and free vortex characters are dominant in the ranges $0.0 \leq r/R \leq 0.1$, $0.1 < r/R < 0.3$ and $0.3 \leq r/R < 1.0$, respectively. This is not changed for changing values of Re numbers and for all vertical measurement stations of the cyclone body. These flow ranges are also be expressed in terms of fluid discharge pipe radius, R_d;

$$0.0 \leq r/R_d \leq 0.225 \quad \text{for forced vortex flow regime} \qquad 4.19$$

$$0.225 < r/R_d < 0.680 \quad \text{for compound vortex flow regime} \qquad 4.20$$

$$0.680 \leq r/R_d \text{ and } r/R < 1.0 \quad \text{for free vortex flow regime} \qquad 4.21$$

The values of the dimensionless radial position, r_m/R at which the maximum value of the dimensionless tangential velocity, $V_{tm}+$ observed, is obtained as 0.208, 0.195, 0.190 and 0.180 at the vertical stations of $Z/h=0.412$, $Z/h=0.667$, $Z/h=0.813$ and $Z/h=0.979$, respectively. This indicates that the forced vortex flow tend to be more dominant than the compound vortex flow downstream of the cyclone inlet. The maximum value of the dimensionless tangential velocity, $V_{tm}+$ decreases linearly from 1.85 to 1.75, when Re increases. The characteristic values of the dimensionless tangential velocity distributions which are shown in Fig. 4.24, 4.25, 4.26 and 4.27, are given in Table 4.1. It is seen that, the values of the free vortex exponent, n in eq. (4.18) remain constant at different Re numbers for the same vertical measurement station, however it increases slightly from 0.537 to 0.587 when Z/h increases from 0.412 to 0.979. When Re increases, the dimensionless angular velocity, ω in eq. (4.17) decreases at all vertical heights of cyclone body. This indicates the increase of friction losses between the free and forced vortex type flow regimes when Re increases. Whereas, the value of ω increases when Z/h increases indicating the dominance of forced vortex flow regime on the compound vortex flow regime increases downstream of the cyclone cylindrical body. When Re increases, the value of the dimensionless free vortex strength, C decreases linearly with ω. Whereas, the value of C decreases with increasing values of ω and increasing values of Z/h.

As a result of above discussion, we may conclude that the increase of Re (i.e., increase of swirl strength) increases the losses caused by viscosity, turbulence and friction. When Re increases, the values of the dimensionless free vortex strength, C and the dimensionless forced vortex angular velocity, ω decrease at all vertical heights on the cyclone body. The value of the dimensionless maximum tangential velocity, V_{tm}^{+} also decrease due to the decrease in C and ω when Re increases. The values of the free vortex

exponent, n and the dimensionless radial position of the maximum tangential velocity, r_m/R are not affected from Re. However, n and r_m/R have different values at different vertical measurement stations on the cyclone body.

The effect of dimensionless fluid discharge pipe diameter, D_d/D on the tangential velocity distribution in the cyclone is shown in Figures 4.28. a, b and c. The characteristic values of the dimensiomless tangential velocity distributions for different D_d/D ratios of the cyclone are given in Table 4.2 referring to Figure 4.23. It is seen from Fig. 4.28 that, the dimensionless radial position of the maximum tangential velocity, r_m/R shows dependence on the D_d/D ratio of the cyclones, are given below;

$$r_m/R = 0.083 \quad \text{for } D_d/D = 0.192 \qquad\qquad 4.22$$

$$r_m/R = 0.125 \quad \text{for } D_d/D = 0.296 \qquad\qquad 4.23$$

$$r_m/R = 0.186 \quad \text{for } D_d/D = 0.442 \qquad\qquad 4.24$$

$$r_m/R = 0.215 \quad \text{for } D_d/D = 0.504 \qquad\qquad 4.25$$

The r_m/R ratio increases linearly when D_d/D ratio increases. A direct relation between r_m and D_d can be established by using the relation;

$$(r_m/R) . 1/(D_d/D) = r_m/R_d \qquad\qquad 4.26$$

Using equation (4.26) along with values of r_m/R for different D_d/D values, the values of r_m/R_d obtained as 0.433, 0.422, 0.421 and 0.427 for $D_d/D=0.192$, 0.296, 0.442, 0.504, respectively. Thus, we see that the radial position, r_m is almost equal to the 0.425 of the R_d for all values of D_d/D ratios of the cyclone.

The magnitude of the maximum tangential velocity is also affected by the D_d/D ratios of the cyclones. The $V_{tm}+$ increases steeply when D_d/D decreases for $D_d/D \geq 0.296$, however it slightly decreases when D_d/D decreases for $D_d/D < 0.296$. There is a threshold value of the D_d/D for obtaining a strong swirl in the cyclone. If the value of D_d/D below this critical

value, the blockage of the fluid discharge outlet of the cyclone is being increased to a value at which the central forced vortex does not freely grow and the axial flow changes its direction to the bottom dust discharge of the cyclone. In other words, the overflow of the cyclone fluid is prevented when the D_d/D decreased to a value lower than the critical value of 0.3, and the under flow of the cyclone fluid through the dust discharge of the cyclone is increased rapidly.

As is seen from Fig. 4.29. a, b, c and d, the effect of Re on the dimensionless tangential velocity distribution does not change when the D_d/D ratio of the cyclone changes. The increase of Re decreases the values of C and ω, thus the value of $V_{tm}+$ decreases. The effect of vertical position on the radial distribution of tangential velocity is not affected by D_d/D ratios of the cyclone.

The effect of dimensionless dust discharge diameter, D_u/D on the dimensionless tangential velocity distribution is shown in Figures 4.30. a, b and c. Figure 4.30 show the radial distribution of dimensionless tangential velocity, V_t+ for different D_u/D ratios of the cyclone at Re=70666 and Z/h=0.412, Z/h=0.813 and Z/h=0.979. The effect of Re number on the radial distribution of V_t+ for different D_u/D ratios of the cyclone configuration is shown in Fig. 4.31. a, b, c and d. The characteristic values of the tangential velocity profiles which are shown in Figures 4.30 and 4.31, are given in Table 4.3. It is seen from Figure 4.30 and Table 4.3 that, the change of D_u/D ratio for $D_u/D \leq 0.25$ does not affect the effective zone of forced and free vortex flow regimes, whereas for $D_u/D > 0.25$, the effective zone of forced vortex flow increases when D_u/D increases. The increase in effective region of forced vortex flow shifts the compound vortex region towards the cyclone wall thus the effective region of the free vortex flow decreases. For the same Re and for any vertical position in the cyclone, the free vortex exponent, n has approximately constant values for $D_u/D \leq 0.25$ and it increases with a rather high rate when D_u/D increases for $D_u/D > 0.25$.

The dimensionless free vortex strength, C stays constant for different D_u/D ratios at a given Re and Z/h. For $D_u/D \leq 0.25$, the dimensionless forced vortex angular velocity, ω increases slightly when D_u/D ratio increases. This is due to sudden enlargement of the effective zone of forced vortex flow regime at a given Re and Z/h. When $D_u/D \geq 0.25$ and for increasing D_u/D

ratio, the compound vortex region shifts toward the cyclone wall and the radial position of $V_{tm}+$ occurs near the cyclone wall.

Figure 4.31. a, b, c and d, and Table 4.3 show that, the effects of cyclone inlet Re number on the tangential velocity distribution for different D_u/D ratios of the cyclone configurations do not change. The exponent n stays constant and ω decreases linearly for increasing Re number. For D_u/D ≤ 0.25, C decreases linearly when Re increases, but for $D_u/D>0.25$, C stays constant for increasing Re number. The effect of vertical position, Z/h in the cyclone body on the radial distribution of tangential velocity for different D_u/D ratios is negligible. The exponent n increases linearly when Z/h increases and ω increases with an increasing rate when Z/h increases for all values of D_u/D ratios investigated. C decreases with an increasing rate when Z/h increases for all values of D_u/D ratios.

Effect of the dimensionless height of cyclone cone, h_c/D on the radial distribution of tangential velocity in the cyclone is shown in Figures 4.32. a, b and c, and Table 4.4. It is seen from Fig. 4.32 and Table 4.4 that, the effective zone of forced vortex flow does not change when h_c/D increases for $h_c/D \geq 1.5$. The decrease of h_c/D below 1.5, slightly enlarges the effective zone of forced vortex flow field and therefore n increases slightly when h_c/D decreases for $h_c/D<1.5$, but it stays constant for $h_c/D \geq 1.5$. C stays constant for all h_c/D values at a given Re and Z/h. ω stays constant for all h_c/D values for constant Re and Z/h.

It is seen from Figure 4.33. a, b, c and d, and Table 4.4 that, n stays constant when Re increases for different h_c/D ratios of the cyclones at a given vertical measurement station. n increases linearly when Z/h increases for constant Re numbers. C decreases linearly when Re increases for each vertical measurement station and each h_c/D ratio. C decreases when Z/h increases for a given value of h_c/D ratio of the cyclone and for a given value of Re number. ω decreases with a decreasing rate when Re increases for any h_c/D ratio at a given vertical measurement station. Whereas ω increases with an increasing rate when Z/h increases for a given h_c/D ratio and a given Re number.

Figures 4.34. a, b and c show the effect of dimensiomless fluid discharge pipe depth, S/D on the radial distribution of V_t^+ at vertical measurement stations of Z/h=0.412, Z/h=0.813 and Z/h=0.979. It is seen from Fig. 4.34 that, the magnitude of V_{tm}^+ and r_m/R increase for increasing

values of S/D when S/D<a/D=0.583. However, V_t^+ and r_m/R stay almost constant for S/D≥a/D. This indicates that, for S/D<a/D, the short-circuiting flow between the tangential inlet and the fluid discharge pipe of the cyclone decreases the magnitudes of V_t^+ and r_m/R. The effect of Re number on the radial distribution of V_t^+ is shown in Figures 4.35. a, b, c and d. It is seen from Fig. 4.35 that, V_t^+ decreases slightly for increasing Re number in the outer region of 0.1≤r/R<1.0 on the cyclones having S/D values of 0.000, 0.292, 0.708 and 1.500.

The effect of a/D and b/D ratios of the cyclone tangential inlet on the radial distribution of V_t^+ is shown in Figures 4.36. a, b and c at vertical measurement stations of Z/h=0.412, Z/h=0.813 and Z/h=0.979. It is seen from Fig. 4.36 that, when a/D increases and b/D decreases the magnitudes of V_t^+ and r_m/R increase slightly at vertical measurement station of Z/h=0.412 where is near to the cyclone tangential inlet. V_t^+ and r_m/R do not change at vertical measurement stations of Z/h=0.813 and Z/h=0.979. This indicates that, the transition of tangential inlet cross-section from square to rectangular shapes increases the strength of swirl in the region near to the tangential inlet of the cyclone, whereas, for increasing Z/h values the effects of a/D and b/d are negligible. As is seen from Figures 4.37. a, b, c and d, the effect of Re number on the radial distribution of V_t^+ in the cyclones having different values of a/D and b/D is same with the previously obtained effect of Re number on V_t^+ in the cyclones having different values of characteristic cyclone dimensions. V_t^+ decreases slightly in the outer region of 0.1≤r/R<1.0 for increasing Re number.

4.3.3 Effects of Re and Characteristic Cyclone Dimensions on the Radial Distribution of Axial Velocity in the Cyclone

The measurements show that, the axial fluid velocity is directed downwards in the near-wall region of the cyclone cylindrical body, its magnitude decreases from its value at the wall region to zero at a radial position which is slightly greater than the radius of fluid discharge pipe. For radial positions smaller than this critical radius, it turns upwards and it reaches its maximum value at a radial position which is not right at the center line of the cyclone body, but is located at some distance apart from

the axis. The axial fluid velocity within the intermediate region of 0.45 $R_d \leq r \leq R_d$ is almost constant for high Re numbers, but it increases slightly when r/R decreases for decreasing Re number. The maximum value of upward directed axial velocity is much larger than the maximum value of downward directed axial velocity.

The radial distribution of axial fluid velocity on the cyclone can be described by means of Figure 4.38 which shows the characteristic distribution of the dimensionless axial velocity in radial direction. There are some critical points on Fig. 4.38 as that; r_0/R is a dimensionless radial position at which the magnitude of axial fluid velocity becomes zero. V_{au}^+ is the maximum value of upward directed dimensionless axial velocity which is obtained at a dimensionless radial position, r_u/R. V_{ad}^+ is the maximum value of downward directed dimensionless axial velocity. The negative sign of V_a^+ on this figure shows that, the axial fluid velocity directed to downward (i.e., - z direction). The effects of Re and the characteristic cyclone dimensions on the radial distribution of axial velocity in the cyclone can be explained by referring to the Fig. 4.38 and mentioned critical values of V_{au}^+, V_{ad}^+, r_0/R and r_u/R.

The effect of Re number on the radial distribution of axial velocity in the cyclone is shown in Fig. 4.39, 4.40, 4.41 and 4.42. The variation of axial velocity profile due to the change of vertical position on the cyclone body can also be seen from these figures. It is seen that, the dimensionless axial velocity profile in radial direction is almost independent from Re number. The magnitudes of V_{au}^+ and V_{ad}^+ depend upon the vertical position, Z/h of the measurement station on the cyclone cylindrical body. V_{au}^+ decreases slightly when Z/h increases. V_{ad}^+ decreases linearly from -0.750 to -0.480 when Z/h increases from 0.412 to 0.979. This indicates that the ratio of the maximum upward velocity, V_{au}^+ to maximum downward velocity, V_{ad}^+ increases linearly from 2.080 to 3.125 when Z/h increases from 0.412 to 0.979. The r_0/R of the axial velocity profile has a constant value for a Re number range of $35000 \leq Re \leq 125000$ at all Z/h. r_0/R decreases linearly from 0.650 to 0.600 as Z/h increases. Therefore, one may relate the value of r_0 to the radius of fluid discharge pipe, R_d, the cyclone diameter, D and the effective height of the cyclone cylindrical body, (Z-S) as;

$$r_0/R = 0.650 \quad \text{for} \quad Z/h = 0.412 \quad \text{and} \quad \text{for} \quad R_d/R = 0.458 \qquad 4.27$$

$r_0/R = 0.622$ for $Z/h = 0.667$ and   "   4.28

$r_0/R = 0.606$ for $Z/h = 0.813$ and   "   4.29

$r_0/R = 0.600$ for $Z/h = 0.979$ and   "   4.30

Therefore;

$$r_0 = R_d + D/[\ 10 + 6.5\ (Z-S)/h\ ] \qquad\qquad 4.31$$

In the above relationship, S shows the depth of fluid discharge pipe, Z is the vertical height measured from the top of the cyclone body, h is the total height of cyclone cylindrical body, and (Z-S) shows the effective height of the measuring station on the cyclone body.

The effect of dimensionless fluid discharge pipe diameter, D_d/D on the radial distribution of dimensionless axial velocity, V_a^+ is shown in Figures 4.43. a, b and c for Z/h values of 0.412, 0.813 and 0.979, respectively. It is seen from Fig. 4.43. a, b and c that, the direction of dimensionless axial velocity, V_a^+ is downwards at the central core region of the cyclones having $D_d/D \leq 0.296$ at all vertical measurement stations, Z/h. This indicates a suddenly increase in the blockage effect of the fluid discharge pipe for a critical range of $0.296 \leq D_d/D \leq 0.442$. In the central core region of the cyclone where $r/R \leq 0.2$, the direction of dimensionless axial velocity is upwards for $D_d/D \geq 0.442$, but for $D_d/D \leq 0.296$ the direction of axial velocity changes and becomes downwards. Downwards direction of axial fluid velocity in the central core region is an indication of the under flow from the cyclone. This under flow is due to the blockage effect of the fluid discharge pipe when the diameter of the discharge pipe is reduced. There is a critical ratio of D_d/D_u for which the axial fluid velocity in the central core region of the cyclone changes its direction upwards. Figures 4.43. a, b and c also show that, the values of r_0/R ratios of the dimensionless axial velocity distributions for different D_d/D ratios on the cyclone at vertical stations of $Z/h=0.412$, $Z/h=0.813$ and $Z/h=0.979$ are given by equation 4.31.

Figures 4.44. a, b, c and d show the effect of Re number on the radial distribution of V_a^+ for the cyclones having D_d/D ratios of 0.192, 0.296, 0.442 and 0.504 respectively. From Fig. 4.44. a, b, c and d, it is seen that the Re number has no effect on the radial distribution of V_a^+ for $0.2 \leq r/R \leq 0.4$. The variation in the radial distribution of V_a^+ in the range of $0.2 \leq r/R \leq 0.4$ with Re

is due to the wake growth around the fluid discharge pipe, when the fluid enters from the annular region between the discharge pipe and cyclone wall into the discharge pipe with increasing Re number. The effect of Re on axial velocity in the pipe inlet sections, corner effect, suppresses the fluid at the other Z/h values for $D_d/D \geq 0.442$. For $D_d/D \leq 0.296$, the direction of V_a^+ is downwards at the central core region, so that corner effect was not observed and there were no effect of Re on V_a^+.

Figures 4.45. a, b and c show the radial distribution of the dimensionless axial velocity, V_a^+ on the cyclones for D_u/D ratios of 0.125, 0.250, 0.375 and 0.500, respectively. It can be seen from Fig. 4.45. a, b and c that, as D_u/D ratio increases the direction of V_a^+ changes from upwards to downwards. This indicates that the fluid is leaving the cyclone from the bottom dust discharge opening for increased D_u/D ratios. The same character of V_a^+ have been obtained for $D_d/D \leq 0.296$. It can be concluded that, there must be a relation between D_u/D and D_d/D ratios of the cyclones giving upwards directed axial velocity in the central core region of $r/R \leq 0.2$. We have obtained a relation between D_u/D and D_d/D ratios from the static pressure loss measurements; the outlet-to-inlet area ratio, A_r of the cyclone must be greater than 1.5 to obtain a cyclone design resulting in low pressure loss, (eq. 4.12).

From Figures 4.43. a, b, c and Figures 4.45. a, b, c, and the comparison of the cyclone configurations used for the measurements to determine the effects of D_d/D and D_u/D ratios on the swirling flow field in the cyclones; one may conclude that for a cyclone having dust separation capability the following relation are required.

$$D_u/D \leq D_d/D - 1/4 \, D_{in}/D \qquad\qquad 4.32$$

or

$$D_d/D \geq D_u/D + 1/4 \, D_{in}/D \qquad\qquad 4.33$$

It is also seen from Fig. 4.45. a, b and c that, the location of the point of zero V_a^+, r_0/R do not change for $D_u/D \leq 0.250$. The effect of Re on the radial distribution of V_a^+ on the cyclones having different D_u/D ratios is shown in Figures 4.46. a, b, c and d. Excluding the range of $0.2 \leq r/R \leq 0.4$ where there is a corner effect for $D_u/D \leq 0.250$, Re number has no effect on the radial distribution of V_a^+ in the cyclones having different D_u/D ratios.

As is seen from Figures 4.47. a, b and c, h_c/D ratios of the cyclone configurations do not affect the radial distribution of V_a^+ in the cyclone cylindrical body. Effect of Re on the radial distribution of V_a^+ on the cyclones having different h_c/D ratios is shown in Figures 4.48. a, b, c and d. It may be seen from Fig. 4.48 that the Re number has a negligible effect on the radial distribution of V_a^+ for the cyclones having different h_c/D ratios.

The effect of dimensionless fluid discharge pipe depth, S/D on the radial distribution of axial velocity, V_a^+ is shown in Figures 4.49. a, b and c. It is seen from Fig. 4.49 that, the magnitude of maximum upward directed axial velocity, V_{au}^+ is almost constant for S/D≥0.583. Whereas, V_{au}^+ decreases suddenly when S/D<0.583. The critical value of S/D ratio is equal to the value of a/D=0.583 of the cyclone configuration used. When S/D<a/D, the short- circuiting of flow occurs between the tangential fluid inlet and the fluid discharge pipe. The short-circuiting fluid flow decreases the amount of circulating fluid in the cyclone. As a result, the magnitude of upward directed axial velocity, V_{au}^+ decreases for S/D<a/D. When S/D≥a/D, the short-circuiting fluid flow does not form and the magnitude of V_{au}^+ remains constant. For S/D≥a/D, V_{au}^+ decreases slightly from 1.4 to 1.25 for increasing Z/h values.

It can also be seen from Fig. 4.49 that, r_u/R and r_0/R ratios increase for increasing S/D. This is due to the enlargement of central core region where forced vortex type flow is dominant. Enlargement of the core region moves the point of transition from forced vortex to free vortex flow toward the cyclone wall. However, the values of r_u/R and r_0/R remains constant for S/D >a/D. This is due to the stabilization of the effective regions of both forced and free vortex flows.

Figures 4.50. a, b, c and d show the radial distribution of V_a^+ on the cyclones having different S/D ratios as a function of Re number. It is seen from Fig. 4.50 that, the effect of Re on the radial distribution of V_a^+ is negligible except for the region of 0.2≤r/R≤0.4 where corner effect was seen. When Re increases, the upward directed axial velocities in the region of 0.2≤ r/R≤0.4 decrease slightly at a given S/D ratio of the cyclone.

The effects of a/D and b/D ratios of the cyclone on the radial distribution of V_a^+ is shown in Figures 4.51. a, b and c. During the transition of the tangential inlet cross-section of the cyclone from square to rectangular shapes (i.e., when a/D increases and b/D decreases), V_{au}^+ increases.

When a/D increases and b/D decreases, the forced vortex flow region in the cyclone enlarges slightly resulting in an increase of r_u/R ratio of the dimensionless axial velocity profile. r_0/R ratio do not change for different a/D and b/D ratios of the cyclone, whereas r_0/R ratio decreases slightly from 0.65 to 0.60 when Z/h increase from 0.412 to 0.979. This is caused by the shift of free vortex type flow toward the axis of cyclone when the swirl decays gradually. Figures 4.52. a, b, c and d show that, the increase of Re decreases the V_a^+ slightly in the region of $0.2 \leq r/R \leq 0.4$ for different a/d and b/D ratios of the cyclone. However, we can say that the effect of Re on the radial distribution of V_a^+ is negligible.

4.3.4 Effects of Re and Characteristic Cyclone Dimensions on the Radial Distribution of Radial Velocity in the Cyclone

The radial velocities measured in the cyclone cylindrical body are relatively small and constant with the motion slightly outward (i.e., positive) near the cyclone wall, and inward (i.e., negative) toward the axis of cyclone. There is an imaginary cylindrical plane at a fixed radial position in the cyclone, slightly greater than the fluid discharge pipe radius, where the radial velocity becomes zero at all vertical measurement stations on the cyclone body.

The radial velocity profiles, shown in Fig. 4.53, 4.54, 4.55 and 4.56 are difficult to interpret unequivocally although trends in data can be seen. In general, the dimensionless radial velocity, V_r^+ at any radial position except for the near axis region, is less than 0.2 and usually in the order of $V_r^+ \leq 0.1$. For $r/R \geq 0.690$, V_r^+ is slightly positive, or outward, and constant for all values of Re number at all vertical measurement stations on the cyclone body. The magnitude of V_r^+ becomes zero at a dimensionless radius of $r/R \cong 0.690$, this radial position can be related to the cyclone geometry by the relation;

$$r_0 = R_d + D / 11.5 \qquad\qquad 4.34$$

The magnitude of dimensionless radial velocity becomes negative (i.e., directed inwards) for $r/R < 0.690$. For $R_d/R \leq r/R < 0.690$, the magnitude of V_r^+ increases slightly to a value of -0.1. V_r^+ is negative and constant for a range of $R_d/2R \leq r/R \leq R_d/R$. V_r^+ shows a fluctuation and decreases to a minimum value in negative sign at a radial position of $r/R = 0.44$ R_d/R

corresponding to the radial position of the maximum tangential velocity, r_m/R. For $r/R \leq 0.2 \cong 0.44$ R_d/R, firstly V_r^+ increases steeply to its minimum value and then decreases steeply in negative sign. V_r^+ has a small non-zero value which is positive, or outward, on the axis of cyclone body at all vertical measurement stations for all values of Re numbers. According to above discussion and Fig. 4.53 to 4.56, one may conclude that the radial distribution of V_r^+ does not depend on Re number and vertical position, Z/h on the basic cyclone configuration.

Figures 4.57. a, b and c show the effect of D_d/D ratio on the radial distribution of dimensionless radial velocity, V_r^+ in the cyclone cylindrical body at vertical measurement stations of $Z/h=0.412$, $Z/h=0.813$ and $Z/h=0.979$, respectively. It is seen from Fig. 4.57 that, the effect of D_d/D ratio on the radial distribution of V_r^+ is negligible in the region of $0.5 < r/R < 1.0$ where free vortex type flow is dominant, for all of the vertical measurement stations. For $0.2 \leq r/R \leq 0.5$, the sign of the dimensionless radial velocity is observed to be negative indicating that radial velocity is directed inwards and its magnitude decreases as D_d/D ratio increases. Even though the magnitude of V_r^+ at the axis of cyclone must be zero for an axisymetric flow, for $D_d/D \leq 0.296$ V_r^+ have non-zero magnitudes. The non-zero magnitude of V_r^+ at the axis shows that there is a slight axi-asymmetry for $D_d/D \leq 0.296$. For $D_d/D \leq 0.296$, investigation of Fig. 4.57. a, b and c show steep variations in the magnitude and direction of V_r^+, indicating that in the central core region of $r/R \leq 0.2$ wild mixing is taking place. This is due to the unestablished swirling flow in the region of $r/R \leq 0.2$ for $D_d/D \leq 0.296$. For $D_d/D \geq 0.442$, in the region of $r/R \leq 0.2$, since the swirling flow is established there were no steep variations in V_r^+ and its magnitude is about 0.1 of the average fluid inlet velocity. It is directed towards the cyclone axis, being zero at the axis. The effect of Re on the radial distribution of V_r^+ on the cyclones having different D_d/D ratios is shown in Figures 4.58. a, b, c and d. It is seen from Fig. 4.58 that, the effect of Re on the radial distribution of V_r^+ is negligible.

The effect of D_u/D ratio of the cyclone on the radial distribution of V_r^+ is shown in Figures 4.59. a, b and c. As it is shown in these figures for $D_u/D \leq 0.375$, the magnitude of V_r^+ increases slightly in the region of $0.3 \leq r/R \leq 0.6$ for increasing values of D_u/D. Whereas V_r^+ decreases suddenly for $D_u/D=0.500$ in this region of $0.3 \leq r/R \leq 0.6$. This indicates that, the fluid is leaving the cyclone from the bottom dust discharge opening for $D_u/D \geq D_d/D=0.442$ and the strength of swirl decreases due to the short-path of fluid

61

between the cyclone inlet and dust discharge opening. In the central core region of $r/R \leq 0.2$, the magnitude of V_r^+ increases for increasing D_u/D. The effect of Re number on the radial distribution of V_r^+ is seen from Figures 4.60. a, b, c and d as being negligible on the cyclones having different D_u/D ratios.

As is seen from Figures 4.61. a, b and c, the effect of h_c/D ratio of the cyclone on the radial distribution of V_r^+ is negligible at vertical measurement stations of $Z/h=0.412$, $Z/h=0.813$ and $Z/h=0.979$. However, the magnitude of V_r^+ for $h_c/D=1.5$ is slightly lower than the values of V_r^+ for $h_c/D=0.650$ and $h_c/D=2.125$ throughout the crossection of cyclone cylindrical body for all vertical measurement stations. The effect of Re number on the radial distribution of V_r^+ is negligible on the cyclones having different h_c/D ratios that is shown in Figures 4.62. a, b, c and d.

Figures 4.63. a, b and c show the effect of S/D ratio on the radial distribution of V_r^+ for the cyclones having different S/D ratios. It is seen from Fig. 4.63 that, for $S/D \leq 0.583$ the magnitude of V_r^+ decreases at all radial positions for increasing values of S/D. Whereas, the magnitude of V_r^+ stays almost constant for $S/D \geq 0.583$ at all radial positions of the cyclones for the vertical measurement stations of $Z/h=0.412$, $Z/h=0.813$ and $Z/h=0.979$. The effect of Re on the radial distribution of V_r^+ on the cyclones having different S/D ratios as shown in Figures 4.64. a, b, c and d, is negligible.

Figures 4.65. a, b and c shows the effects of a/D and b/D ratios of the cyclone on the radial distribution of V_r^+ at vertical stations of $Z/h=0.412$, $Z/h=0.813$ and $Z/h=0.979$, respectively. It is seen from Fig. 4.65 that, V_r^+ increases slightly for all radial positions in the cyclone at the vertical measurement station of $Z/h=0.412$ for increasing a/D and decreasing b/D values. This indicates that, the transition of the tangential inlet cross-section of the cyclone from square to rectangular shapes increases the magnitude of V_r^+ at the regions near to the tangential fluid inlet. Whereas the effects of a/D and b/D ratios on V_r^+ are negligible at the vertical measurement stations of $Z/h=0.813$ and $Z/h=0.979$. As is seen from Figures 4.66. a, b, c and d, the effect of Re number on the radial distribution of V_r^+ is negligible for the cyclones having different a/D and b/D ratios.

4.3.5 Effects of Re and Characteristic Cyclone Dimensions on the Radial Distribution of Static Pressure in the Cyclone

The results of flow measurements showed that the radial distribution of static pressure coefficient, C_S at a given vertical position of the cyclone body is importantly affected with Re number. Figures 4.67, 4.68, 4.69 and 4.70 show the radial distribution of static pressure coefficient, C_S in the basic cyclone configuration for different values of Re number at vertical measurement stations of Z/h=0.412, Z/h=0.667, Z/h=0.813 and Z/h=0.979. The dimensionless static pressure coefficient, C_S is defined as that;

$$C_S = P_{st} / 1/2 \, \rho \, V_{in}^2 \qquad 4.35$$

From Fig. 4.67, 4.68, 4.69 and 4.70, it may be observed that the swirling motion causes a static pressure coefficient distribution in the cyclone cross-section which has a decreasing trend for the radial positions from cyclone wall towards the central axis. The lowest static pressure coefficient is located at the central axis. The static pressure coefficient firstly rises rapidly in the forced vortex region and then levels off, reaching a maximum value at the cylindrical wall. The radial variation of C_S in free vortex region is very small compared to its variation in forced vortex region. The C_S is almost constant over the axis of cyclone, independent from Re and vertical position, Z/h. C_S decreases in free vortex region and on the cyclone wall when Re increases. This may indicate, the increase of friction losses within the near wall region of cyclone body when Re increases. The axial variation of static pressure coefficient is negligibly small compared to its radial variation. Figures 4.67 to 4.70 also show the static pressure coefficients at the cyclone wall which are measured by means of the wall static pressure tapping. The extrapolation of the static pressure coefficient in close vicinity of the wall which is determined from the readings of the five-tube pressure probe, to the wall is in good agreement with the determined one by wall static tapping.

Figure 4.71 shows that, the static pressure distribution in the radial direction of cyclone can be related to the radial distribution of tangential velocity through the momentum equation in radial direction. This requires the elimination of fluctuating component of velocities and pressure in radial direction. The static pressure $P_{st}(r)$ at any radial position is given by;

$$P_{st}(r) = P_w - \rho_r \int^R V_t^2 / r \, dr \qquad 4.36$$

63

where P_w is the static pressure at the cyclone wall and V_t is the tangential velocity at the corresponding radial position, [17, 29, 30, 31, 32]. It is observed from Figure 4.71 that, eq. (4.36) completely expresses the distribution of static pressure throughout the cyclone cross-section except the center of the cyclone body. For r=0, eq. (4.36) has a singular point and has no meaning. The consistency of eq. (4.36) with the experimental data was obtained for different Re values in different cyclone configurations.

Figures 4.72. a, b and c show the effect of D_d/D ratio on the radial distribution of static pressure coefficient, C_s. It is seen from Fig. 4.72 that, the magnitude of C_s at the axis of cyclone increases for increasing D_d/D, whereas C_s at the cyclone wall decreases for increasing D_d/D ratios. Investigation of Fig. 4.72. a, b and c show that, the radial distribution of C_s for a given D_d/D ratio at different Z/h values have the same characteristic, so that the effect of Z/h on the radial distribution of C_s is negligible. This is due to the low mass density of air. The effect of Re on the radial distribution of C_s on the cyclones having different D_d/D ratios are shown in Figures 4.73. a, b, c and d. It is seen from Fig. 4.73 that, the magnitude of C_s decreases in the outer region of $0.1 \leq r/R \leq 1.0$ for increasing Re number for different D_d/D ratios of the cyclone. Whereas the effect of Re number on the radial distribution of C_s in the central core region is negligible.

Figures 4.74. a, b and c give the effect of D_u/D ratio of the cyclone on the radial distribution of C_s. For $D_u/D \geq 0.375$, C_s decreases in the outer region of $0.1 \leq r/R \leq 1.0$ for increasing values of D_u/D, whereas C_s is almost constant for $D_u/D \leq 0.250$ in this region. C_s increases near the axis of cyclone for increasing values of D_u/D. As is seen from Figures 4.75. a, b, c and d, the magnitude of C_s decreases in the near wall region of the cyclone for increasing Re values on the cyclones having D_u/D ratios of 0.125, 0.250, 0.375 and 0.500. However, the effect of Re on the radial distribution of C_s is negligible in the near axis region of the cyclone.

Figures 4.76. a, b and c show the effect of h_c/D ratio of the cyclone on the radial distribution of static pressure coefficient, C_s. It is seen from Fig. 4.76 that, the effect of h_c/D ratio on the radial distribution of C_s for the near wall region of the cyclone is negligible at a given vertical measurement station on the cyclone. Whereas, C_s increases slightly in the core region for increasing values of h_c/D ratio. The effect of Re number on the radial distribution of C_s is shown in Figures 4.77. a, b, c and d for different h_c/D

ratios of the cyclone. It is seen from Figures 4.77 that, C_S decreases slightly in the near wall region of $0.3 \leq r/R \leq 1.0$, whereas C_S is almost constant in the near axis region of the cyclone for increasing Re number.

Figures 4.78. a, b and c give the effects of S/D ratio on the radial distribution of C_S. The magnitude of C_S is almost constant in the range of 0.3 $\leq r/R \leq 1.0$ for increasing S/D ratio at vertical measurement stations of Z/h=0.412, Z/h=0.813 and Z/h=0.979 in the cyclone. However, For S/D$\leq$ 0.583 in the region of r/R<0.3, C_S decreases for increasing values of S/D ratio. This is due to the increase of swirl strength for increasing fluid discharge pipe depth. The magnitude of C_S in the near axis region of the cyclone r/R<0.3 stays almost constant for S/D$\geq$0.583. This is due to the stabilization of forced and compound vortex flows in the near axis region of the cyclone for S/D$\geq$a/D=0.583. As is seen from Figures 4.79. a, b, c and d, the S/D ratio of the cyclone does not change the effect of Re number on the radial distribution of C_S. C_S decreases in the near wall region of the cyclone, whereas C_S stays almost constant in the near axis region of the cyclone for increasing values of Re number.

The effects of a/D and b/D ratios of the cyclones on the radial distribution of C_S are shown in Figures 4.80. a, b and c. It is seen from Fig. 4.80 that, the effects of a/D and b/D ratios are negligible on the radial distribution of C_S. Figures 4.81. a, b, c and d show that, the effect of Re number on the radial distribution of C_S for the cyclones having different a/D and b/D ratios is same with those previously observed effects of Re number on the cyclones having different values of D_d/D, D_u/D, h_c/D and S/D.

4.3.6 Conclusions

Swirling flow in the cyclone separators having different values of the characteristic dimensions, D_d, D_u, h_c, S, a and b were investigated experimentally and following conclusions are drawn from the results of the present experiments.

1. Swirling flow in the cyclone is slightly axi-asymmetric at the region near to the tangential inlet of the cyclone, however it tends to become axisymmetric when the swirl gradually decays.

2. Tangential velocity profile in the radial direction of cyclone cylindrical body may be divided into three parts. Namely, part belonging to a near axis core of forced vortex, part belonging to an intermediate region of compound vortex and part belonging to an outer region of free vortex.

3. The forced, compound and free vortex flow regimes are dominant in the ranges of $r \leq 0.225 R_d$, $0.225 R_d \leq r \leq 0.680 R_d$ and $0.680 R_d < r < R$, respectively. These ranges did not change for different values of Re numbers and for different vertical measurement stations on the cyclone body.

4. The radial position of maximum tangential velocity, r_m in the cyclone has an average value of $0.425 \, R_d$ throughout the cyclone cylindrical body height. r_m decreases slightly for increasing values of Z/h. r_m does not change with Re. r_m does not change for $D_u/D < D_d/D$, whereas for $D_u/D \geq D_d/D$, it increases. r_m does not change for $S/D \geq a/D$, whereas for $S/D < a/D$, it decreases. r_m increases slightly, when a/D increases and b/D decreases. r_m does not change with h_c/D.

5. The maximum value of dimensionless tangential velocity, V_{tm}^+ decreases slightly for increasing values of Re number. V_{tm}^+ increases slightly with Z/h. V_{tm}^+ increases steeply for increasing values of D_d/D. V_{tm}^+ stays constant for $D_u/D < D_d/D$, whereas for $D_u/D \geq D_d/D$ it decreases. V_{tm}^+ stays almost constant for $S/D \geq a/D$, whereas for $S/D < a/D$ it decreases. V_{tm}^+ increases slightly, when a/D increases and b/D decreases. V_{tm}^+ does not change with h_c/D.

6. The measurements show that, the axial fluid velocity is directed downwards in the near-wall region of the cyclone cylindrical body. It turns upwards at a radial position which is slightly greater than the radius of fluid discharge pipe. For radial positions smaller than this critical radius, it increases and reaches its maximum value at a radial position which is not right at the center line of the cyclone body, but is located at some distance apart from the axis. The maximum value of upward directed axial velocity is much larger than the maximum value of downward directed axial velocity.

7. The effect of Re number on the radial distribution of dimensionless axial velocity, V_a^+ is negligible except for the region of $0.425 R_d \leq r \leq R_d$ on the cyclones having different values of characteristic cyclone dimensions, D_d, D_u, h_c, S, a and b. Whereas for the region of $0.425 R_d \leq r \leq R_d$, the magnitude

of V_a^+ decreases slightly due to the corner effect of fluid discharge pipe and wake growth with increasing Re number.

8. The magnitudes of V_{au}^+ and V_{ad}^+ depend upon the vertical position, Z/h of the measurement station on the cyclone cylindrical body. V_{au}^+ decreases slightly when Z/h increases, whereas V_{ad}^+ decreases linearly when Z/h increases. Therefore V_{au}^+ / V_{ad}^+ increases linearly when Z/h increases. V_{au}^+ is almost constant for $S/D \geq a/D$, whereas it decreases suddenly when $S/D < a/D$. V_{au}^+ increases when a/D increases and b/D decreases. V_{au}^+ does not change with h_c/D.

9. The r_0/R of the axial velocity profile is independent from Re number. r_0/R decreases linearly as Z/h increases. r_0/R increases for increasing D_d values. Therefore, one may relate the value of r_0 to the radius of fluid discharge pipe, R_d, the cyclone diameter, D and the effective height of the cyclone cylindrical body, $(Z-S)$ as;

$$r_0 = R_d + D/[\ 10 + 6.5\ (Z\text{-}S)/h\ ]$$

10. For obtaining a cyclone design resulting in an efficient particle separation from fluid, there is a critical ratio of D_d/D_u for which the axial fluid velocity, in the central core region of the cyclone, changes its direction upwards. One may obtain this ratio from the following relation;

$$D_u/D \leq D_d/D - 1/4\ D_{in}/D$$

11. The radial velocities measured in the cyclone cylindrical body are relatively small and constant with the motion slightly outward (i.e., positive) near the cyclone wall, and inward (i.e., negative) toward the axis of cyclone.

12. In general, the magnitude of radial velocity at any radial position except for the near axis region of the cyclone, is less than 0.2 and usually it is in the order of 0.1 of the average fluid inlet velocity.

13. The effect of Re number on the radial distribution of V_r^+ is negligible on the cyclones having different values of characteristic cyclone dimensions, D_d, D_u, h_c, S, a and b.

14. There is an imaginary cylindrical plane at a fixed radial position in the cyclone, slightly greater than the fluid discharge pipe radius, where the radial velocity becomes zero at all vertical measurement stations on the

cyclone body. This radial position is related to the cyclone geometry by the relation;

$$r_0 = R_d + D / 11.5$$

15. The swirling motion causes a static pressure distribution in the cyclone cross-section which has a decreasing trend for the radial positions from cyclone wall towards the central axis. The lowest static pressure is located at the central axis. The static pressure firstly rises rapidly in the forced vortex region and then levels off, reaching a maximum value at the cylindrical wall. The radial variation of static pressure in free vortex region is very small compared to its radial variation in forced vortex region.

16. The static pressure coefficient, C_S is almost constant in the near axis region of the cyclone, independent from Re and vertical position, Z/h. Whereas C_S decreases except for the near axis region of the cyclone and on the cyclone wall for increasing values of Re number for the cyclones having different values of characteristic cyclone dimensions, D_d, D_u, h_c, S, a and b.

17. The variation of static pressure in the axial direction is negligibly small compared to its variation in the radial direction.

18. The static pressure at the cyclone wall which is measured by means of the wall static pressure tapping is in good agreement with the extrapolation of the static pressure in close vicinity of the wall which is determined from the readings of the five-tube pressure probe, to the wall.

19. The radial distribution of experimentally determined static pressures excluding the center of the cyclone is given by;

$$P_{st}(r) = P_w - \rho_r \int_r^R V_t^2/r \, dr$$

20. The magnitude of C_S at the near axis core of cyclone increases for increasing values of D_d/D, D_u/D and h_c/D ratios, whereas C_S decreases in this region for increasing values of S/D ratio when S/D$\leq$0.583. The magnitude of C_S at the near wall region of cyclone decreases for increasing values of D_d/D and D_u/D ratios, whereas C_S does not change in this region with h_c/D and S/D ratios. The effects of a/D and b/D ratios are negligible on the radial distribution of C_S.

CHAPTER 5

CONCLUSIONS AND RECOMMENDATIONS FOR FURTHER WORK

In the present study, the effects of Re number and the characteristic cyclone dimensions, D_d, D_u, h_c, S, a and b on the static pressure loss and the swirling flow field of the cyclone separator were experimentally investigated.

The conclusions derived from the experimental investigation of the static pressure loss and the swirling flow fields of the cyclone separator are given in section 4.2.8 and 4.3.6, respectively. The results obtained from the experimental study may be used to obtain a cyclone separator design resulting in low pressure loss and high collection efficiency.

The experimental investigations of the swirling flow were conducted for an air cyclone in this study. In further studies, the applicability of the results drawn from this study for a hydraulic cyclone may be investigated.

A method for the determination of the cyclone collection efficiency and the cyclone critical particle size may be developed together with a detailed dynamic modelling and using the measured swirling flow fields in this study.

As a further work, the effect of Re number and the characteristic cyclone dimensions on the amount of under flow which leaves from the bottom dust discharge opening of the cyclone, may be investigated.

In further studies the effects of Re number, the characteristic cyclone dimensions, the dust particle properties, and the fluid-particle concentration at inlet to the cyclone, on the collection efficiency of cyclone separators may be determined experimentally using the set-up produced in this study.

LIST OF REFERENCES

1. Chigier, N.A., Cervinsky, A.1967 " Experimental Investigation of Swirling Vortex Motion in Jets " Jornual of Applied Mechanics. June pp. 443-451.

2. Yajnik,K.S.,Subbaiah,M.V., 1973 " Experiments on Swirling Turbulent Flows Part 1. Similarity in Swirling Flows " J. Fluid Mech. Vol. 60, part4, pp.665-687.

3. Riahi, A., Hill, P. G. 1993 "Turbrlent Swirling Flow in Short Cylindrical Chambers " Journal of Fluids Engineering. September , Vol.115, pp. 444-451.

4. Prikhod'ko, V. P., Dytnerskii, Yu.I., Khalpanov, L. P. and Kozlovskii, E.V. 1989 " Calculating Hydraulic Drag of a Concurrent Cyclone " Theoretical Foundation of Chemical Engineering. January, Vol.23, No.1, pp. 94-100.

5. Ovchinnikov, A. A., Nikolaev, N. A. 1989 " Investigation of the Influence of Pre swirling a Gas Flow on the Hydraulic Drag of a Swirl Device " November, Vol. 23, No. 6, pp. 761-766.

6. Migay, V. K., Golubev, L. K. 1970 " Friction and Heat Transfer in Turbulent Swirl Flow with a Variable Swirl Generator in a Pipe " Heat Transfer - Soviet Research.Vol. 2, No. 3, pp. 68-73.

7. Yowakim, F. M., Kind, R. T. 1988 " Mean Flow and Turbulence Measurements of Annular Swirling Flow s " Trans. ASME J. of Fluids , Engineering . September, Vol. 110, pp. 257-263.

8. Sampers, W. F. J., Lamers, A.P.G.G., Steenhaven, A.A. 1993 " Analysis of Experimental and Numerical Results of a Turbulent Swirling Flow in a Tube " Chemical Engineering Communications., May, Vol. 125, pp. 187- 196.

9. Backshall, R.G., Landis, F. 1969 " The Boundary Layer Velocity Distribution   in Turbulent Swirling Pipe Flow " Trans. ASME J. of Basic Engineering., December, pp. 728-733.

10. Nag, P.K., Debray, B. 1987 "Effect of Spiral Turbulator on Heat Transfer from an Immersed Vertical Heated Cylinder to a Fluidized Bed of

Coarse Particles " Indian Journal of Technology., October, Vol.25, No.10, pp.427-433.

11. Nakamura, Y., Hama, T., Yasuhara, M. 1982 " Axisymmetric Inviscid Swirling Flows Produced by Bell Mouth and Centerbody " AIAA Journal., April, Vol.20, No.4, pp.561-562.

12. Algifri, A.H., Bhardwaj, R.K., Rao, Y.V.N. 1988 " Heat Transfer in Turbulent Decaying Swirl Flow in a Circular Pipe " Int. J. Heat and Mass Transfer., Vol.31, No.8, pp.1563-1568.

13. Sarpkaya, T. 1974 " Effect of the Adverse Pressure Gradient on Vortex Breakdown " AIAA Journal., May, Vol.12, No.5, pp.602-607.

14. Faler, J.H., Leibovich, S. 1978 " An Experimental Map of the Internal Structure of a Vortex Breakdown " J. Fluid Mech., August, Vol.86, Part2, pp.313-335.

15. Hallett, W.L.H. 1986 " Swirl Generator for Independent Variation of Swirl and Velocity Profile " AIAA Journal., July, Vol.24, No.7, pp.1212-1213.

16. Chigier, N.A., Beer, J.M. 1964 " Velocity and Static Pressure Distributions in Swirling Air Jets Issuing from Annular and Divergent Nozzles " Trans. ASME J. Basic Engineering., December, pp.788-796.

17. Uskaner, Y.A. 1994 " Experimental and Theoretical Study of Swirling Flow in Pipes " Ph. D. Thesis, University of Gaziantep, Gaziantep, Turkey.

18. Ito, S., Ogawa, K., Kuroda, C. 1980 " Turbulent Swirling Flow in a Circular Pipe " J. of Chemical Engineering of Japan., Vol.13, No.1, pp.6-9.

19. Escudier, M.P., Bornstein, J., Zehnder, N. 1980 " Observations and LDA Measurements of Confined Turbulent Vortex Flow " J. Fluid Mech. Vol.98, Part 1, pp.49-63.

20. Hay, N., West, P.D. 1975, " Heat Transfer in Free Swirling Flow in a Pipe" Trans. ASME J. of Heat Transfer, August, pp.411-416.

21. Stern, C. 1977 " Air Pollution, Vol.4-Enginnering Control of Air Pollution " Academic Press, INC., Newyork.

22. Lynn, A.D., 1976 " Air Pollution-Threat and Response " Addison-Wesley Publishing Company., Menlo Park, California.

23. Magill, P.L., Holden, F. R., Ackley, C. 1956 "Air Pollution Handbook " Mc Graw-Hill Book Company., Menlo Park, California.

24. Strauss, W. 1971 " Air Pollution Control " John Wiley & Sons, INC. ....

25. Rossano, A.T. 1974 " Air Pollution Control " Mc Graw-Hill Book Company., Washington.

26. Noll, K. 1973 " Industrial Air Pollution Control " Ann Arbor Science Publishers Inc., Michigan.

27. Zhou, L.X., Soo, S.L. 1990 " Gas-Solid Flow and Collection of Solids in a Cyclone Separator " Powder Technology., Vol.63, No.1, pp.45-53.

28. Knowles, S.R., Woods, D.R., Fuerstein, I.A. 1973 " The Velocity Distribution within a Hydrocyclone without an Air Core " Canadian Journal of Chemical Engineers., June, Vol.51, pp.263-271.

29. Hwang, C.C., Shen, H.Q., Zhu, G., Khonsari, M.M. 1993 " On the Main Flow Pattern in Hydrocyclones " J. of Fluids Engineering., March, Vol.115, pp.21-25.

30. Bloor, M.I.G., Ingham, D.B. 1987 " The Flow in Industrial Cyclones " J. of Fluid Mech., Vol.178, pp.507-519.

31. Rietema, K. 1960 " Performance and Design of Hydrocyclones" Chemical Engineering Science., Vol.15, Part 1,2,3,4., pp.298-325.

32. Pericleous, K.A.1987 " Mathematical Simulation of Hydrocyclones " Applied Mathematical Modelling., August, Vol.11, pp.242-255.

33. Xu, J., Qian, L., Qiu, J. 1989 " The Investigation of the Internal Pressure loss in Hydrocyclones " Separation Science and Technology., Vol.24, No.14, pp.1167-1178.

34. Gebica, M. 1988 " A Contribution to Pressure Loss and Dedusting Efficiency of Cyclones " AUFTAK., Vol.29, No.7, pp.395-402.

35. Clift, R., Ghadiri, M., Hoffman, A.C. " A Critique of Two Models for Cyclone Performance " AICHE Journal., Vol.37, No.2, pp.285-289.

36. Dietz, P.W., 1981 " Collection Efficiency of Cyclone Separators " AICHE Journal. November, Vol.27, No.6, pp.888-892.

37. Vedernikov, V.B. 1990 " Optimization of Cyclone Designs " Theoretical Foundations of Chemical Eng., Vol.24, No.1, pp.82-87.

38. Mothes, H., Löeffler, F. 1988 " Prediction of Particle Removal in Cyclone Separators " International Chemical Engineering., April, Vol.28, No.2, pp.231-240.

39. Gauthier, T.A., Briens, C.L., Bergougnou, M.A., Galtier, P. 1990 " Uniform Cyclone Efficiency Study " Powder Technology., Vol.62, No.3, pp.217-225.

40. Koch, W.H., Licht, W. 1977 " New Design Approacch Boosts Cyclone Efficiency " Chemical Engineering., November, Vol.7, pp.80-88.

41. Sherstyuk, A.N., Aslamova, V.S. 1990 " An Emprical Method of Evaluating Separation Efficiency in Cyclones " Thermal Engineering.,May, Vol.37, No.5, pp.253-255.

42. Leith, D., Mehta, D. 1973 " Cyclone Performance and Design " Atmospheric Environment., Vol.7, pp.527-549.

43. Cooper, D.W. 1983 " Cyclone Design: Sensitivity , Elasticity and Error Analysis " Atmospheric Environment., Vol.17, pp.485-489.

44. Tucker, A.R., Carr, J.F., Pekers, J.E. " Experimental Study of Hopper Evacuation Effects on Multiple Cyclone Performance " JAPCA.(J. of Air Pollution Control Association., Vol.39, No.12, pp.1614-1618.

45. Uskaner F., 1991 "Design, Construction and Testing of a Model Blower Type Wind Tunnel" Ms. Thesis, Gaziantep Üniversitesi, Gaziantep, Turkey.

46. BS 1042, " Method of the Measurement of the fluid flow in pipes " British Standard Institution., London.

47. Bryer, D.W., Punkhurst, R.C. 1971 " Pressure-Probe Methods for Determining Wind Speed and Flow Direction " NPL., Her Majesty 's Stationary Office, London.

48. Ayık, M., 1990, " Establishment of A Cyclone Test-Rig and Experimental Determination of Cyclone Performance " Ms. Thesis, Gazi Üniversitesi,   Ankara, Turkey.

APPENDICES

APPENDIX 1

SPECIFICATIONS OF THE DRIVE UNIT OF FAN

The drive unit of fan was consisted by an electric motor and the AC motor variable speed controller which have the following specifications;

Electric motor

Input:3∅, 220/380 V, 50 Hz

Power rating: 2.95 HP / 2.2 kW

Rotational speed: 2835 rpm

Protection class: IP 44 B

AC speed controller

Controller specification: Simovert P.6SE2008-3AA00

Input: 3∅, 380/500V±10%, 14/12 A, 47-63 Hz

Output:3∅, 380/500V, 12/11 A, 0-400 Hz

Power rating: 8.3 kVA, motor: 7.5 HP/5.5 kW

Protection class: IEC 529 IP 20

Temperature range: 0-40°

APPENDIX 2

SPECIFICATIONS OF THE DRIVE UNIT OF PARTICLE FEEDER

The drive unit of particulate feeder was consisted by an electric motor and an AC motor variable speed controller which have the following specifications;

Electric motor

Input: 3∅, 220/380 V, 50 Hz

Power rating: 0.8 HP/0.6 kW

Rotational speed: 1375 rpm

Protection class: KR 80.1/4 TA III (Made in Germany)

AC speed controller

Controller specification: Simovert P.6SE2001-1AA00

Input: 1∅, 220/240 V±10%, 7A, 50-60 Hz

Output: 3∅, 0-220/240 V, 2.5A, 0-120 Hz

Power rating: 0.7 kVA motor: 0.5 HP/0.37 kW

Protection class: IEC 529 IP 20

Temperature range: 0-40°C

APPENDIX 3

SPECIFICATIONS OF THE BLOWER TYPE WIND TUNNEL
AND ITS DRIVE UNIT

Wind tunnel

Type: Blower type

Impeller diameter: 300 mm

Test section size: 140×210×550 mm

Max. crossectional size: 425×640 mm

Wind speed range: 0 -10 m/s

Electric motor

Input: 3∅, 220/380 V, 50 Hz

Power rating: 0.34 HP/255 W

Rotational speed: 1350 rpm

Protection class: KR 71.1/4 TA III (Made in Germany)

AC speed controller

Controller specification: Simovert P.6SE2001-1AA00

Input: 1∅, 220/240 V±10%, 7A, 50-60 Hz

Output: 3∅, 0-220/240 V, 2.5A, 0-120 Hz

Power rating: 0.7 kVA motor: 0.5 HP/0.37 kW

Protection class: IEC 529 IP 20

Temperature range: 0-40°C

TABLES

Table 3.1 Standard Cyclone Configurations in Available Literature.

SOURCE	Purpose	D/D	a/D	b/D	D_d/D	S/D	h/D	h_c/D	H/D	D_u/D
Stairmand [21]	High Efficiency	1	0.50	0.20	0.50	0.50	1.50	2.50	4.00	0.38
Swift [40]	High Efficiency	1	0.44	0.21	0.40	0.50	1.40	2.50	3.90	0.40
Zhou & Soo [27]	High Efficiency	1	0.37	0.38	0.57	0.37	1.31	2.30	3.60	0.40
Mothes & Loeffler [38]	High Efficiency	1	0.53	0.16	0.39	0.53	1.38	1.37	2.75	0.39
Lapple [42]	General Purpose	1	0.50	0.25	0.50	0.63	2.00	2.00	4.00	0.25
Swift [40]	General Purpose	1	0.50	0.25	0.50	0.60	1.75	2.00	3.75	0.40
Peterson & Whitby [21]	General Purpose	1	0.58	0.21	0.50	0.58	1.33	1.84	3.17	0.50
Stairmand [21]	High Throughput	1	0.75	0.38	0.75	0.88	1.50	2.50	4.00	0.38
Swift [40]	High Throughput	1	0.80	0.35	0.75	0.85	1.70	2.00	3.70	0.40
Basic Configuration (Present Work)	General Purpose	1	0.58	0.26	0.44	0.70	2.00	2.00	4.00	0.25
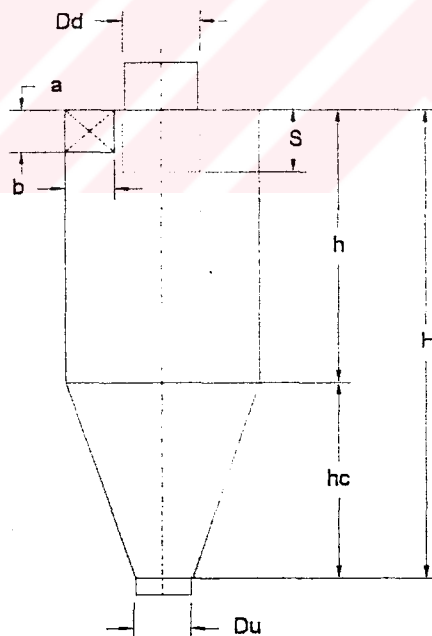
Table 3.2 Configuration List for the Experimentiation of the Tangential Inlet Height and Width of Cyclone.

C.Name	D/D	h/D	h_c/D	a/D	b/D	D_d/D	D_u/D	S/D
ab1	1.0	2.0	1.5	0.458	0.367	0.458	0.25	0.583
ab2	"	"	"	0.583	0.263	"	"	0.708
ab3	"	"	"	0.658	0.233	"	"	0.783
ab4	"	"	"	0.863	0.177	"	"	0.988

S=a+D/8 from standara designs
A_{in}=a*b= constant
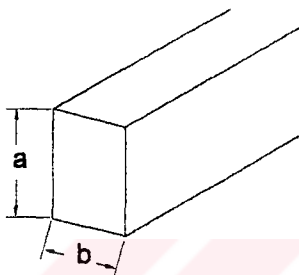
Table 3.3 Configuration List for the Experimentiation of the Fluid Discharge Pipe Depth of Cyclone.

C.Name	D/D	h/D	h_c/D	a/D	b/D	D_d/D	D_u/D	S/D
S1	1.0	2.0	1.5	0.583	0.266	0.458	0.25	0.000
S2	"	"	"	"	"	"	"	0.292
S3	"	"	"	"	"	"	"	0.583
S4	"	"	"	"	"	"	"	0.708
S5	"	"	"	"	"	"	"	1.050
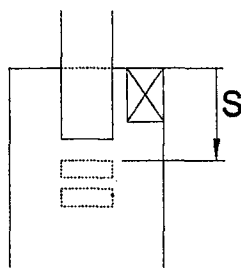
Table 3.4 Configuration List for the Experimentiation of the Fluid Discharge Pipe Diameter of Cyclone.

C.Name	D/D	h/D	h_c/D	a/D	b/D	D_d/D	D_u/D	S/D
Dd1	1.0	2.0	1.5	0.583	0.266	0.192	0.458	0.708
Dd2	"	"	"	"	"	0.296	"	"
Dd3	"	"	"	"	"	0.442	"	"
Dd4	"	"	"	"	"	0.504	"	"

Dd
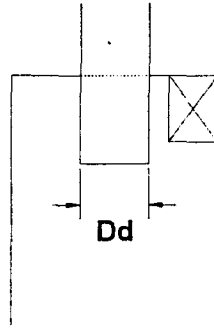
Table 3.5 Configuration List for the Experimantation of the Under Flow Diameter of Cyclone.

C.Name	D/D	h/D	h_c/D	a/D	b/D	D_d/D	D_u/D	S/D
Du1	1.0	2.0	1.75	0.583	0.266	0.442	0.125	0.708
Du2	"	"	1.50	"	"	"	0.250	"
Du3	"	"	1.25	"	"	"	0.375	"
Du4	"	"	1.00	"	"	"	0.500	"

$h_c = ((D-D_u)/2) \tan\varepsilon$

D=cst

hc=varying

E=cst(76)

Du=varying

81
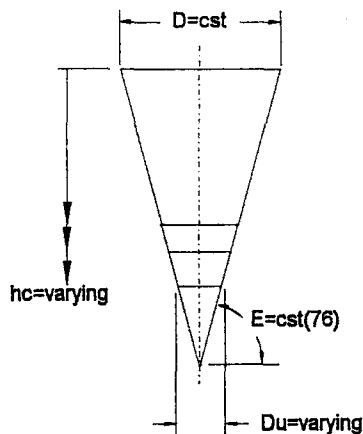
Table 3.6 Configuration List for the Experimentiation of the Cone Heights of the Cyclone

C.Name	D/D	h/D	h_c/D	a/D	b/D	D_d/D	D_u/D	S/D
hc1	1.0	2.0	0.650	0.583	0.266	0.442	0.25	0.708
hc2	"	"	1.110	"	"	"	"	"
hc3	"	"	1.500	"	"	"	"	"
hc4	"	"	2.125	"	"	"	"	"
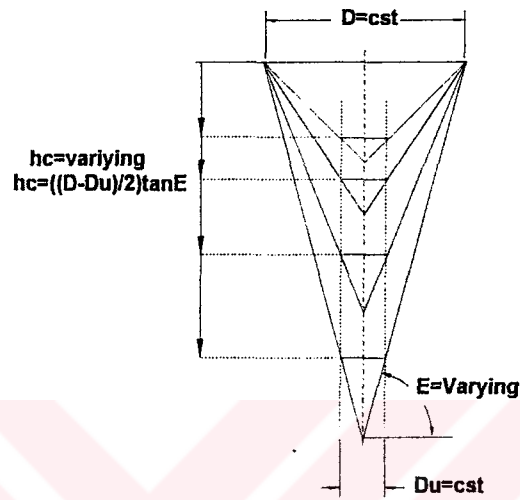
Table 4.1 The Characteristic Values of the Dimensionless Tangential Velocity Distributions which are Shown in Fig. 4.24, 4.25, 4.26 and 4.27, Referring to eq. (4.17) and (4.18).

Z/h	Re $*10^4$	Free Vortex Flow			Forced Vortex Flow			V_{tm}^+	r_m/R	V_{tc}^+/V_{tm}^+	r_c/r_m
		n	C	Effective Region	n	ω	Effective Region				
0.979	3.53	0.593	0.848	0.3≤r/R≤1.0	1.0	18.156	0 ≤r/R≤ 0.1	1.853	0.186	1.457	0.769
	5.30	0.588	0.835	"	"	17.760	"	1.835	"	1.411	0.784
	7.07	0.583	0.828	"	"	17.536	"	1.825	"	1.397	0.781
	8.83	0.590	0.797	"	"	17.525	"	1.810	"	1.386	0.770
	12.4	0.585	0.781	"	"	17.126	"	1.766	"	1.383	0.766
0.813	3.53	0.568	0.880	0.3≤r/R≤1.0	1.0	17.550	0 ≤r/R≤ 0.1	1.852	0.190	1.405	0.780
	5.30	0.561	0.855	"	"	17.220	"	1.830	"	1.375	0.769
	7.07	0.565	0.847	"	"	16.910	"	1.823	"	1.370	0.777
	10.6	0.570	0.810	"	"	16.694	"	1.790	"	1.357	0.766
	12.4	0.563	0.795	"	"	16.498	"	1.763	"	1.344	0.756
0.667	3.53	0.547	0.910	0.3≤r/R≤1.0	1.0	16.650	0 ≤r/R≤ 0.1	1.855	0.196	1.371	0.783
	5.30	0.545	0.892	"	"	16.560	"	1.845	"	1.355	0.775
	7.07	0.554	0.858	"	".	16.530	"	1.825	"	1.350	0.765
	8.83	0.554	0.860	"	"	16.500	"	1.775	"	1.389	0.766
	11.5	0.550	0.830	"	"	15.785	"	1.760	"	1.341	0.767
0.412	3.53	0.540	0.935	0.3≤r/R≤1.0	1.0	16.620	0 ≤r/R≤ 0.1	1.870	0.208	1.372	0.741
	5.30	0.532	0.920	"	"	16.476	"	1.840	"	1.362	0.731
	7.07	0.533	0.900	"	"	16.320	"	1.833	"	1.345	0.726
	8.83	0.540	0.869	"	"	16.080	"	1.801	"	1.342	0.723
	10.6	0.538	0.848	"	"	15.612	"	1.775	"	1.323	0.723
	12.4	0.540	0.821	"	"	15.00	"	1.753	"	1.297	0.729

Table 4.2 The Characteristic Values of the Dimensionless Tangential
Velocity Distributions which are Shown in Fig. 4.28. a, b and
c, and Fig. 4.29. a, b, c and d, Referring to eq. (4.17) and (4.18).

			Free Vortex Flow			Forced Vortex Flow				
Z/h	D_d/D	Re $*10^4$	n	C	Effective Region	n	ω	Effective Region	V_{tm}^+	r_m/R
0.979		3.53	0.702	0.668	$0.2 \leq r/R \leq 1.0$	1.0	48.825	$0 \leq r/R \leq 0.08$	3.203	0.09
	0.192	7.07	0.759	0.584	"	"	41.500	"	2.765	"
		10.6	0.776	0.576	"	"	26.347	"	2.536	"
		3.53	0.736	0.596	$0.25 \leq r/R \leq 1.0$	1.0	42.343	$0 \leq r/R \leq 0.09$	3.156	0.120
	0.296	7.07	0.770	0.635	"	"	29.525	"	2.950	"
		10.6	0.799	0.562	"	"	26.606	"	2.735	"
		3.53	0.593	0.848	$0.3 \leq r/R \leq 1.0$	1.0	18.156	$0 \leq r/R \leq 0.1$	1.853	0.186
		5.30	0.588	0.835	"	"	17.760	"	1.835	"
	0.442	7.07	0.583	0.828	"	"	17.536	"	1.825	"
		8.83	0.590	0.797	"	"	17.525	"	1.810	"
		12.4	0.585	0.781	"	"	17.126	"	1.766	"
		3.53	0.579	0.832	$0.33 \leq r/R \leq 1.0$	1.0	12.036	$0 \leq r/R \leq 0.12$	1.710	0.215
	0.504	7.07	0.546	0.852	"	"	11.650	"	1.715	"
		10.6	0.533	0.827	"	"	11.250	"	1.660	"
0.813	0.192	7.07	0.670	0.670	$0.2 \leq r/R \leq 1.0$	1.0	30.564	$0 \leq r/R \leq 0.08$	2.550	0.100
	0.246		0.704	0.674	$0.25 \leq r/R \leq 1.0$	"	27.427	$0 \leq r/R \leq 0.09$	2.700	0.130
	0.442		0.554	0.858	$0.3 \leq r/R \leq 1.0$	"	16.530	$0 \leq r/R \leq 0.1$	1.825	0.195
	0.504		0.493	0.894	$0.33 \leq r/R \leq 1.0$	"	11.244	$0 \leq r/R \leq 0.12$	1.655	0.225
0.412	0.192	7.07	0.735	0.608	$0.2 \leq r/R \leq 1.0$	1.0	31.266	$0 \leq r/R \leq 0.08$	2.625	0.110
	0.296		0.720	0.690	$0.25 \leq r/R \leq 1.0$	"	25.800	$0 \leq r/R \leq 0.09$	2.795	0.150
	0.442		0.533	0.900	$0.3 \leq r/R \leq 1.0$	"	16.320	$0 \leq r/R \leq 0.1$	1.833	0.208
	0.504		0.502	0.950	$0.33 \leq r/R \leq 1.0$	"	9.338	$0 \leq r/R \leq 0.12$	1.726	0.250

Table 4.3 The Characteristic Values of the Dimensionless TangentialVelocity Distributions which are Shown in Fig. 4.30. a, b and c, and Fig. 4.31. a, b, c, Referring to eq. (4.17) and (4.18).

	Free Vortex Flow				Forced Vortex Flow						
Z/h	D_u/D	$Re *10^4$	n	C	Effective Region	n	ω	Effective Region	V_{tm}^+	r_m/R	V_{tc}^+/V_{tm}^+	r_c/r_m
0.979		3.53	0.593	0.845	$0.3{\leq}r/R{\leq}1.0$	1	16.932	$0{\leq}r/R{\leq}0.1$	1.791	0.180	1.440	0.846
	0.125	7.07	0.589	0.813	"	"	16.421	"	1.775	"	1.396	0.838
		11.3	0.594	0.767	"	"	15.577	"	1.751	"	1.345	0.840
		3.53	0.593	0.848	$0.3{\leq}r/R{\leq}1.0$	1	18.156	$0{\leq}r/R{\leq}0.1$	1.853	0.186	1.457	0.769
		5.30	0.588	0.835	"	"	17.760	"	1.835	"	1.411	0.784
	0.250	7.07	0.583	0.828	"	"	17.536	"	1.825	"	1.397	0.781
		8.83	0.590	0.797	"	"	17.525	"	1.810	"	1.386	0.770
		12.4	0.585	0.781	"	"	17.126	"	1.766	"	1.383	0.766
		3.53	0.625	0.802	$0.35{\leq}r/R{\leq}1.0$	1	13.130	$0{\leq}r/R{\leq}0.13$	1.870	0.200	1.257	0.895
	0.375	7.07	0.616	0.808	"	"	12.510	"	1.824	"	1.259	0.918
		10.6	0.624	0.795	"	"	11.125	"	1.740	"	1.259	0.985
		3.53	0.651	0.816	$0.40{\leq}r/R{\leq}1.0$	1	12.600	$0{\leq}r/R{\leq}0.15$	1.675	0.295	1.433	0.646
	0.500	7.07	0.638	0.826	"	"	11.840	"	1.605	"	1.452	0.667
		10.6	0.646	0.820	"	"	10.850	"	1.571	"	1.438	0.706
		12.4	0.642	0.817	"	"	10.000	"	1.542	"	1.411	0.737
0.813	0.125	7.07	0.556	0.847	$0.3{\leq}r/R{\leq}1.0$	1	15.745	$0{\leq}r/R{\leq}0.1$	1.775	0.190	1.356	0.784
	0.250		0.554	0.858	$0.3{\leq}r/R{\leq}1.0$	"	16.530	$0{\leq}r/R{\leq}0.1$	1.825	0.195	1.350	0.765
	0.375		0.588	0.852	$0.35{\leq}r/R{\leq}1.0$	"	11.340	$0{\leq}r/R{\leq}0.13$	1.810	0.235	1.327	0.834
	0.500		0.610	0.860	$0.40{\leq}r/R{\leq}1.0$	"	8.198	$0{\leq}r/R{\leq}0.15$	1.610	0.310	1.255	0.795
0.412	0.125	7.07	0.521	0.902	$0.3{\leq}r/R{\leq}1.0$	1	15.300	$0{\leq}r/R{\leq}0.1$	1.781	0.210	1.336	0.740
	0.250		0.527	0.900	$0.3{\leq}r/R{\leq}1.0$	"	15.900	$0{\leq}r/R{\leq}0.1$	1.833	0.208	1.323	0.733
	0.375		0.550	0.896	$0.35{\leq}r/R{\leq}1.0$	"	10.800	$0{\leq}r/R{\leq}0.13$	1.815	0.255	1.194	0.787
	0.500		0.580	0.893	$0.40{\leq}r/R{\leq}1.0$	"	7.325	$0{\leq}r/R{\leq}0.15$	1.556	0.315	1.243	0.838

Table 4.4 The Characteristic Values of the Dimensionless Tangential Velocity Distributions which are Shown in Fig. 4.32. a, b and c, and Fig 4.33. a, b, c and d, Referring to eq. (4.17) and (4.18).

			Free Vortex Flow			Forced Vortex Flow						
Z/h	h_c/D	Re $*10^4$	n	C	Effective Region	n	ω	Effective Region	V_{tm}^+	r_m/R	V_{tc}^+/V_{tm}^+	r_c/r_m
0.979		3.53	0.685	0.779	$0.3 \le r/R \le 1.0$	1.0	18.105	$0 \le r/R \le 0.1$	1.980	0.200	1.414	0.773
	0.650	7.07	0.677	0.760	"	"	16.745	"	1.860	"	1.425	0.790
		10.6	0.676	0.736	"	"	16.196	"	1.810	"	1.414	0.791
		3.53	0.596	0.848	$0.3 \le r/R \le 1.0$	1.0	18.876	$0 \le r/R \le 0.1$	1.853	0.186	1.457	0.769
		5.30	0.588	0.835	"	"	17.760	"	1.835	"	1.411	0.784
	1.500	7.07	0.583	0.828	"	"	17.536	"	1.825	"	1.397	0.781
		8.83	0.590	0.797	"	"	17.525	"	1.810	"	1.386	0.770
		12.4	0.585	0.781	"	"	17.126	"	1.766	"	1.383	0.766
		3.53	0.595	0.807	$0.3 \le r/R \le 1.0$	1.0	18.040	$0 \le r/R \le 0.1$	1.842	0.190	1.396	0.751
	2.125	7.07	0.589	0.776	"	"	17.260	"	1.765	"	1.388	0.747
		10.6	0.598	0.751	"	"	16.750	"	1.715	"	1.399	0.754
0.813	0.650	7.07	0.602	0.840	$0.3 \le r/R \le 1.0$	1.0	15.150	$0 \le r/R \le 0.1$	1.850	0.210	1.346	0.783
	1.500		0.565	0.847	$0.3 \le r/R \le 1.0$	"	16.910	$0 \le r/R \le 0.1$	1.823	0.200	1.370	0.777
	2.125		0.546	0.838	$0.3 \le r/R \le 1.0$	"	15.853	$0 \le r/R \le 0.1$	1.776	0.210	1.333	0.711
0.412	0.650	7.07	0.556	0.901	$0.3 \le r/R \le 1.0$	1.0	14.682	$0 \le r/R \le 0.1$	1.865	0.225	1.310	0.739
	1.500		0.533	0.900	$0.3 \le r/R \le 1.0$	"	16.320	$0 \le r/R \le 0.1$	1.833	0.210	1.345	0.726
	2.125		0.525	0.896	$0.3 \le r/R \le 1.0$	"	15.200	$0 \le r/R \le 0.1$	1.780	0.225	1.334	0.695

FIGURES
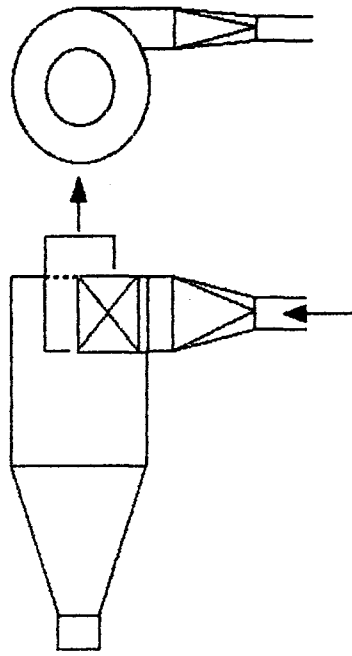
(a) Tangential inlet with axial discharge
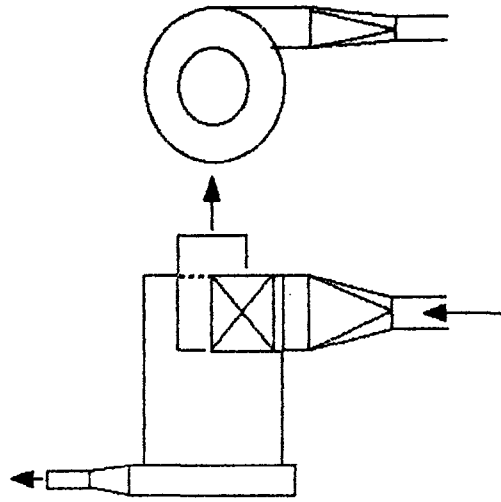
(b) Tangential inlet with peripheral discharge
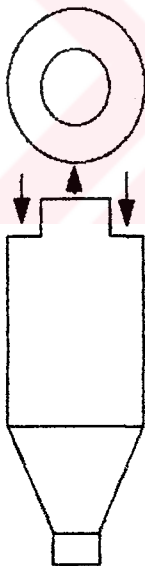
(c) Axial inlet through vanes with axial discharge
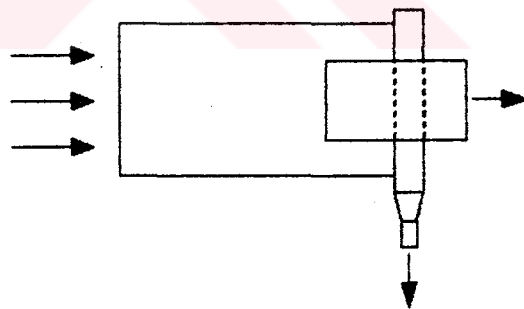
(d) Axial inlet through vanes with peripheral discharge

Figure 2.1 Types of cyclone configurations in common use
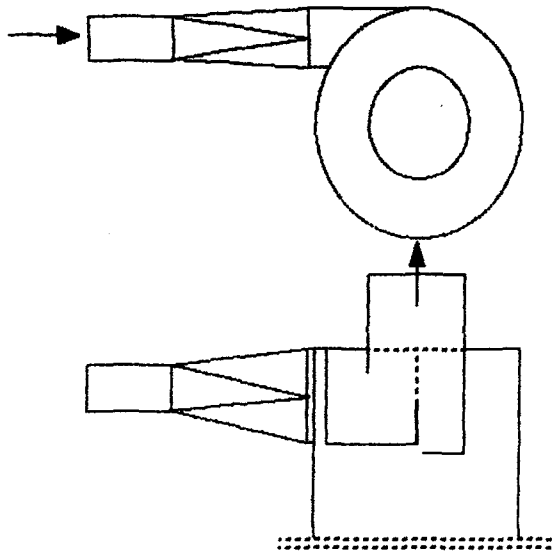
(A) Standard inlet
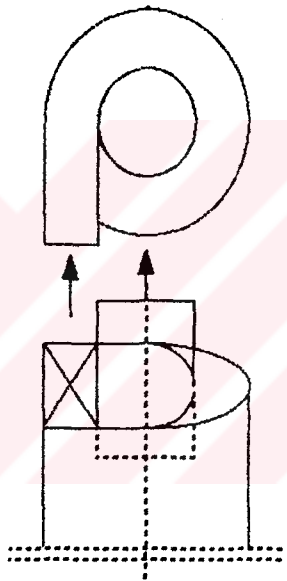
(B) Helical inlet
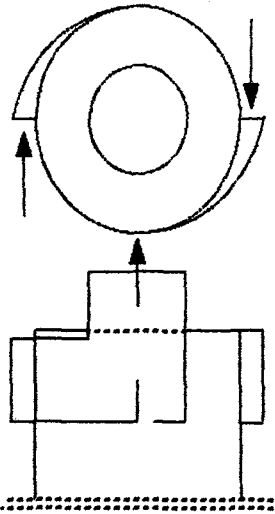
(C) Involute inlet

Figure 2.2 Types of tangential inlets
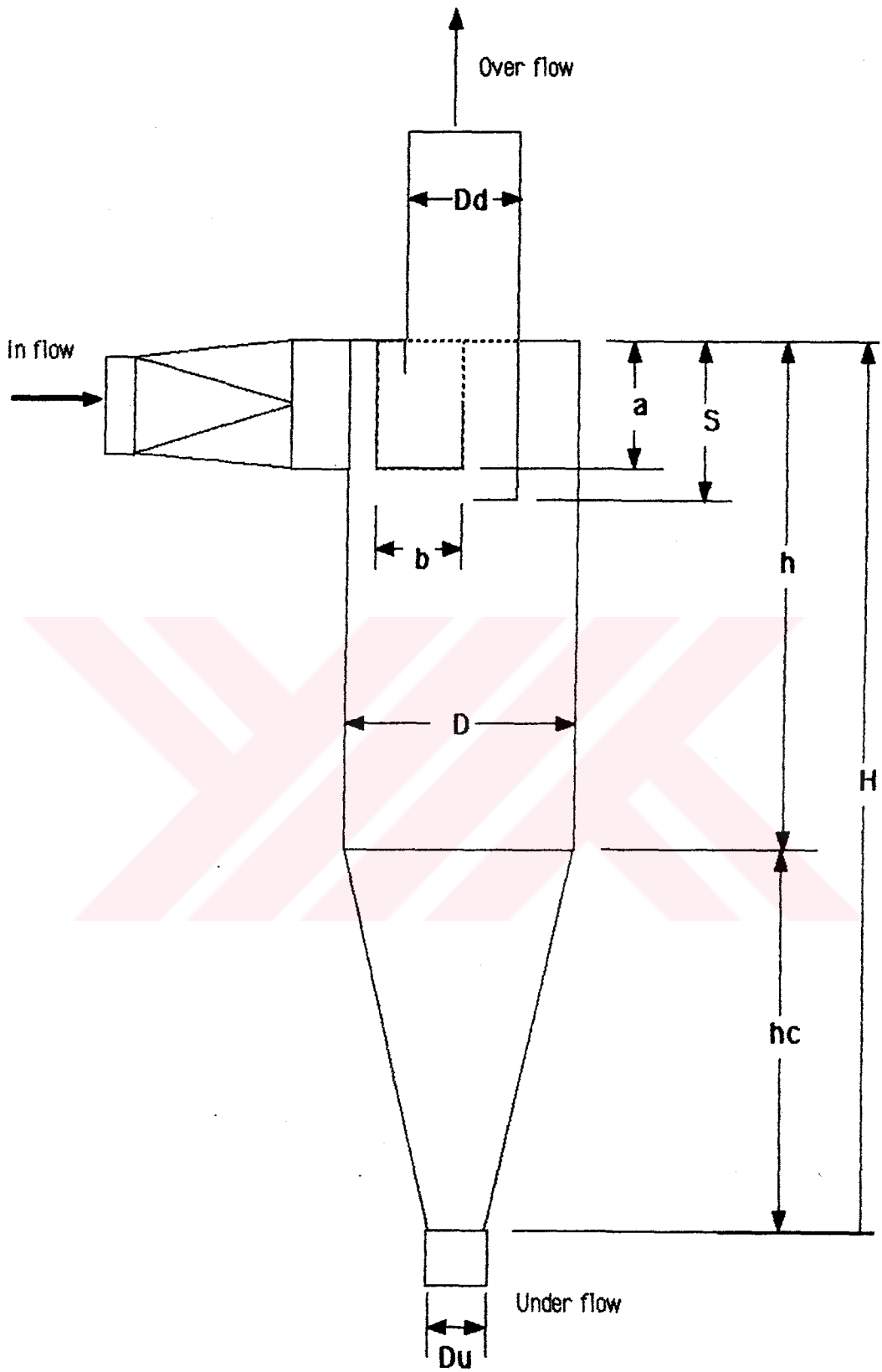
Figure 2.3   Typical cyclone geometry with dimensions
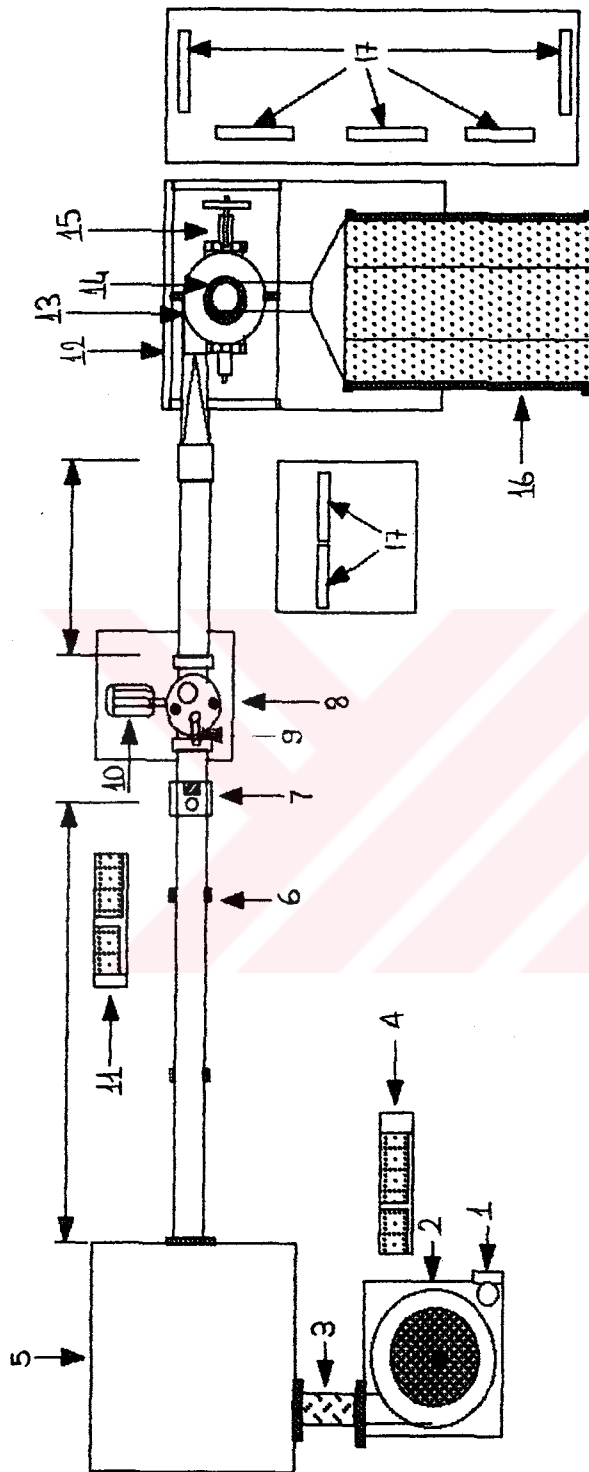
1. 2.95 HP, 2835 rpm motor
2. Fan unit
3. Flexible duct
4. AC motor speed controller of fan unit
5. Settling tank
6. Pipe supports
7. Pitot traverse and wall static pressure tappings
8. Particulate feeder
9. Short-circuit flow linkage
10. 0.8 HP, 1375 rpm motor
11. AC motor speed controller of feeding unit
12. Supporting roof of cyclones
13. Cyclone cylindrical body
14. Fluid discharge pipe
15. Five-hole probe and its traverse mechanism
16. Bag filter
17. Manometers

Figure 3.1. General view of the experimental set-up

90
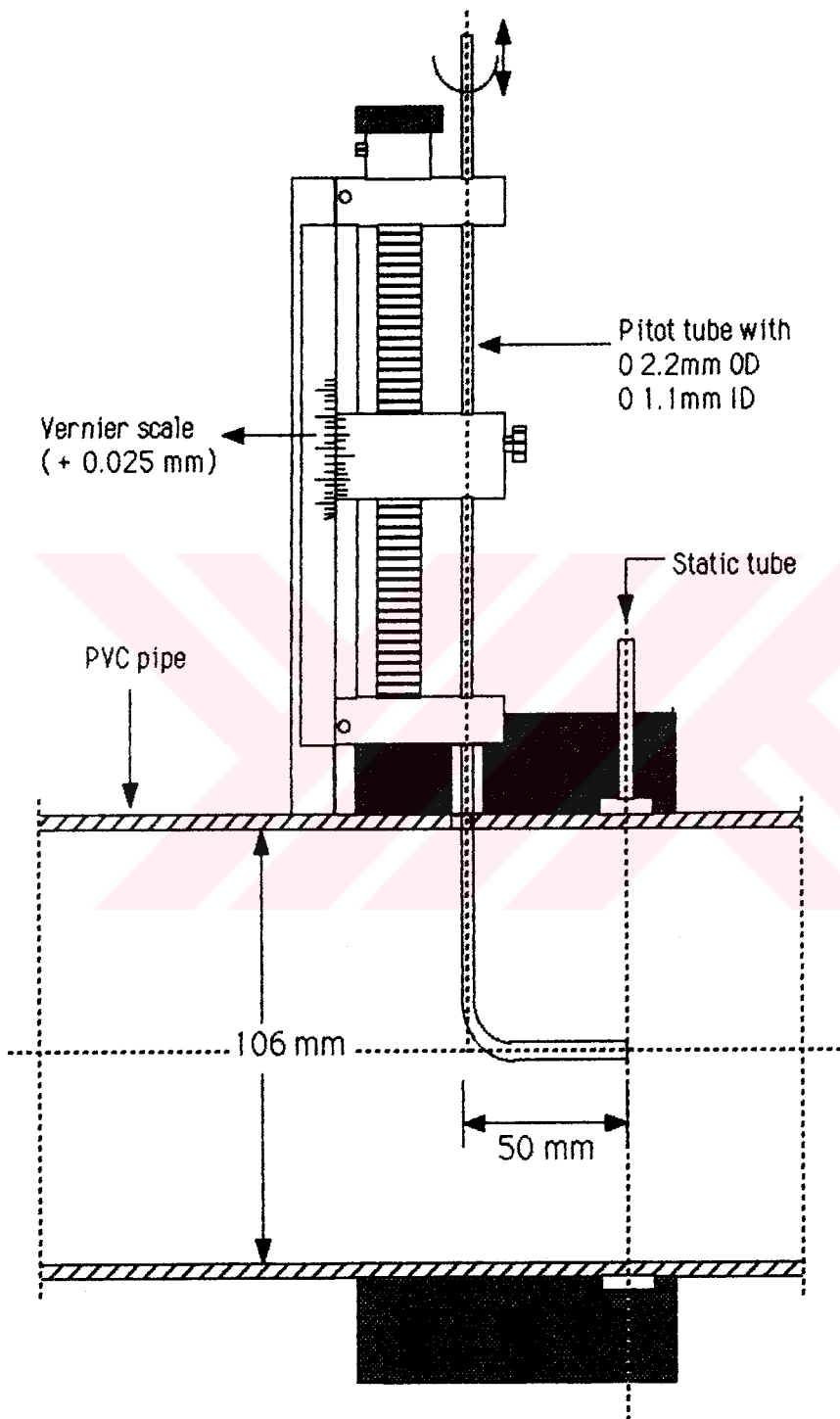
Figure 3.2. Pitot tube and traverse mechanism

The following labels appear in the figure:

- Pitot tube with O 2.2mm OD O 1.1mm ID
- Vernier scale (+ 0.025 mm)
- Static tube
- PVC pipe
- 106 mm
- 50 mm
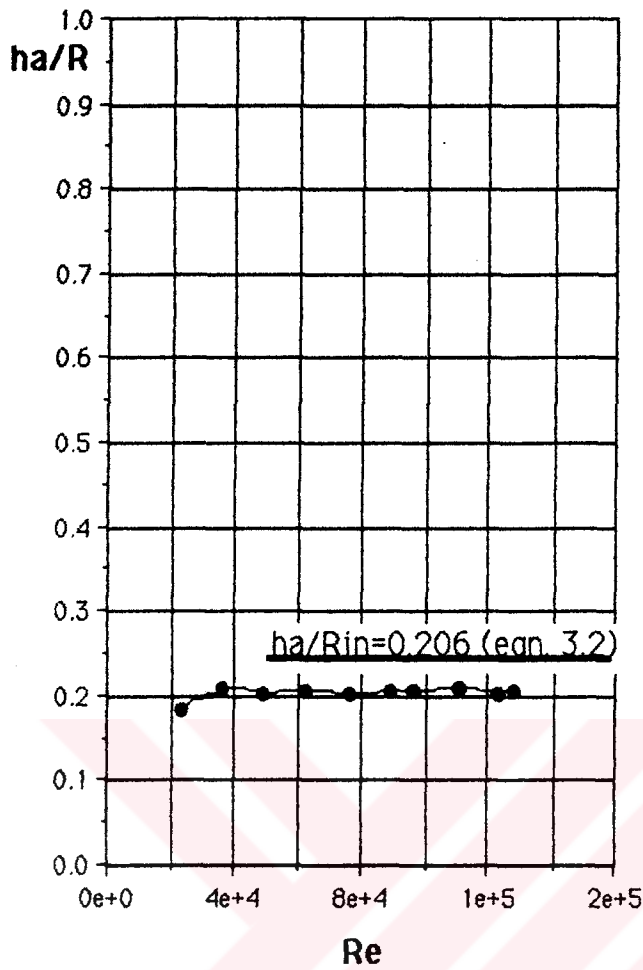
R.N	fan RPM	Va(m/s)	Re(x10	ha/R
1	567	3.32	2.346	0.185
2	851	5.12	3.619	0.208
3	1134	6.95	4.914	0.204
4	1418	8.85	6.251	0.206
5	1701	10.77	7.607	0.202
6	1985	12.60	8.901	0.205
7	2126	13.63	9.635	0.205
8	2268	15.63	11.042	0.209
9	2552	17.40	12.301	0.203
10	2835	18.11	12.75	0.206
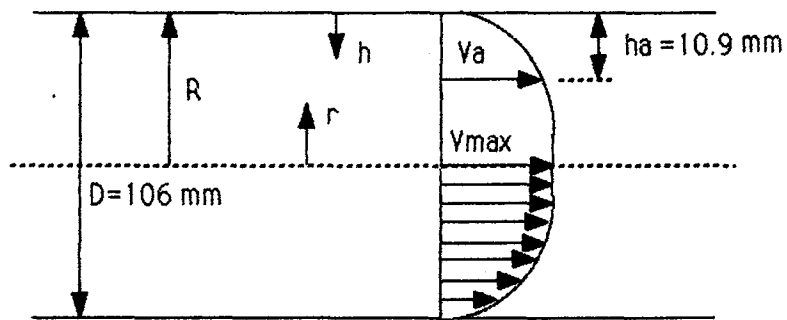
Figure 3.3. Calibration of average fluid velocity in the inlet pipe of cyclone configurations
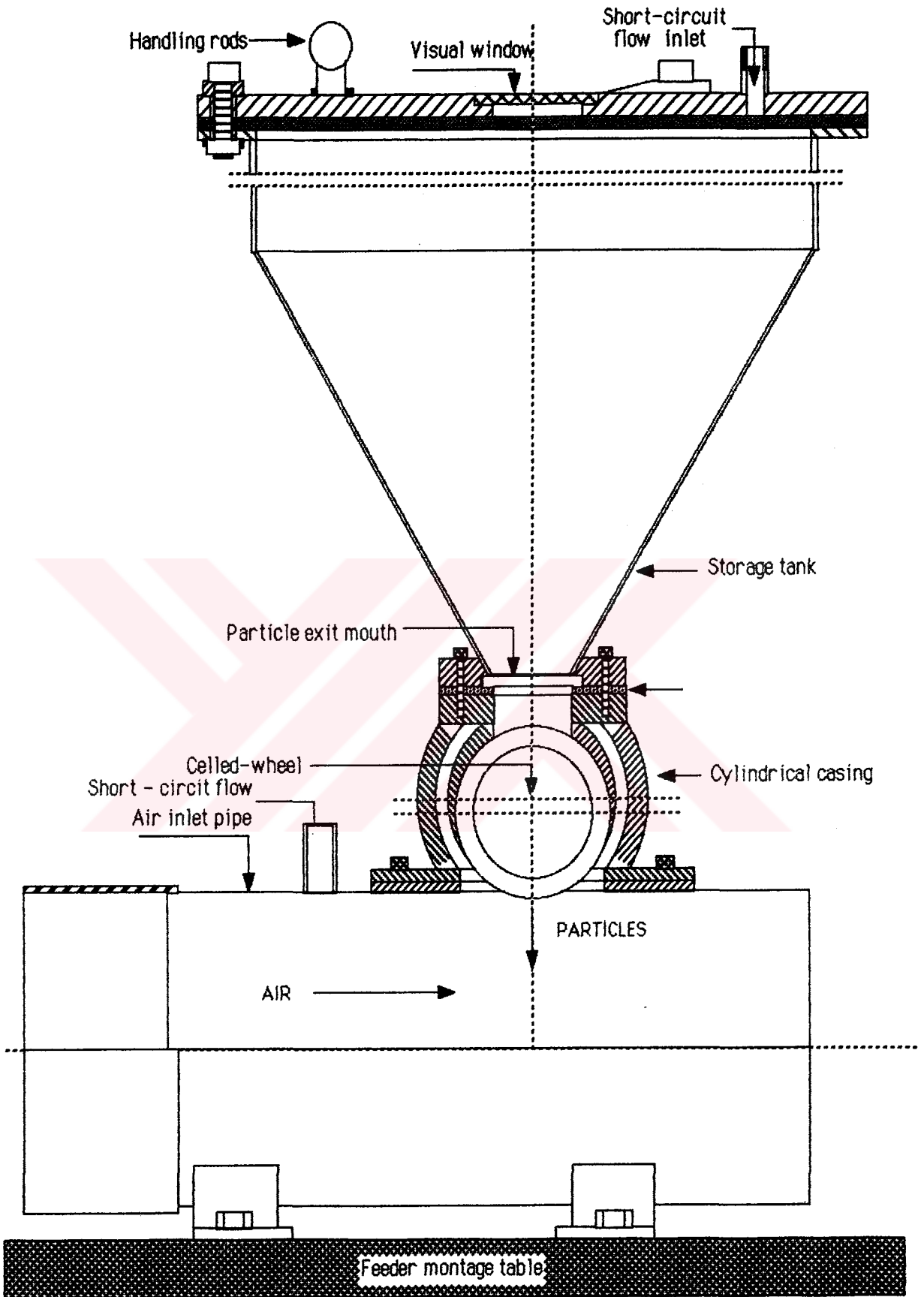
Figure 3.4. Particulate feeder (Side crossectional-view)

93
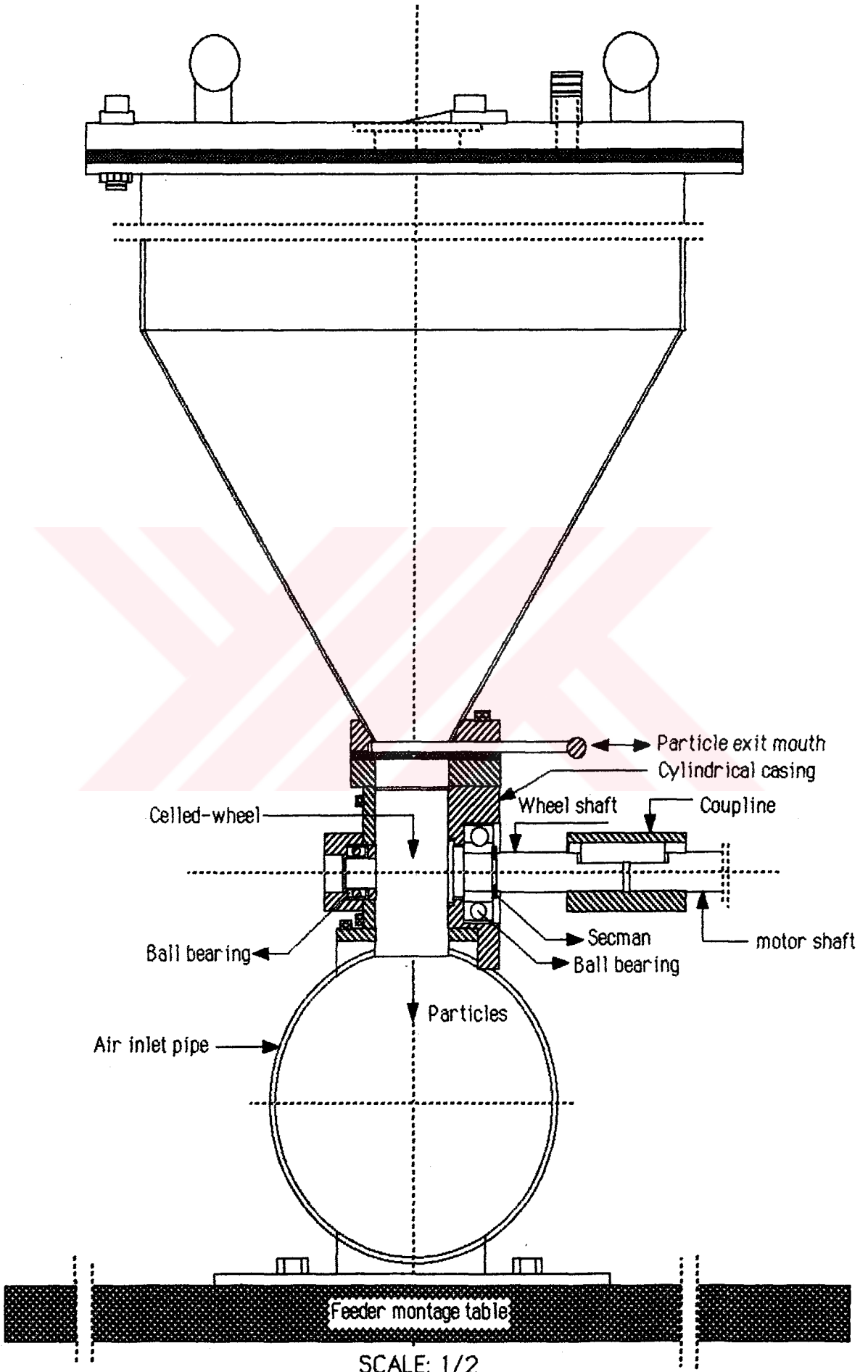
Figure 3.5. Particulate feeder (Front crossectional-view)

Labels in figure:
- Particle exit mouth
- Cylindrical casing
- Wheel shaft
- Coupline
- Celled-wheel
- Secman
- motor shaft
- Ball bearing
- Ball bearing
- Particles
- Air inlet pipe
- Feeder montage table

SCALE: 1/2

94.

Do=60 · Di · 10

12.5 (Secman slot)

15 · 21 · 25

5x2.5 (Key way)

9 · 30 · 11 · 24 · 30

1.5 · 3.5 · 1

110
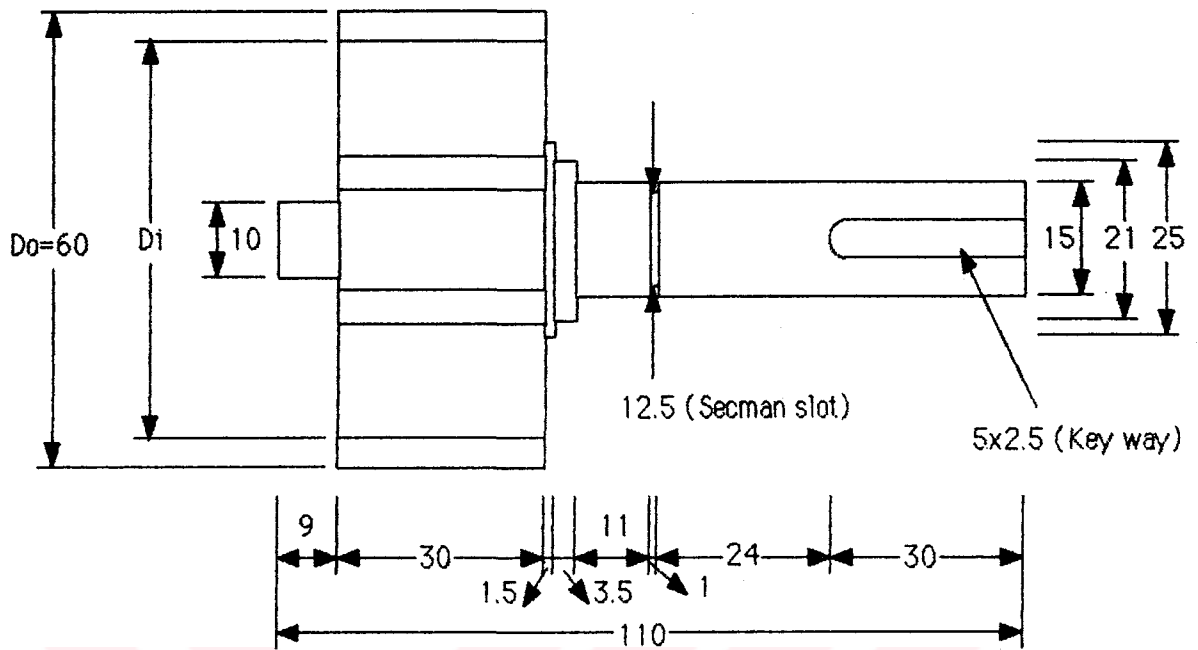
SCALE : 1/1

Rotor code	Di (mm)	t (mm)	n	V (m3/rev)
R1	55	4	8	1.115E-5
R2	52	4.5	6	1.787E-5
R3	30	2	6	5.822E-5

WHERE;

Di; inner diameter of wheel

t ; thickness of wheel blade

n; total number of blades

v ; rotational volume of wheel

Figure 3.6. Types of celled-wheels used in the particulate feeder

95
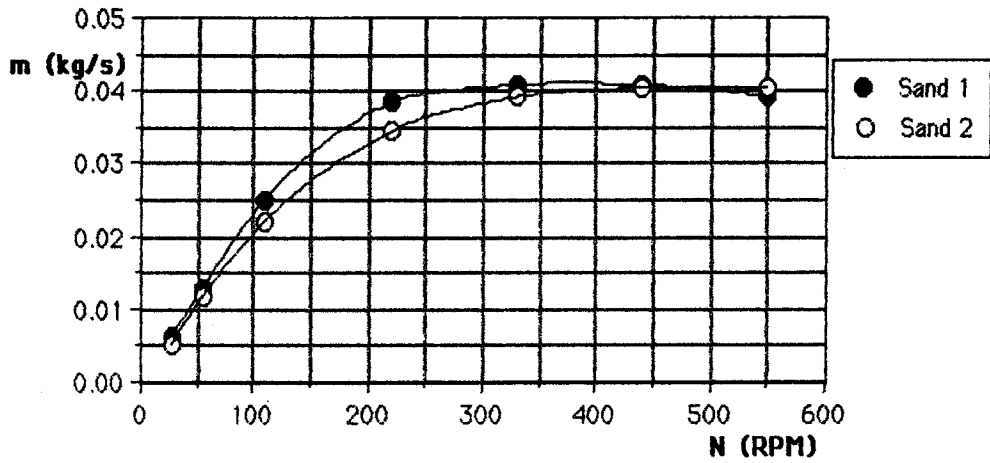
(a)
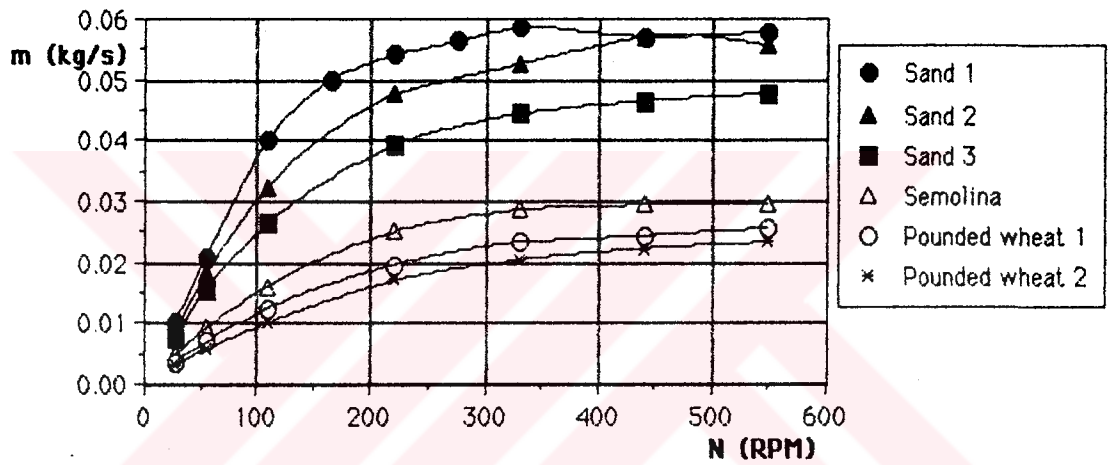
(b)
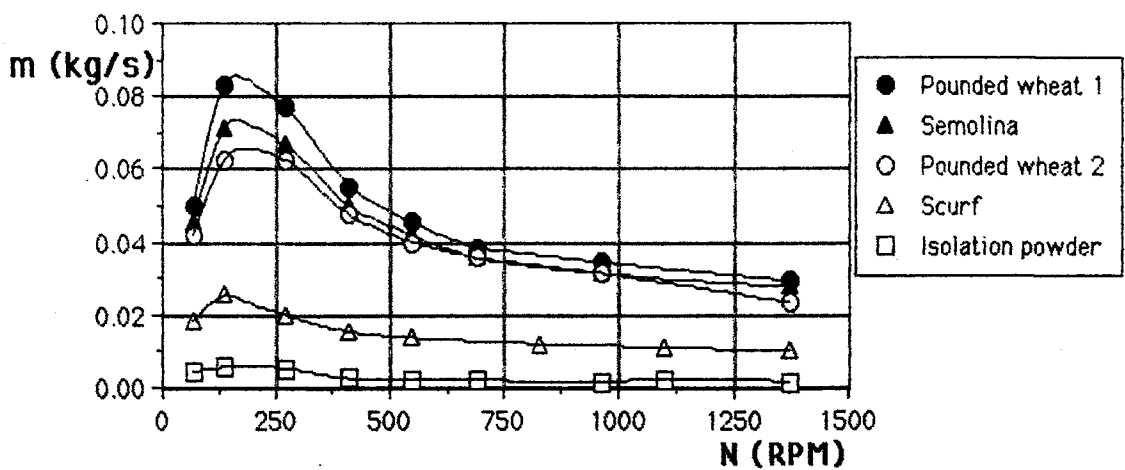
(c)

Figure 3.7 Variation of the particle mass flowrate as a function of wheel speed for three types of celled-wheels, (a), (b), (c) for different rotors given in Fig. 3.6.
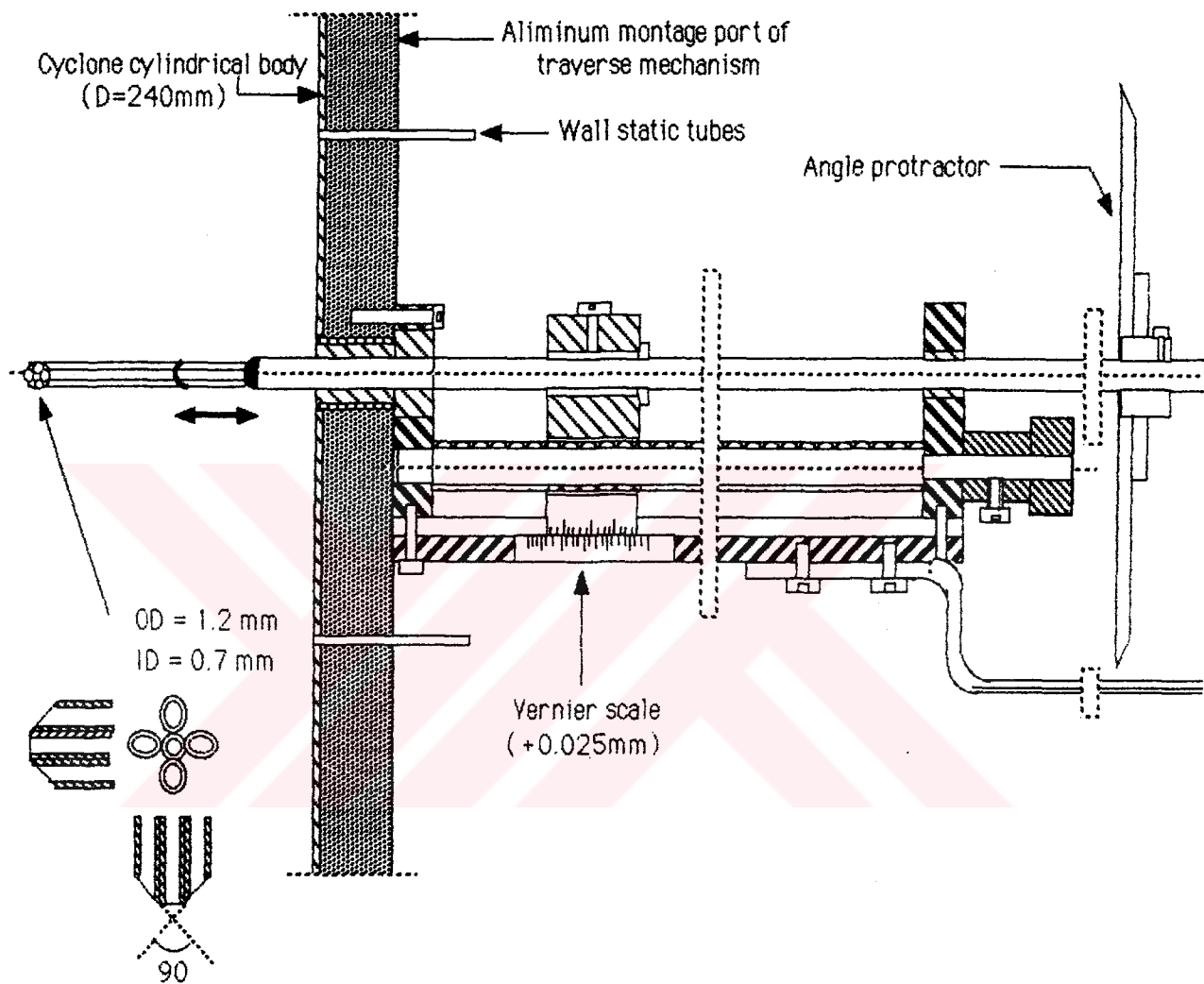
Figure 3.8 Five-tube yawmeter and its traverse mechanism mounted on the cyclone cylindrical body
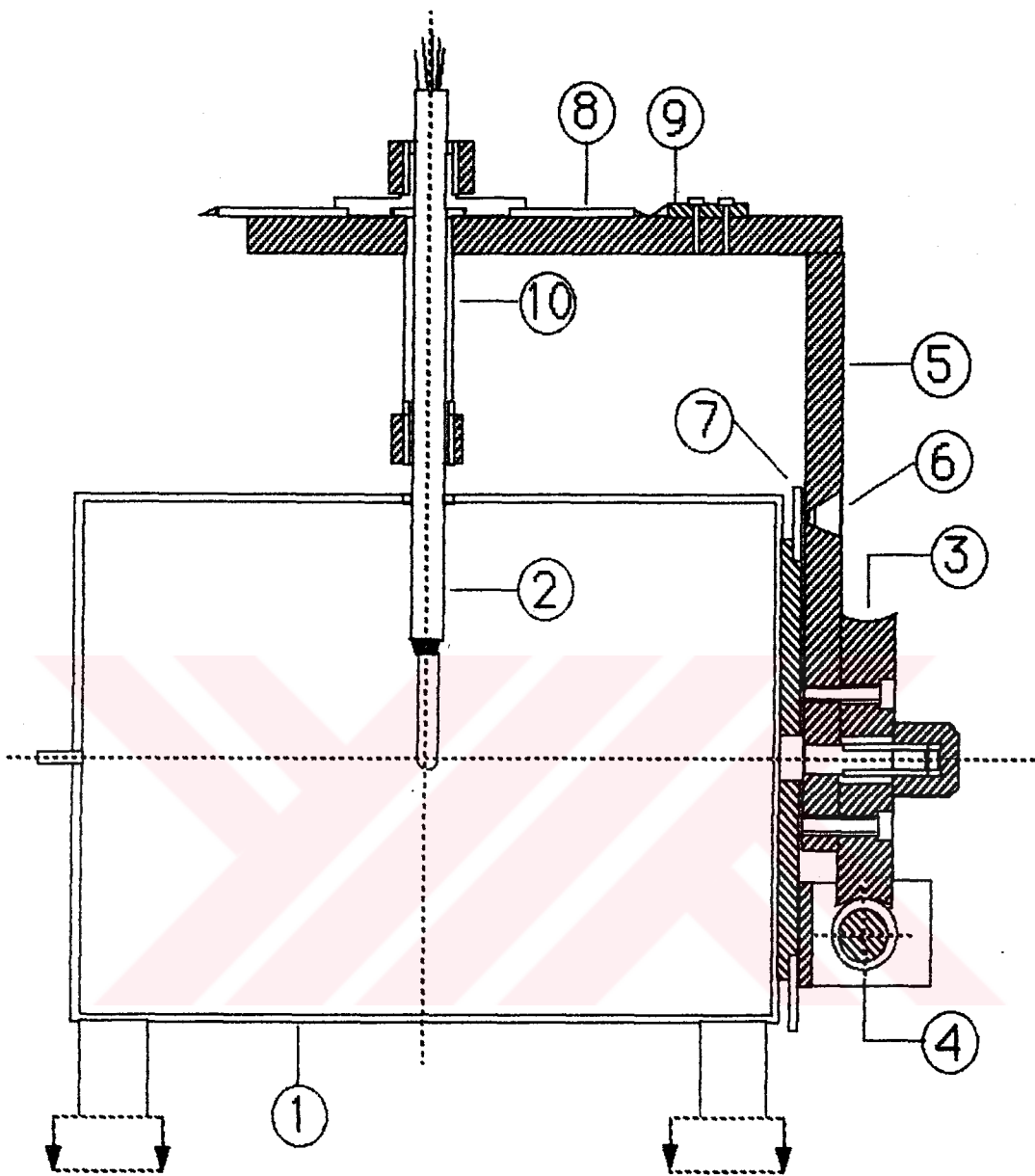
1. Wind tunnel test section
2. Five-tube yawmeter
3. Worm gear
4. Helical Gear
5. L-shaped arm
6. Visualization hole
7. Pitch angle protractor
8. Yaw angle protractor
9. Yaw angle vernier
10. Four-groove coupline

Figure 3.9 Calibration mechanism of the five-tube yawmeter probe

$$f(\varphi) = \frac{P_2 - P_4}{P_5 - P_m}$$

$$f(\alpha) = \frac{P_3 - P_1}{P_5 - P_m}$$
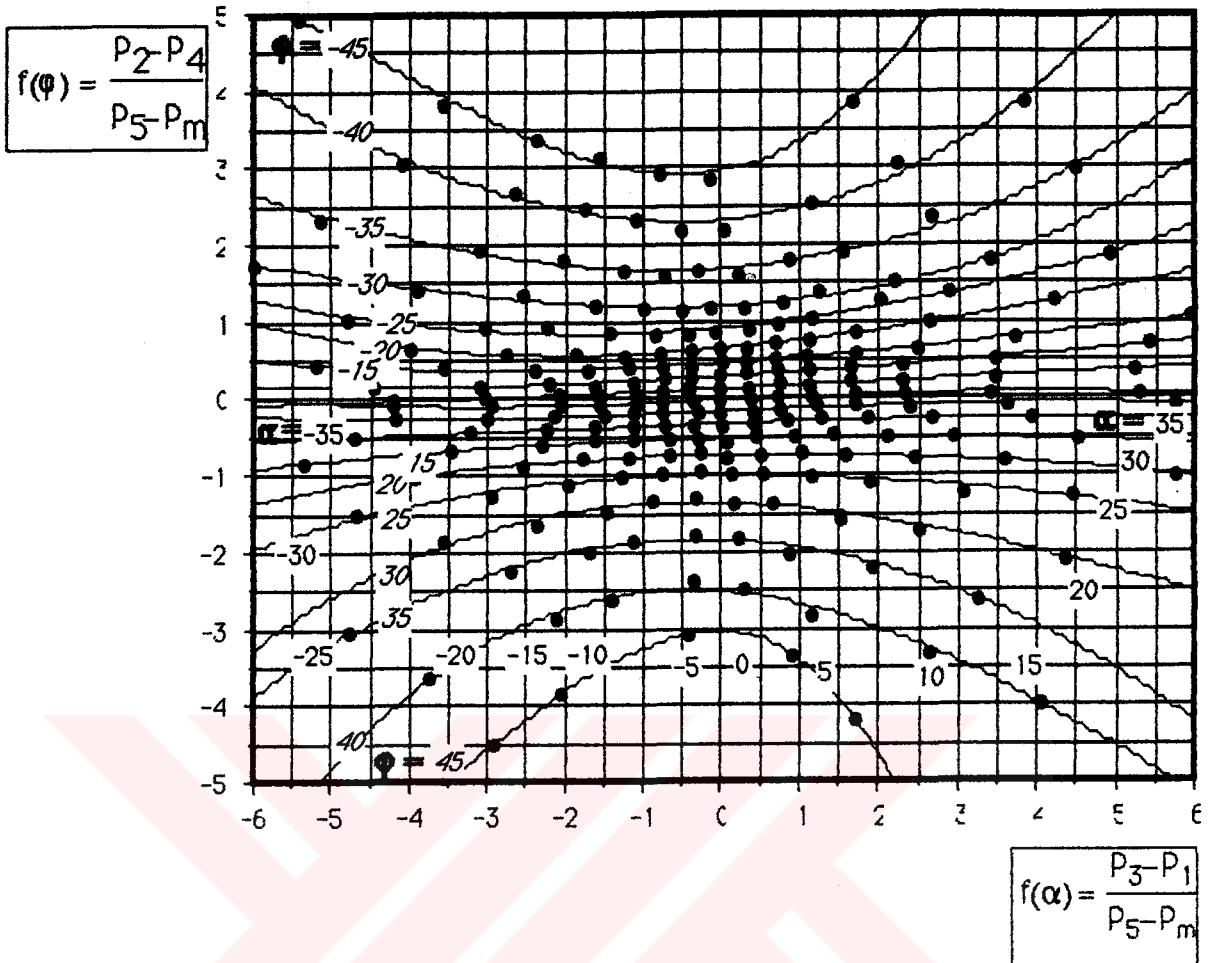
Figure 3.10 (a) The calibration factors $f(\alpha)$ and $f(\varphi)$
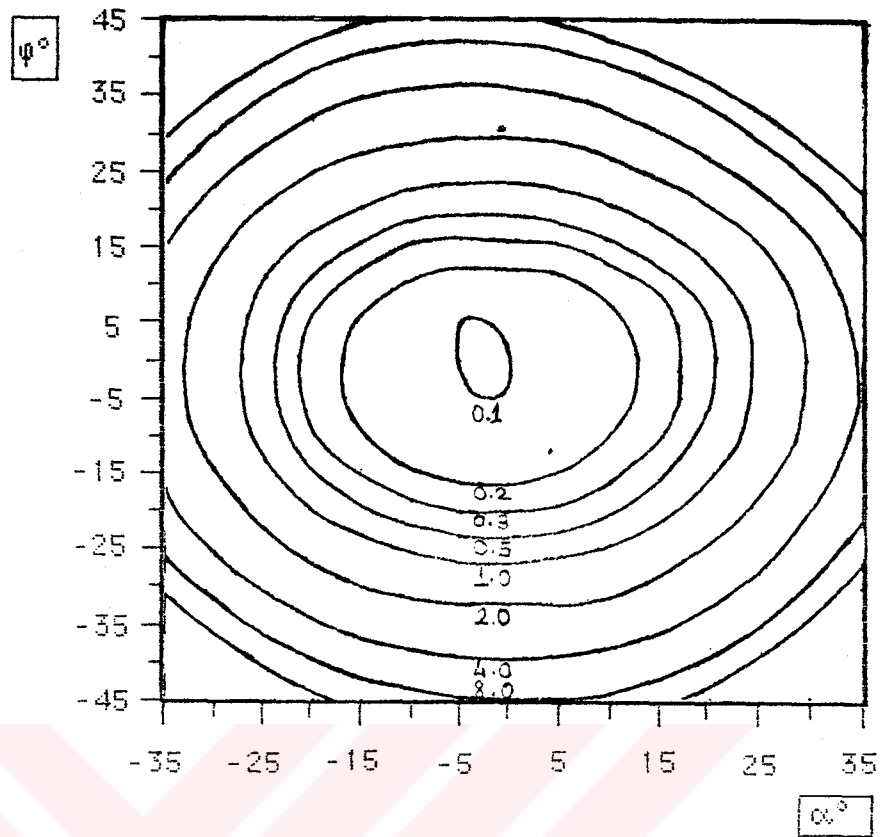
Figure 3.10. **(b)** The calibration factor S_p
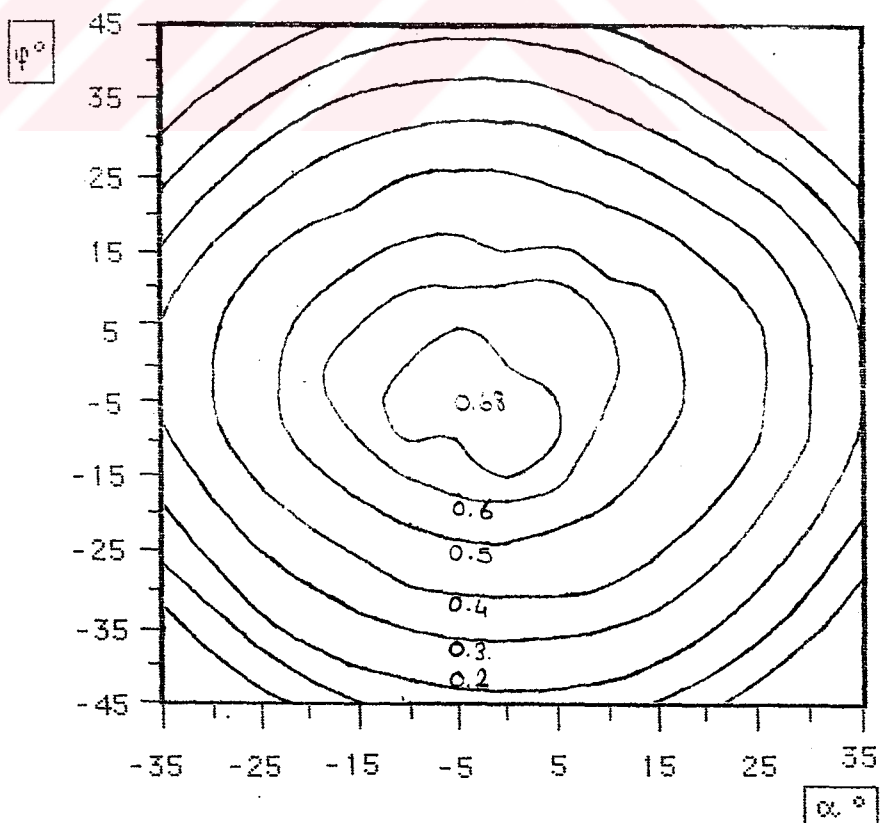
Figure 3.10. **(c)** The calibration factor Q_p
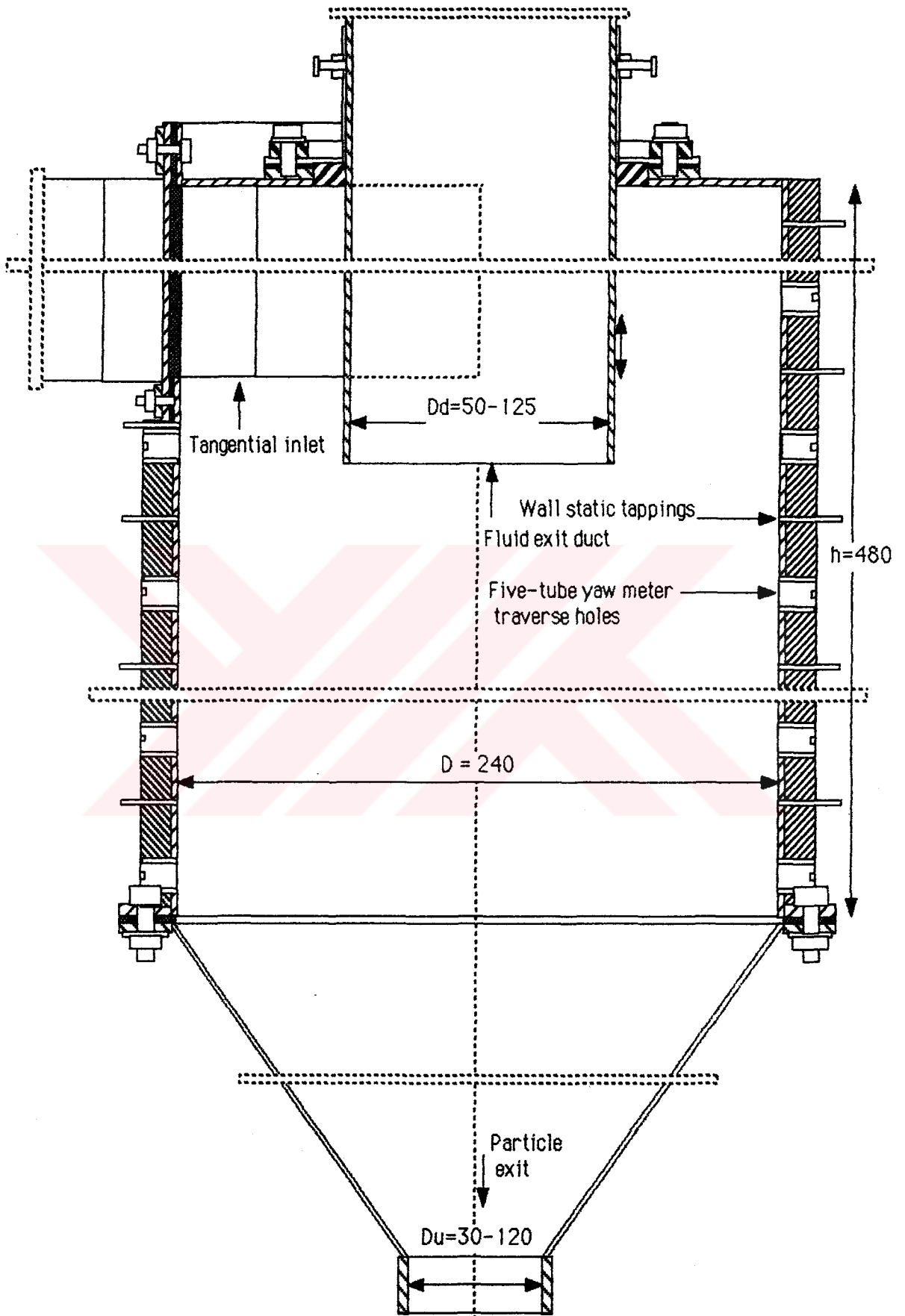
Figure 3.11 Section view of the cylindrical cyclone body
with the all of mounting sections.

The following labels appear in the figure:

- Tangential inlet
- Dd=50-125
- Wall static tappings
- Fluid exit duct
- Five-tube yaw meter traverse holes
- h=480
- D = 240
- Particle exit
- Du=30-120
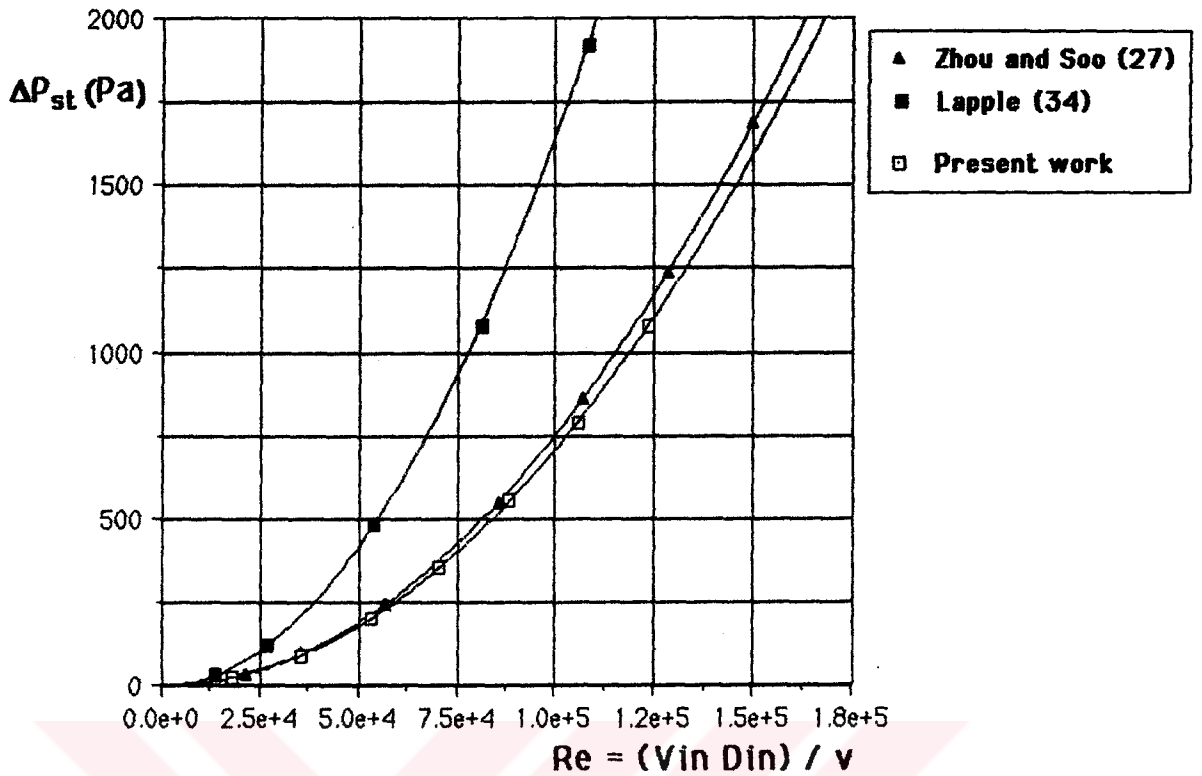
Figure 4.1 Variation of the cyclone static pressure loss as a function of Re for the basic cyclone configuration and used with (27, 34).
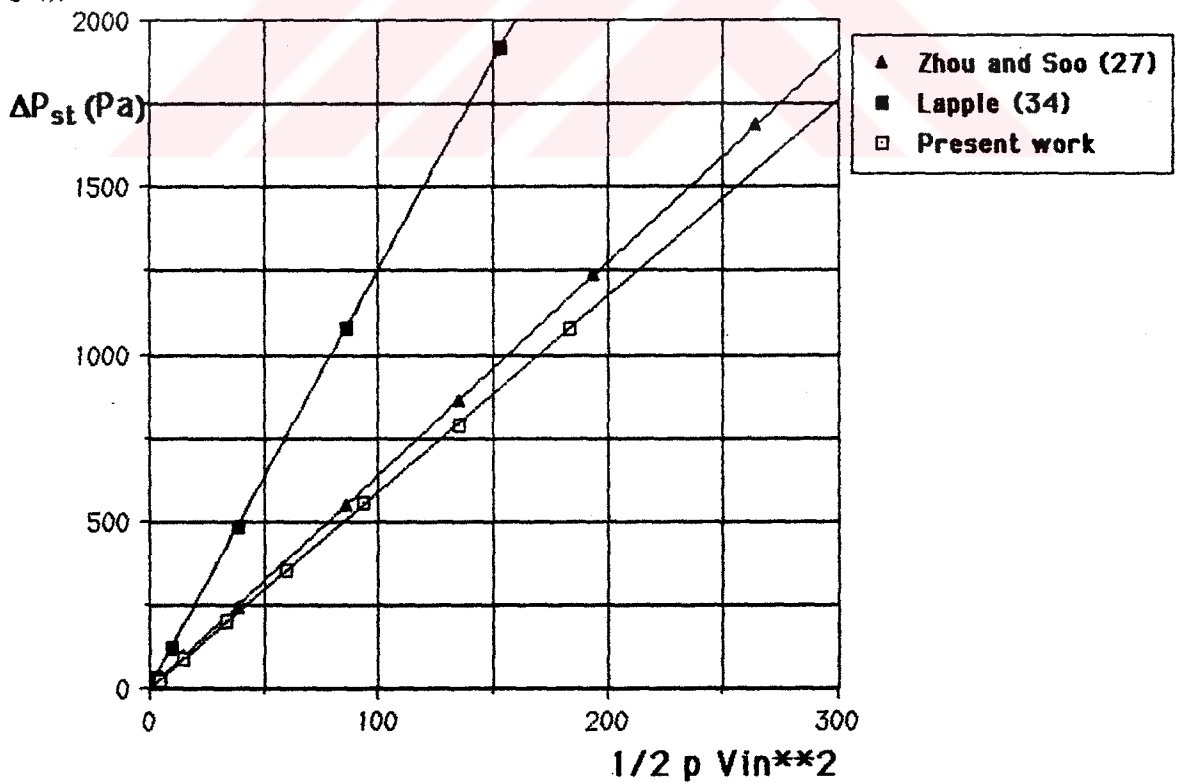
Figure 4.2 Variation of the cyclone static pressure loss as a function of inlet dynamic pressure for the basic cyclone configuration and used with (27,34).
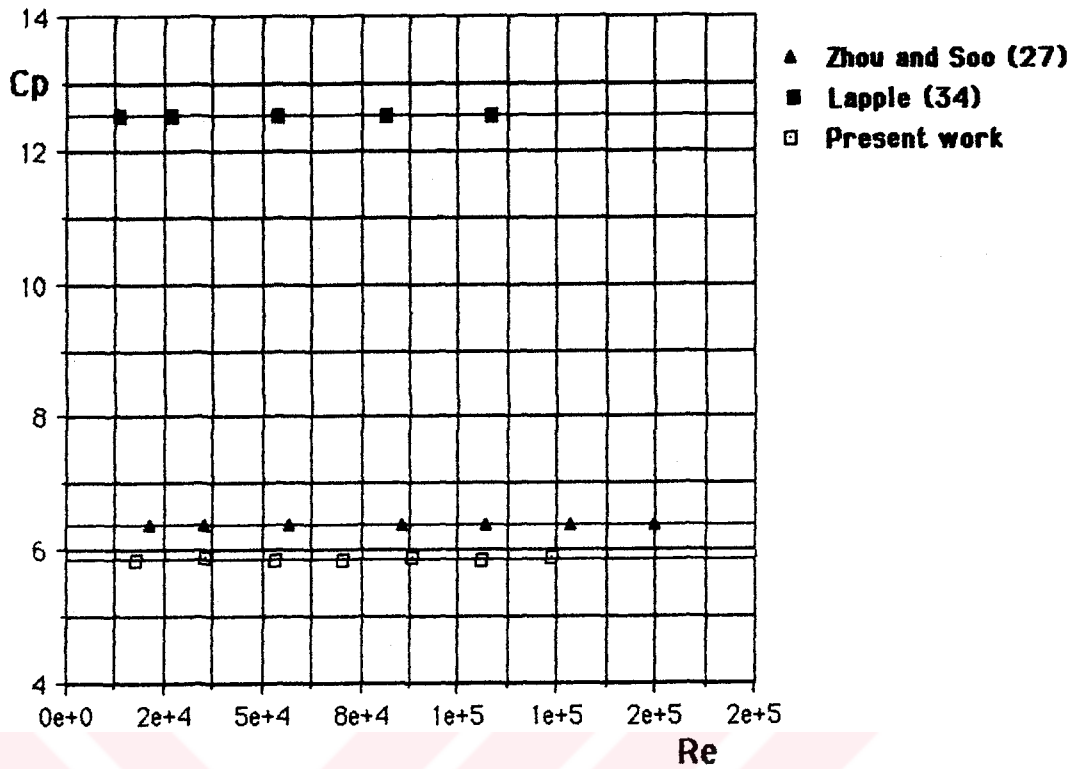
Figure 4.3 Variation of C_p as a function of Re for the basic cyclone configuration and, used with investigators in references (27, 34).
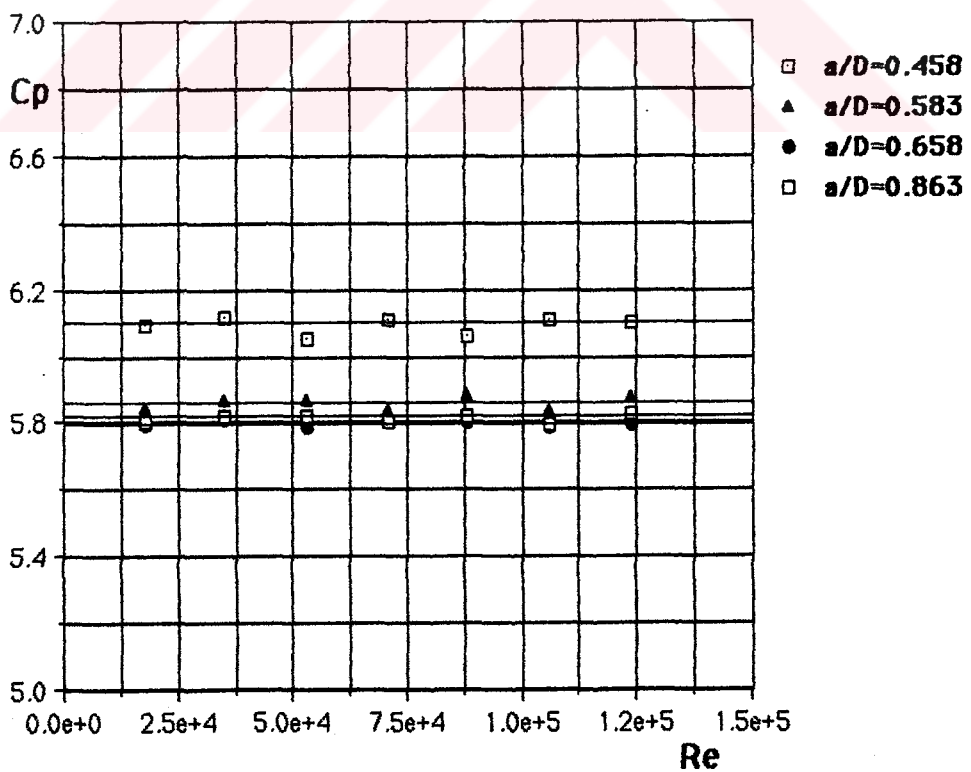
Figure 4.4 Variation of C_p as a function of Re for different a/D ratios of the cyclone.
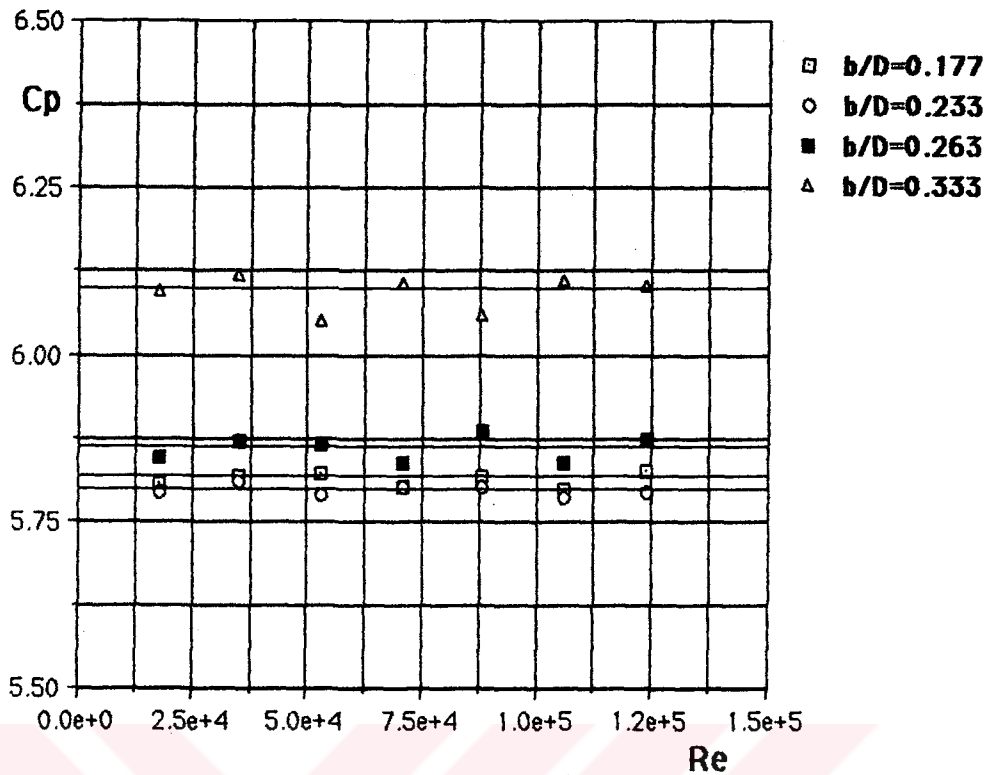
Figure 4.5 Variation of C_p as a function of Re for different b/D ratios of the cyclone.
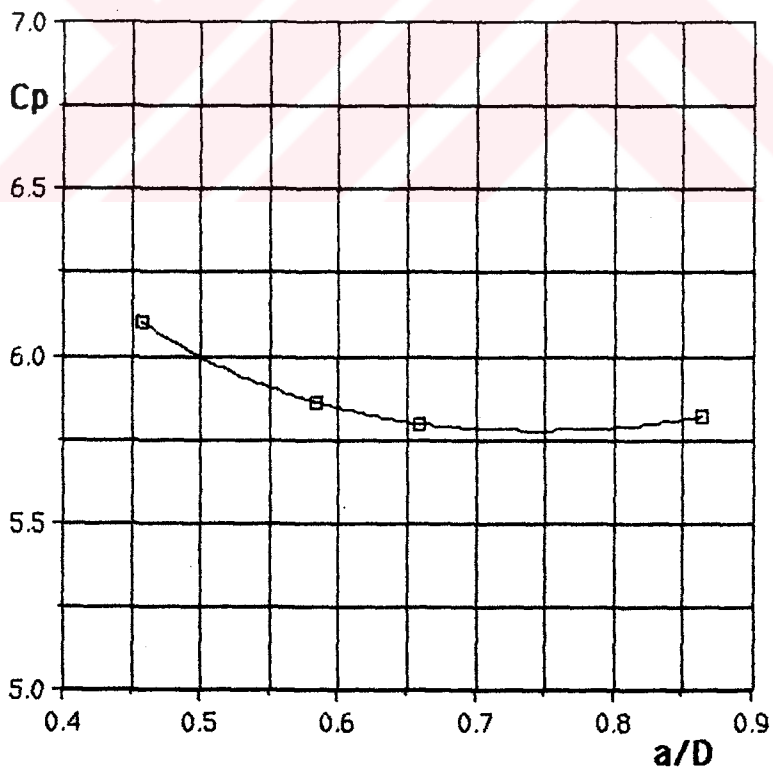
Figure 4.6 Variation of C_p as a function of a/D ratio of the cyclone, independent from Re number.
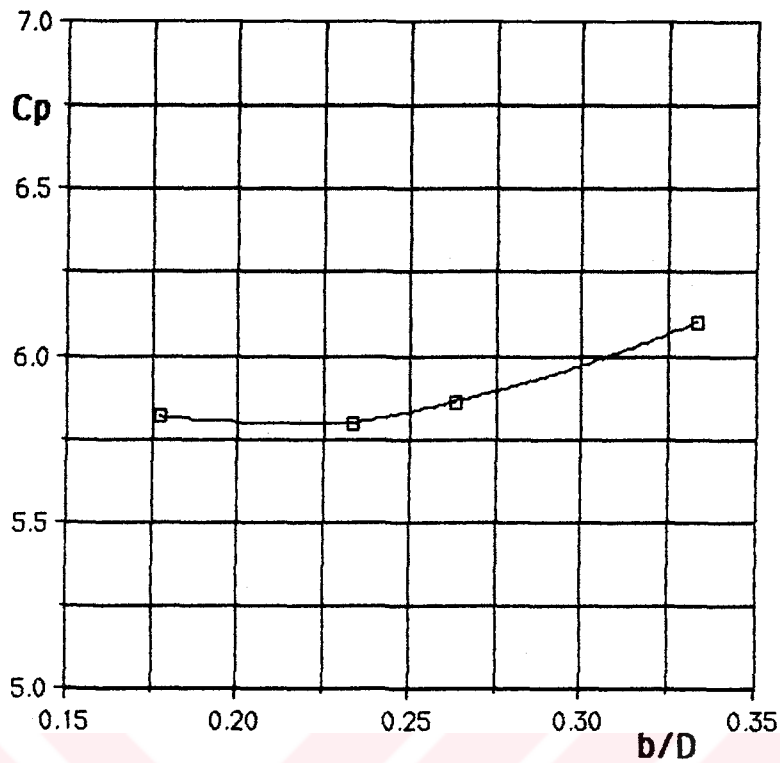
Figure 4.7 Variation of C_p as a function of b/D ratio of the cyclone, independent from Re number.
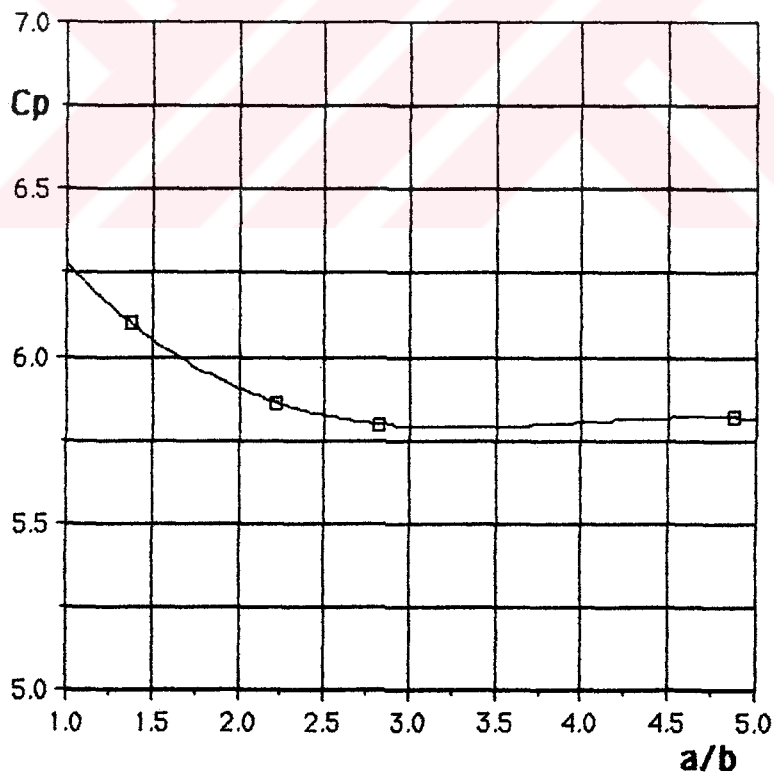
Figure 4.8 Variation of C_p as a function of a/b ratio of the cyclone, independent from Re number.
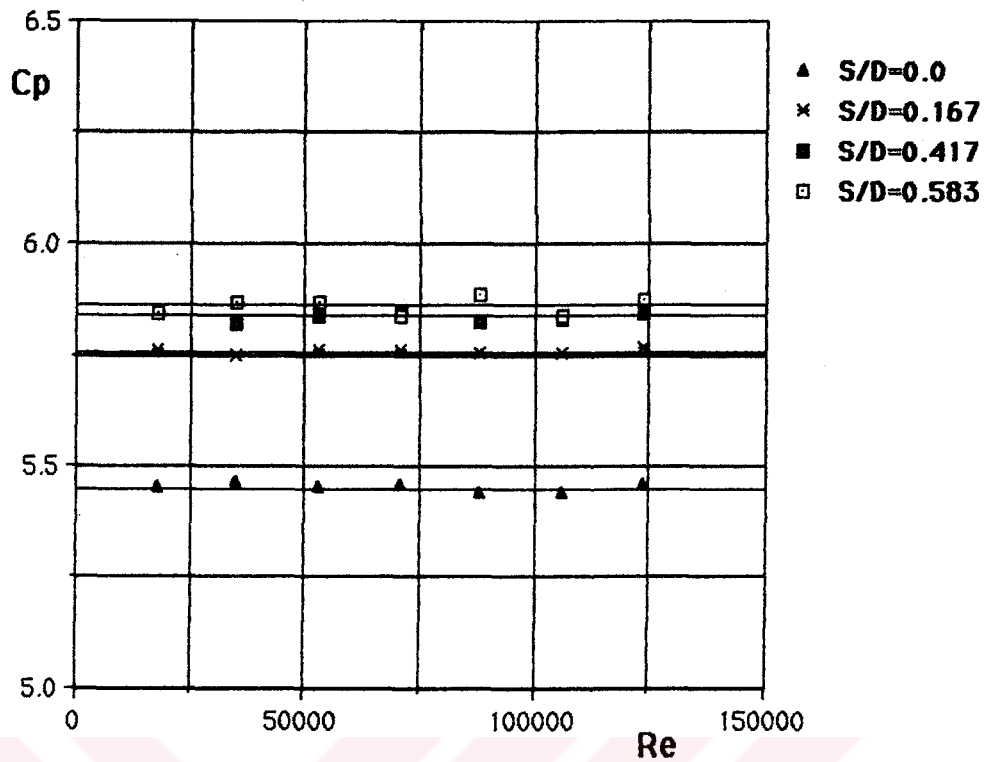
Figure 4.9 Variation of C_p as a function of Re for different S/D ratios of the cyclone.
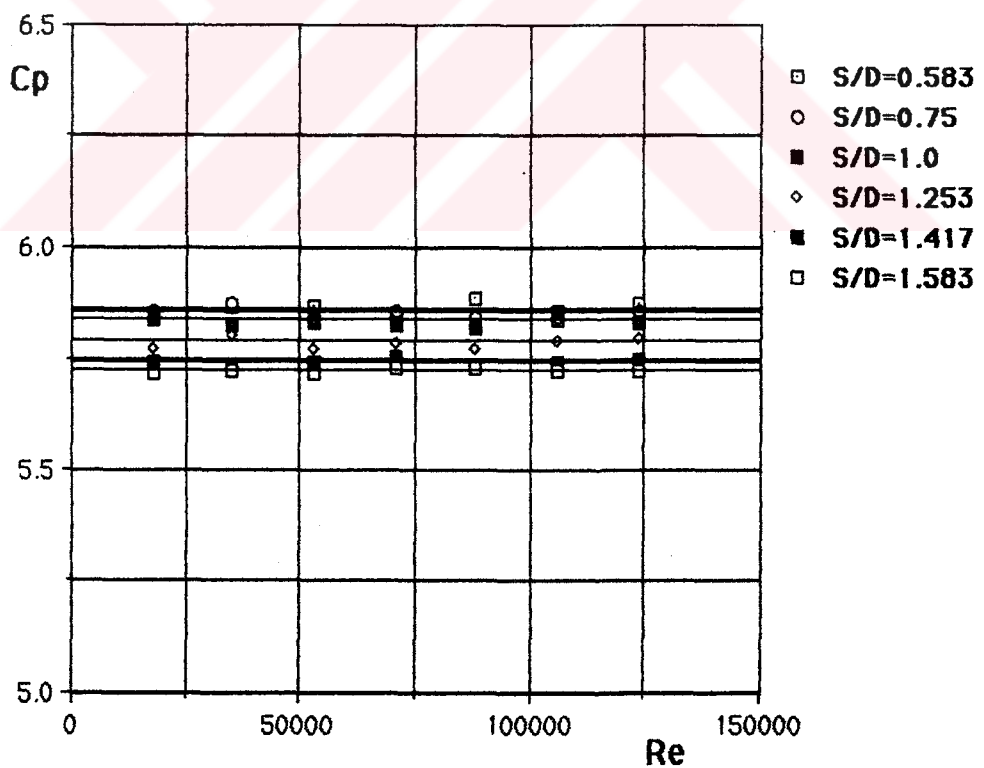
Figure 4.10 Variation of C_p as a function of Re for different S/D ratios of the cyclone.

106
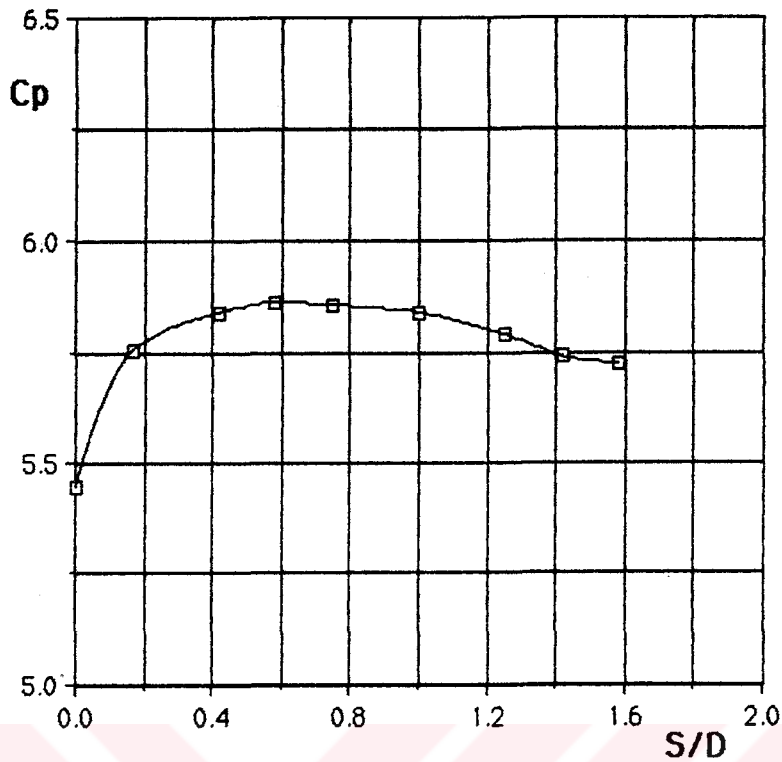
Figure 4.11 Variation of Cp as a function of S/D ratio of the cyclone, independent from Re number.
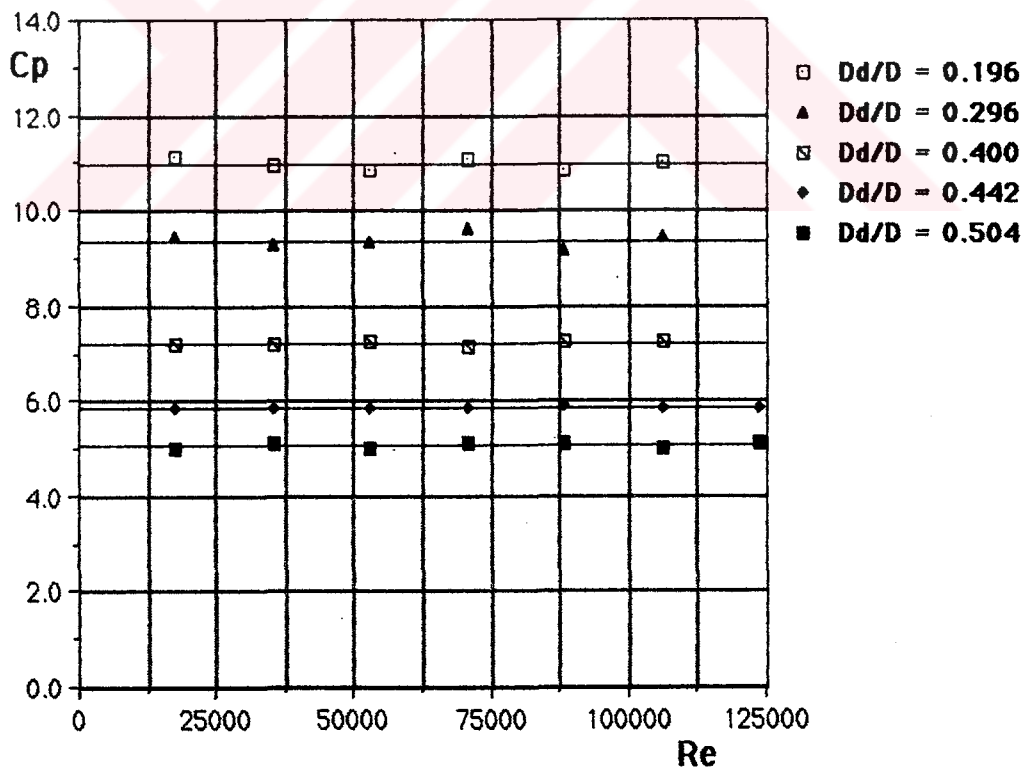
Figure 4.12 Variation of Cp as a function of Re for different Dd/D ratios of the cyclone.
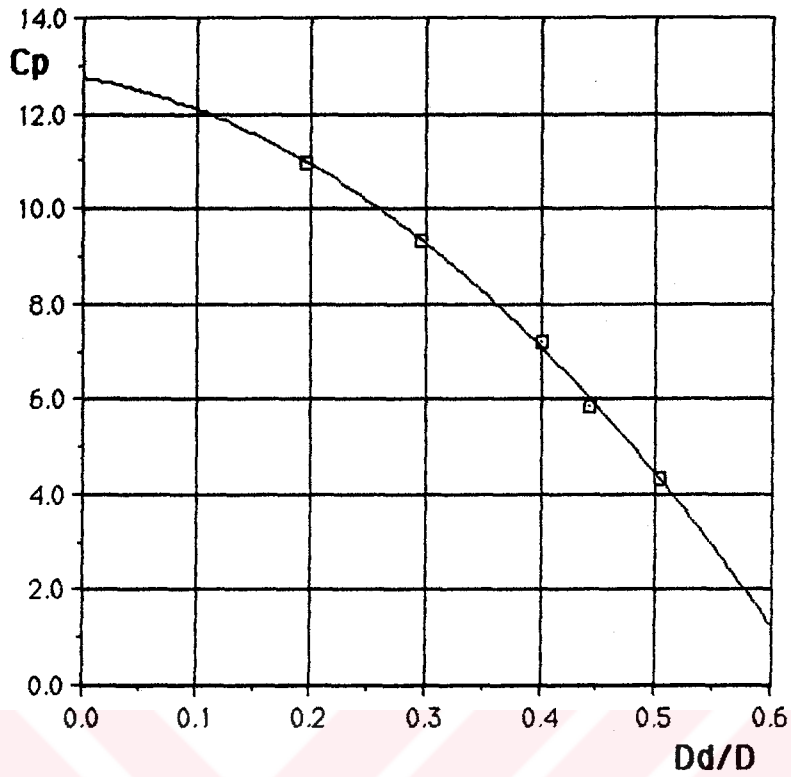
Figure 4.13 Variation of C_p as a function of D_d/D ratio of the cyclone, independent from Re number.
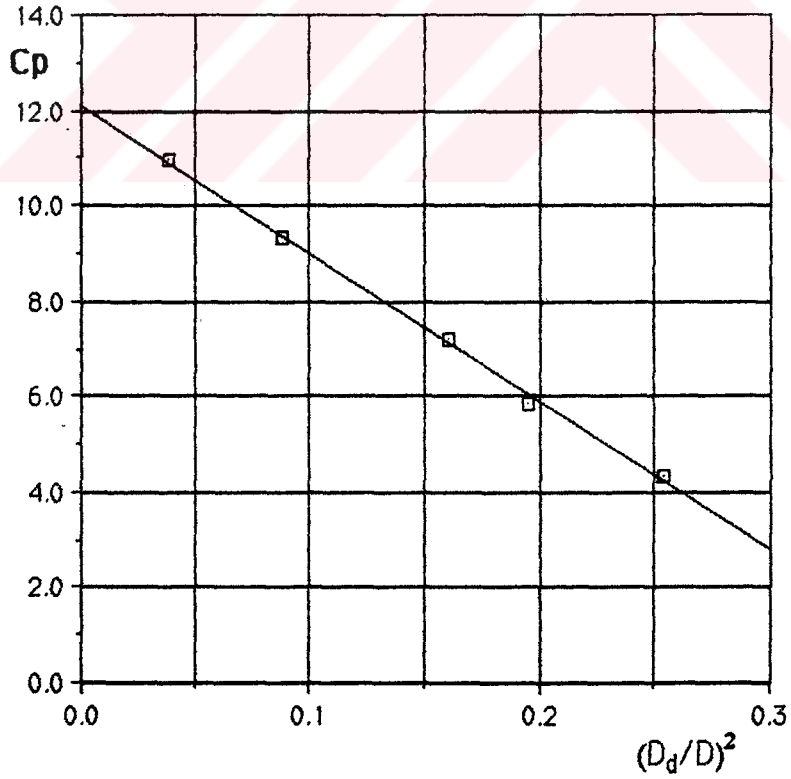
Figure 4.14 Variation of C_p as a function of $(Dd/D)^2$, independent from Re number.
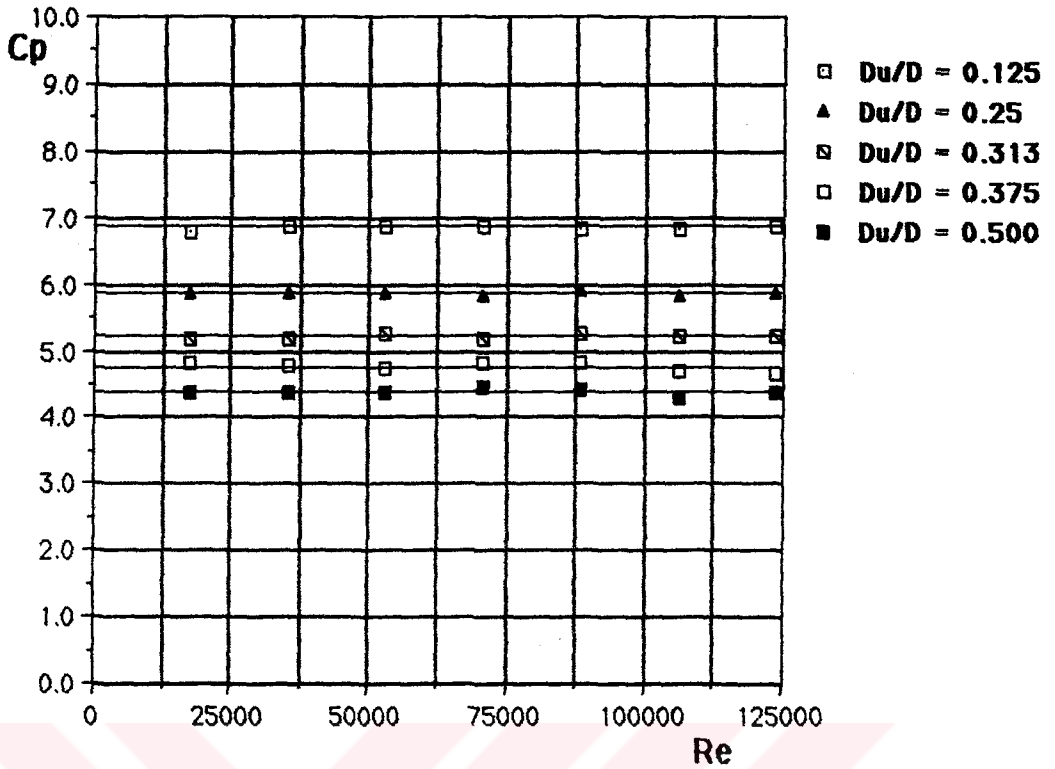
Figure 4.15 Variation of C_p as a function of Re for different D_u/D ratios of the cyclone.
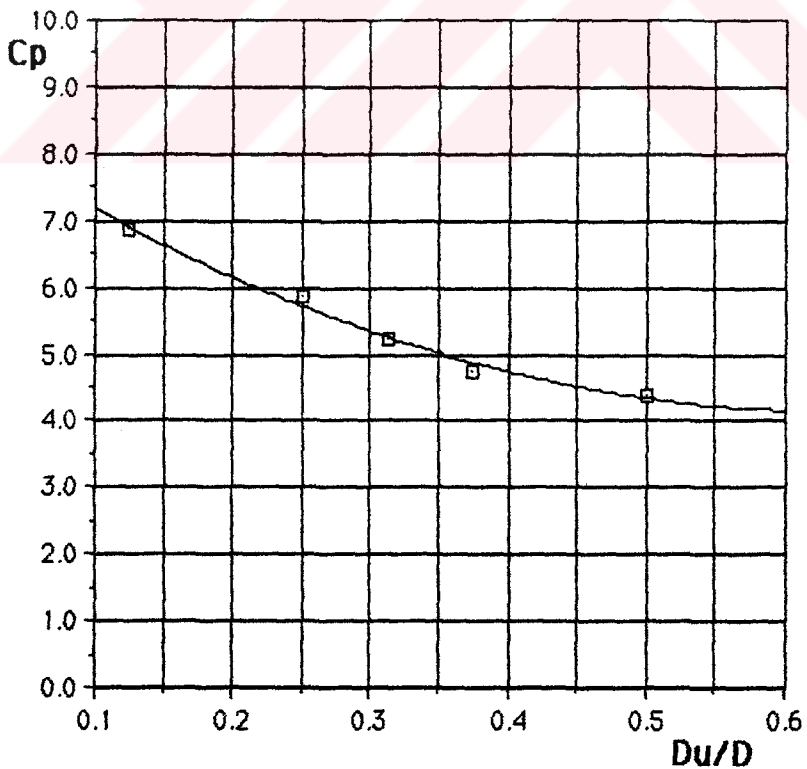
Figure 4.16 Variation of C_p as a function of D_u/D ratio of the cyclone, independent from Re number.
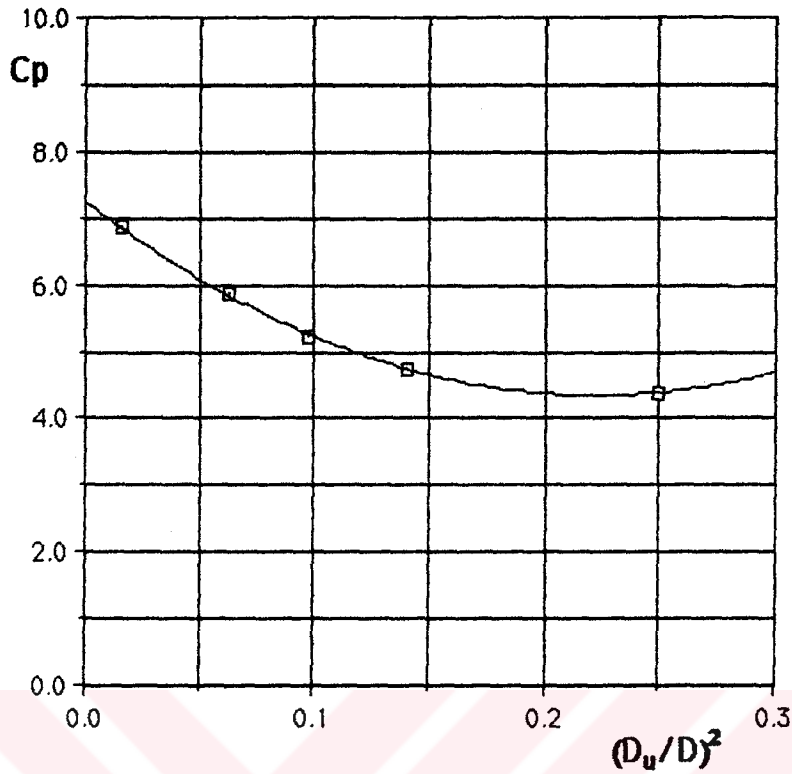
Figure 4.17 Variation of C_p as a function of $(D_u/D)^2$, independent from Re.
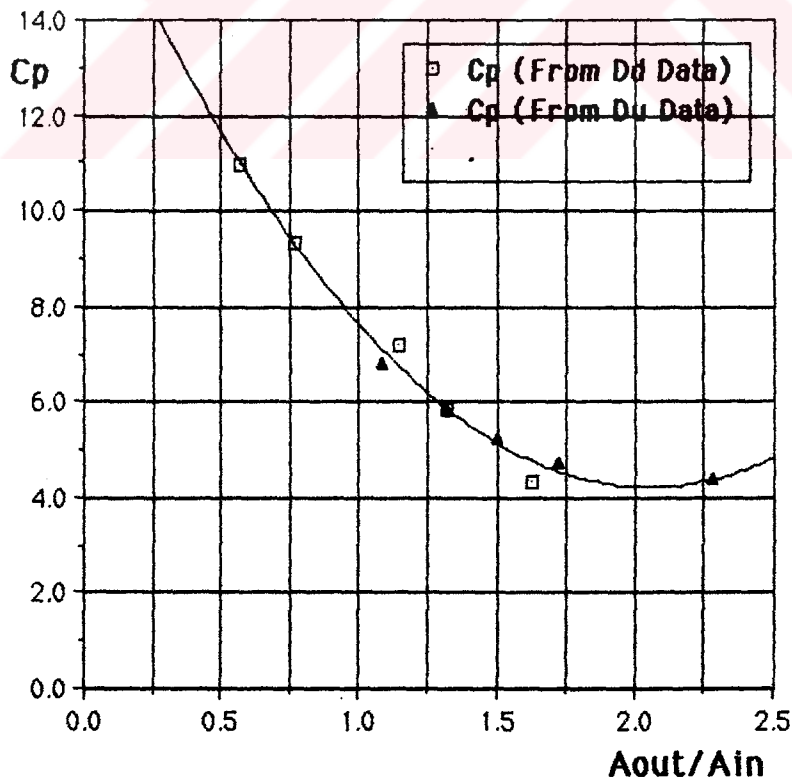
Figure 4.18 Variation of C_p as a function of A_{out}/A_{in} ratio of the cyclone, independent from Re number.
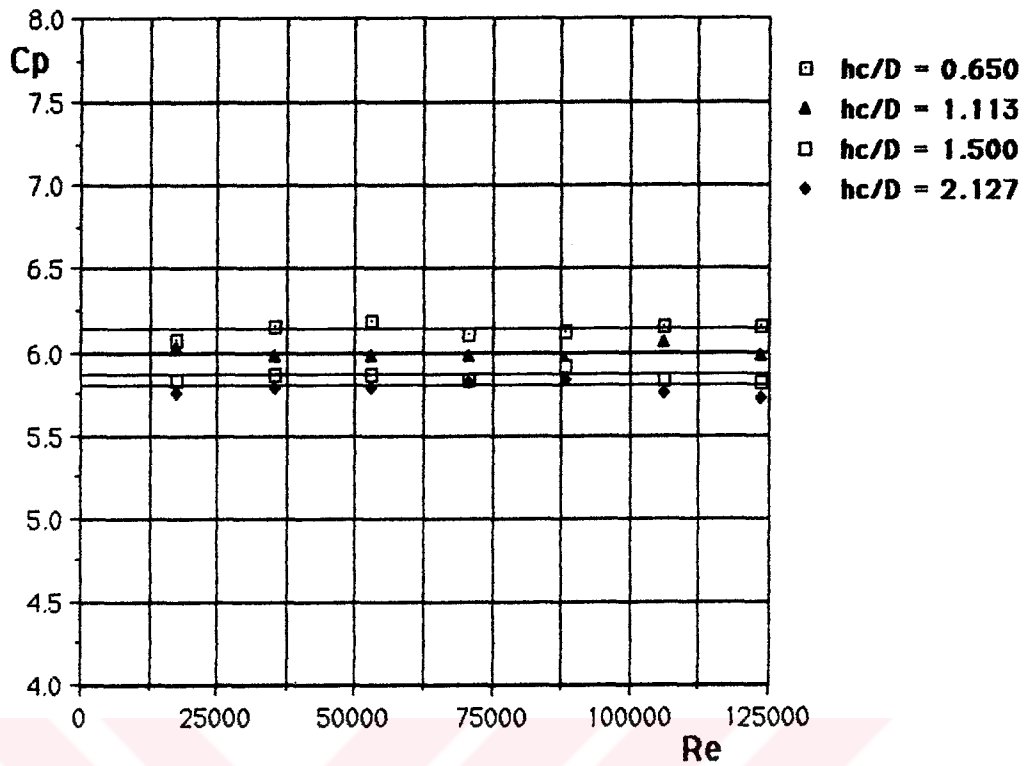
Figure 4.19 Variation of C_p as a function of Re for different h_C/D ratios of the cyclone.
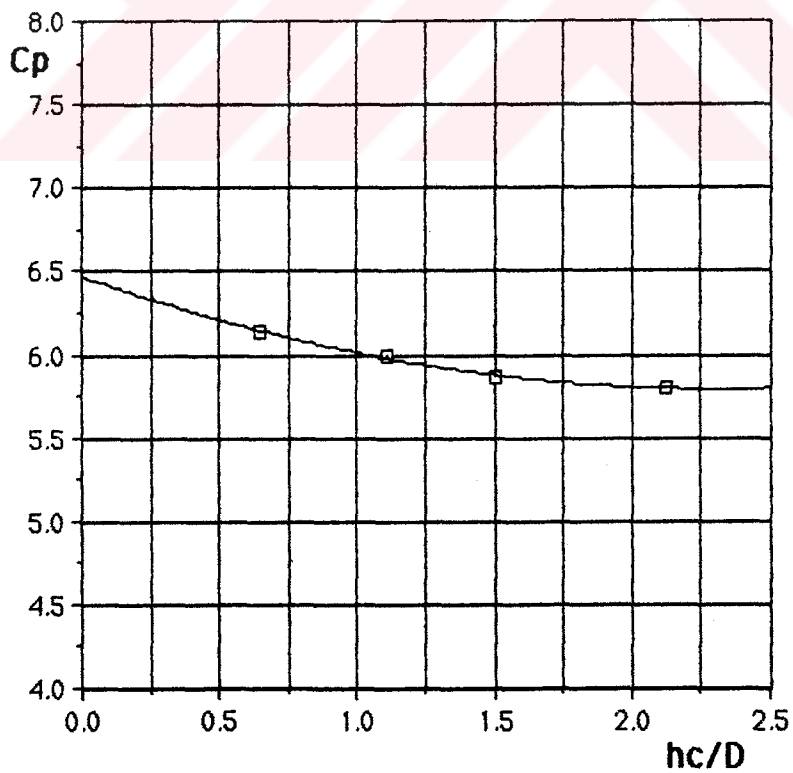
Figure 4.20 Variation of C_p as a function of h_C/D ratio of the cyclone, independent from Re number.
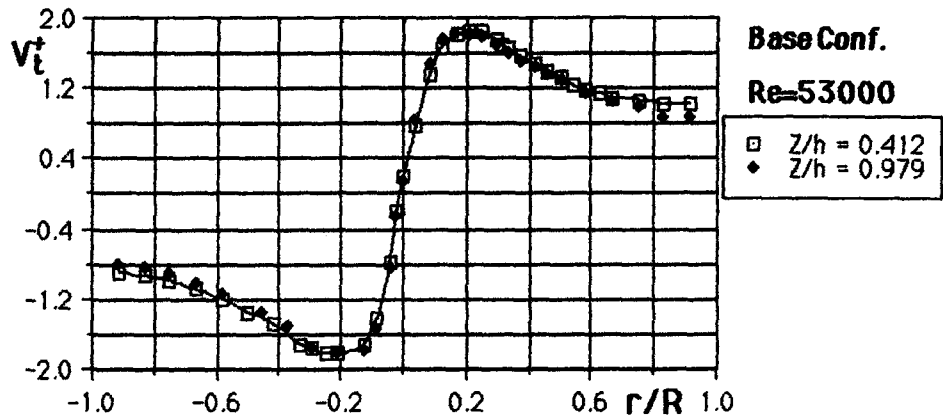
(a)
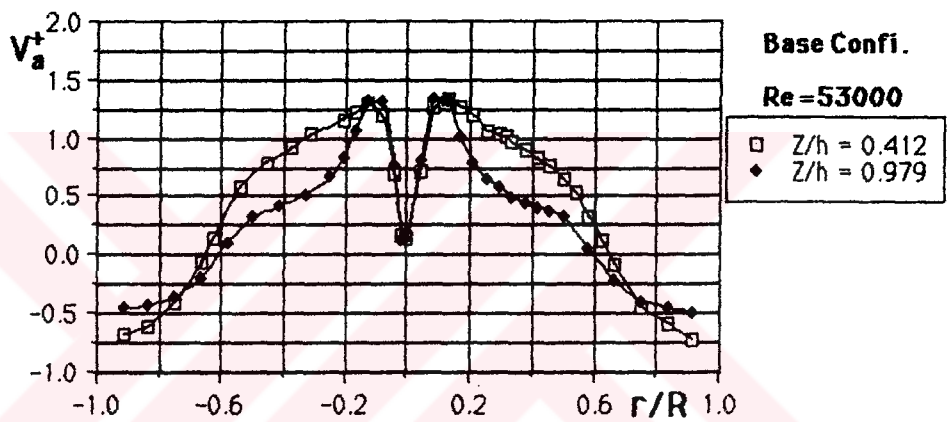
(b)
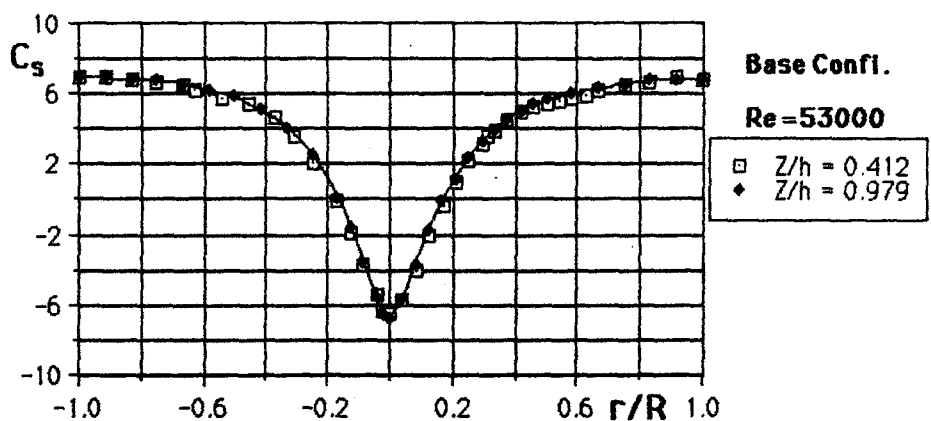
(c)

Figure 4.21 Radial distributions of dimensionless tangential velocity (a), axial velocity (b), and static pressure coefficient (c) on the cyclone at vertical measurement stations of Z/h =0.412 and Z/h=0.979 for Re=53000.
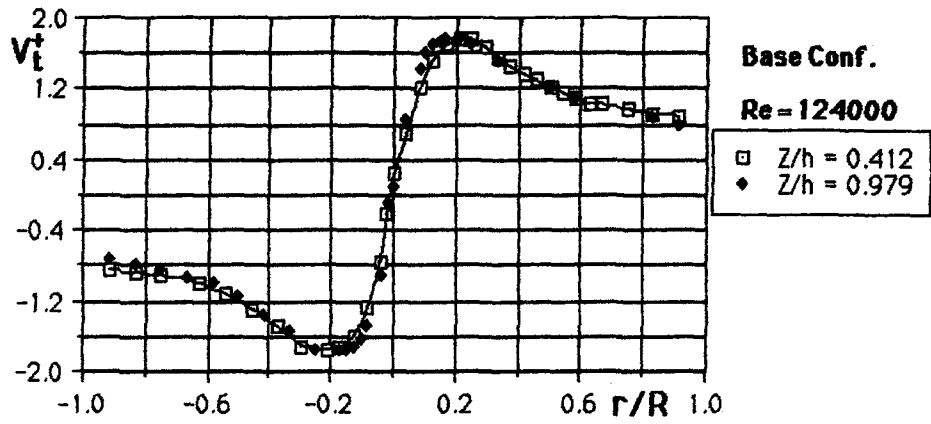
(a)
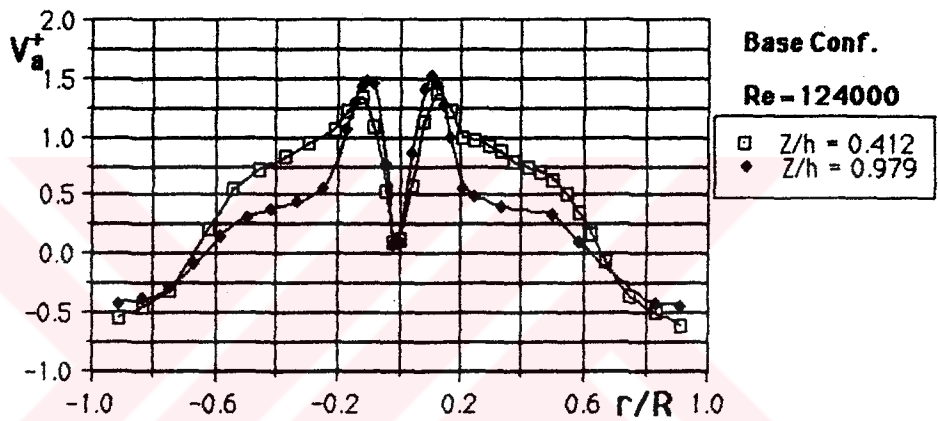
(b)
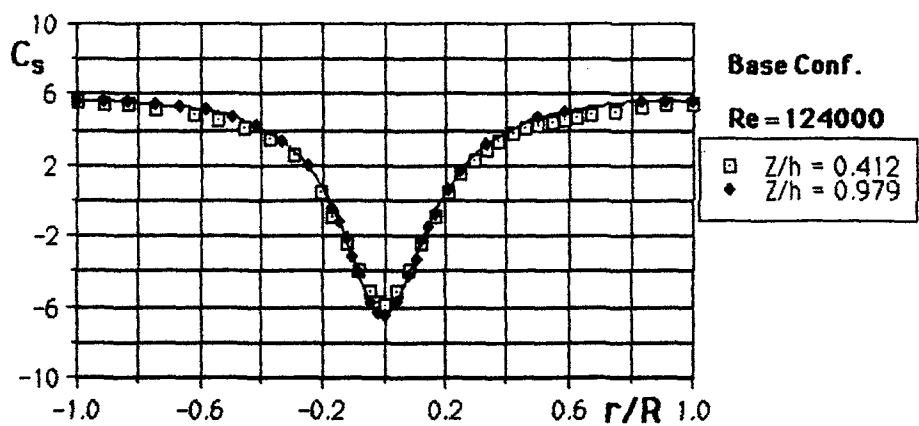
(c)

Figure 4.22 Radial distributions of dimensionless tangential velocity (a), axial velocity (b), and static pressure coefficient (c) on the cyclone at vertical measurement stations of Z/h =0.412 and Z/h=0.979 forRe=124000.
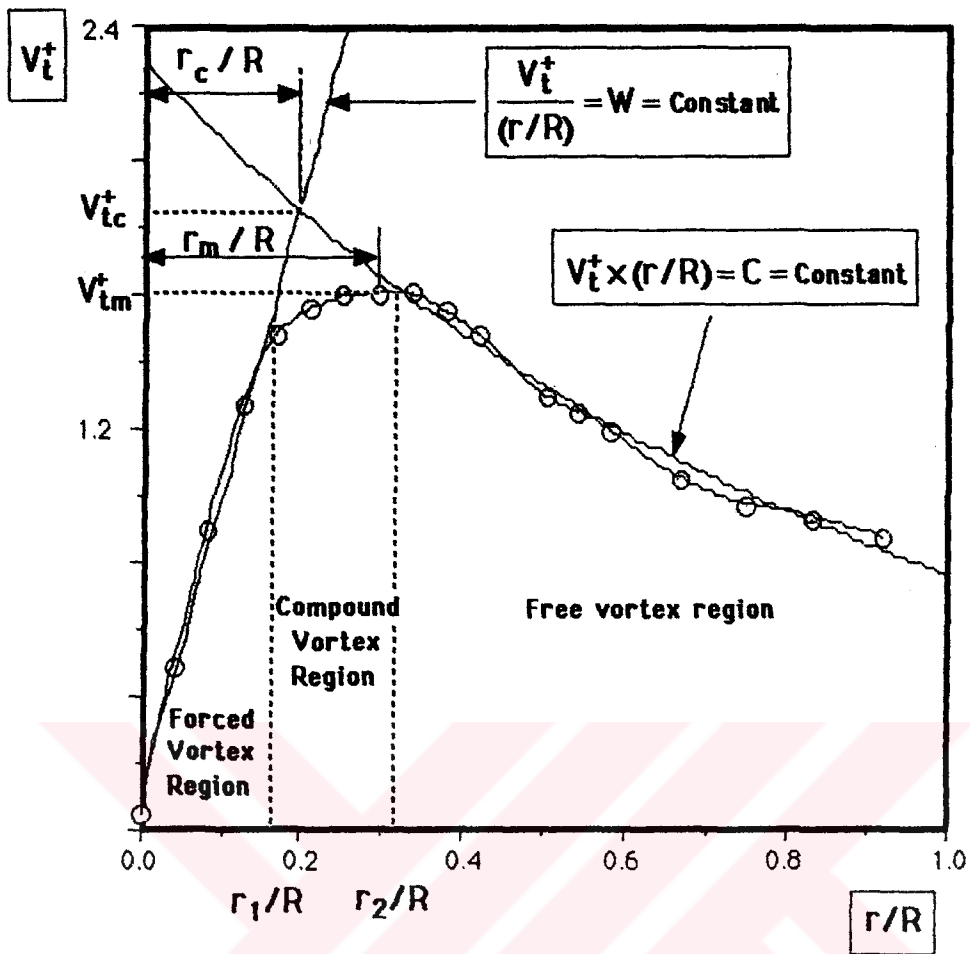
Figure 4.23 Characteristic radial distribution of the dimensionless tangential velocity on the cyclone cylindrical body.
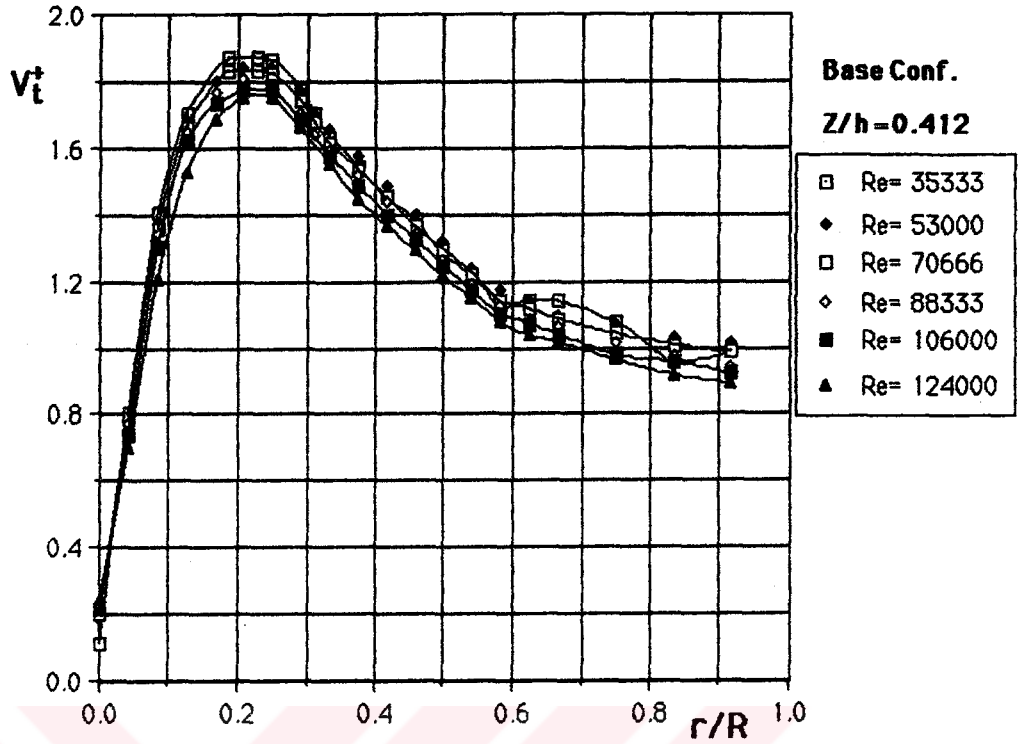
Figure 4. 24 Radial distribution of dimensionless tangential velocity on the basic cyclone configuration for different Re values at Z/h=0.412.
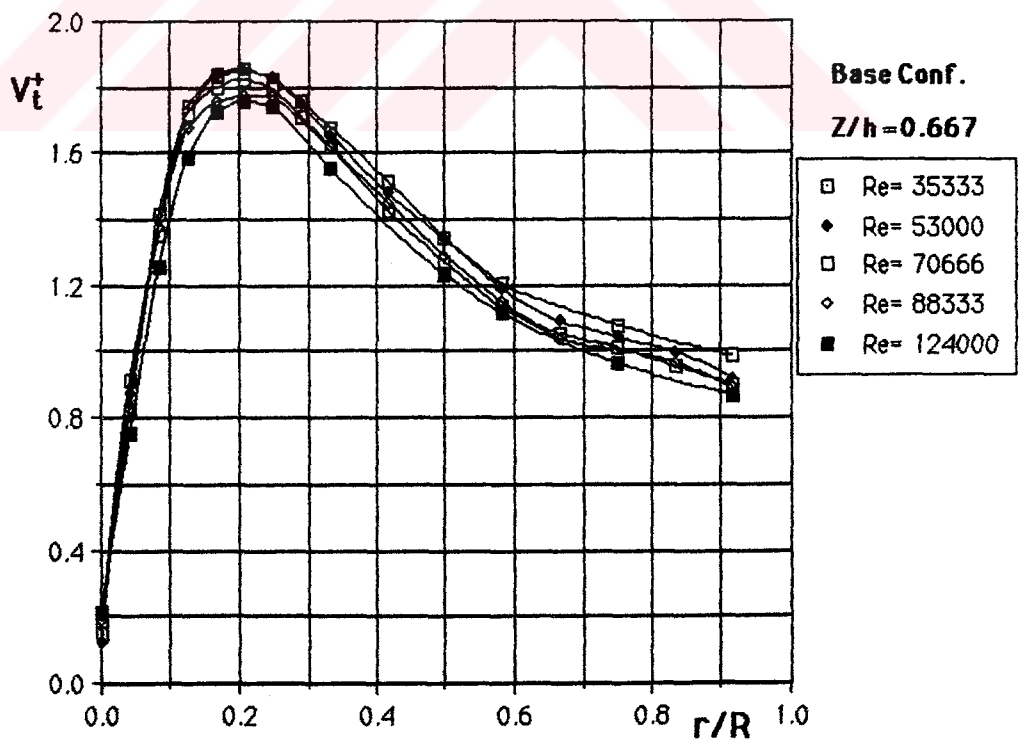
Fig. 4. 25 Radial distribution of dimensionless tangential velocity on the basic cyclone configuration for different Re values at Z/h=0.667.
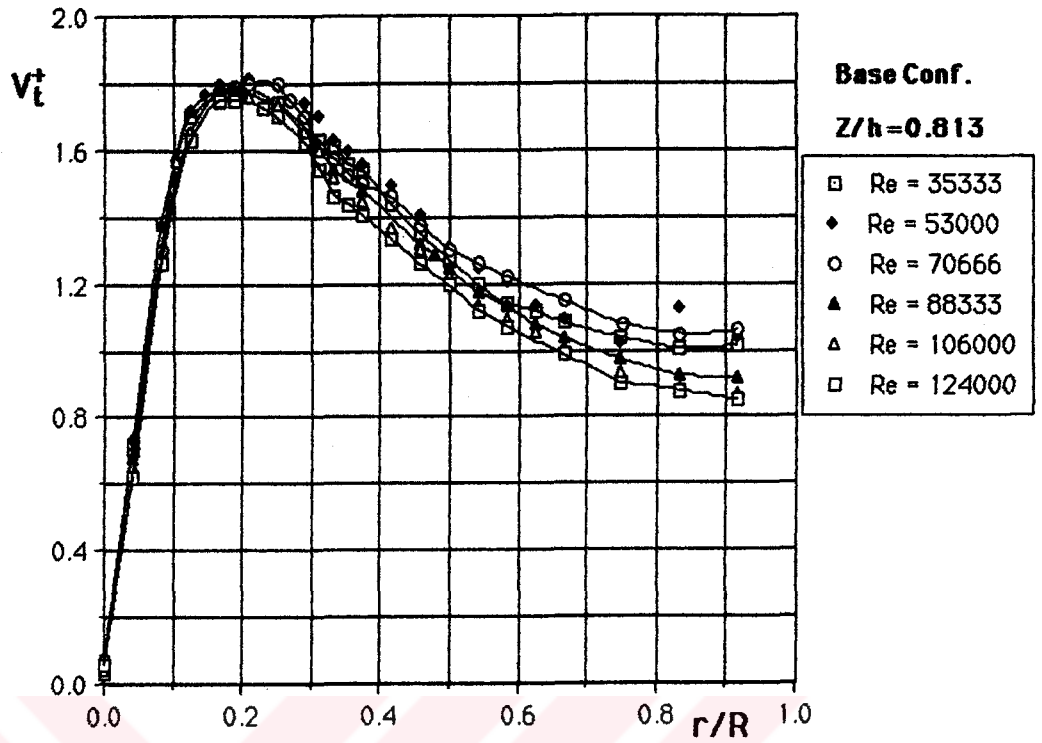
Figure 4. 26 Radial distribution of dimensionless tangential velocity on the basic cyclone configuration for different Re values at Z/h=0.813.
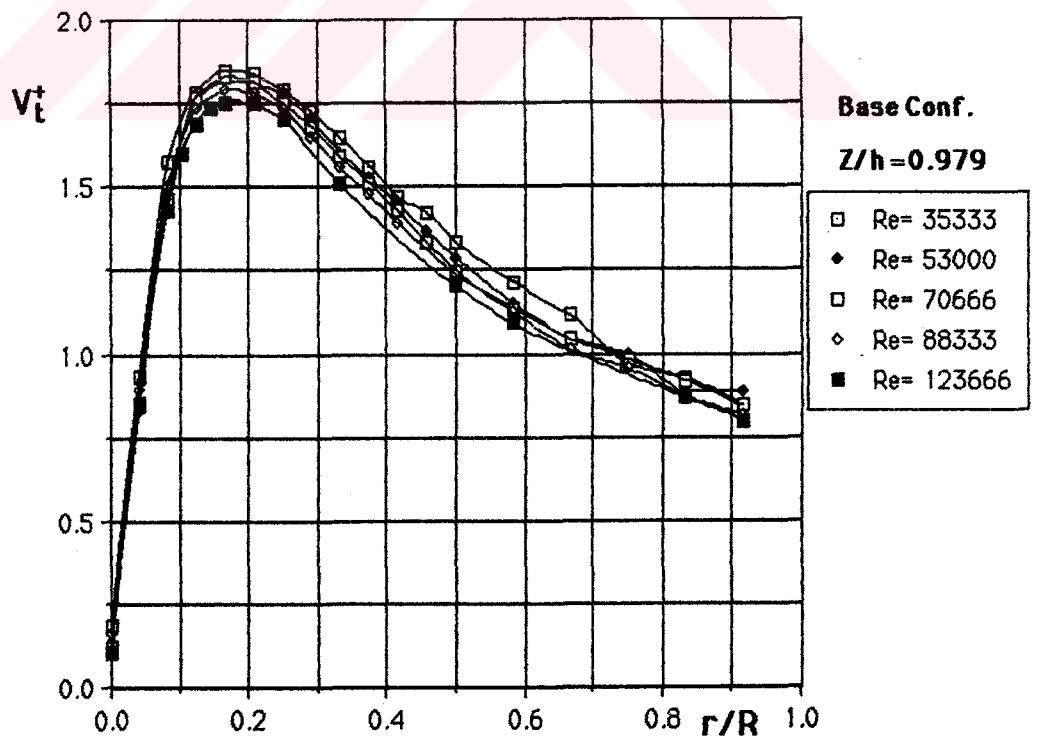
Figure 4. 27 Radial distribution of dimensionless tangential velocity on the basic cyclone configuration for different Re values at Z/h=0.979.
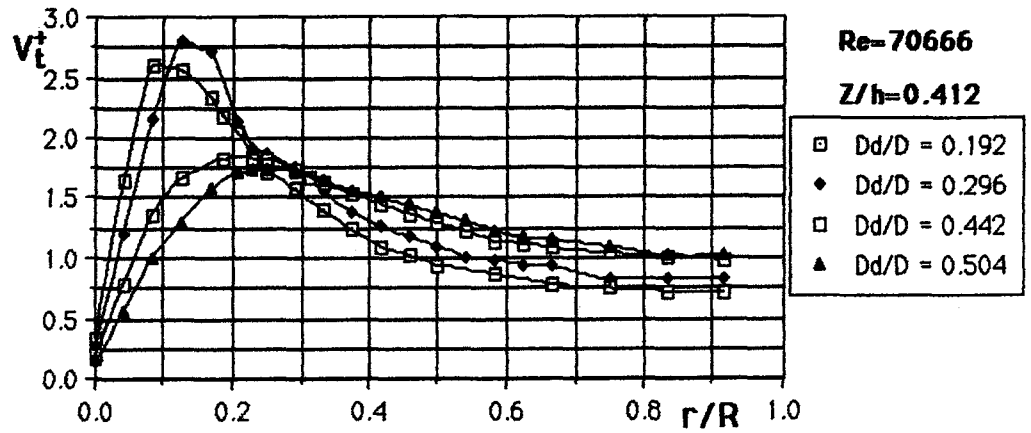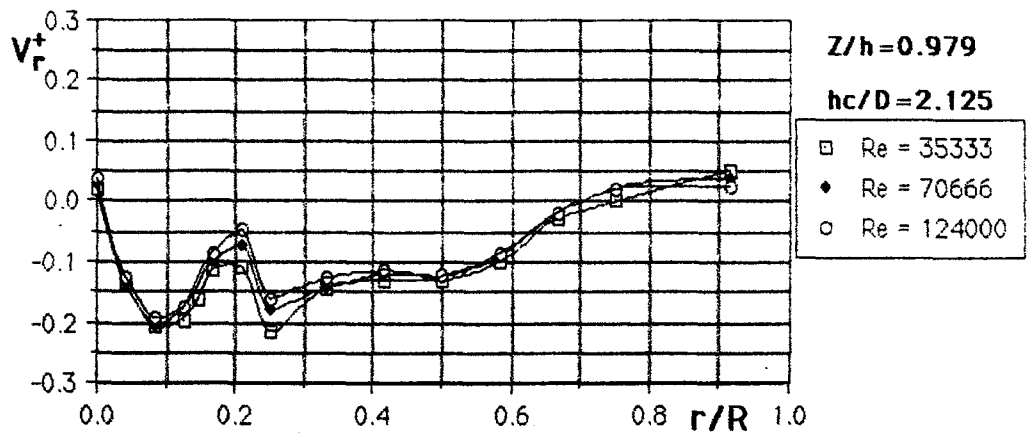
(a)
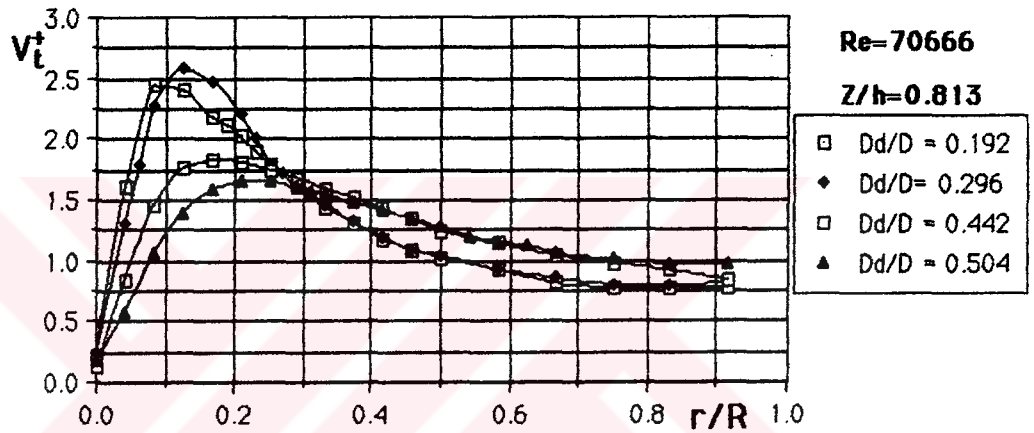
(b)
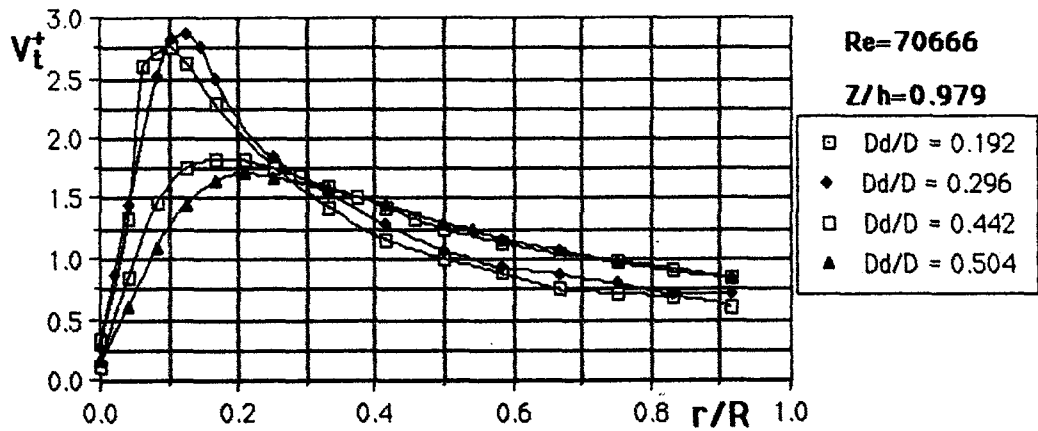
(c)

Figure 4.28 Radial distribution of dimensionless tangential velocity on the cyclone having different Dd/D ratios for Re= 70666 at Z/h=0.412, Z/h=0.813 and Z/h=0.979, respectively.
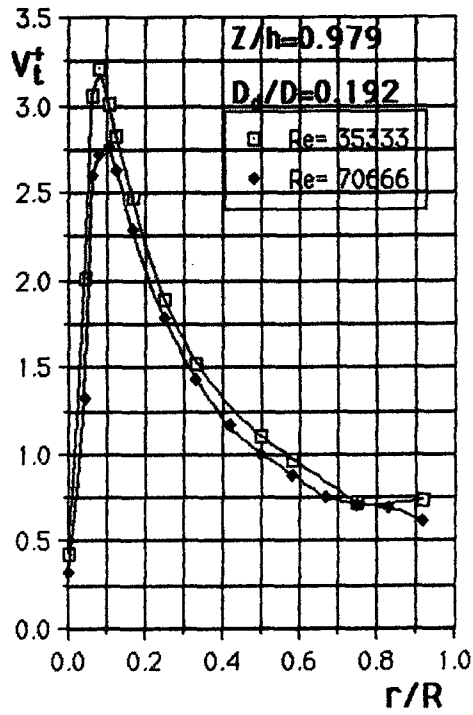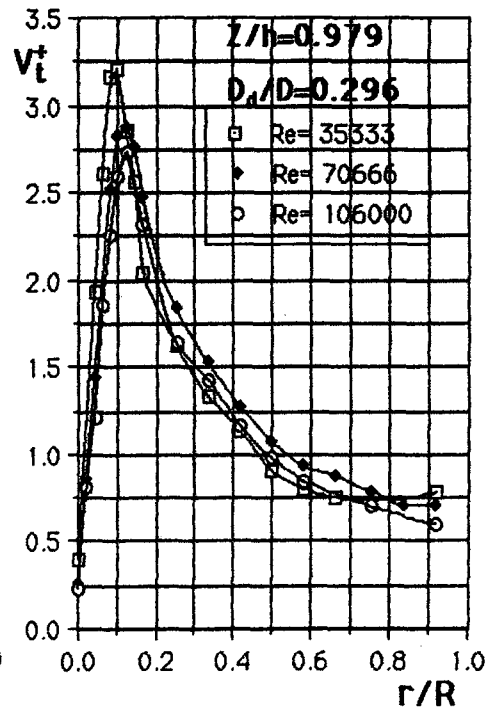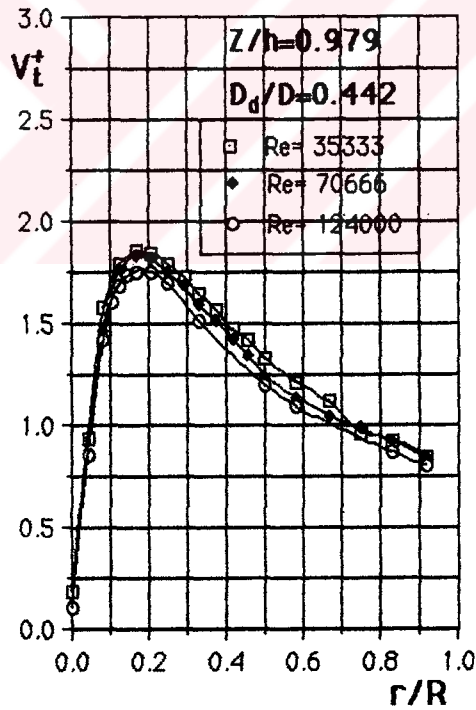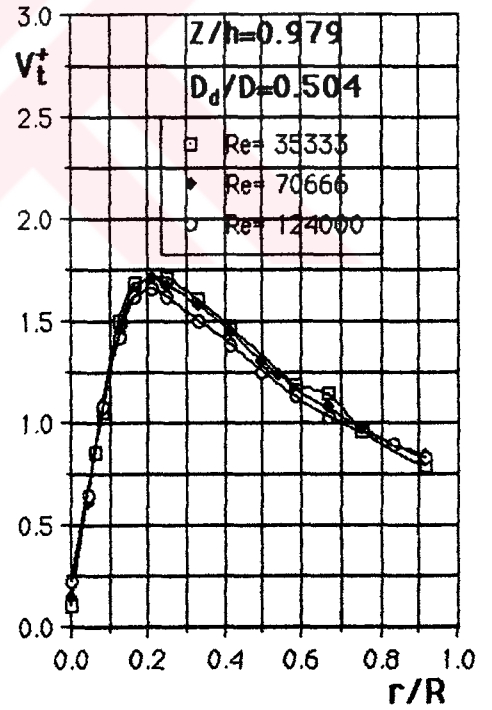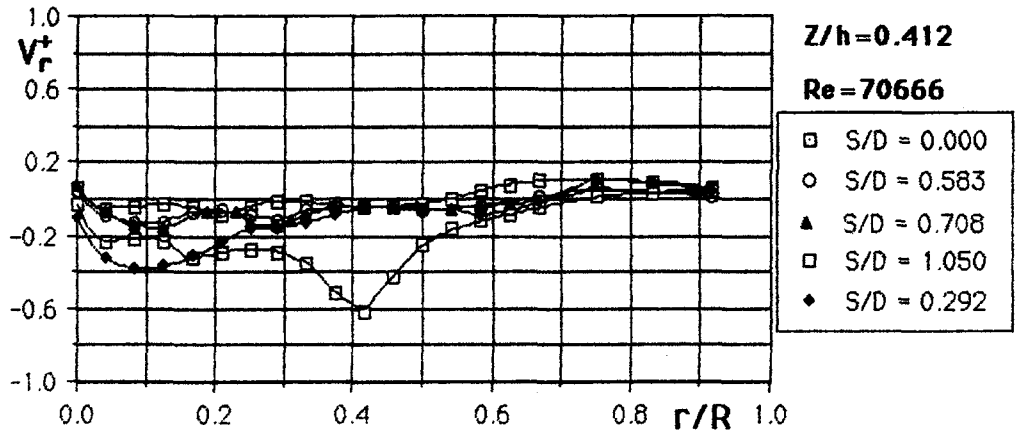
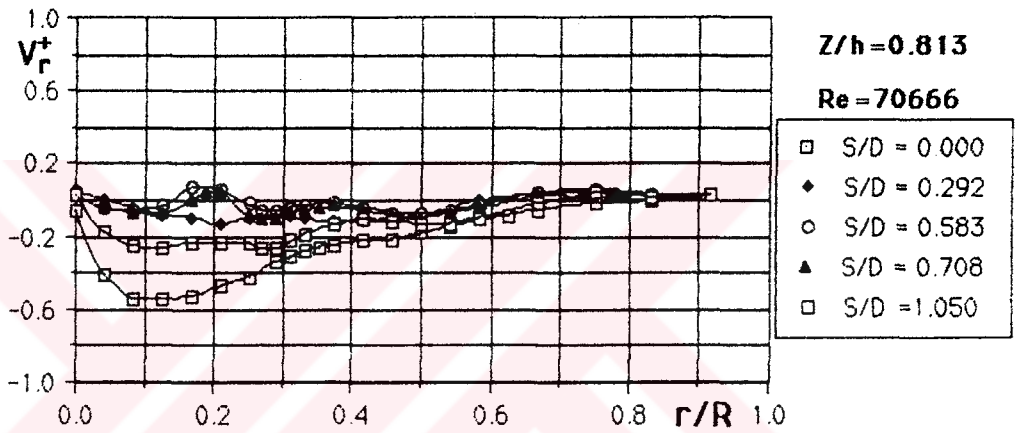Figure 4.29 Radial distributions of dimensionless tangential velocity for different Re values on the cyclone having De/D ratios of 0.192, 0.296, 0.442 and 0.504 at Z/h=0.979, respectively.
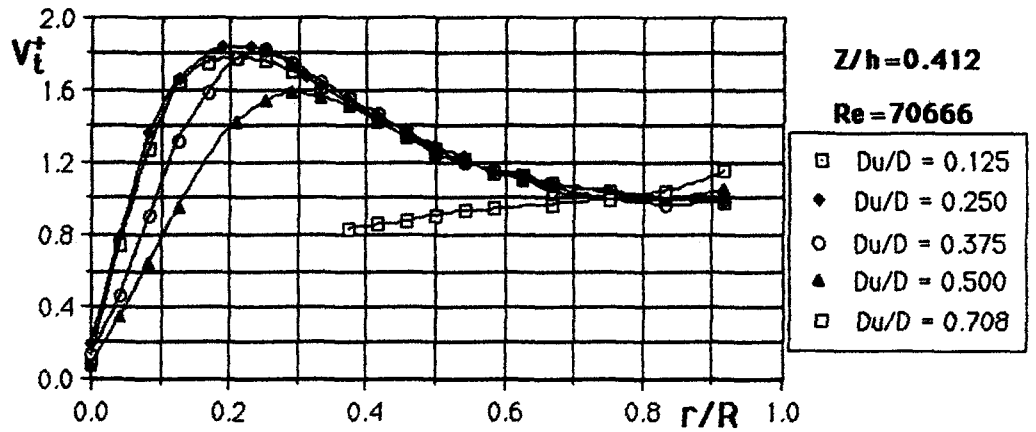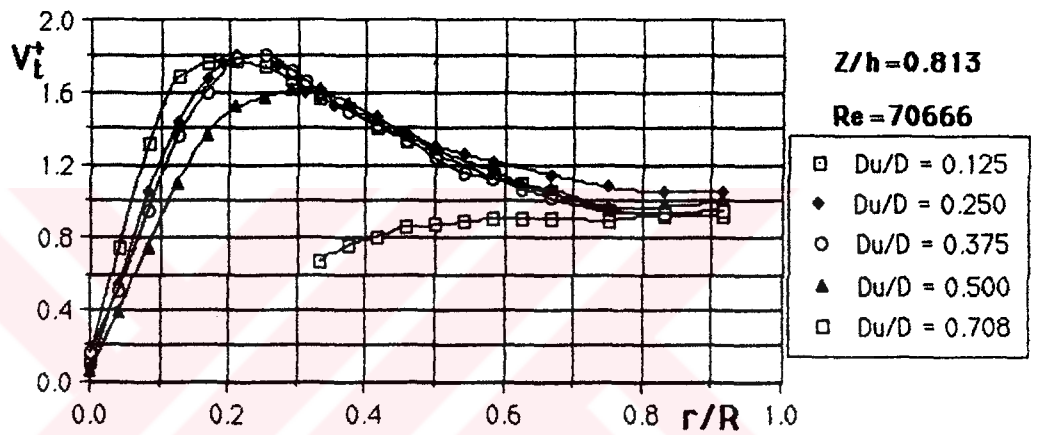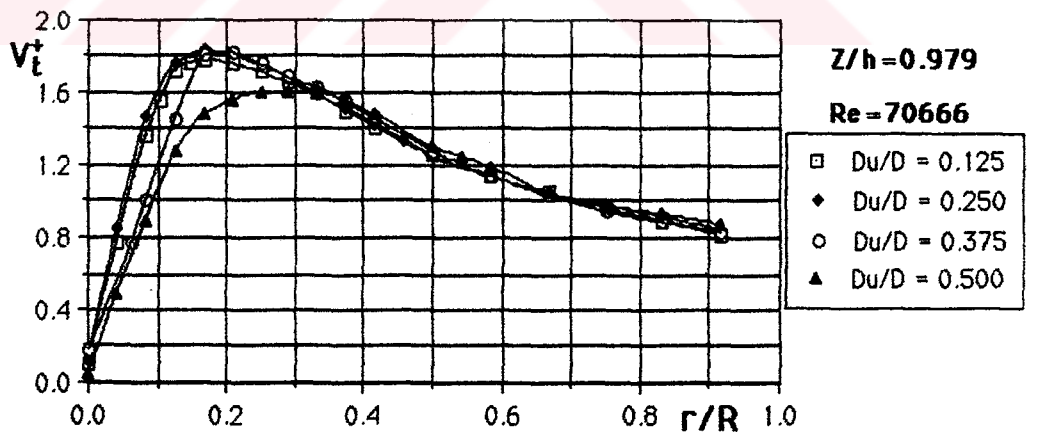
Figure 4.30 Radial distributions of dimensionless tangential velocity on the cyclone having different Du/D ratios for Re=70666 at Z/h= 0.412, Z/h=0.813 and Z/h=0.979, respectively.
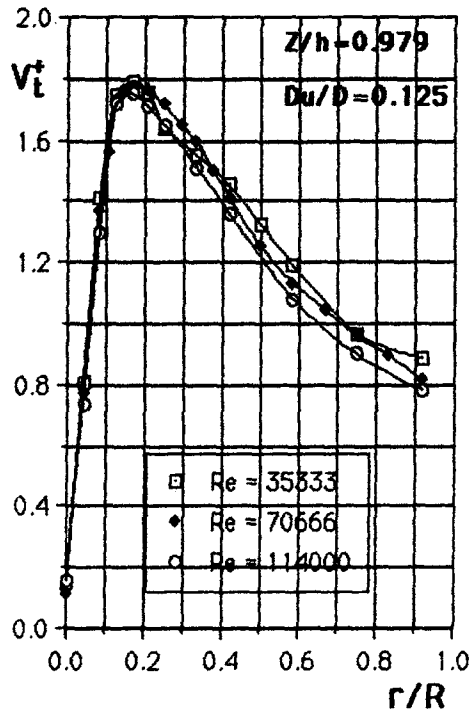
(a)
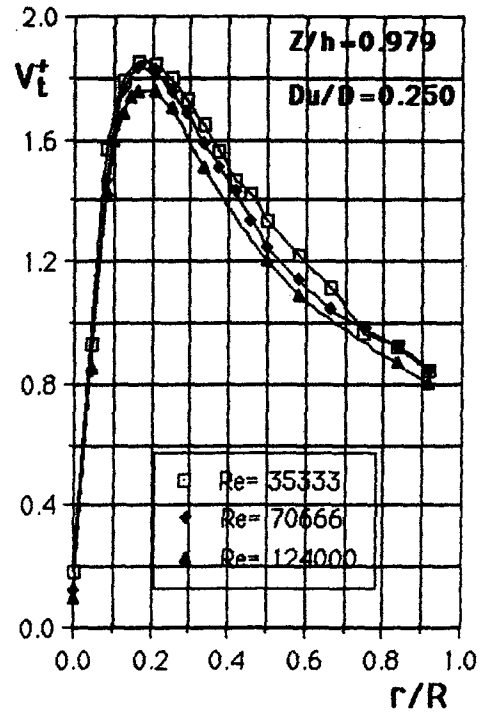
(b)
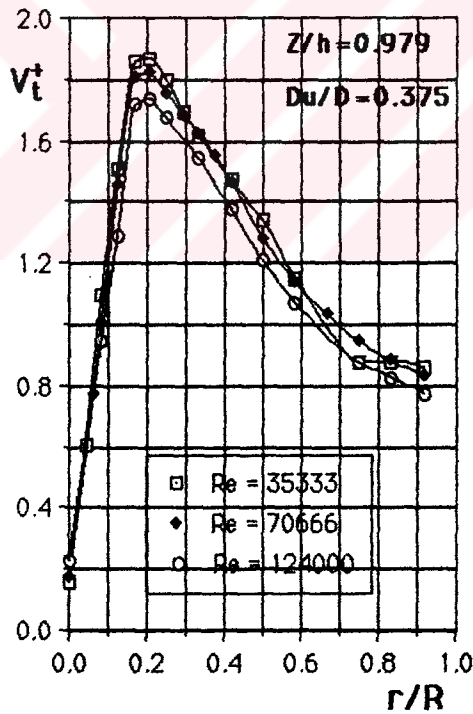
(c)
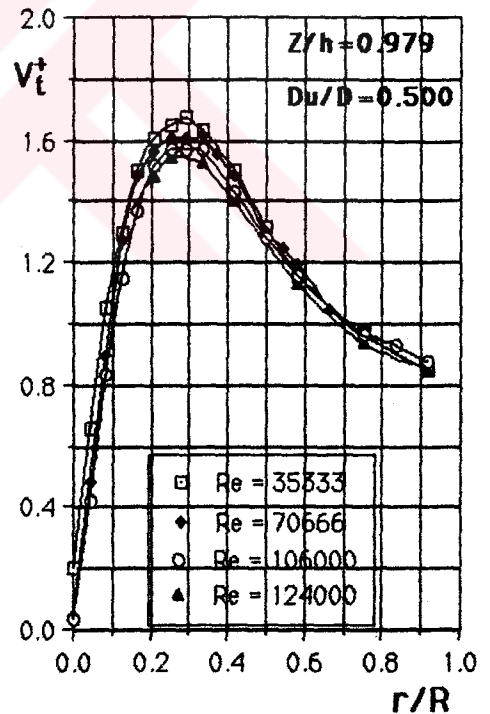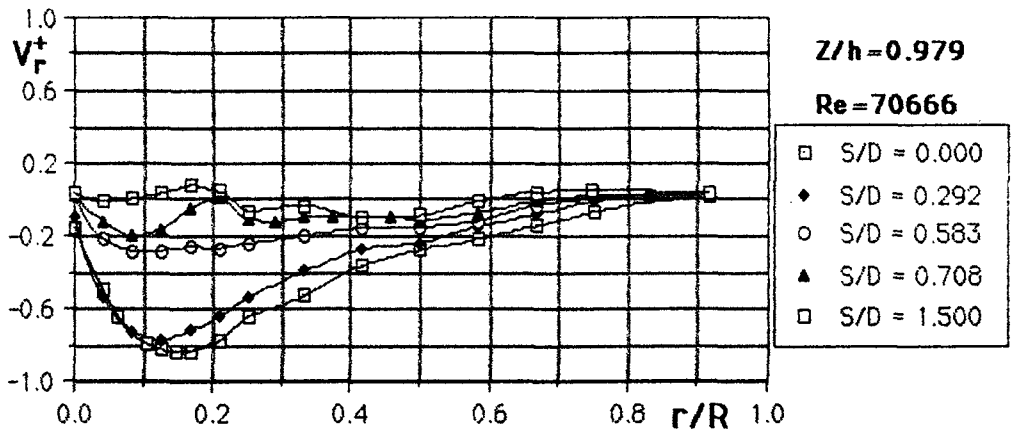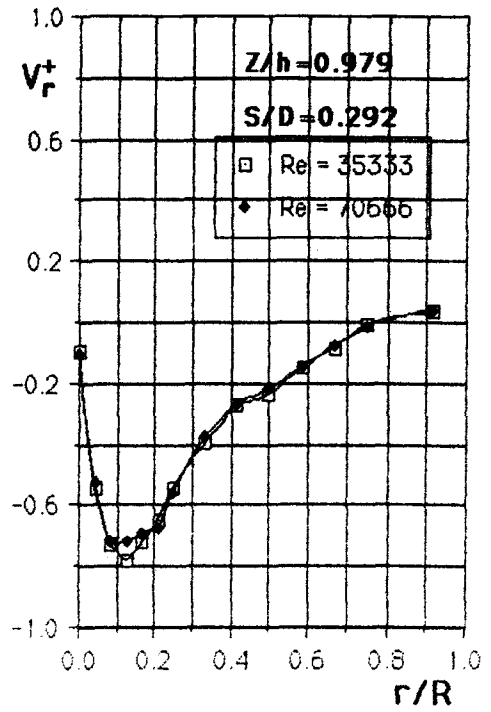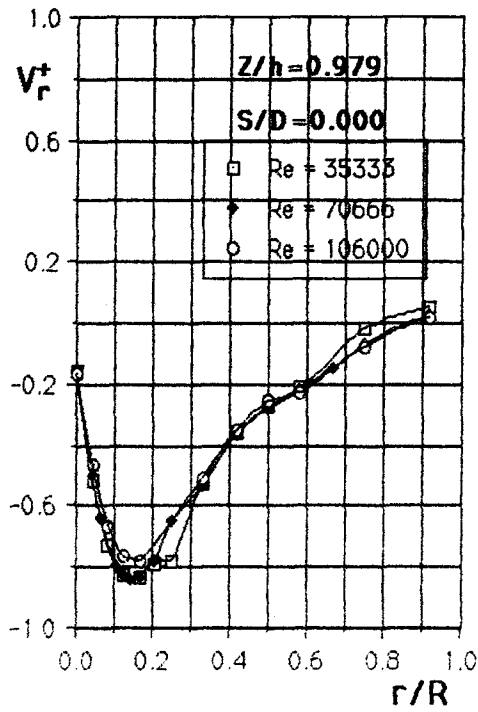
(d)

Figure 4.31 Radial distributions of dimensionless tangential velocity for different Re values on the cyclone having Du/D ratios of 0.125, 0.250, 0.375 and 0.500 at Z/h=0.979, respectively.
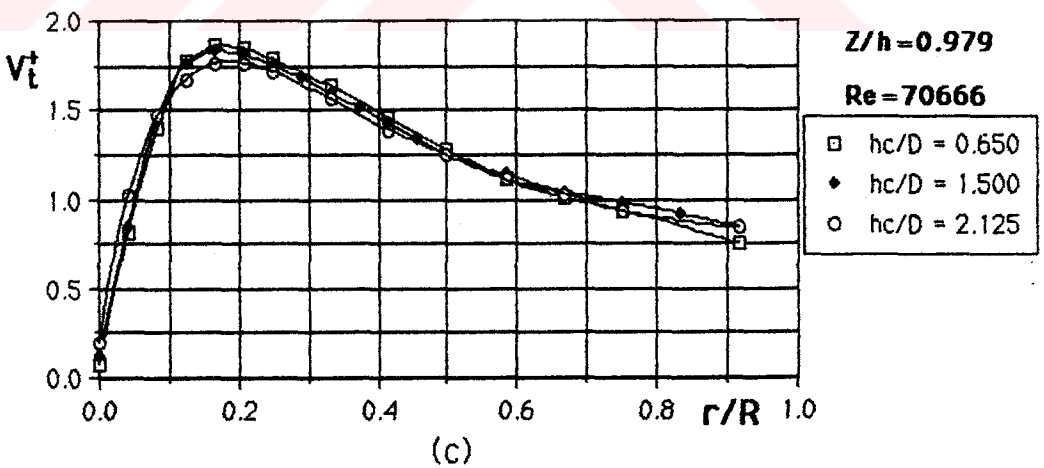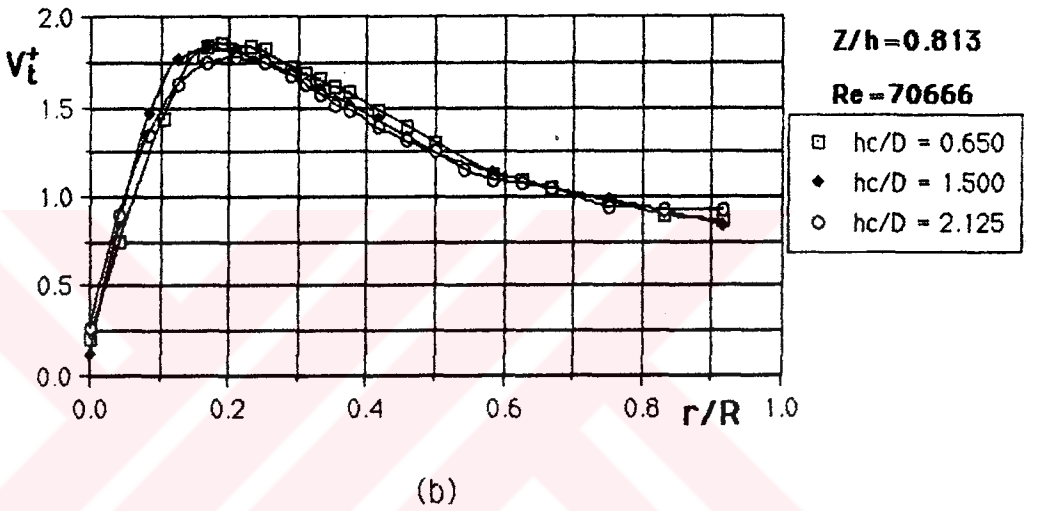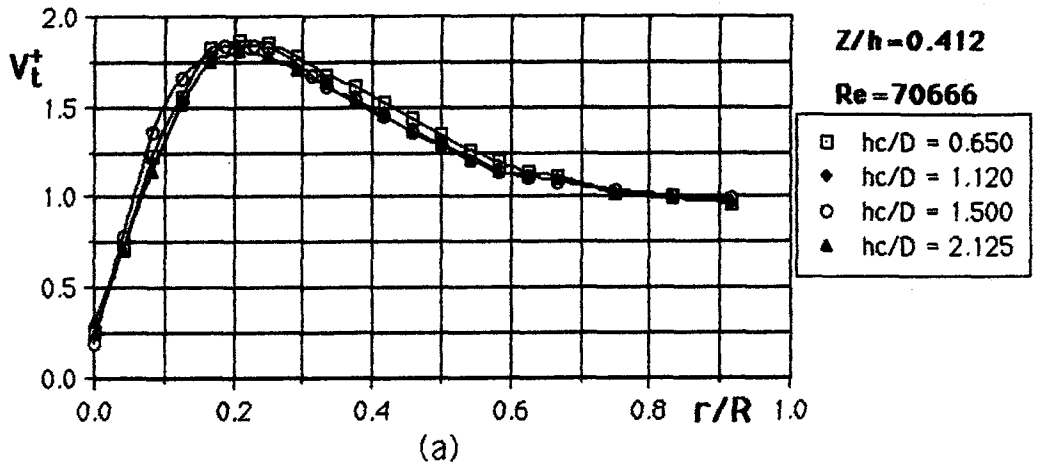
Figure 4.32 Radial distributions of dimensionless tangential velocity on the cyclone having different h_c/D ratios for Re=70666 at Z/h= 0.412, Z/h=0.813 and Z/h=0.979, respectively.
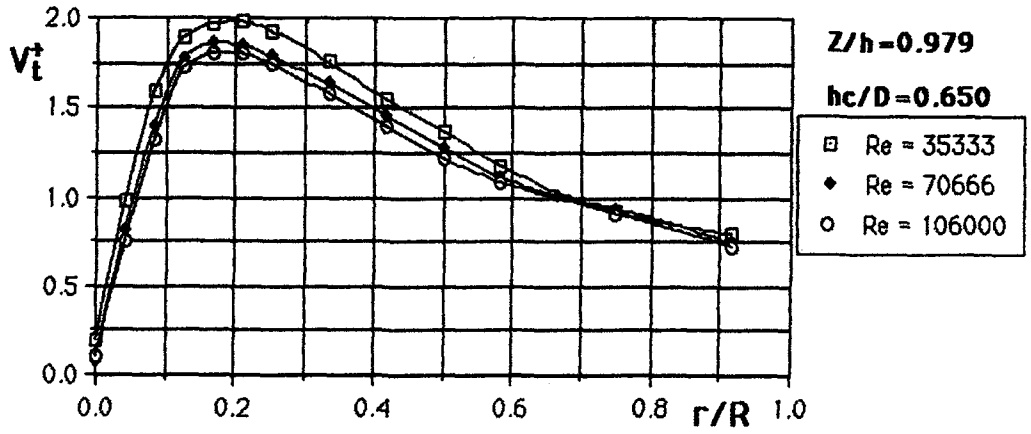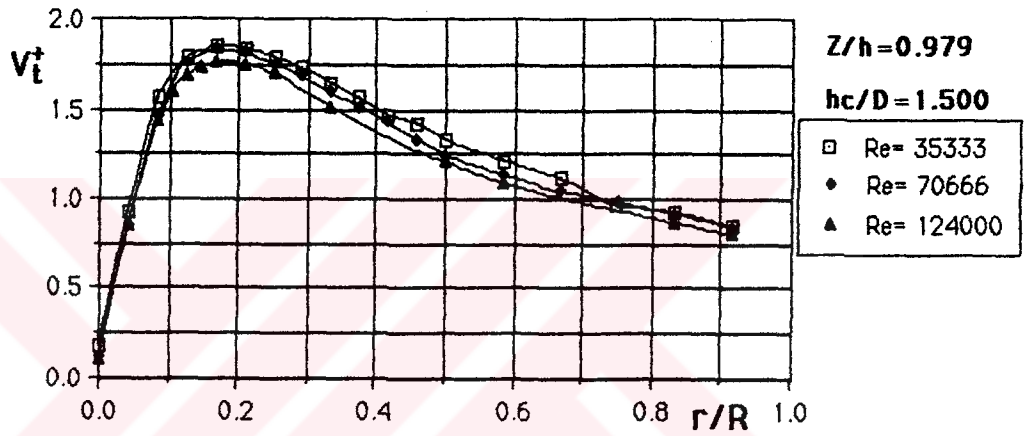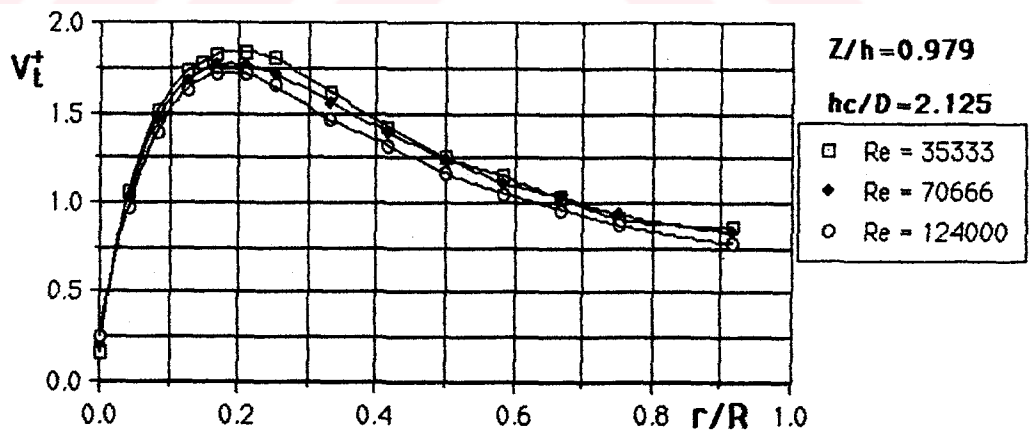
Figure 4.33 Radial distributions of dimensionless tangential velocity for different Re values on the cyclone having h_c/D ratios of 0.650, 1.500 and 2.125 at Z/h=0.979, respectively.
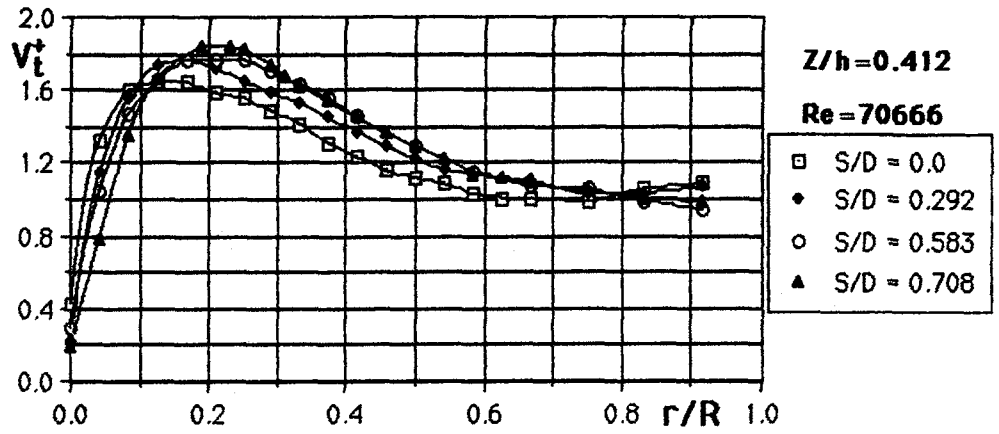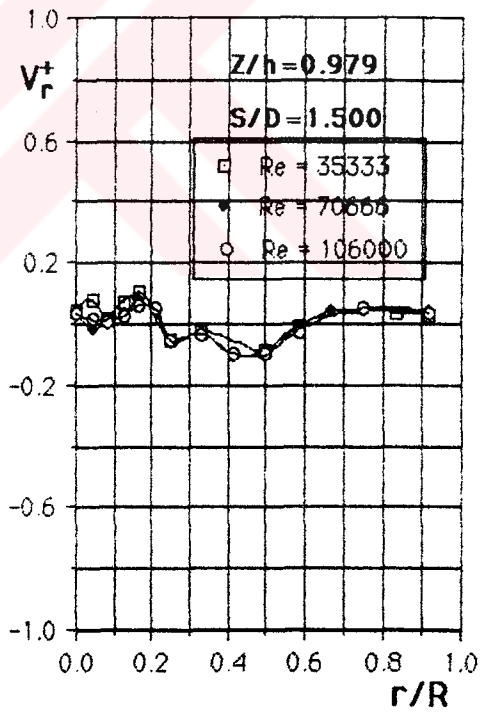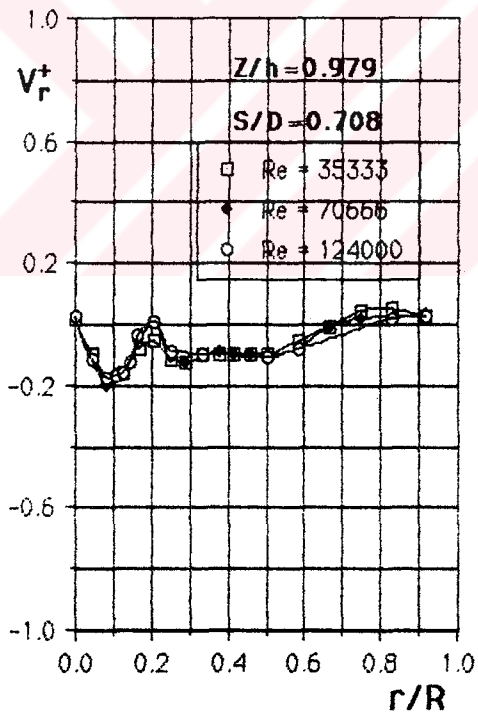
(a)
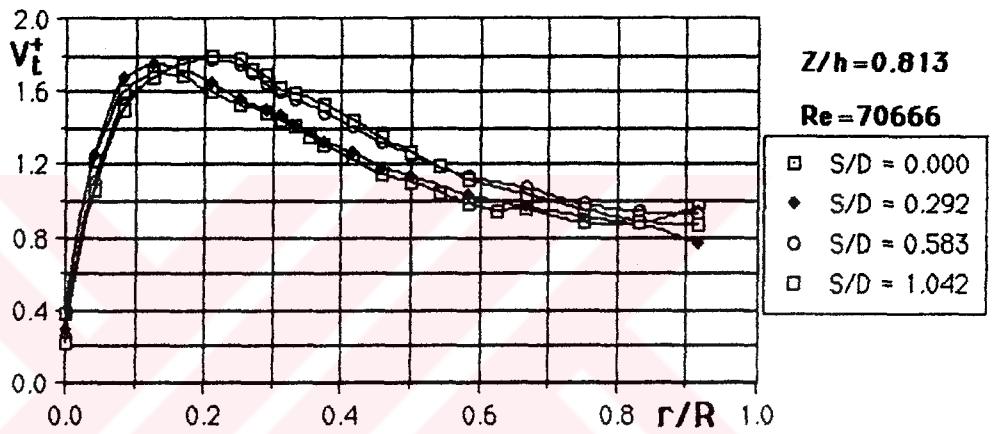
(b)
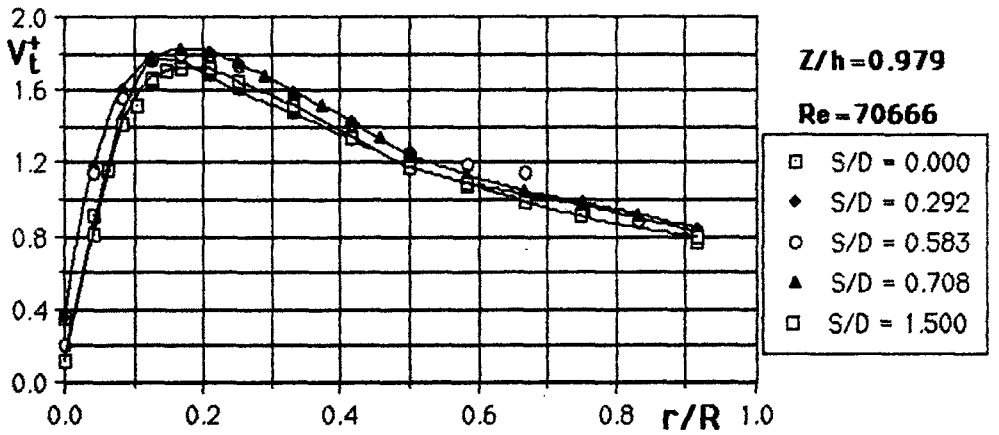
(c)

Figure 4.34 Radial distribution of dimensionless tangential velocity on the cyclone having different S/D ratios for Re=70666 at Z/h= 0.412, Z/h=0.813 and Z/h=0.979, respectively.
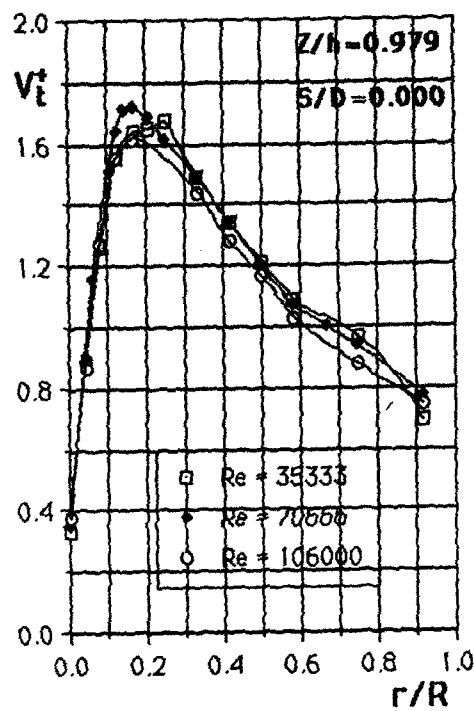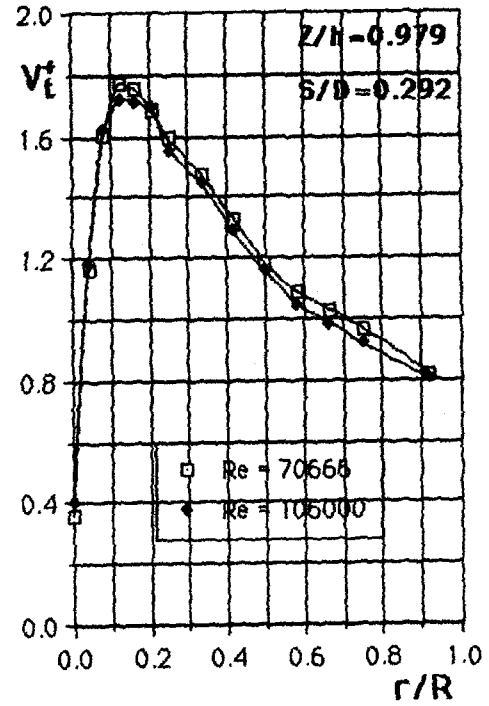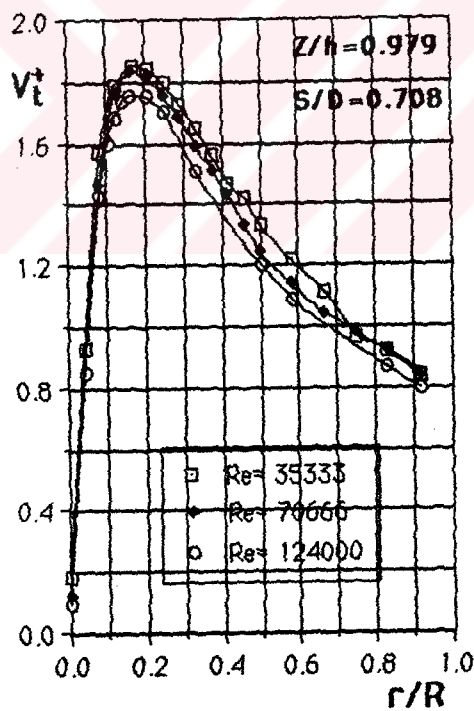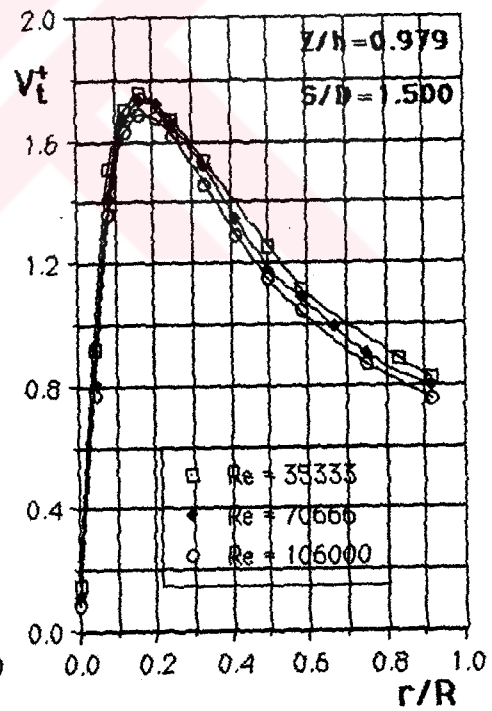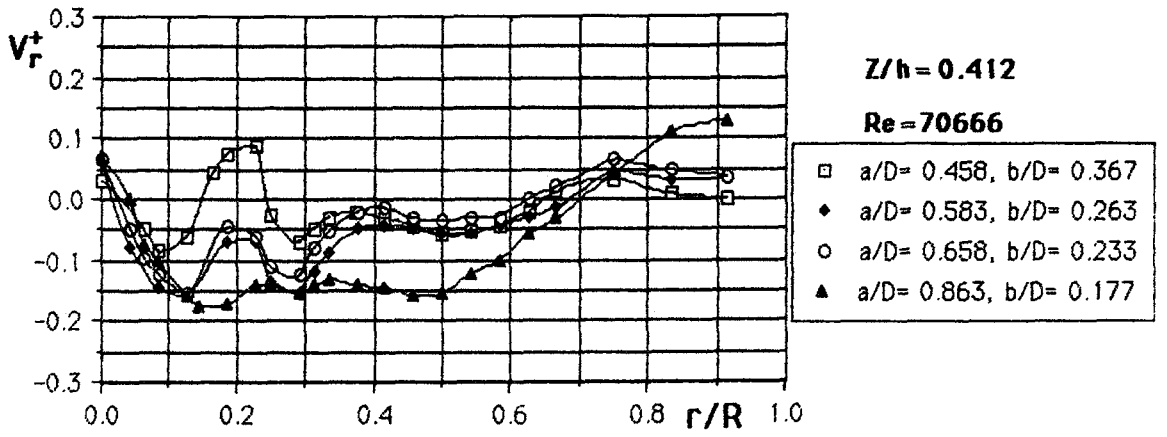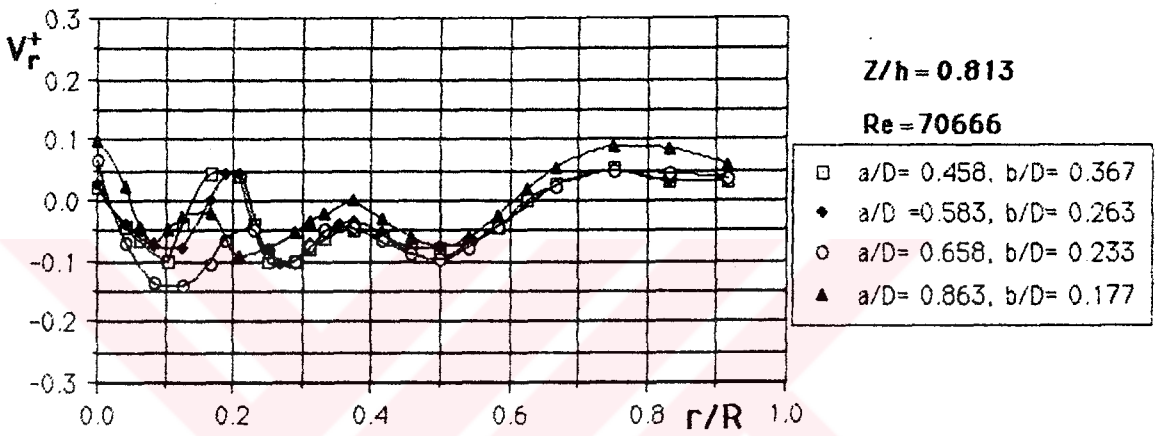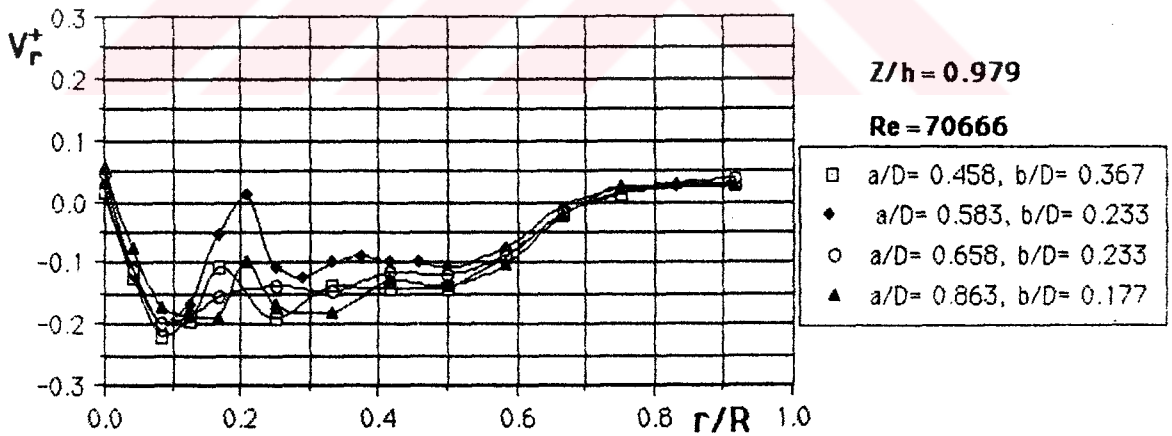
Figure 4.35 Radial distributions of dimensionless tangential velocity for different Re values on the cyclone having S/D ratios of 0.000, 0.292, 0.708 and 1.500 at Z/h=0.979, respectively.
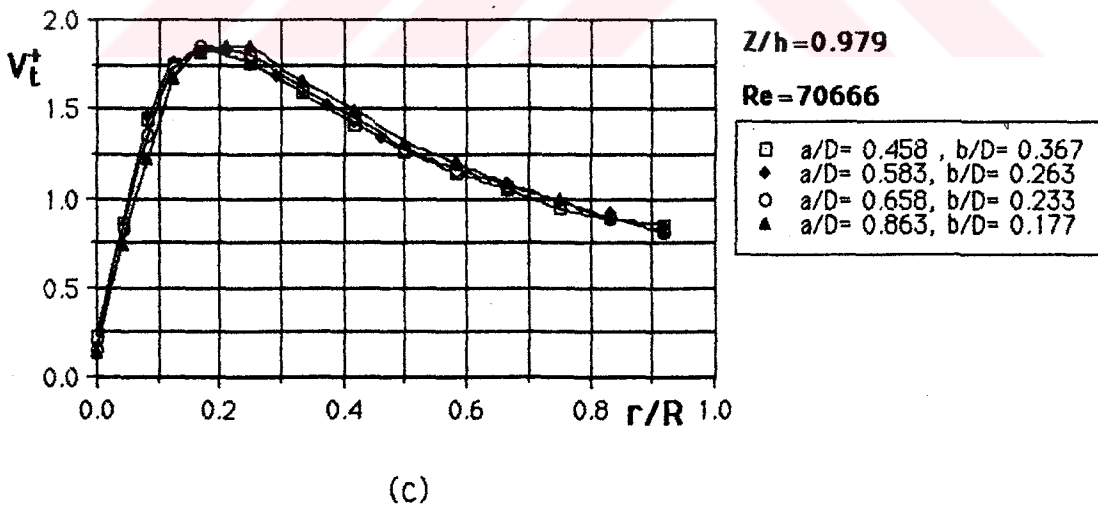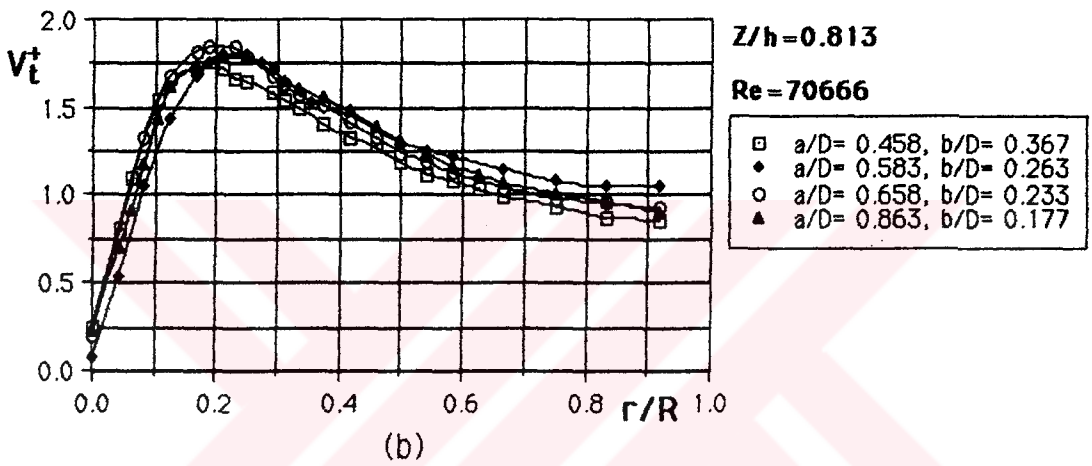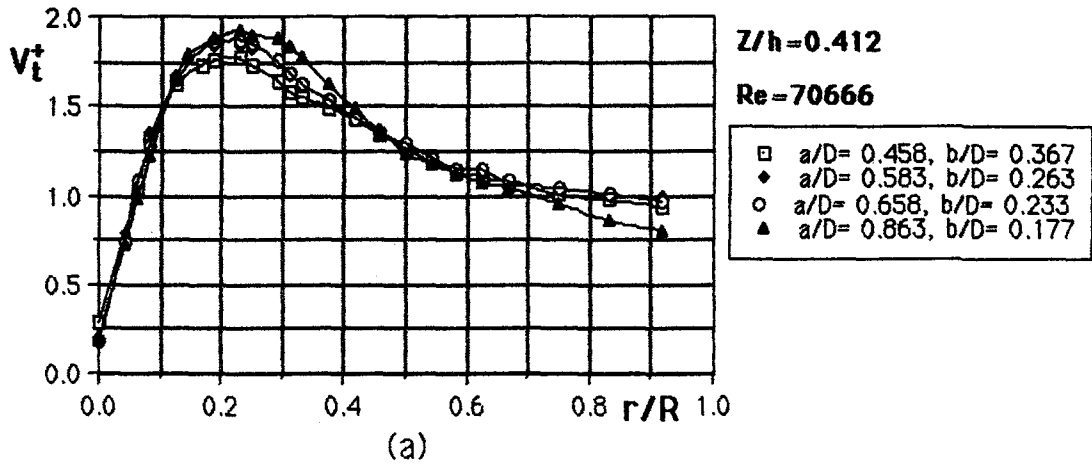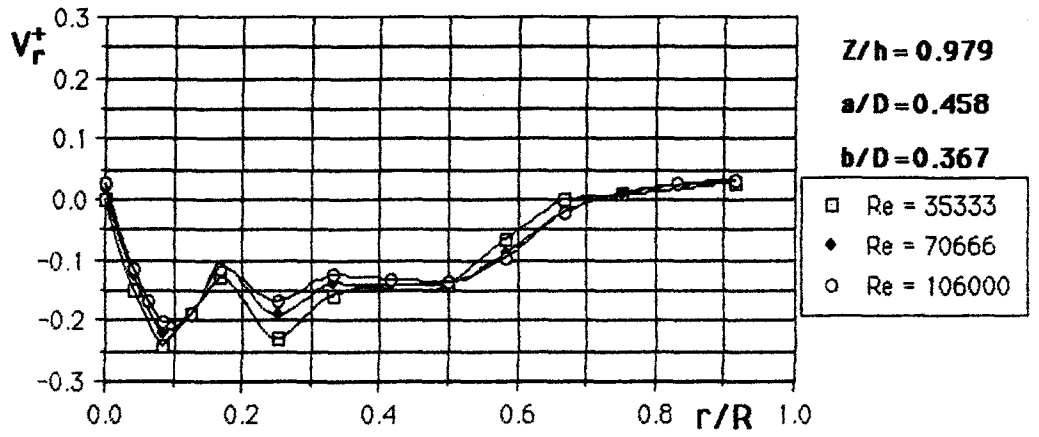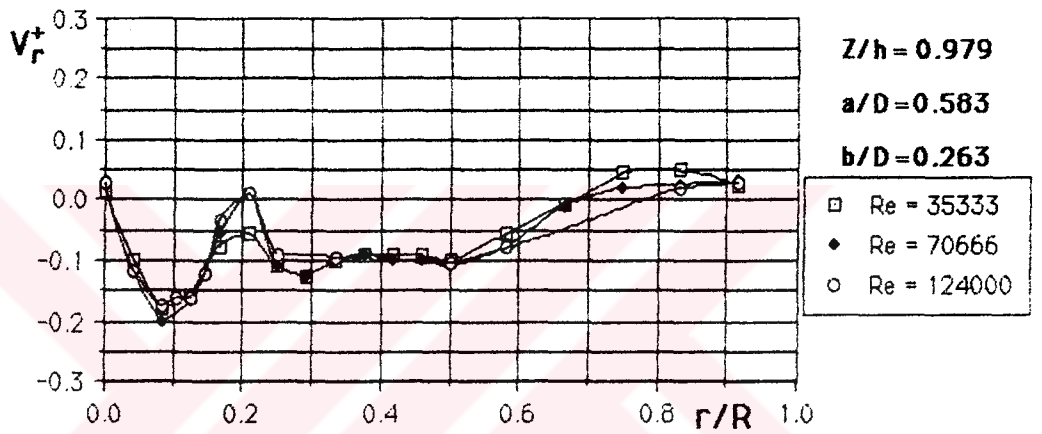
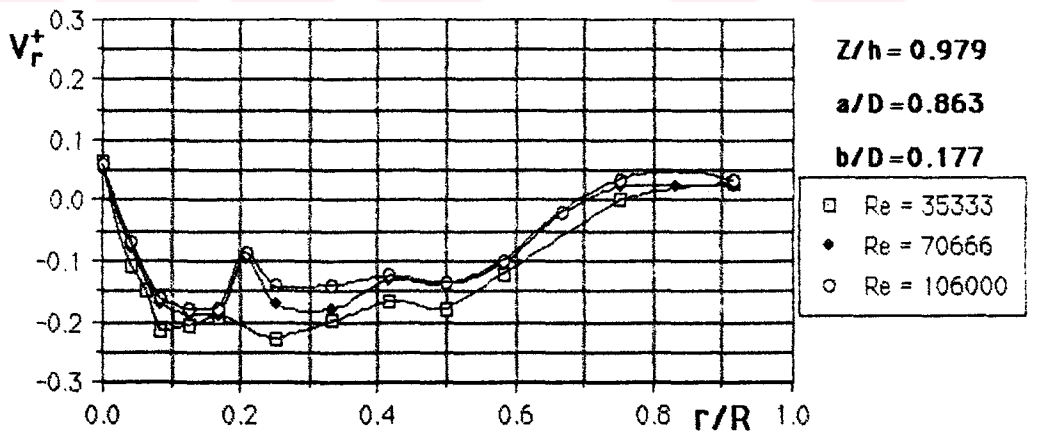Figure 4.36 Radial distributions of dimensionless tangential velocity on the cyclone having different a/D and b/D ratios for Re=70666 at Z/h= 0.412, Z/h=0.813 and Z/h=0.979, respectively.
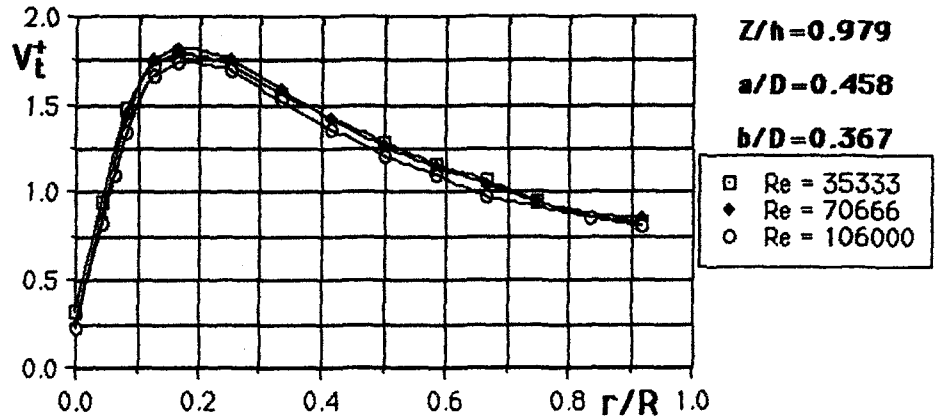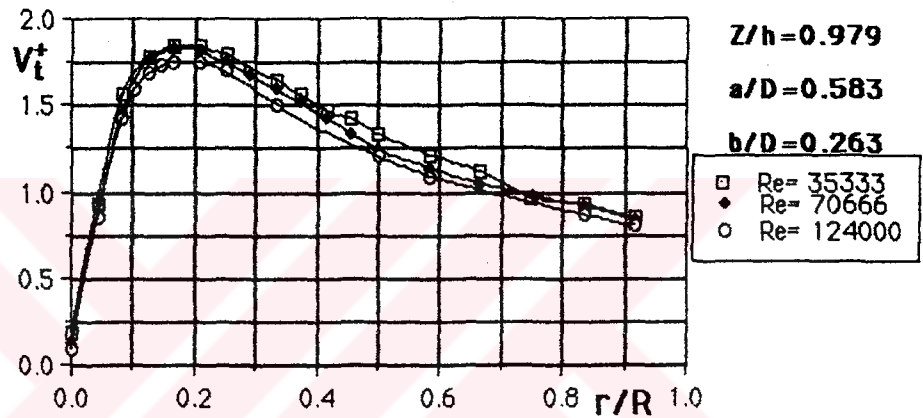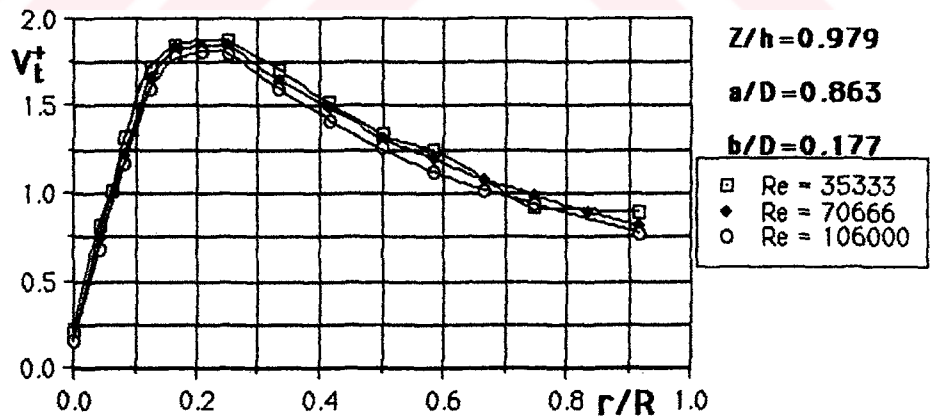
Figure 4.37 Radial distributions of dimensionless tangential velocity for different Re values on the cyclone having a/D ratios of 0.458, 0.583, 0.863 and b/D ratios of 0.367, 0.263, 0.177 at Z/h=0.979, respectively.
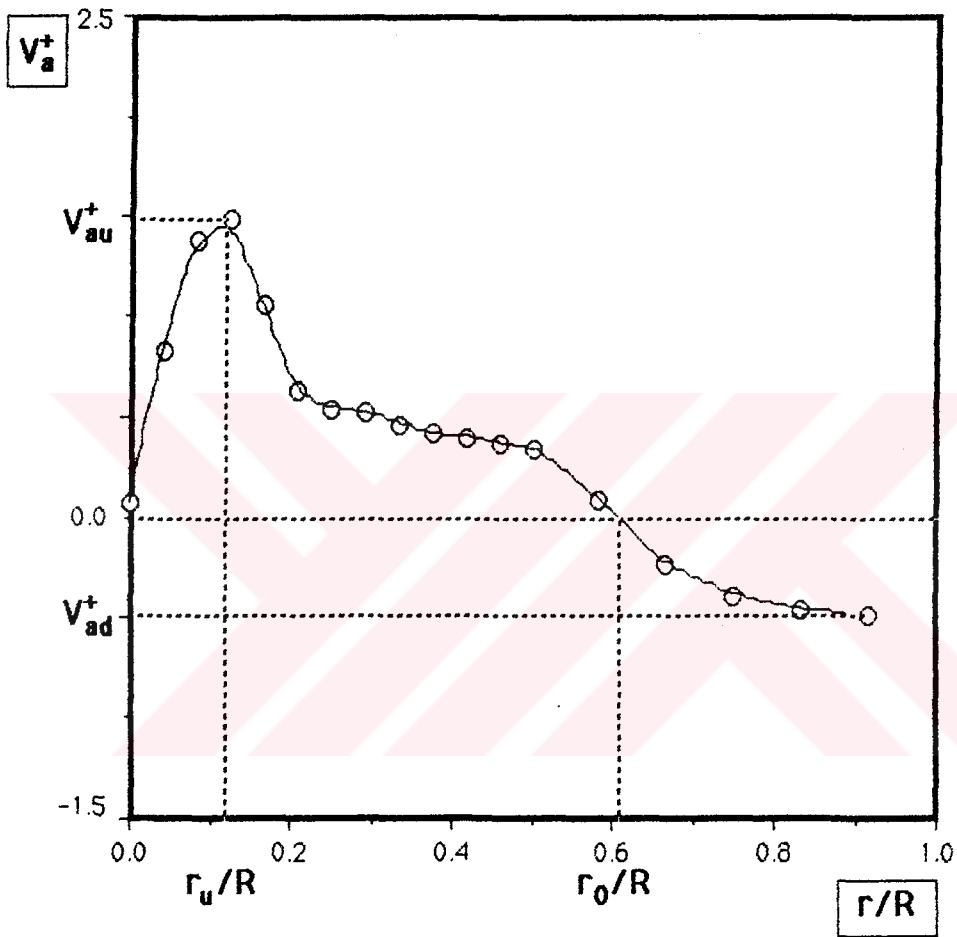
Figure 4.38 Characteristic radial distribution of the dimensionless axial velocity on the cyclone cylindrical body.
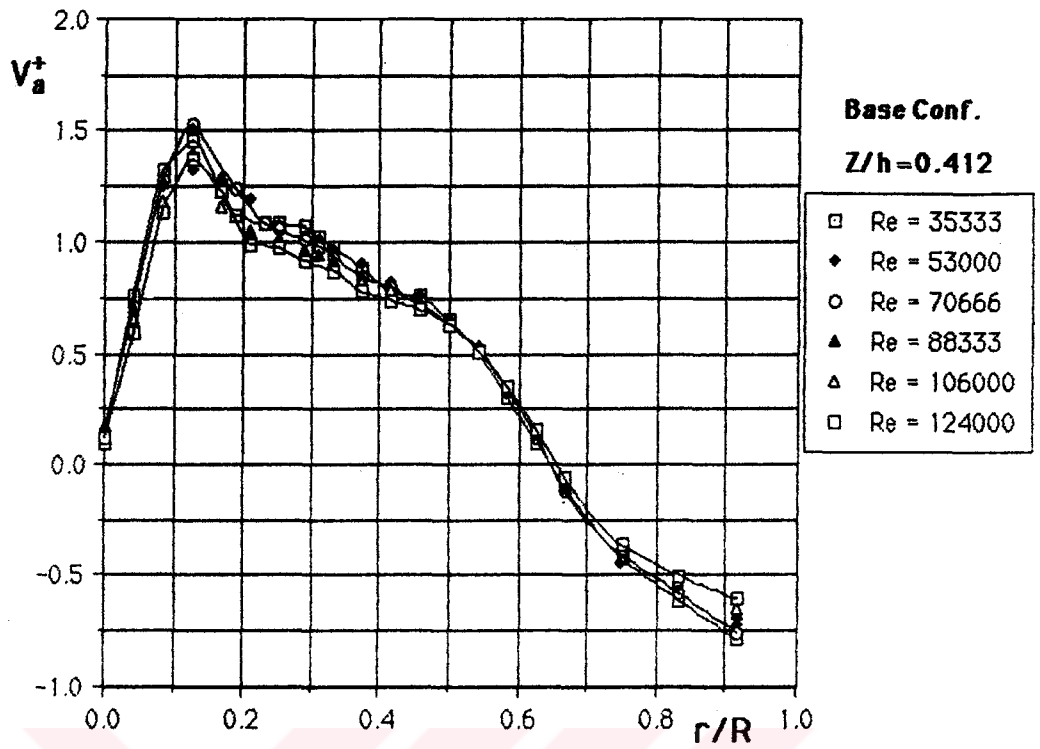
Figure 4.39 Radial distribution of dimensionless axial velocity on
the basic cyclone configuration for different Re values at Z/h =0.412.
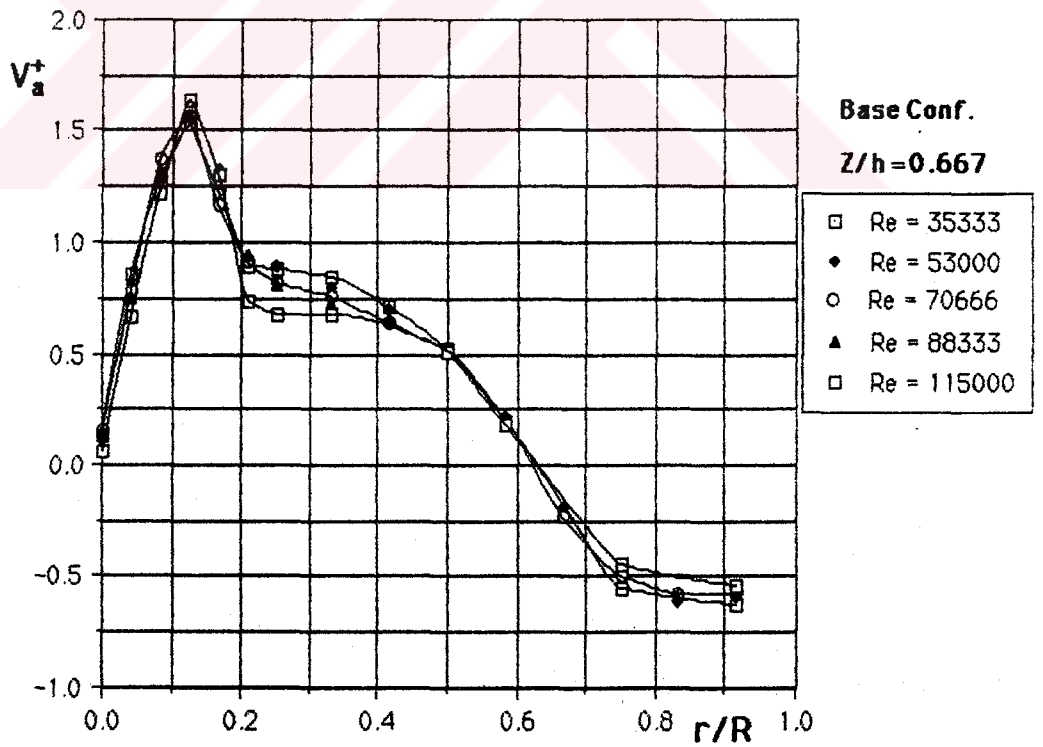
Figure 4.40 Radial distribution of dimensionless axial velocity on
the basic cyclone configuration for different Re values at Z/h =0.667.
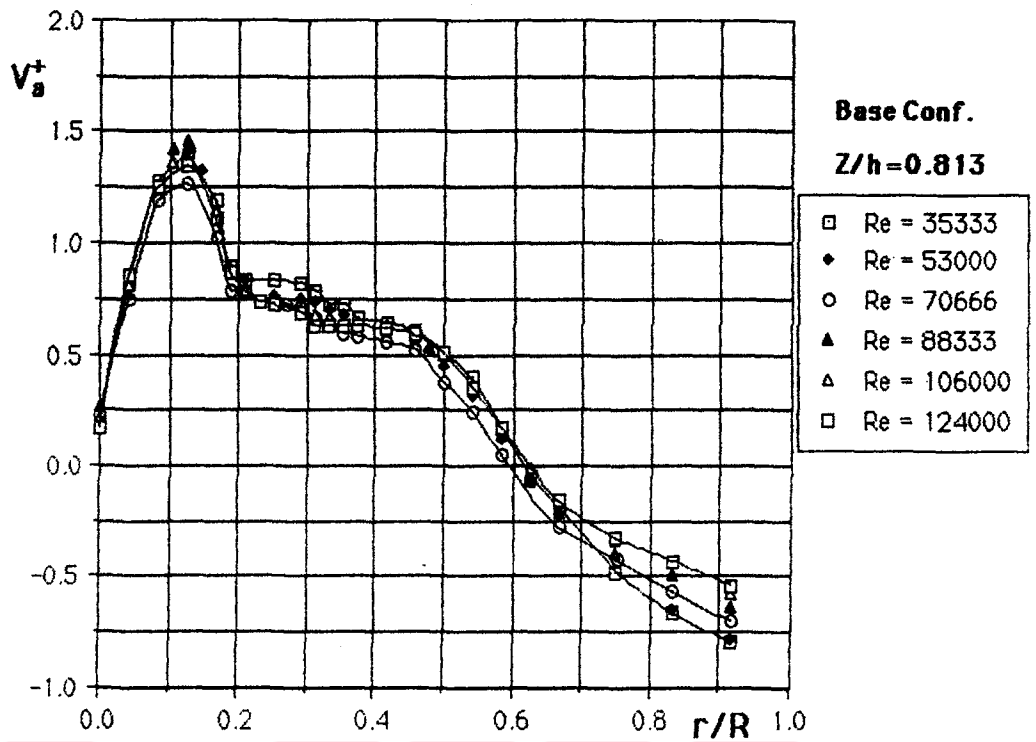
Figure 4.41 Radial distribution of dimensionless axial velocity on the basic cyclone configuration for different Re values at Z/h =0.813.
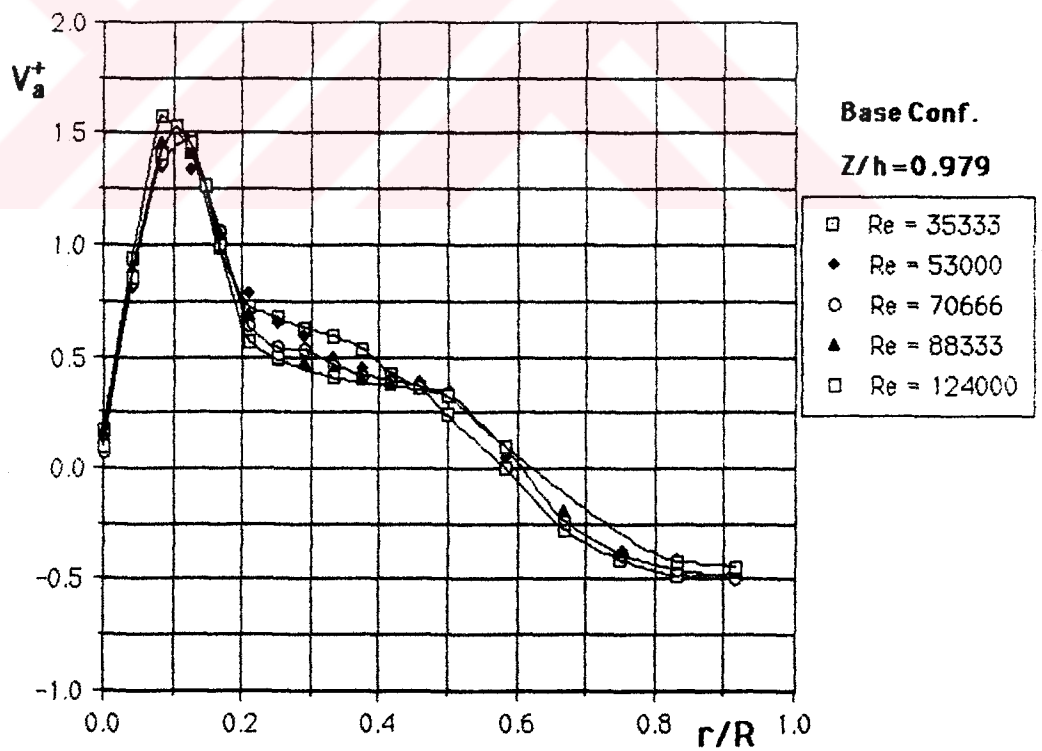
Figure 4.42 Radial distribution of dimensionless axial velocity on the basic cyclone configuration for different Re values at Z/h =0.979.
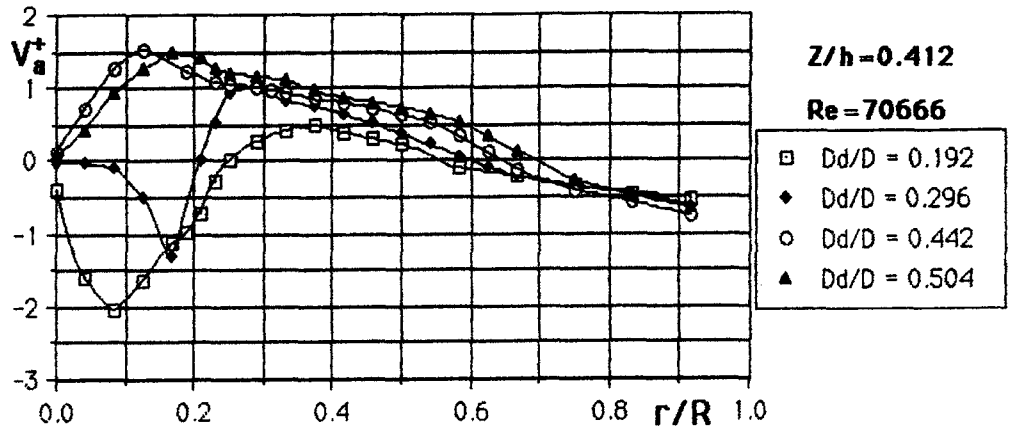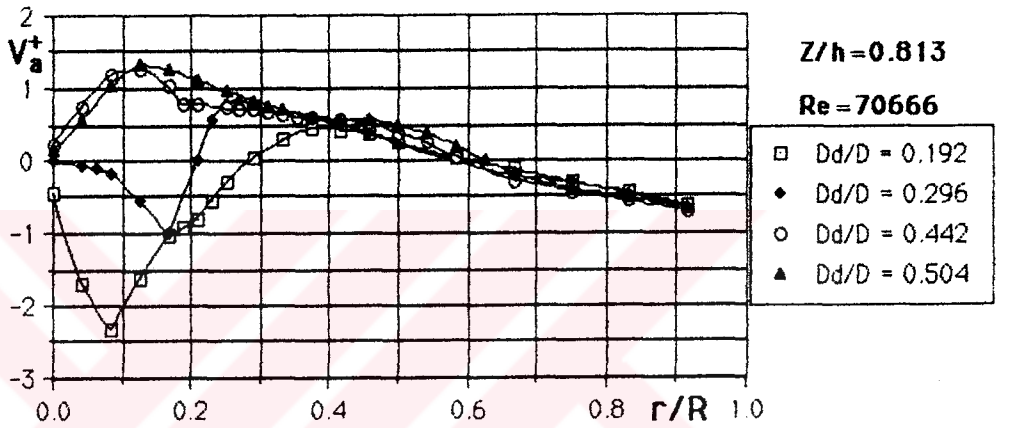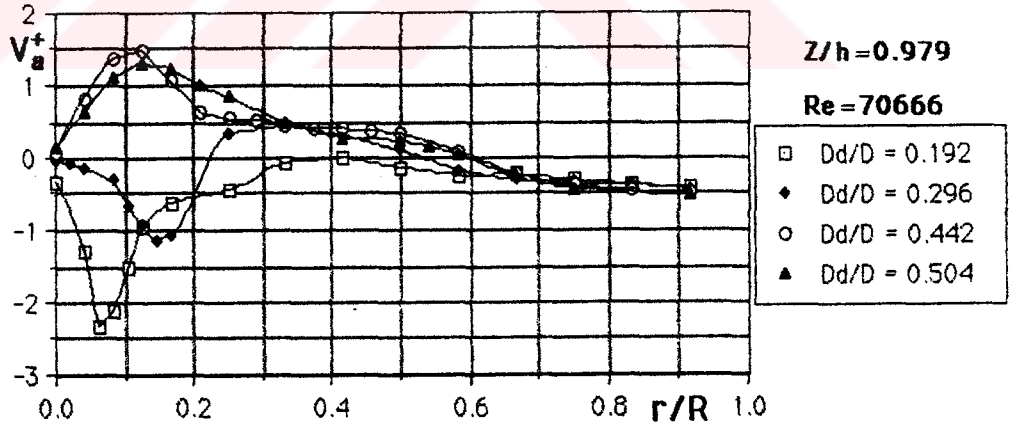
Figure 4.43 Radial distribution of dimensionless axial velocity on the cyclone having different D$_d$/D ratios for Re= 70666 at Z/h=0.412, Z/h=0.813 and Z/h=0.979, respectively.
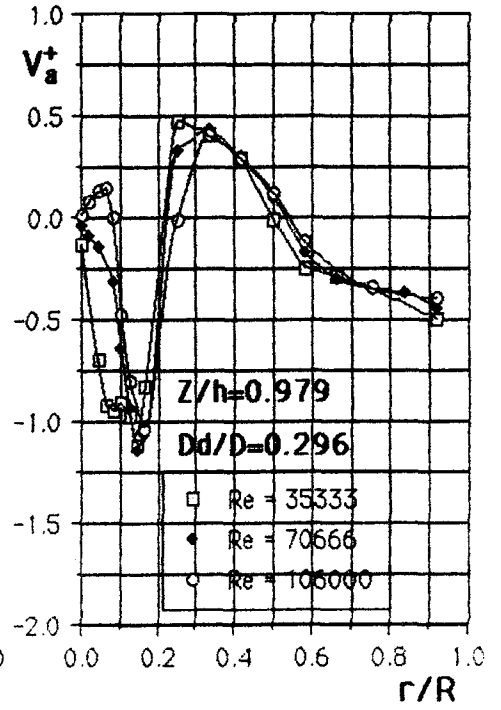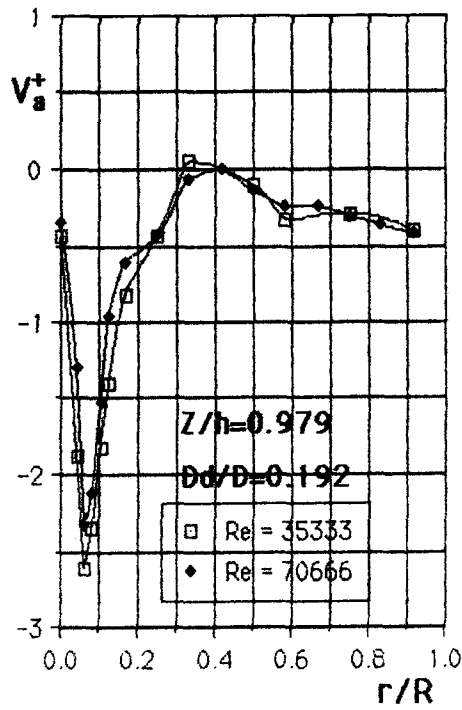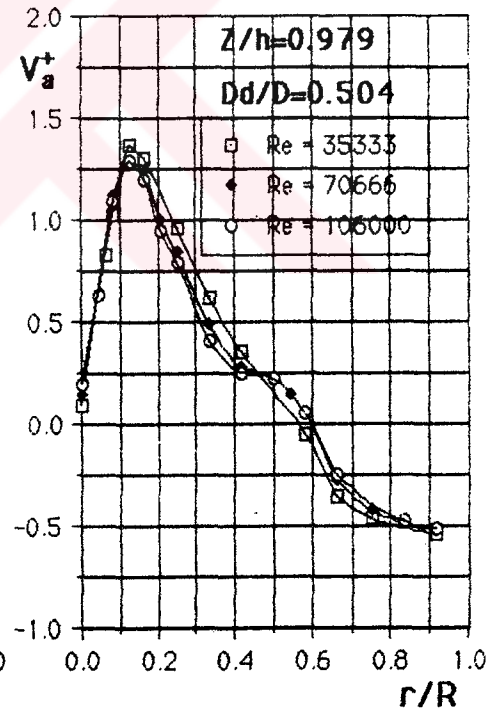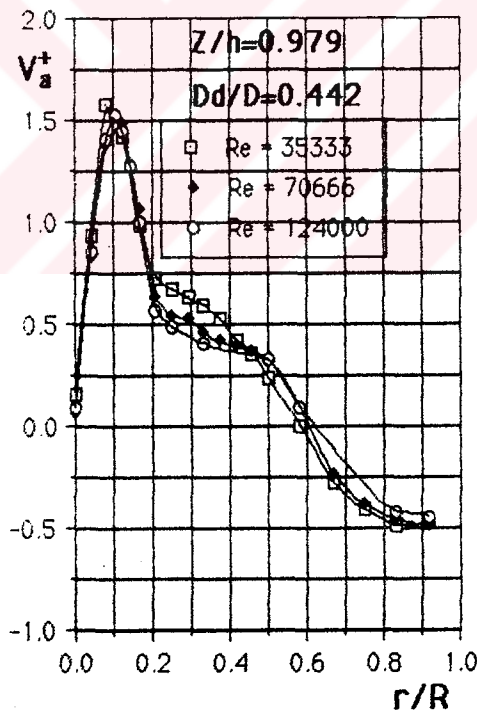
Figure 4.44 Radial distributions of dimensionless axial velocity
for different Re values on the cyclone having Dd/D ratios of 0.192,
0.296, 0.442 and 0.504 at Z/h=0.979, respectively.
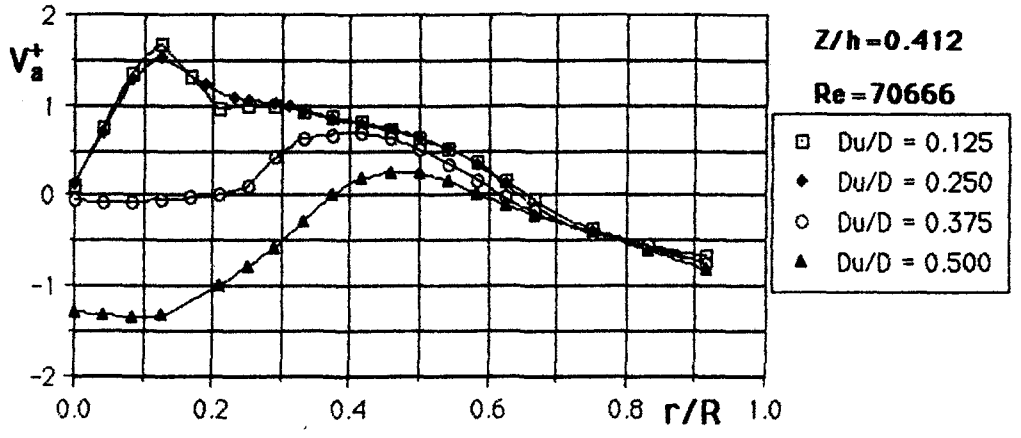
(a)
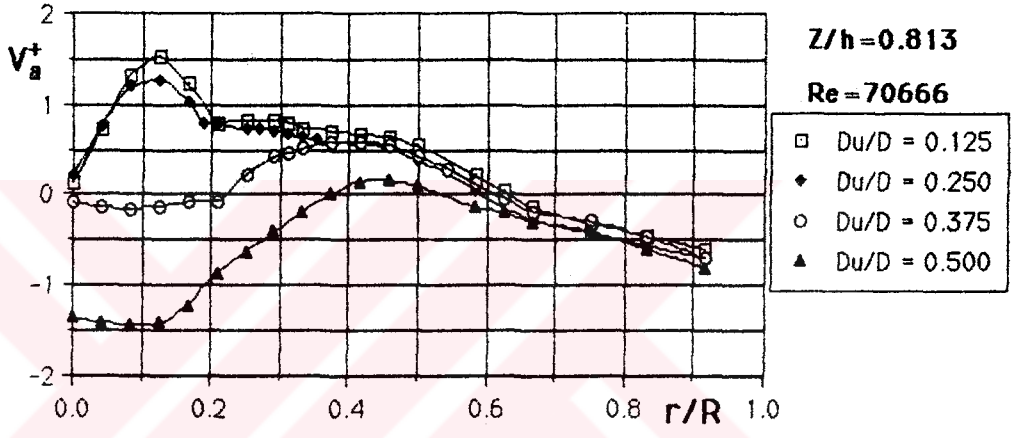
(b)
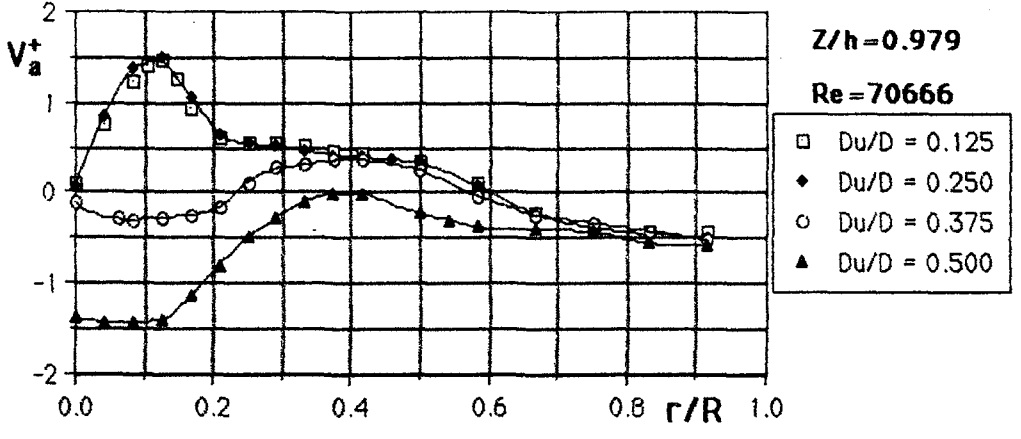
(c)

Figure 4.45 Radial distributions of dimensionless axia velocity on
the cyclone having different Du/D ratios for Re=70666 at Z/h= 0.412,
Z/h=0.813 and Z/h=0.979, respectively.
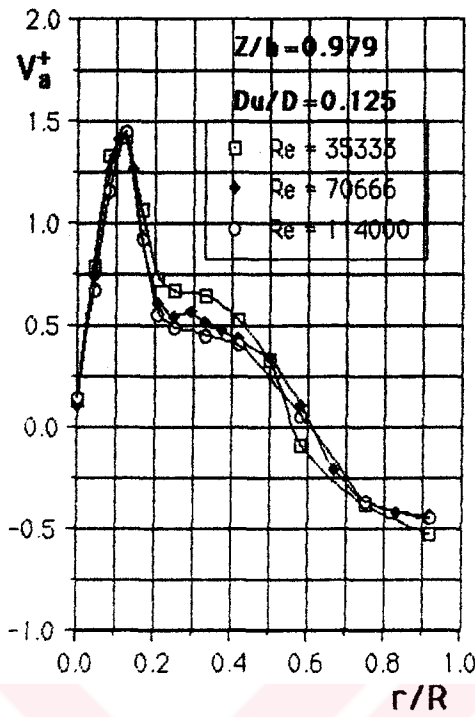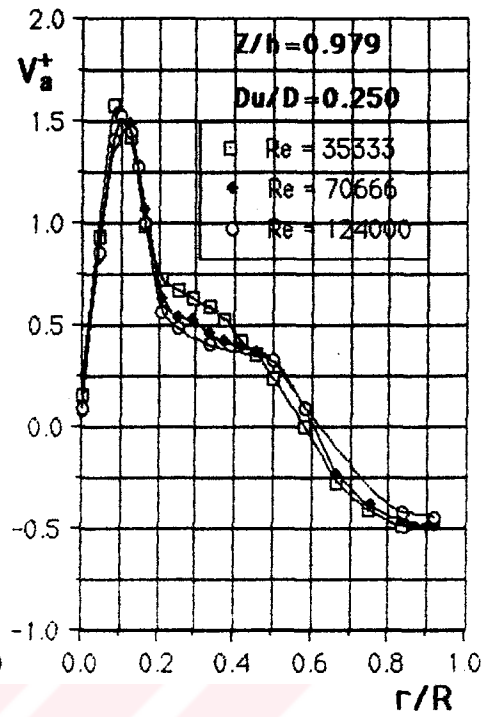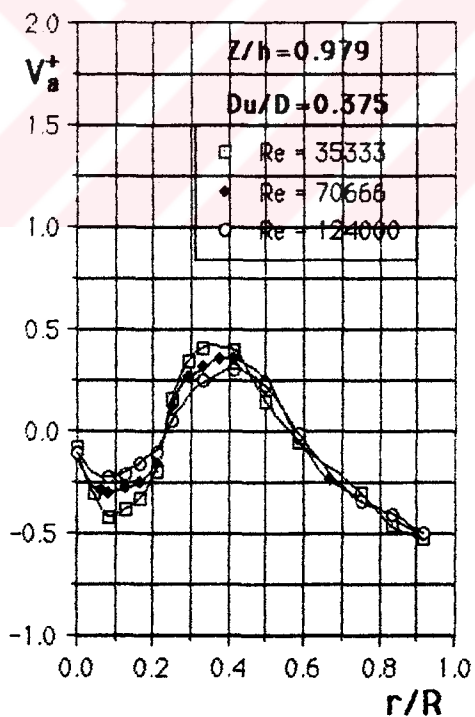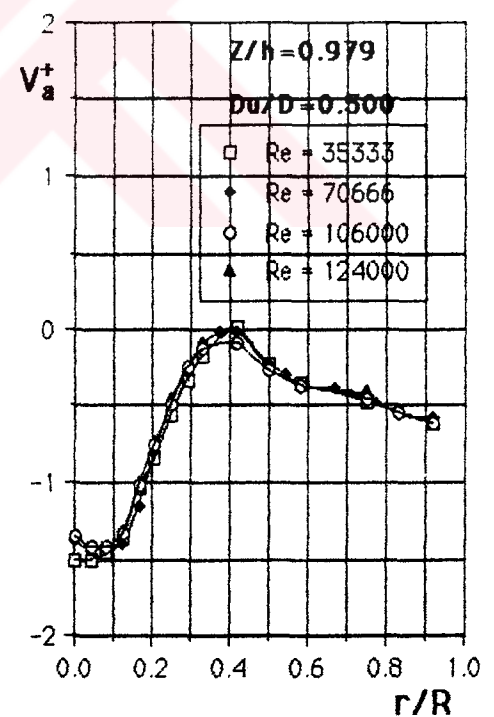
Figure 4.46 Radial distributions of dimensionless axial velocity
for different Re values on the cyclone having Du/D ratios of 0.125,
0.250, 0.375 and 0.500 at Z/h=0.979, respectively.
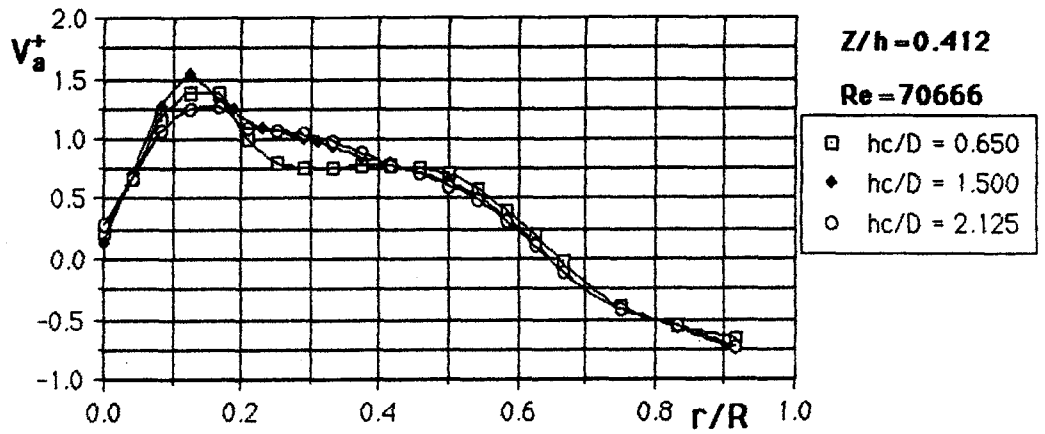
(a)
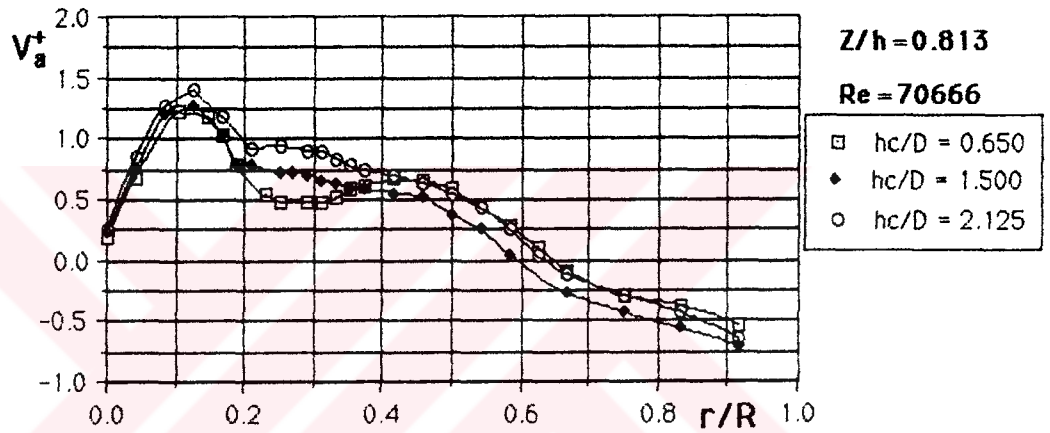
(b)
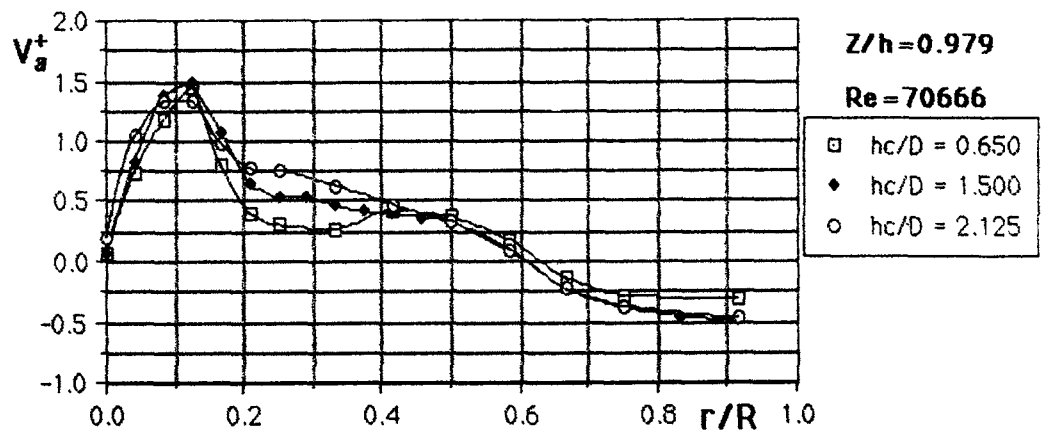
(c)

Figure 4.47 Radial distributions of dimensionless axial velocity on the cyclone having different h_c/D ratios for Re=70666 at Z/h= 0.412, Z/h=0.813 and Z/h=0.979, respectively.
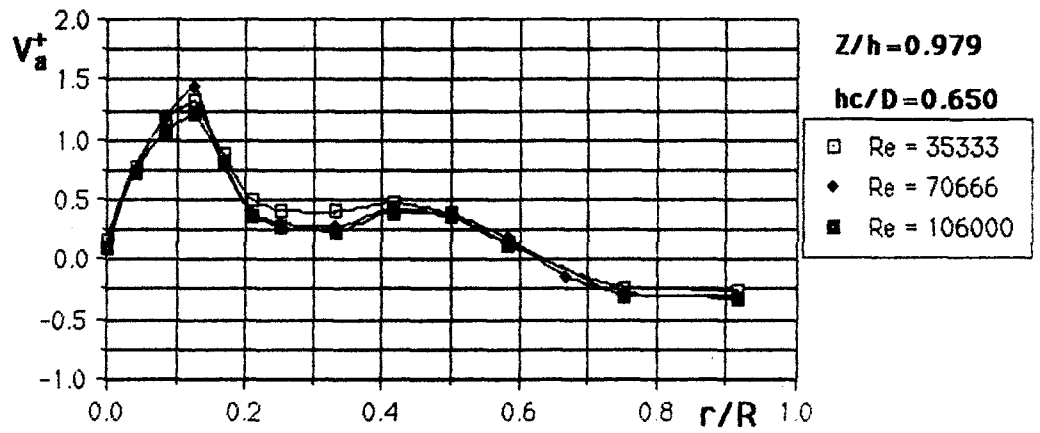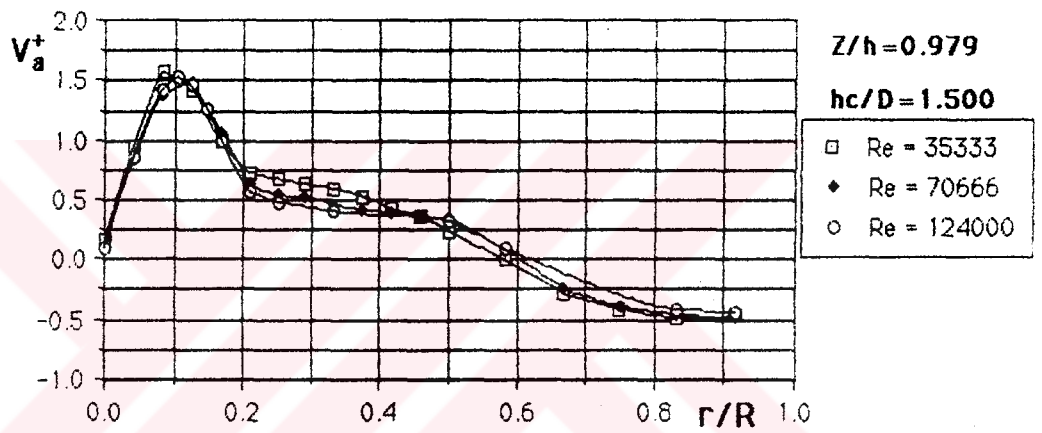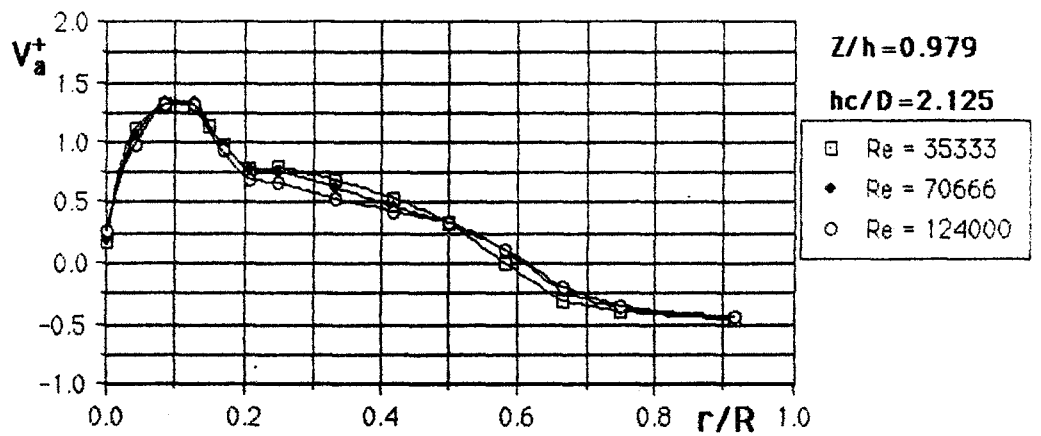
Figure 4.48 Radial distributions of dimensionless tangential velocity for different Re values on the cyclone having h_c/D ratios of 0.650, 1.500 and 2.125 at Z/h=0.979, respectively.
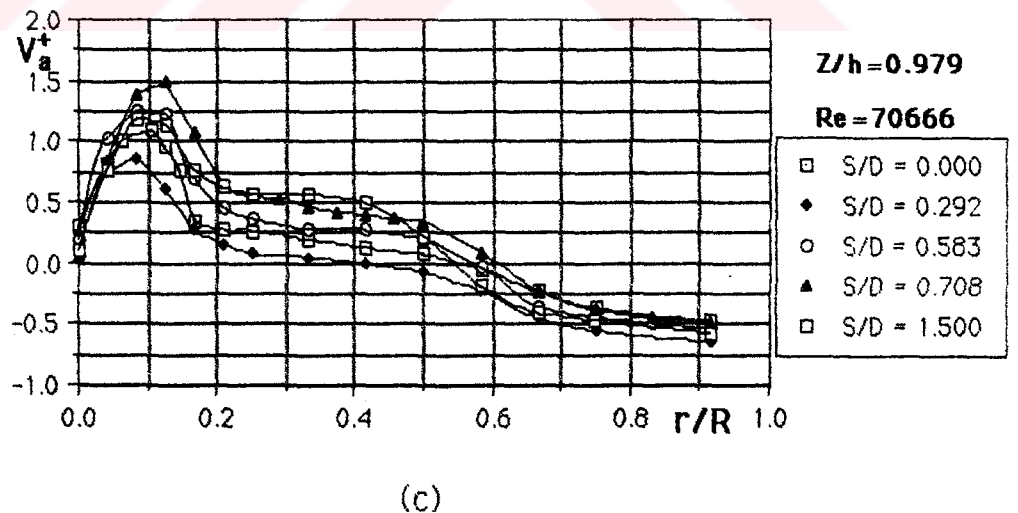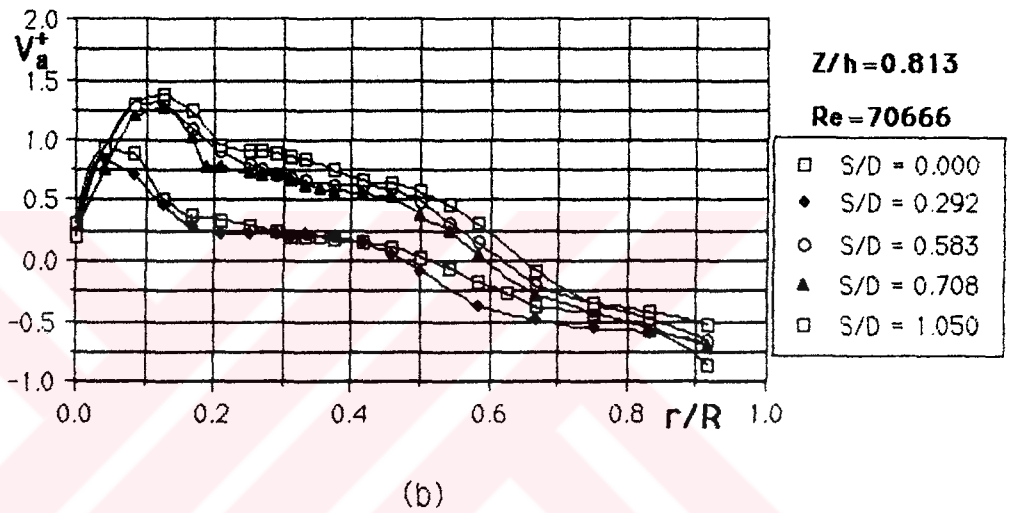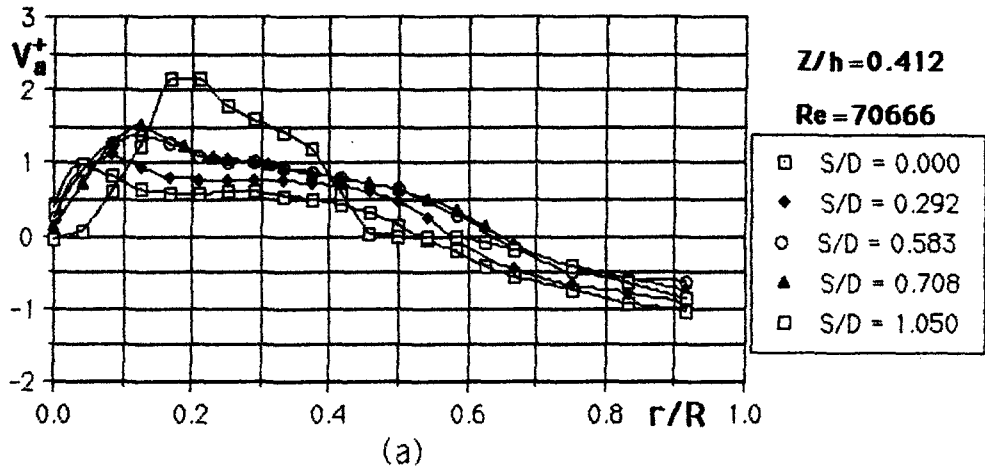
Figure 4.49 Radial distribution of dimensionless axial velocity on the cyclone having different S/D ratios for Re=70666 at Z/h= 0.412, Z/h=0.813 and Z/h=0.979, respectively.
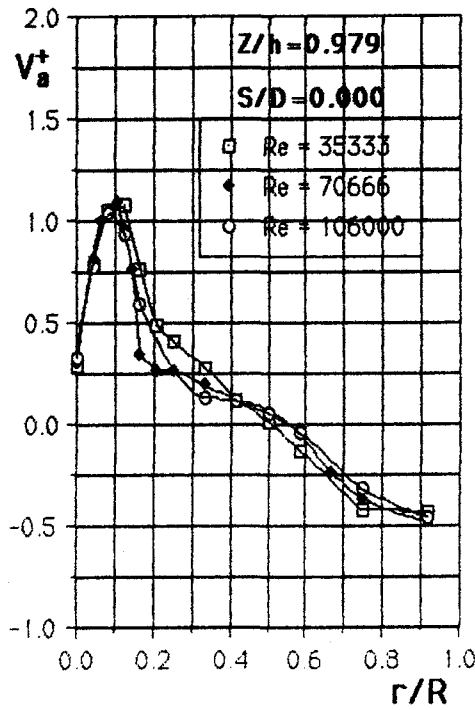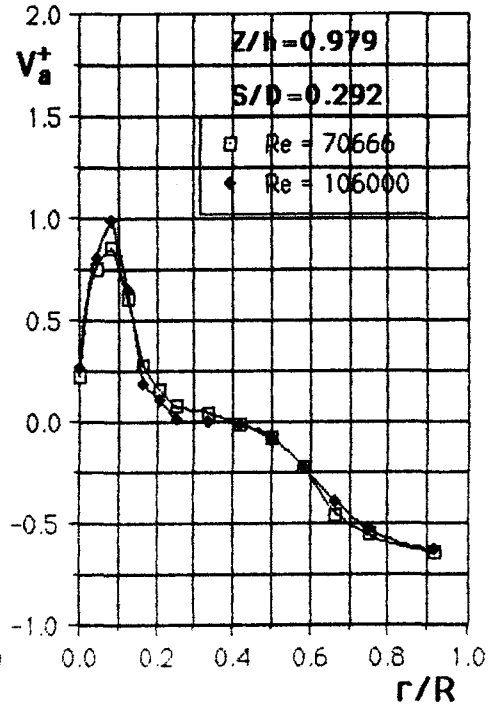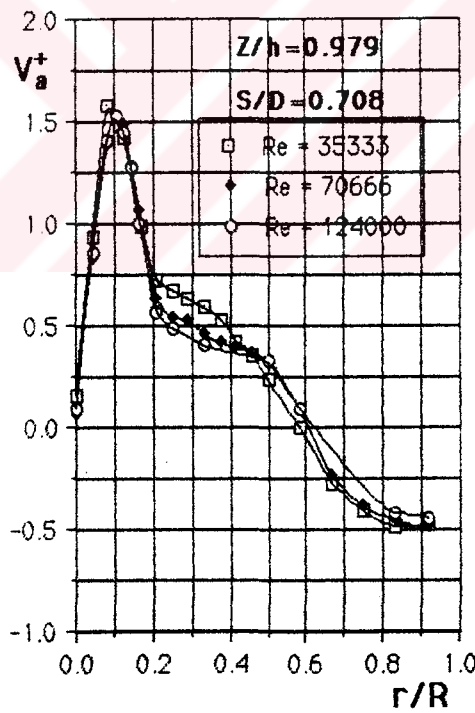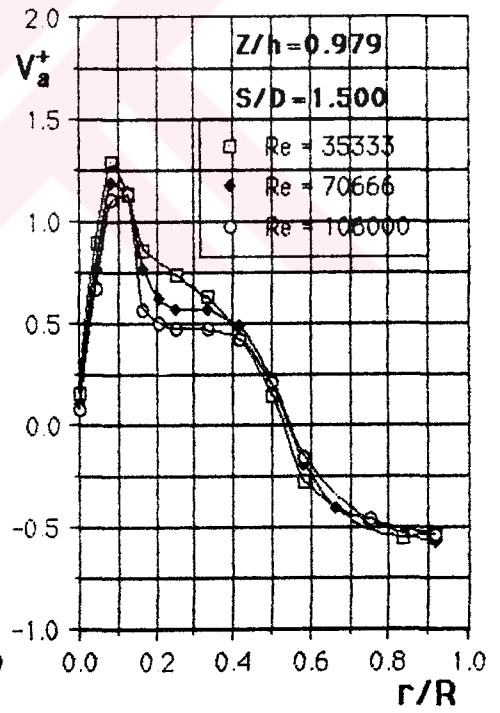
Figure 4.50 Radial distributions of dimensionless axial velocity
for different Re values on the cyclone having S/D ratios of 0.000, 0.292,
0.708 and 1.500 at Z/h=0.979, respectively.
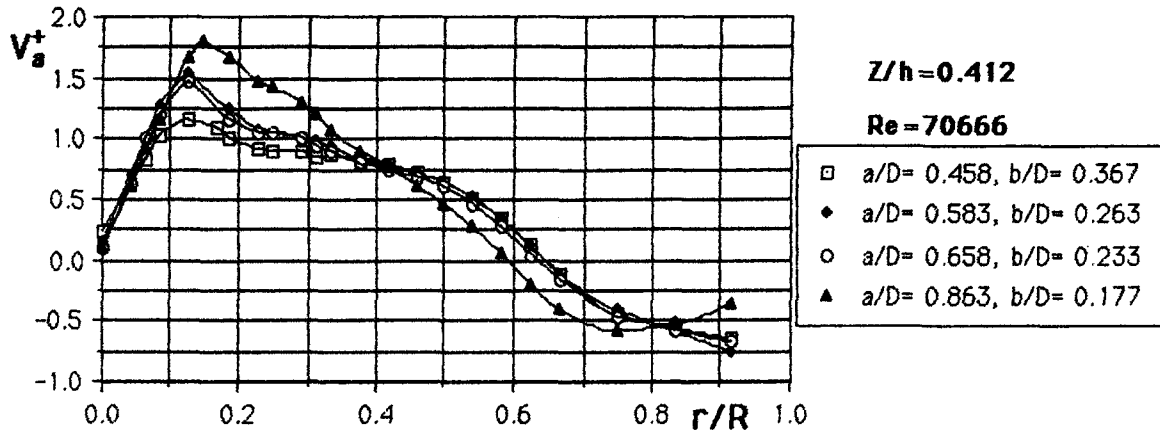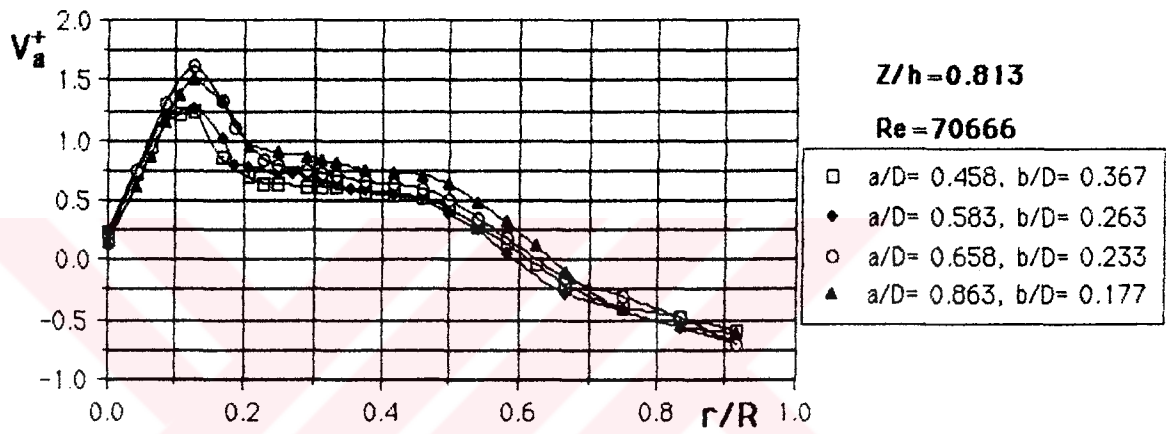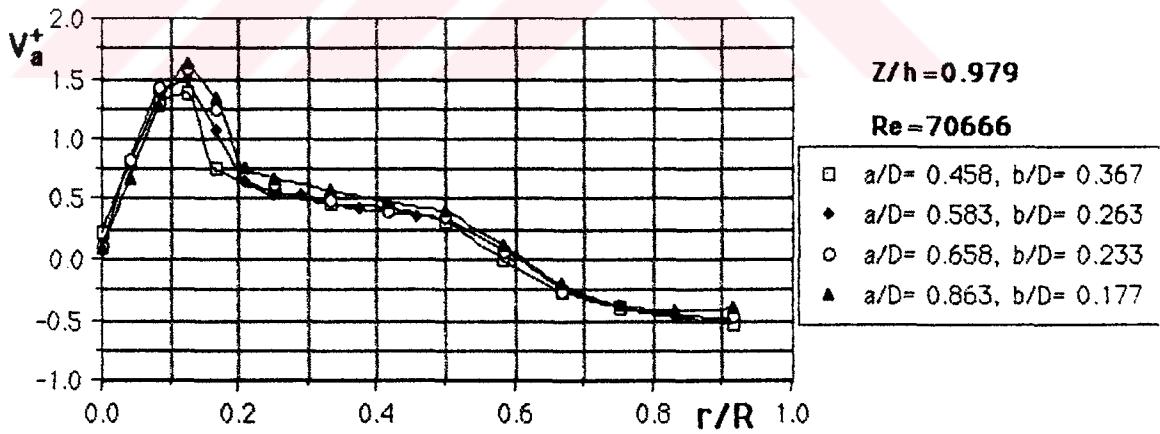
Figure 4.51 Radial distributions of dimensionless axial velocity on the cyclone having different a/D and b/D ratios for Re=70666 at Z/h= 0.412, Z/h=0.813 and Z/h=0.979, respectively.
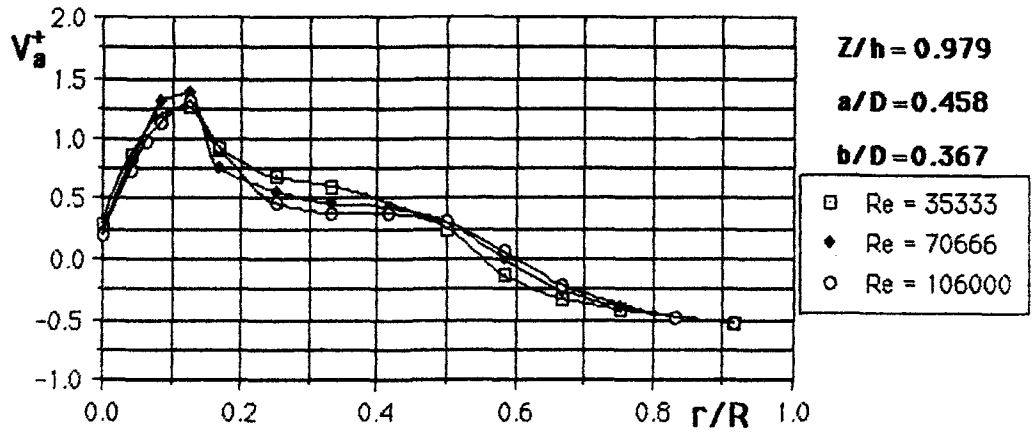
(a)
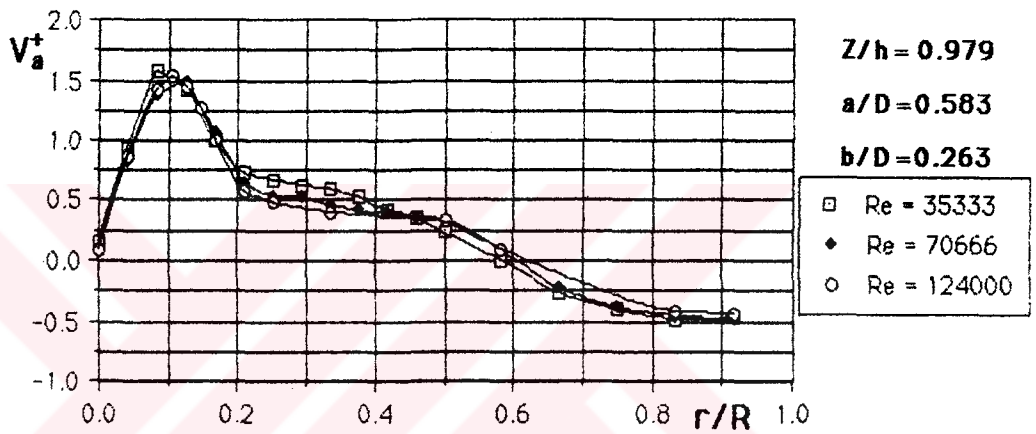
(b)
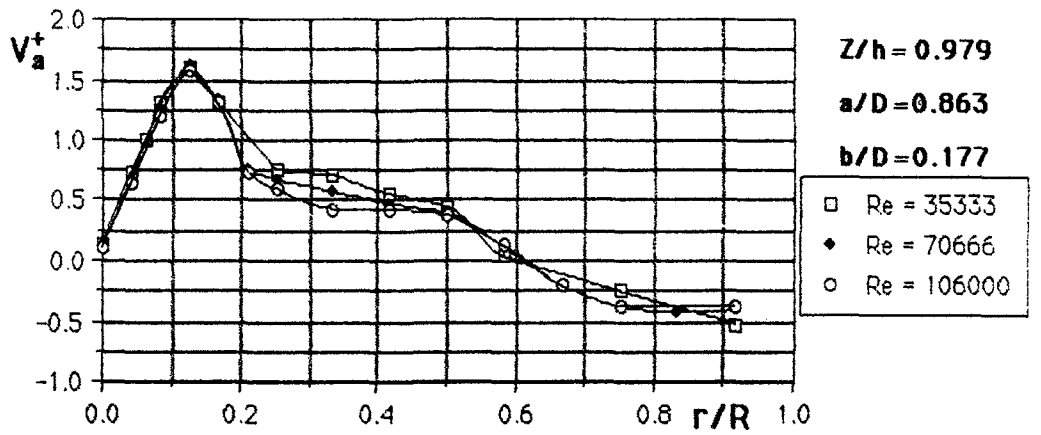
(c)

Figure 4.52 Radial distributions of dimensionless axial velocity for different Re values on the cyclone having a/D ratios of 0.458, 0.583, 0.863 and b/D ratios of 0.367, 0.263, 0.177 at Z/h=0.979, respectively.

139
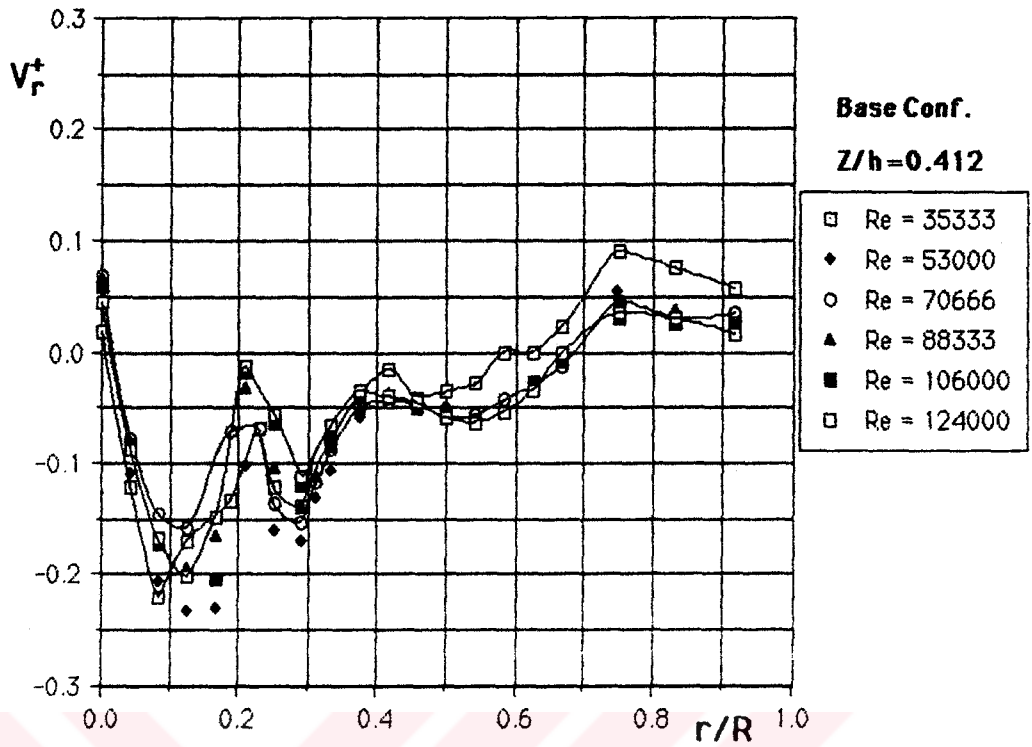
Figure 4.53 Radial distribution of dimensionless radial velocity on the basic cyclone configuration for different Re values at Z/h =0.412.
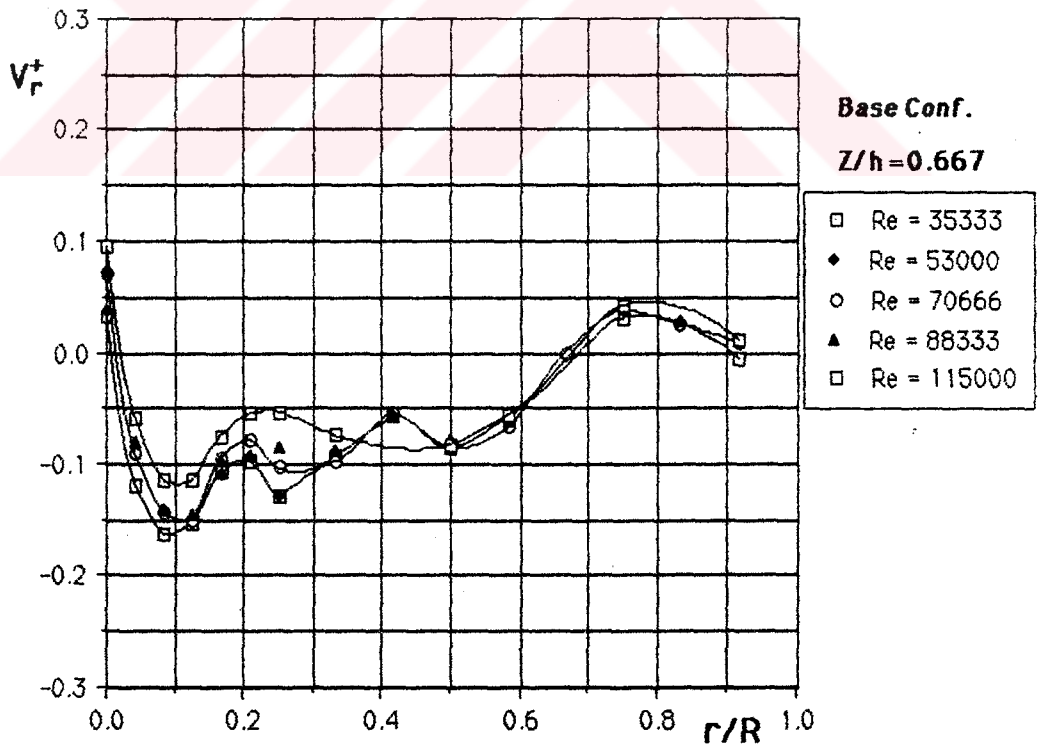
Figure 4.54 Radial distribution of dimensionless radial velocity on the basic cyclone configuration for different Re values at Z/h =0.412.
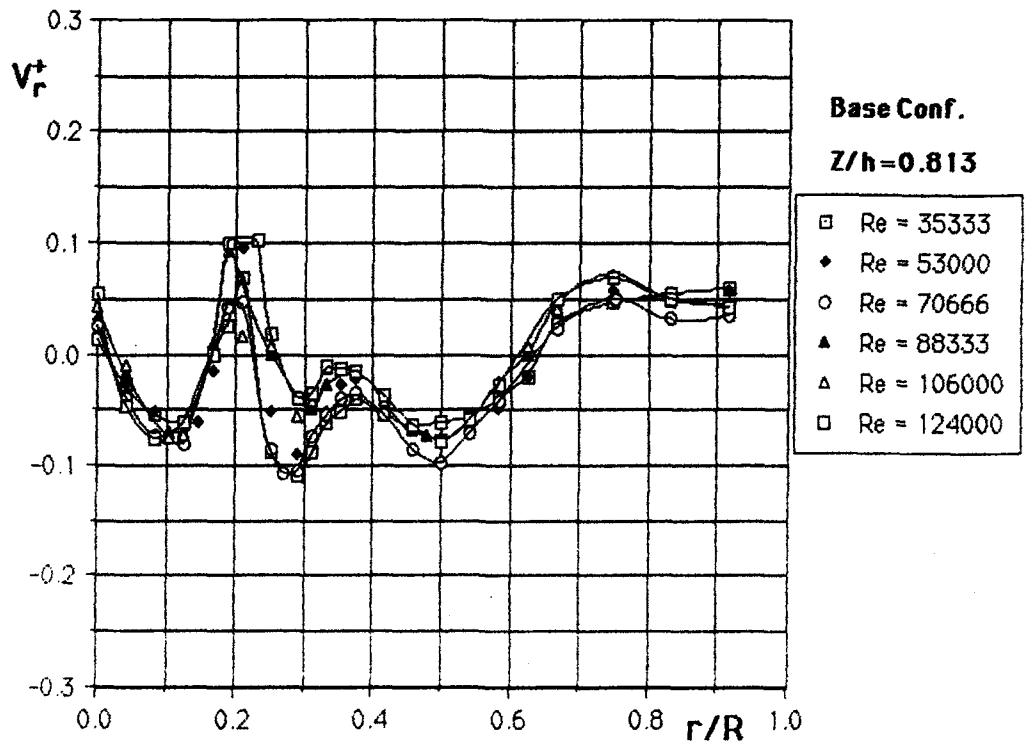
Figure 4.55 Radial distribution of dimensionless radial velocity on the basic cyclone configuration for different Re values at Z/h =0.412.
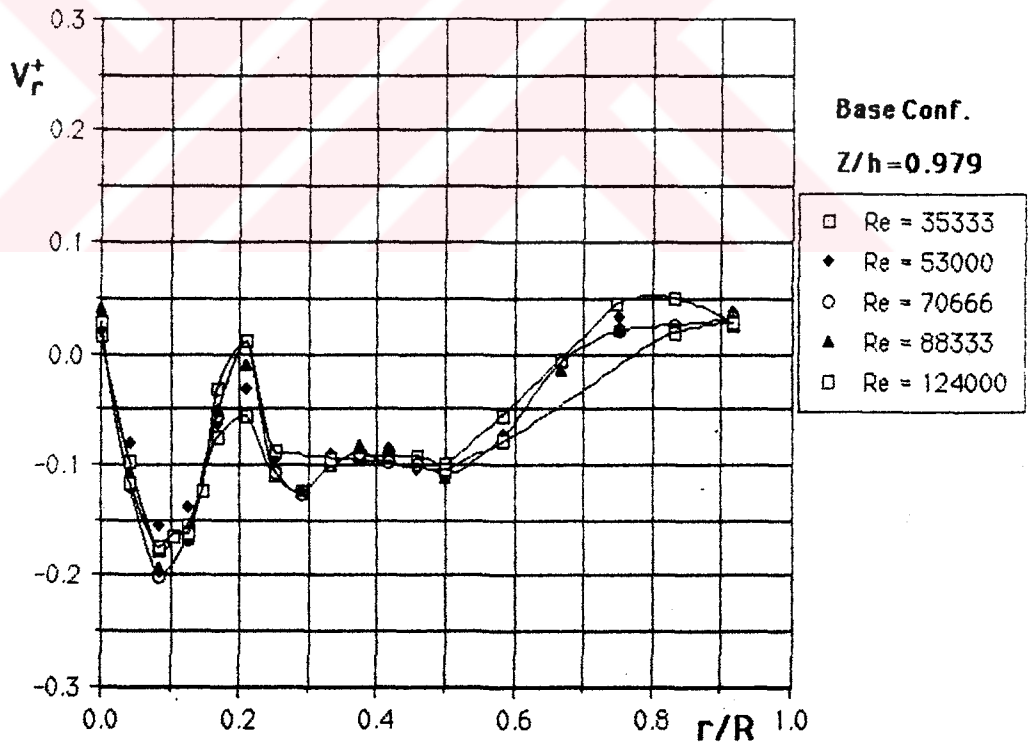
Figure 4.56 Radial distribution of dimensionless radial velocity on the basic cyclone configuration for different Re values at Z/h =0.412.

141
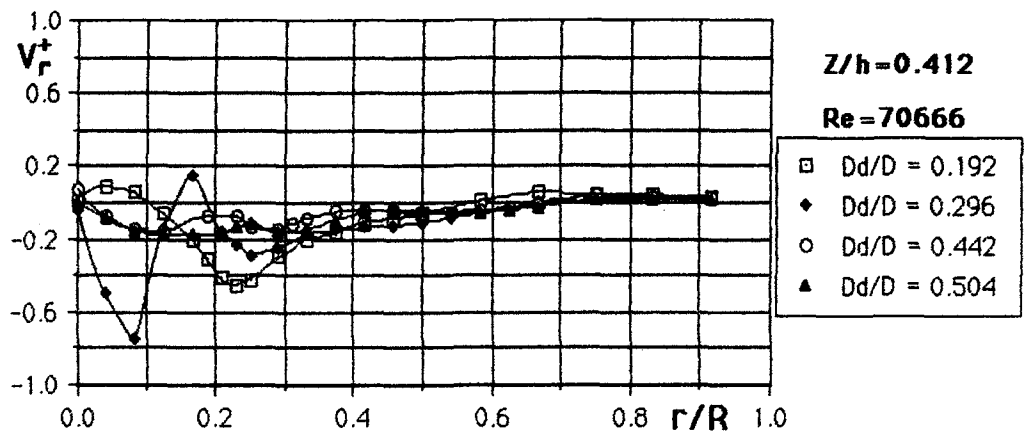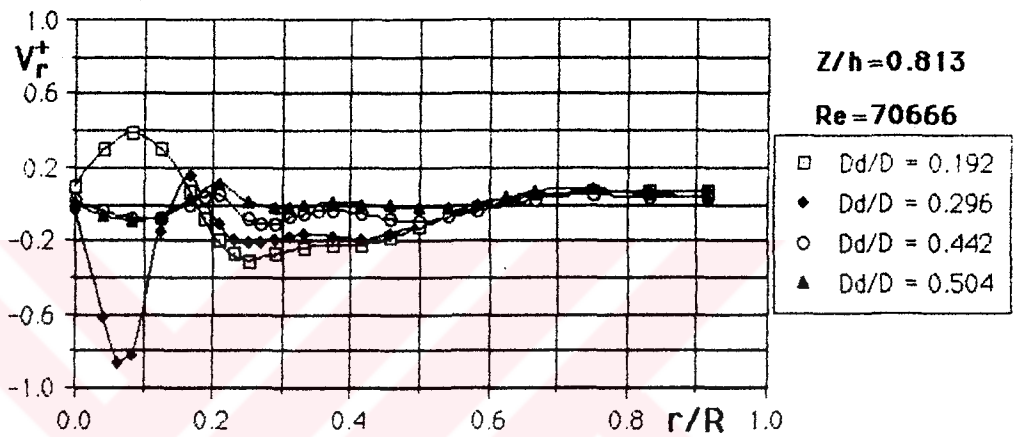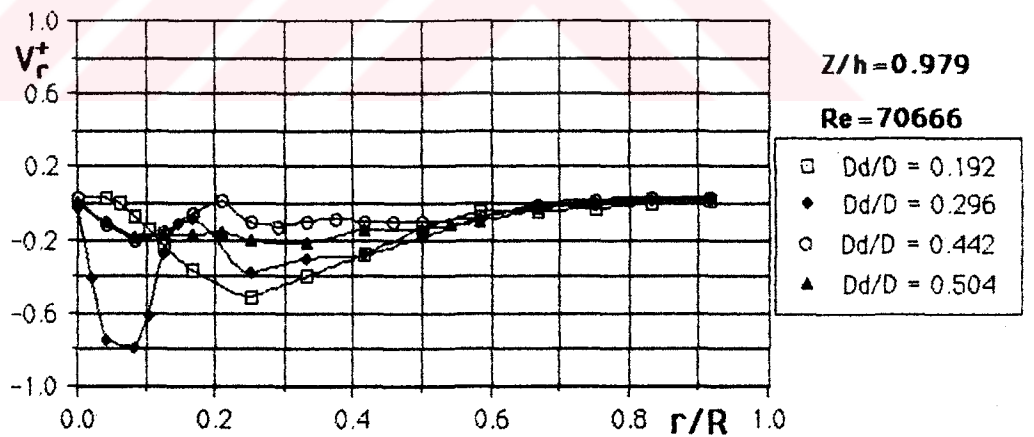
Figure 4.57 Radial distribution of dimensionless radial velocity on the cyclone having different D_d/D ratios for Re= 70666 at Z/h=0.412, Z/h=0.813 and Z/h=0.979, respectively.
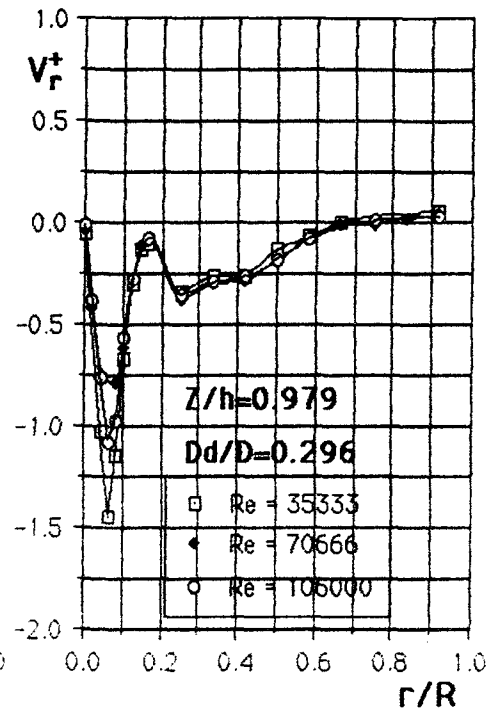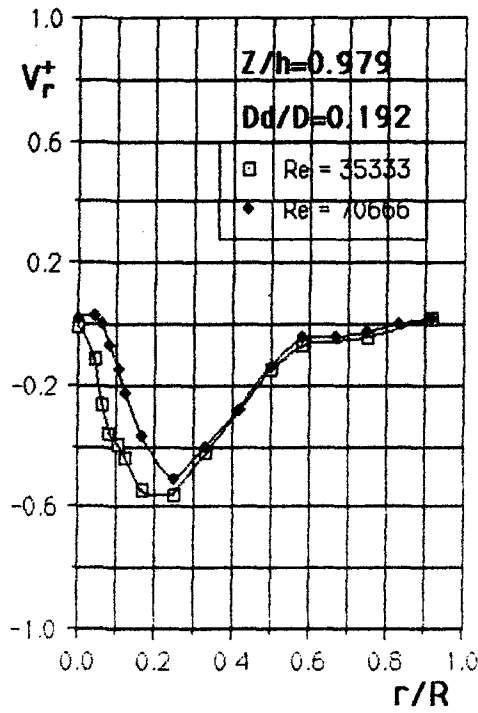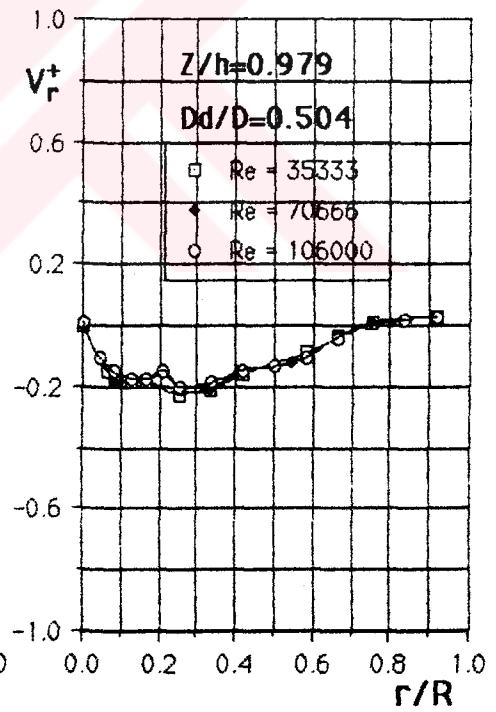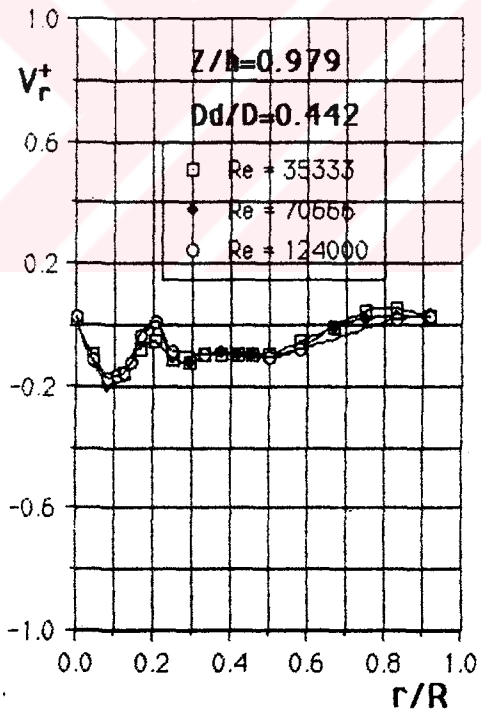
Figure 4.58 Radial distributions of dimensionless radial velocity
for different Re values on the cyclone having Dd/D ratios of 0.192,
0.296, 0.442 and 0.504 at Z/h=0.979, respectively.
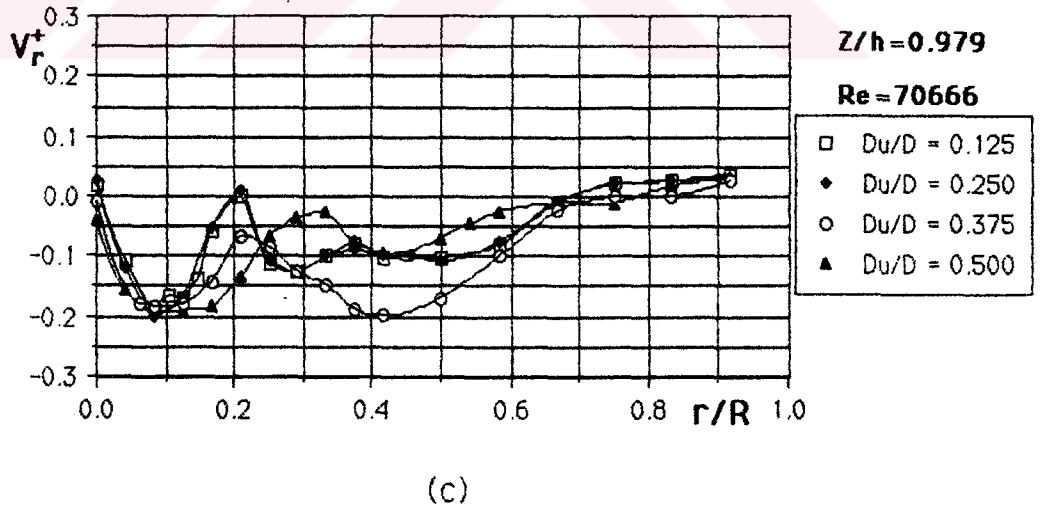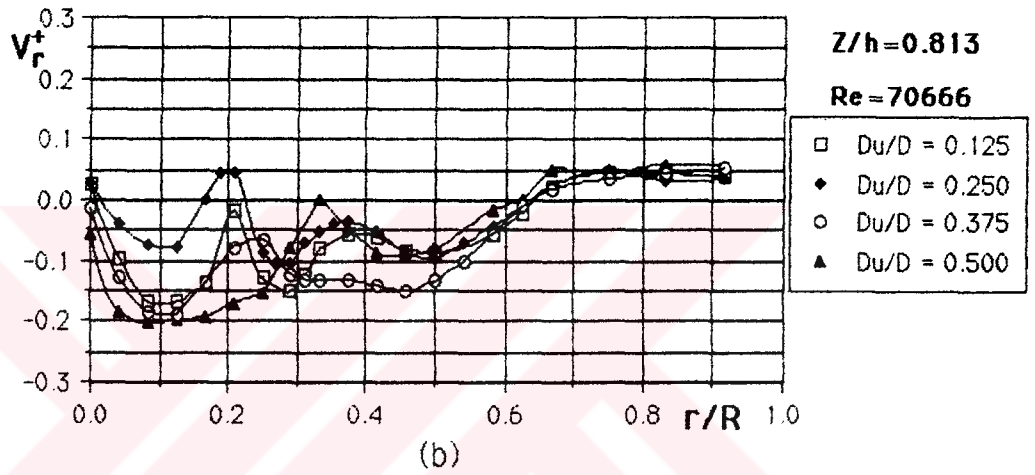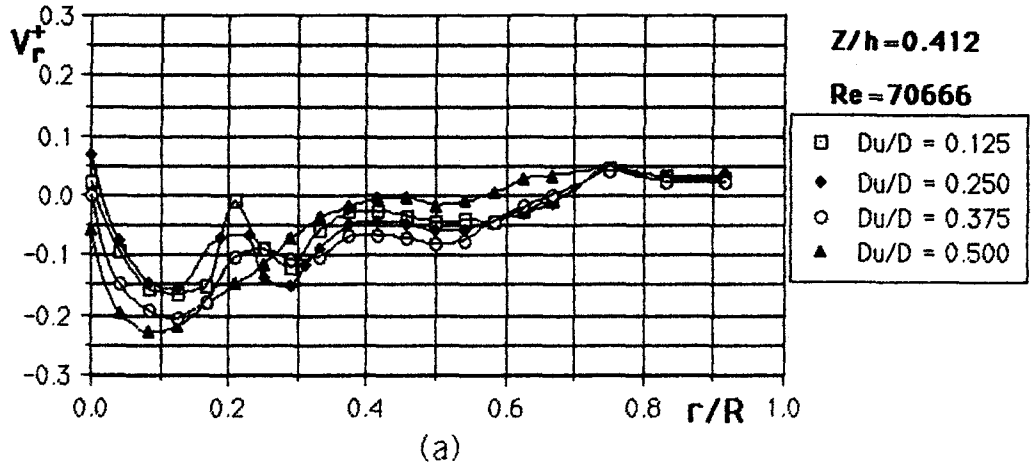
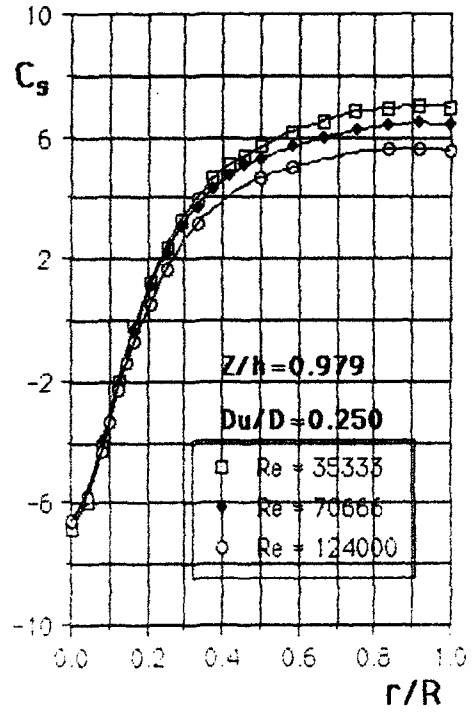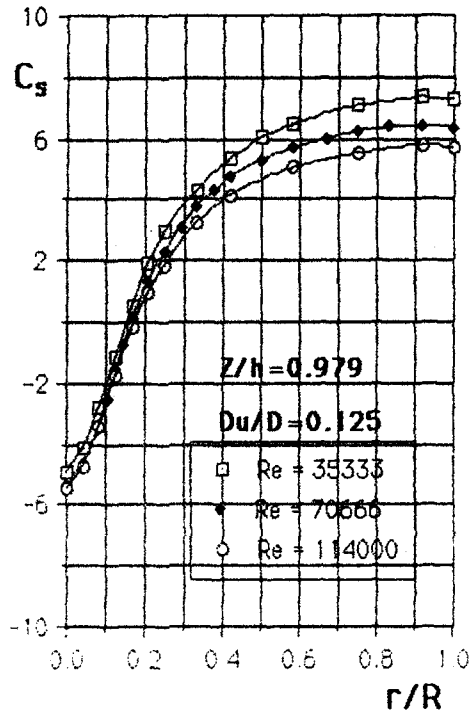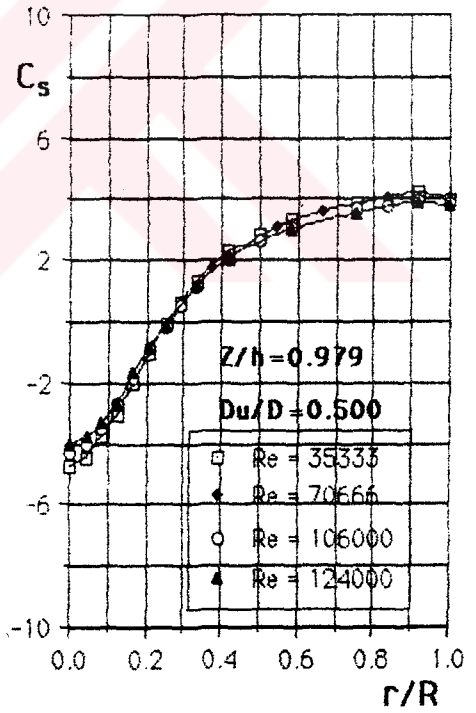Figure 4.59 Radial distributions of dimensionless radial velocity on the cyclone having different Du/D ratios for Re=70666 at Z/h= 0.412, Z/h=0.813 and Z/h=0.979, respectively.
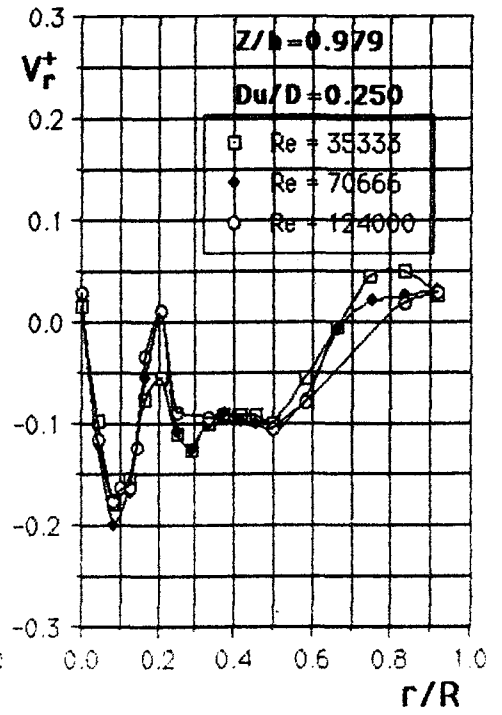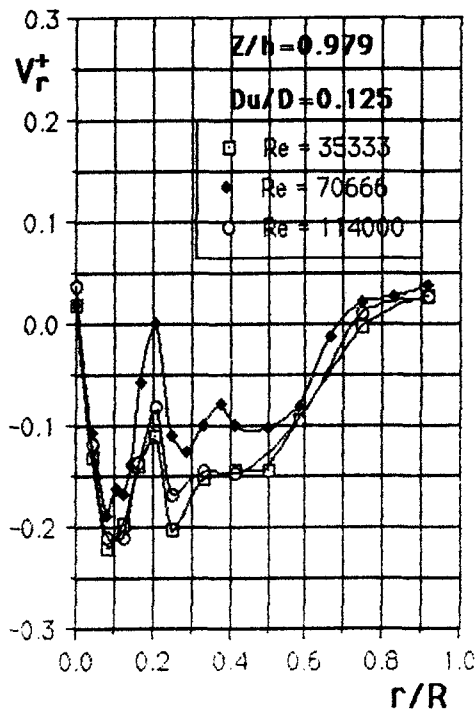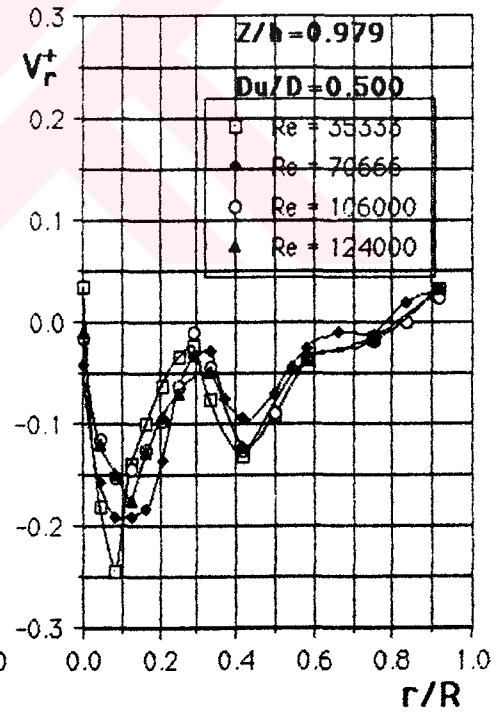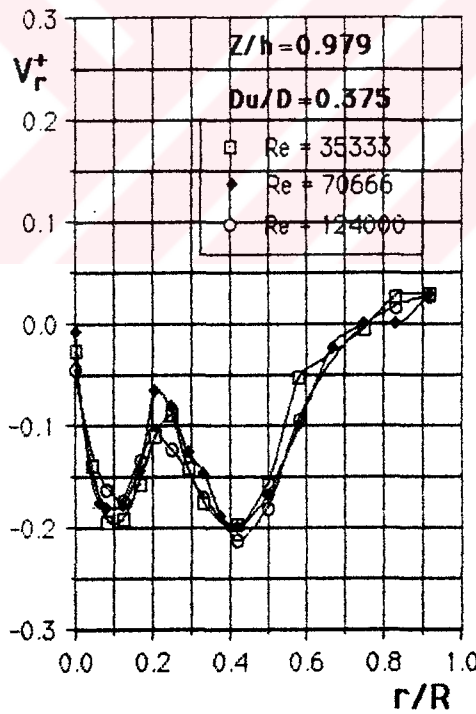
Figure 4.60 Radial distributions of dimensionless radial velocity for different Re values on the cyclone having Du/D ratios of 0.125, 0.250, 0.375 and 0.500 at Z/h=0.979, respectively.
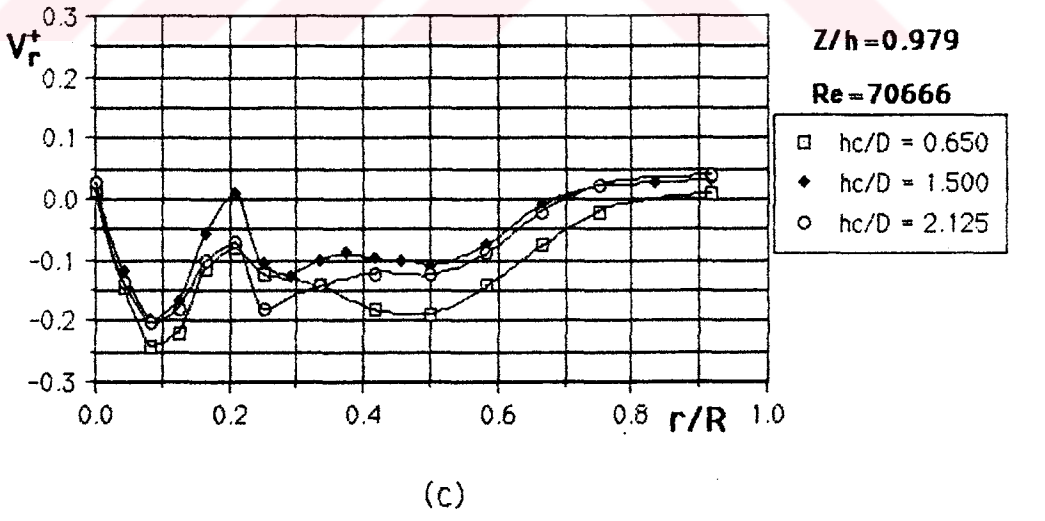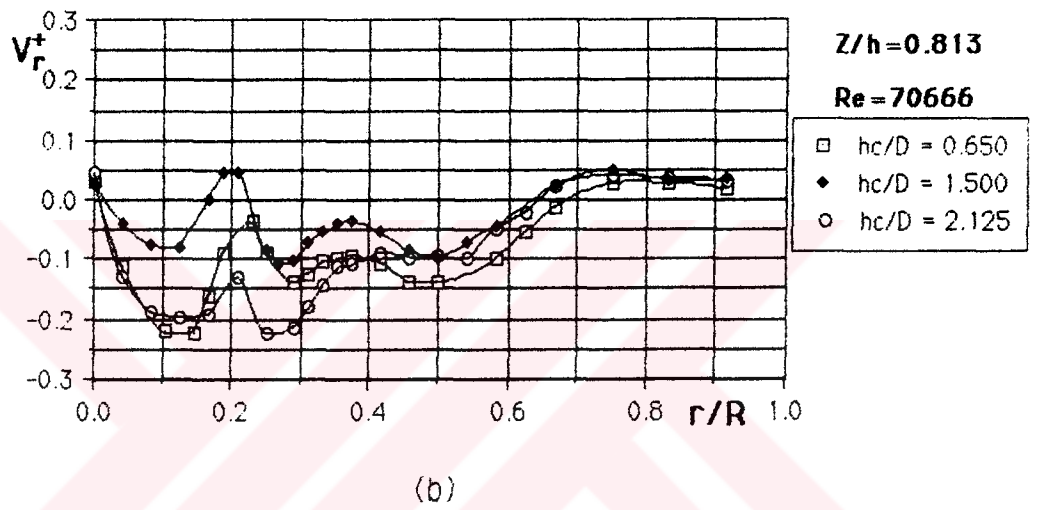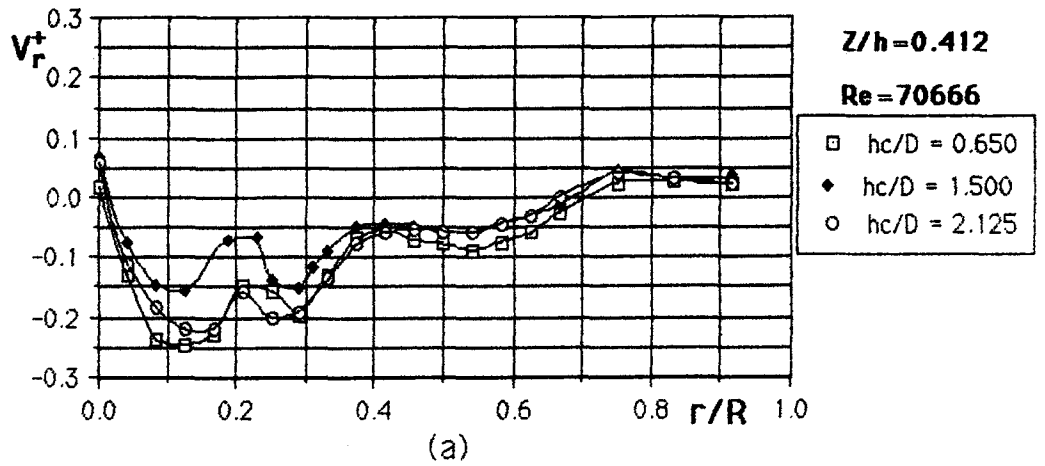
Figure 4.61 Radial distributions of dimensionless radial velocity on the cyclone having different h_c/D ratios for Re=70666 at Z/h= 0.412, Z/h=0.813 and Z/h=0.979, respectively.

1 ͡
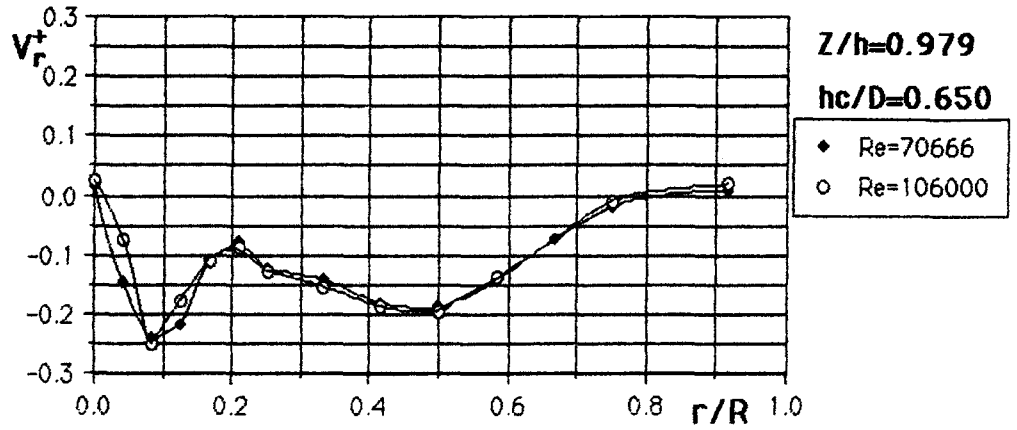
(a)
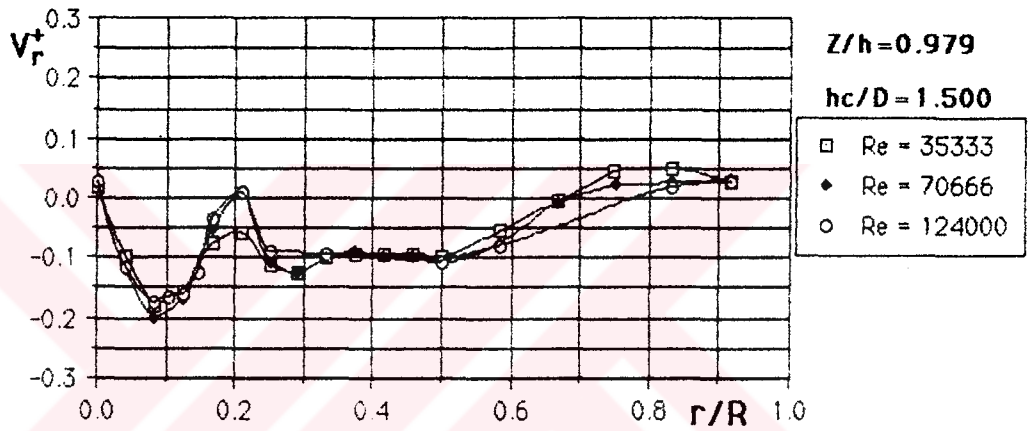
(b)

(c)

Figure 4.62 Radial distributions of dimensionless radial velocity
for different Re values on the cyclone having h_c/D ratios of 0.650, 1.500
and 2.125 at $Z/h=0.979$, respectively.

Figure 4.63 Radial distribution of dimensionless radial velocity on the cyclone having different S/D ratios for Re=70666 at Z/h= 0.412, Z/h=0.813 and Z/h=0.979, respectively.

Figure 4.64 Radial distributions of dimensionless radial velocity for different Re values on the cyclone having S/D ratios of 0.000, 0.292, 0.708 and 1.500 at Z/h=0.979, respectively.

Figure 4.65 Radial distributions of dimensionless radial velocity on the cyclone having different a/D and b/D ratios for Re=70666 at Z/h= 0.412, Z/h=0.813 and Z/h=0.979, respectively.

Figure 4.66 Radial distributions of dimensionless radial velocity
for different Re values on the cyclone having a/D ratios of 0.458, 0.583,
0.863 and b/D ratios of 0.367, 0.263, 0.177 at Z/h=0.979, respectively.

$$C_s = \frac{P_s}{1/2 \, \rho \, V_{in}^2}$$

Base Conf.
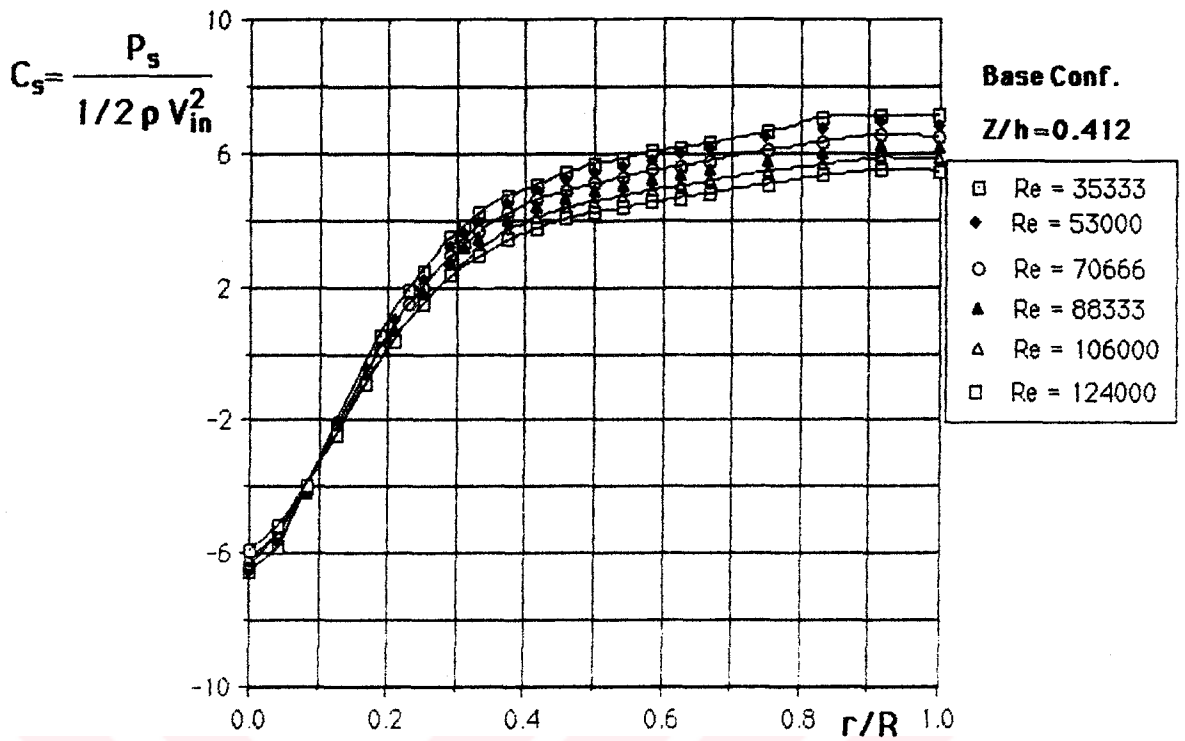
Z/h = 0.412

Figure 4.67 Radial distribution of static pressure coefficient on the basic cyclone configuration for different Re values at Z/h =0.412

Base Conf.
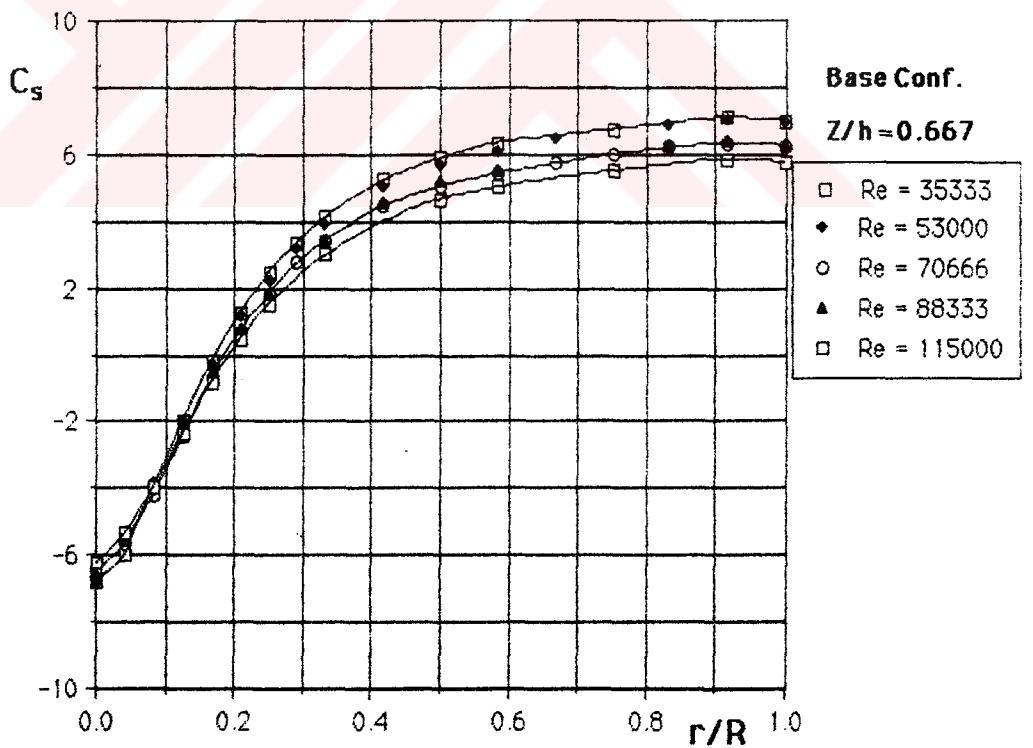
Z/h = 0.667

Figure 4.68 Radial distribution of static pressure coefficient on the basic cyclone configuration for different Re values at Z/h =0.667.
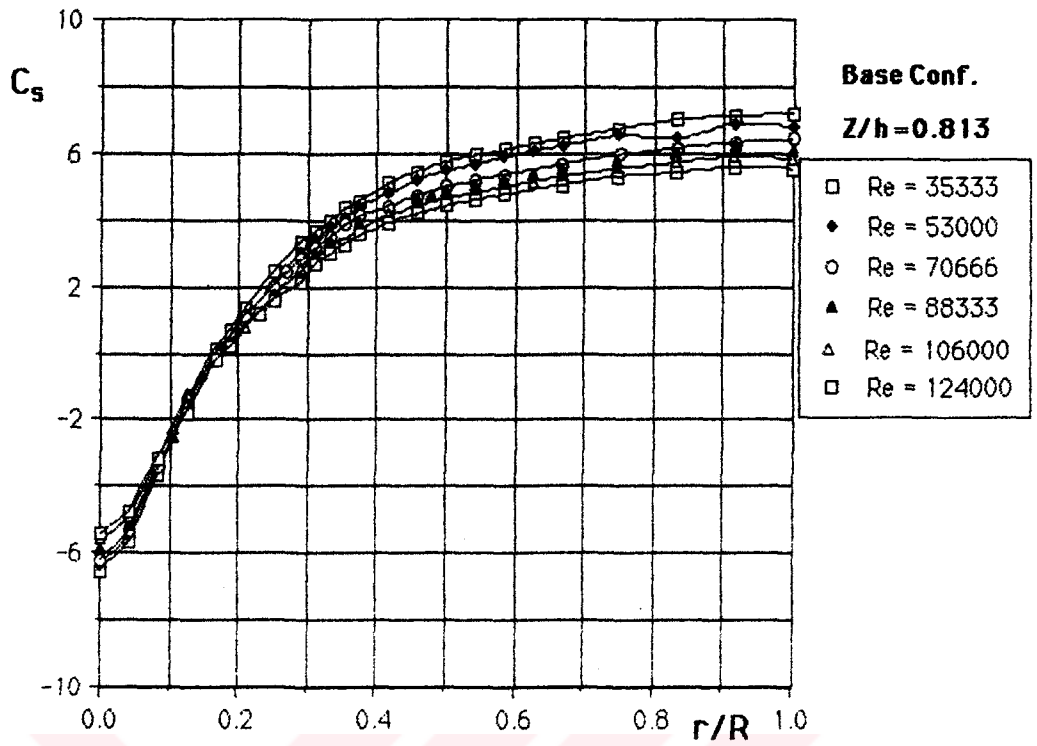
Figure 4.69 Radial distribution of static pressure coefficient on the basic cyclone configuration for different Re values at Z/h =0.813.
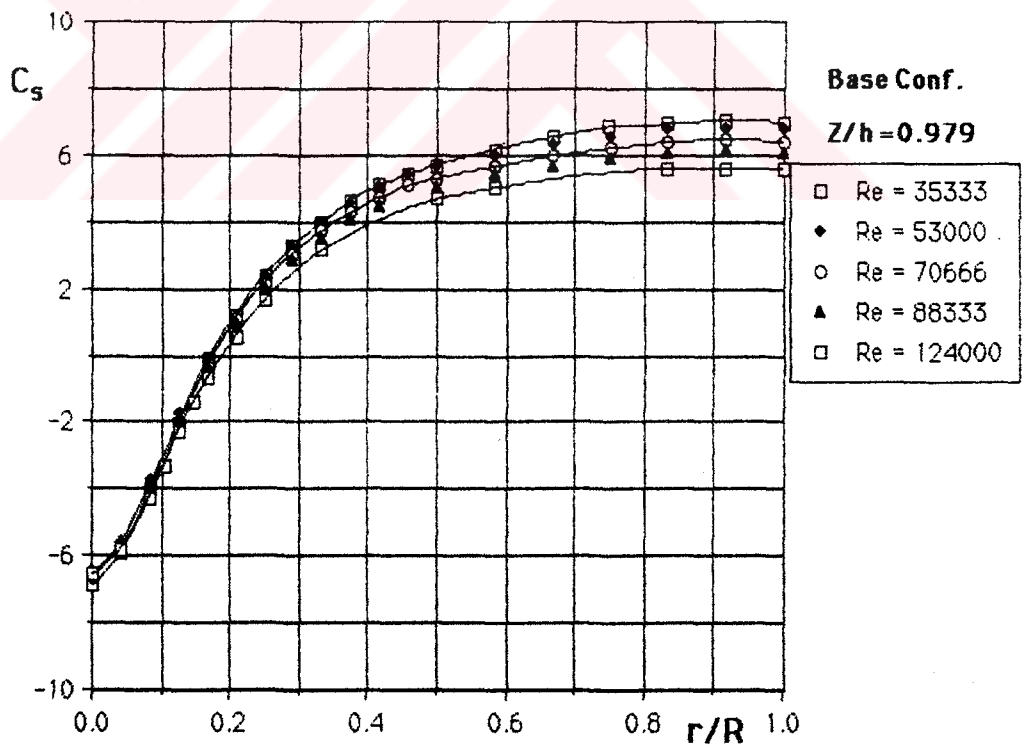
Figure 4.70 Radial distribution of static pressure coefficient on the basic cyclone configuration for different Re values at Z/h =0.979.
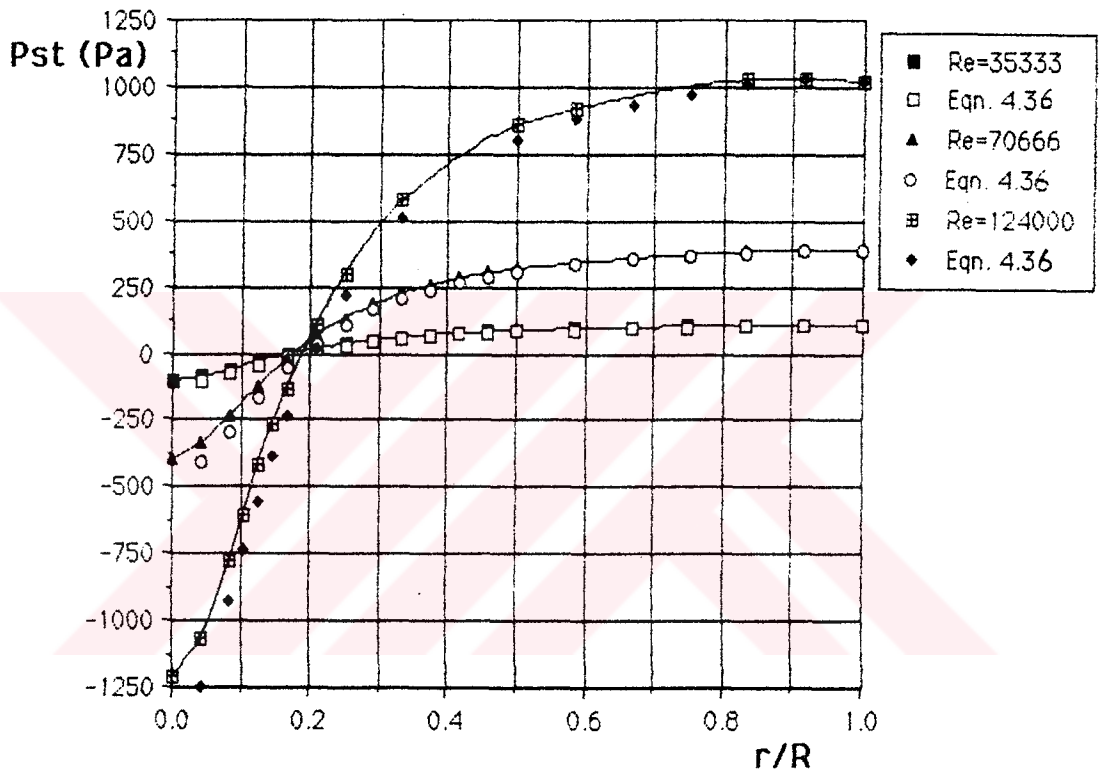
Figure 4.71 Radial distributions of measured static pressure on the basic cyclone configuration for Re number values of 35333, 70666, and124000 and distributions obtained by Eqn. 4.36 at Z/h=0.979.
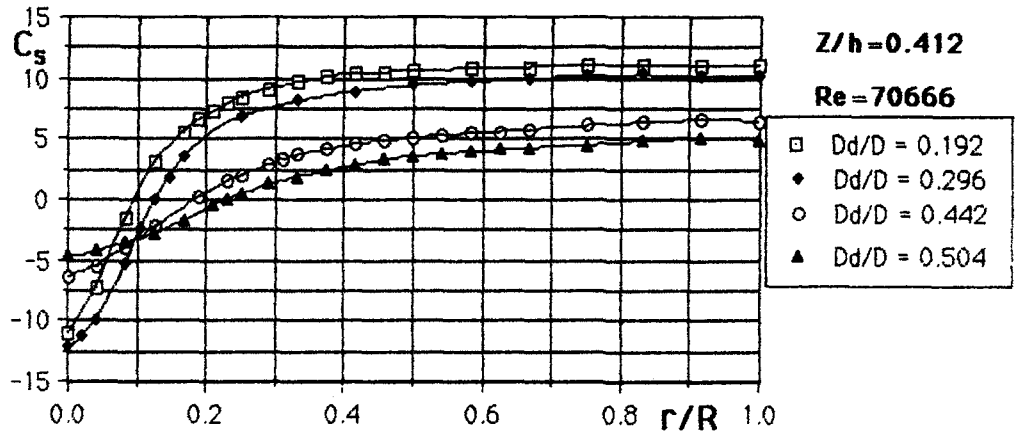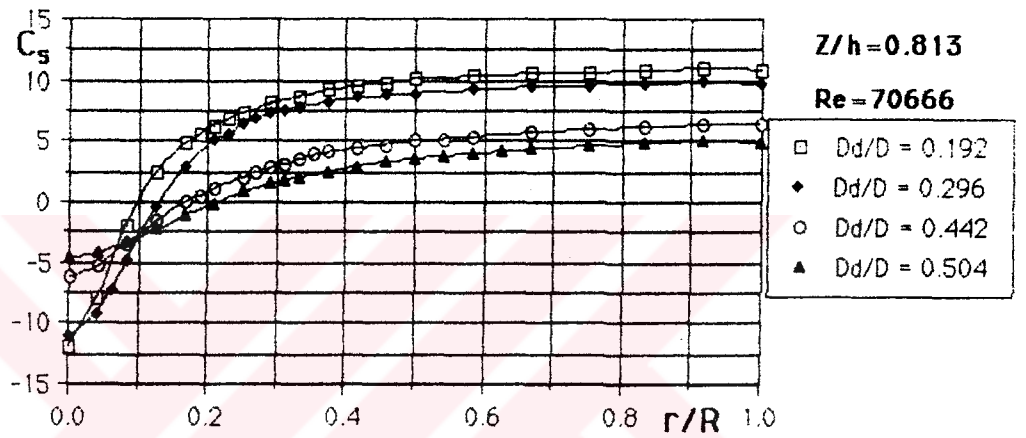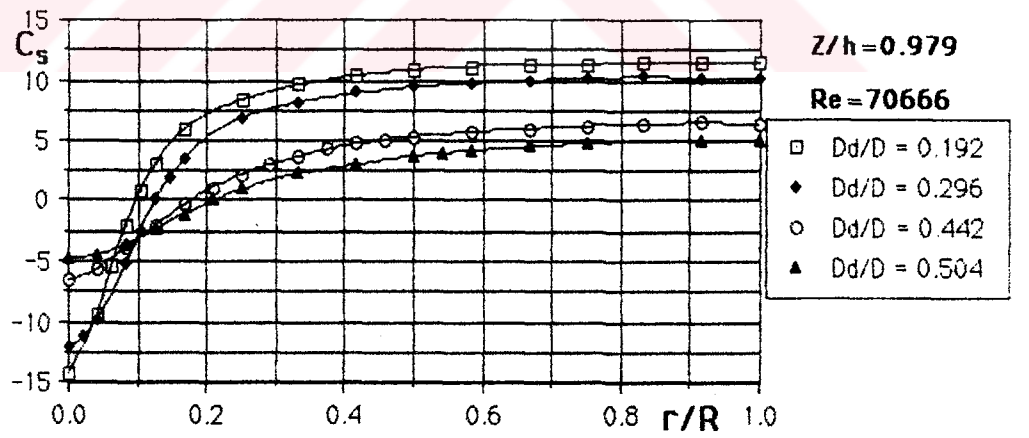
Figure 4.72 Radial distribution of static pressure coefficient on the cyclone having different Dd/D ratios for Re= 70666 at Z/h=0.412, Z/h=0.813 and Z/h=0.979, respectively.
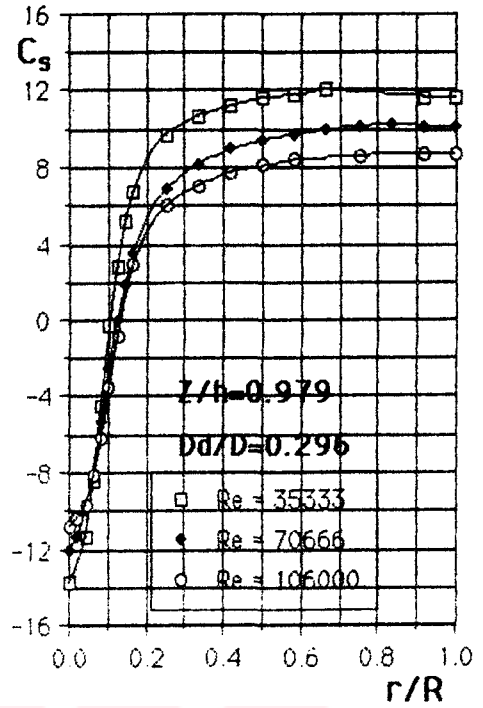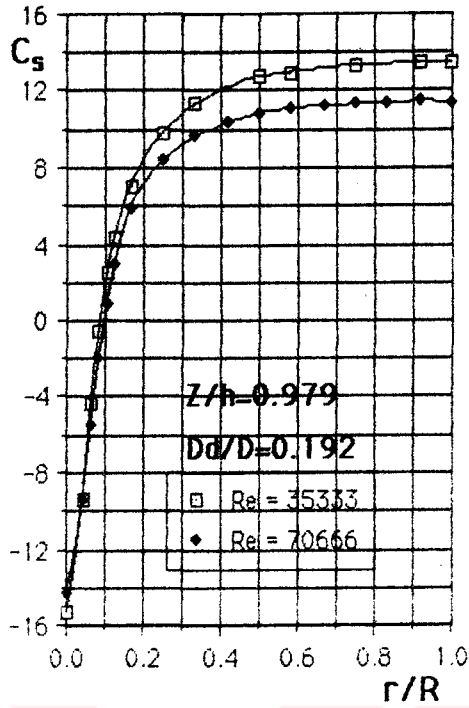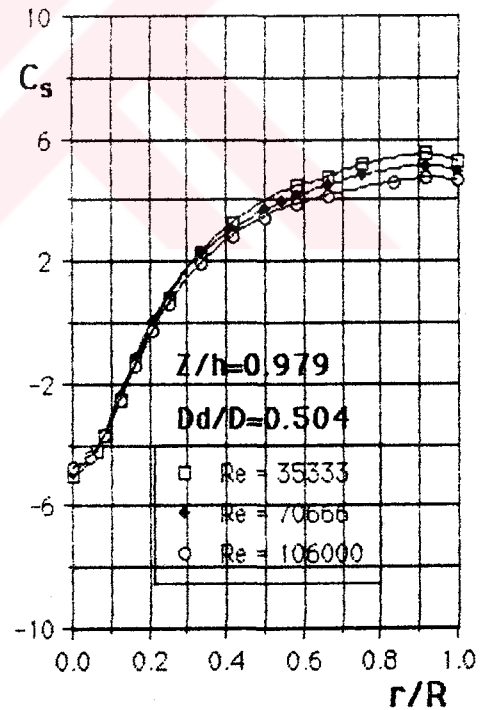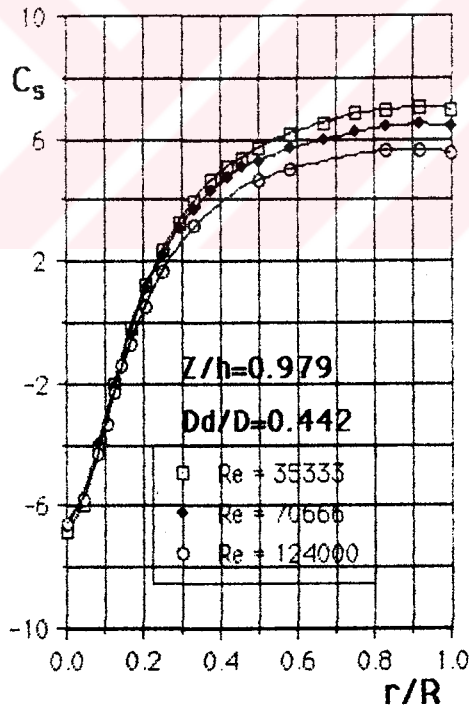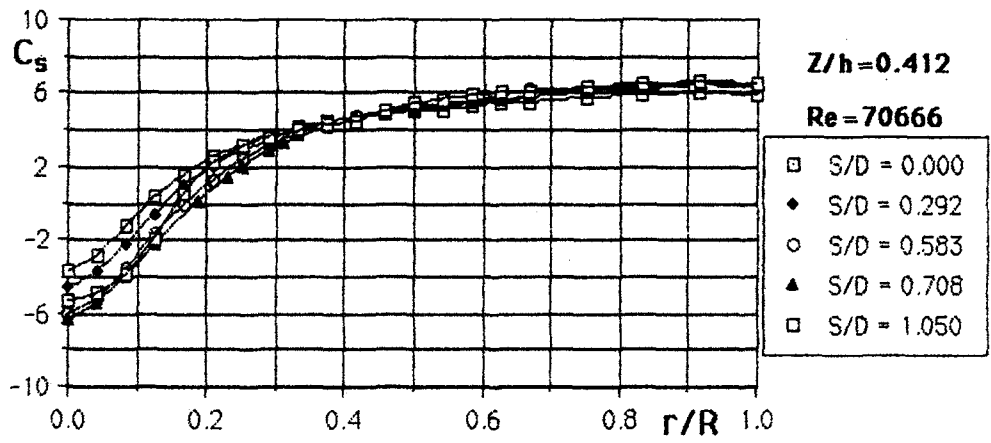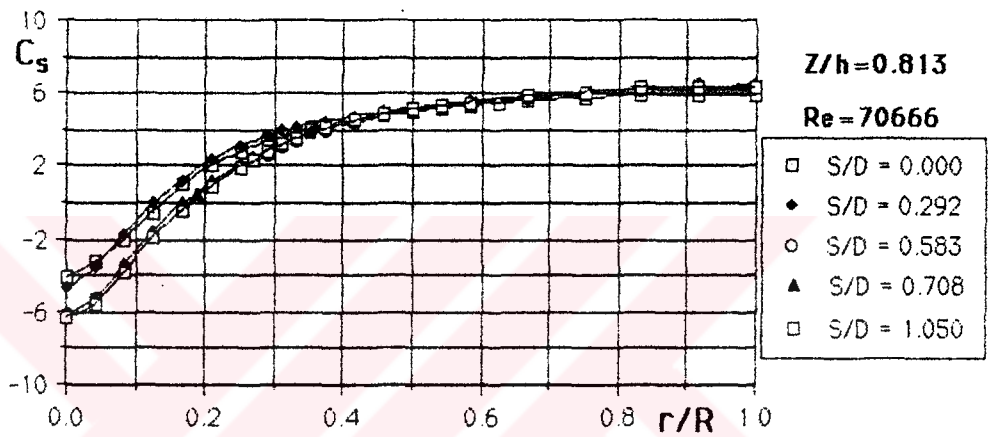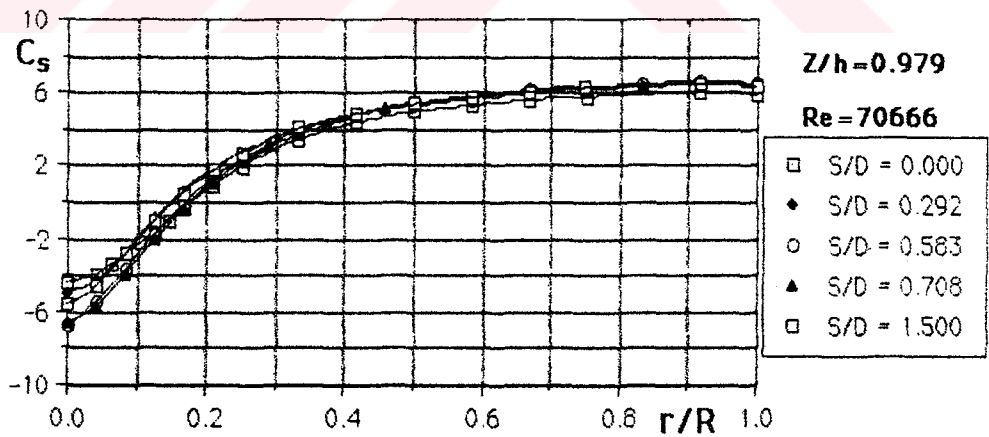
Figure 4.73 Radial distributions of static pressure coefficient for
different Re values on the cyclone having Dd/D ratios of 0.192, 0.296,
0.442 and 0.504 at Z/h=0.979, respectively.
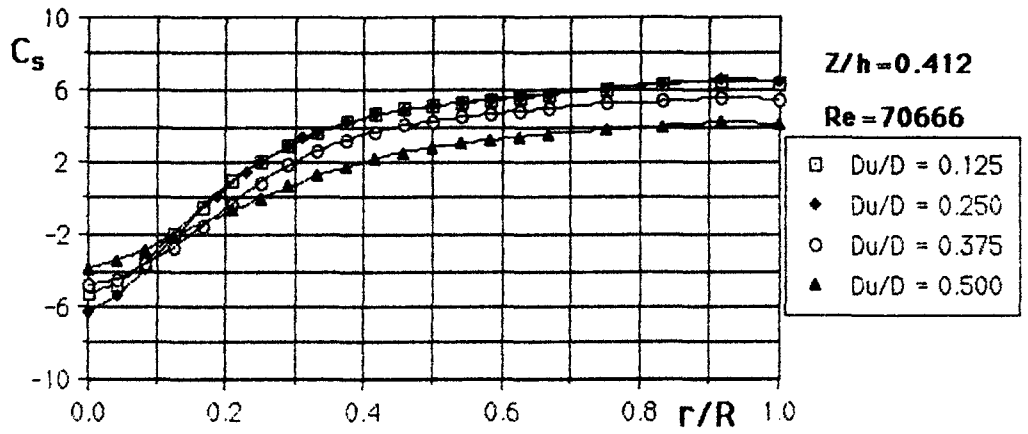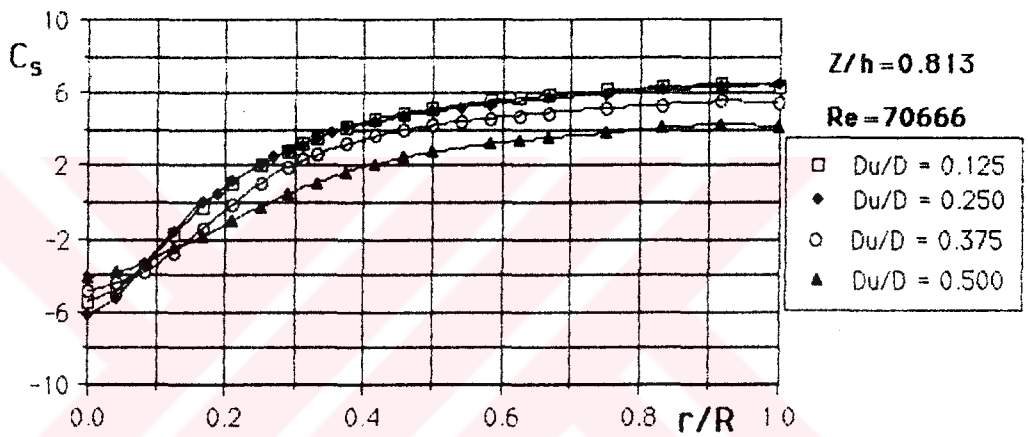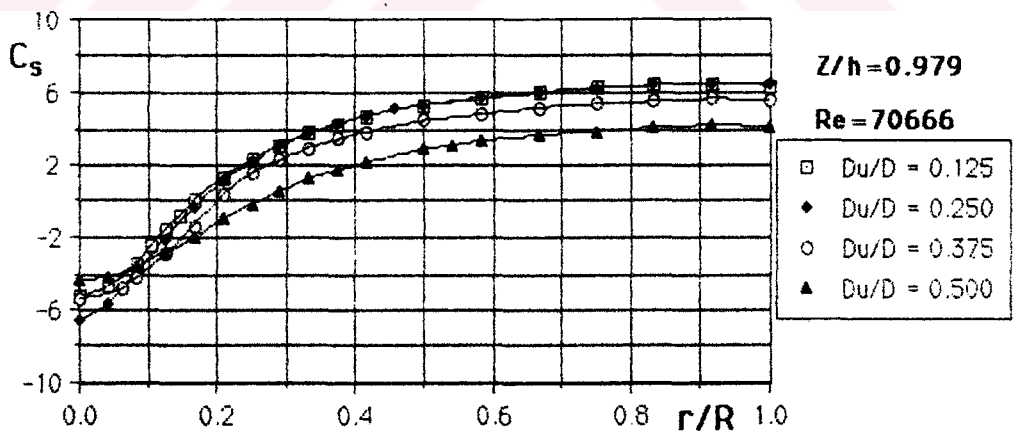
Figure 4.74 Radial distributions of static pressure coefficient on the cyclone having different Du/D ratios for Re=70666 at Z/h= 0.412, Z/h=0.813 and Z/h=0.979, respectively.
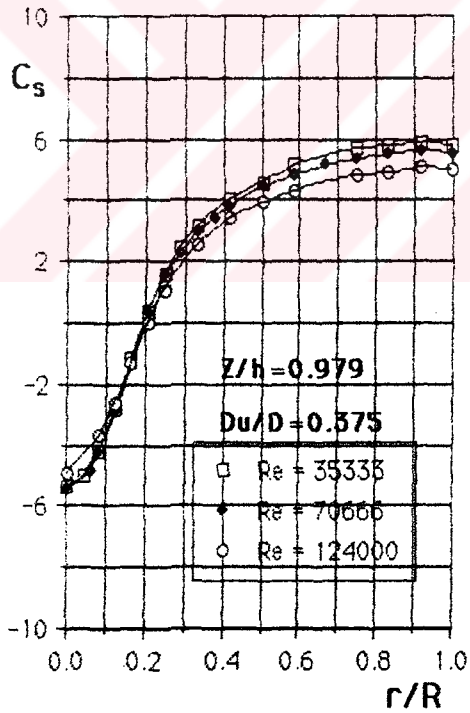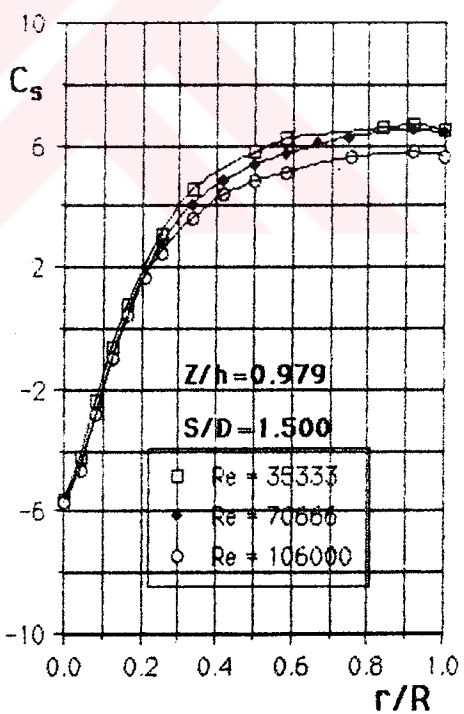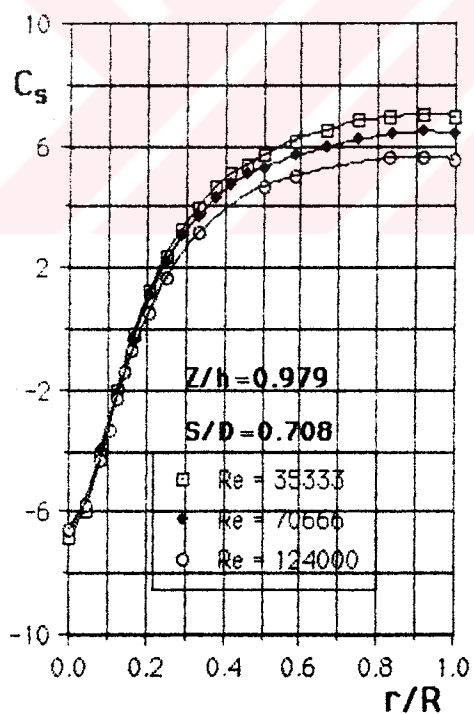
Figure 4.75 Radial distributions of static pressure coefficient for different Re values on the cyclone having Du/D ratios of 0.125, 0.250, 0.375 and 0.500 at Z/h=0.979, respectively.
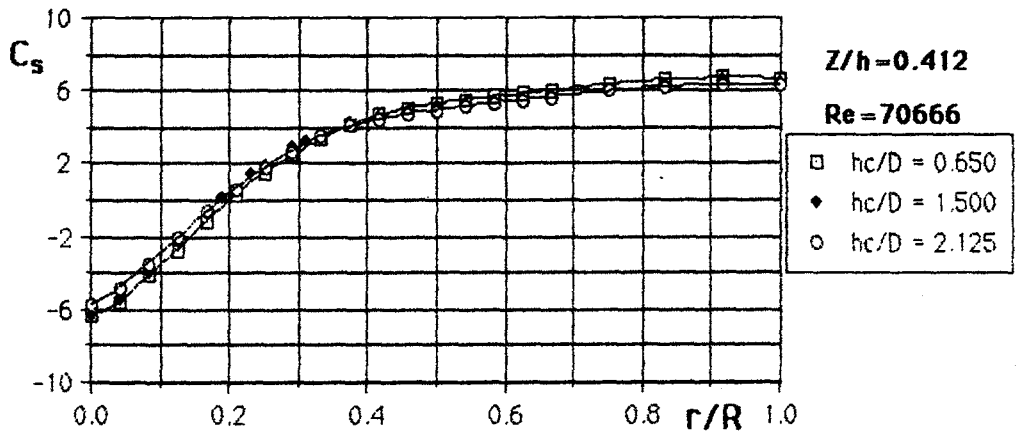
(a)
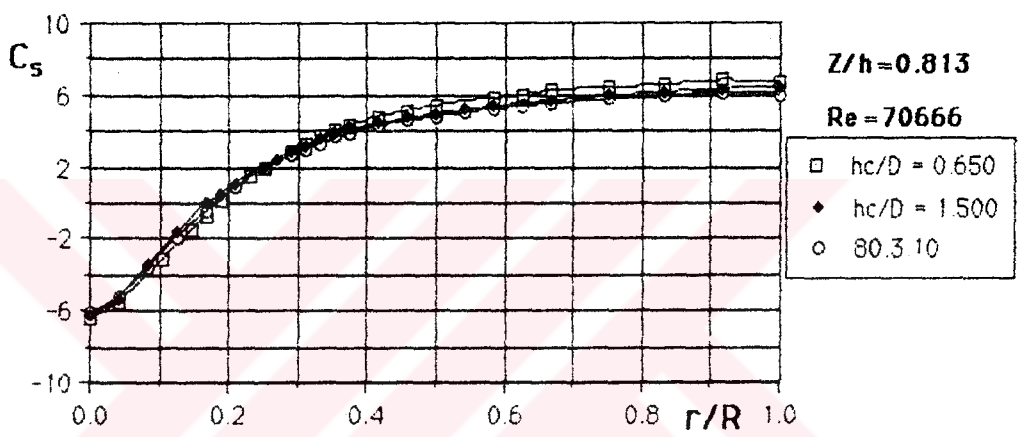
(b)
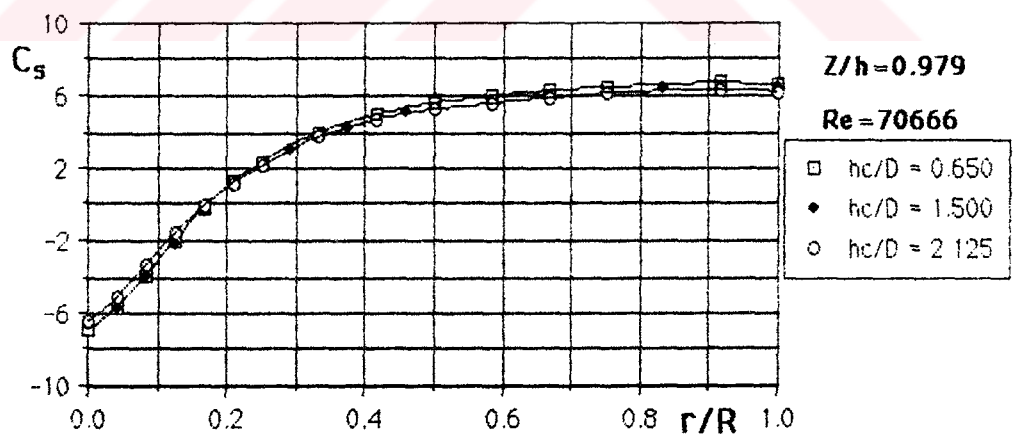
(c)

Figure 4.76 Radial distributions of static pressure coefficient on the cyclone having different h_c/D ratios for Re=70666 at Z/h= 0.412, Z/h=0.813 and Z/h=0.979, respectively.
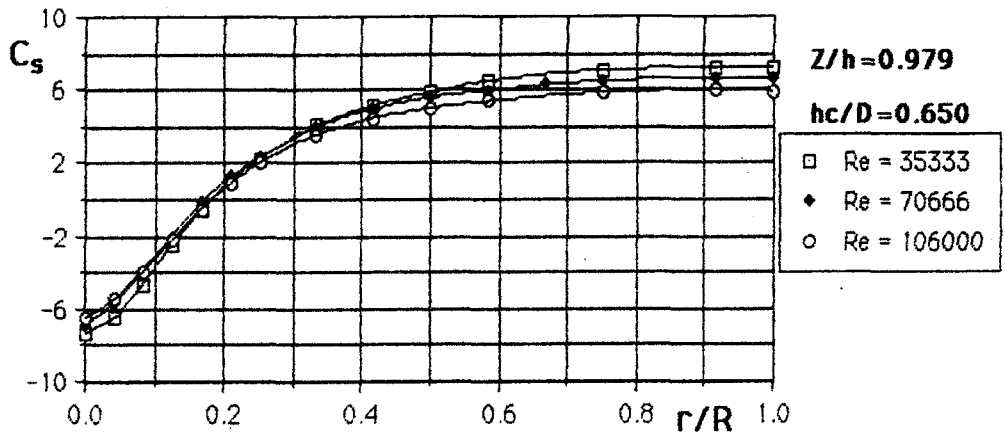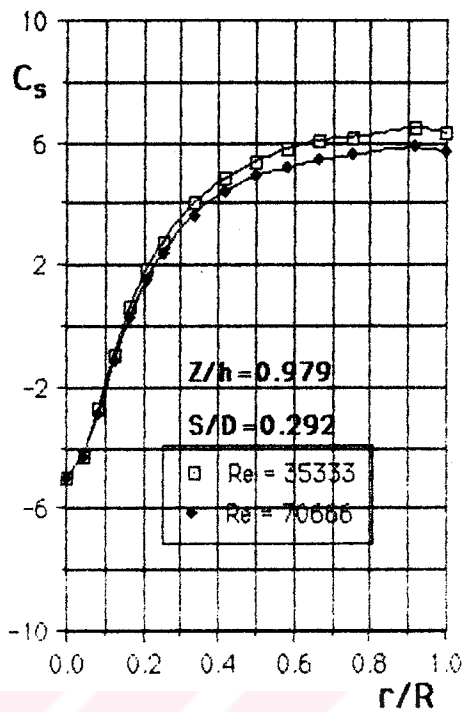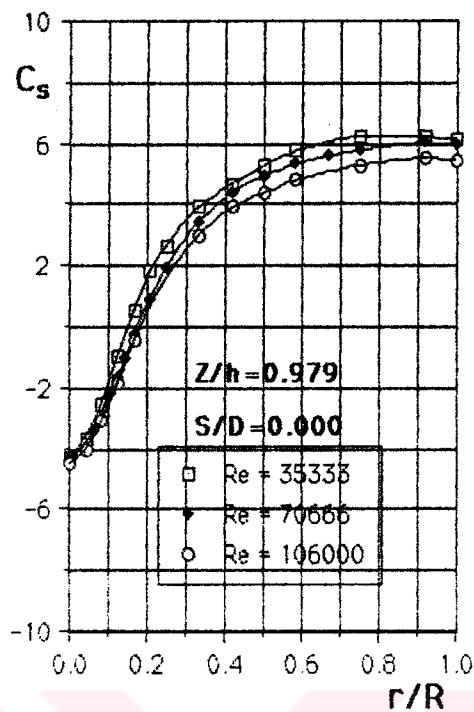
(a)
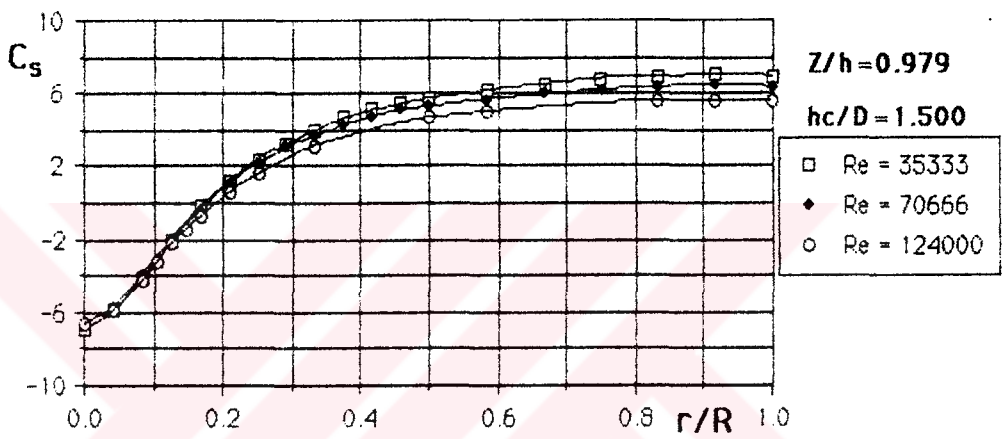
(b)
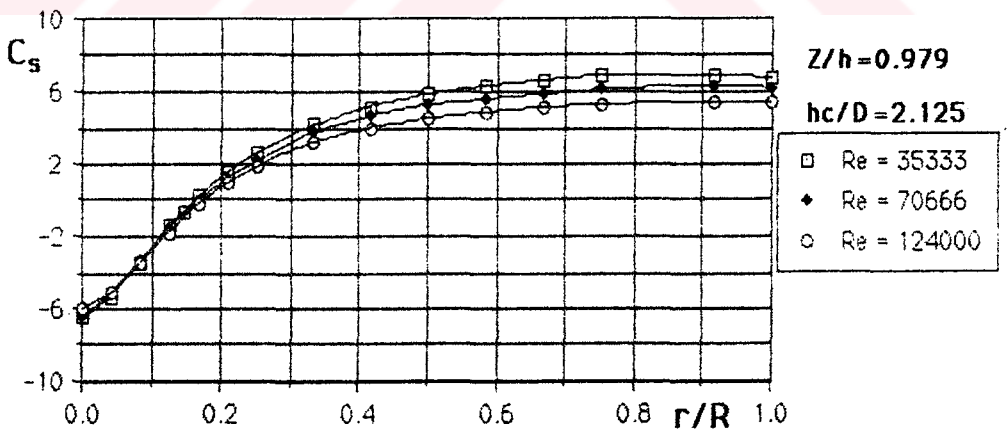
(c)

Figure 4.77 Radial distributions of static pressure coefficient for different Re values on the cyclone having h_c/D ratios of 0.650, 1.500 and 2.125 at $Z/h=0.979$, respectively.

Figure 4.78 Radial distribution of static pressure coefficient on the cyclone having different S/D ratios for Re=70666 at Z/h= 0.412, Z/h=0.813 and Z/h=0.979, respectively.

161

(a)　　　　　　　　(b)

(c)　　　　　　　　(d)

Figure 4.79 Radial distributions of static pressure coefficient for
different Re values on the cyclone having S/D ratios of 0.000, 0.292,
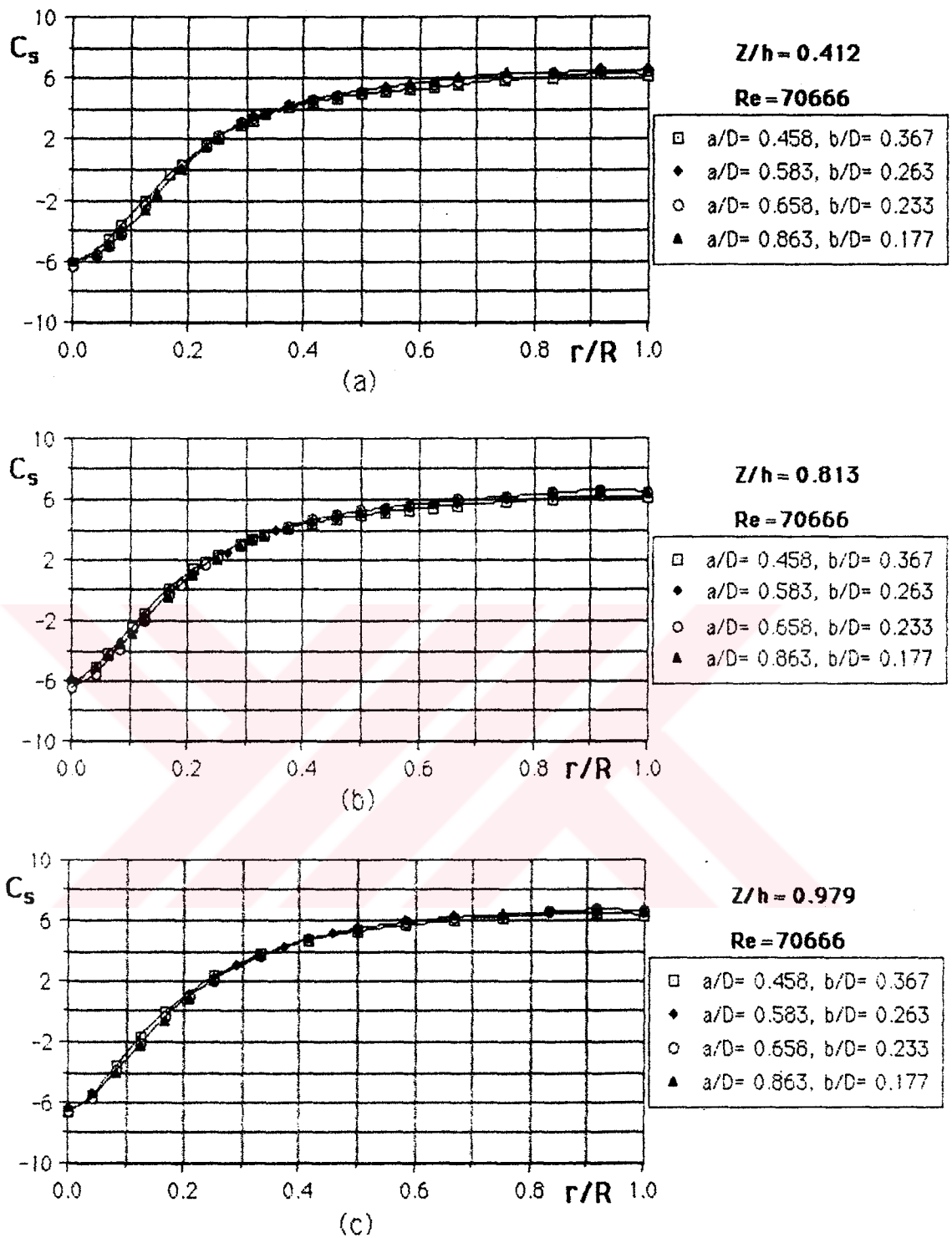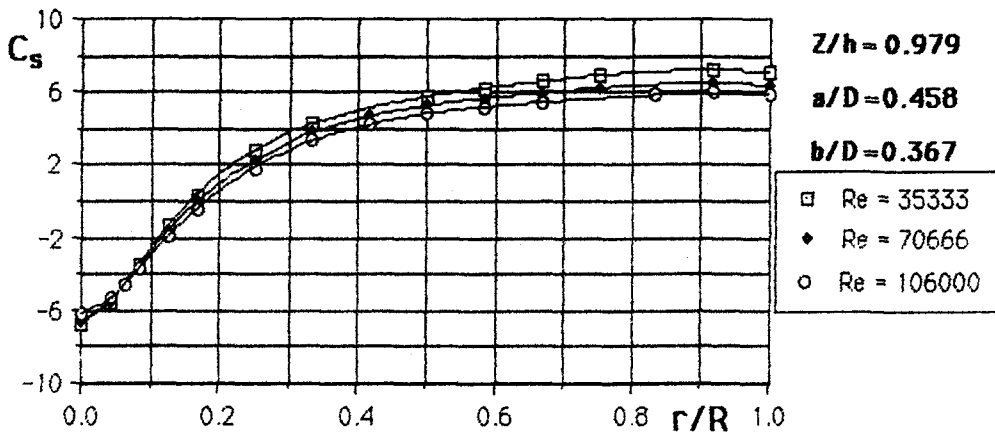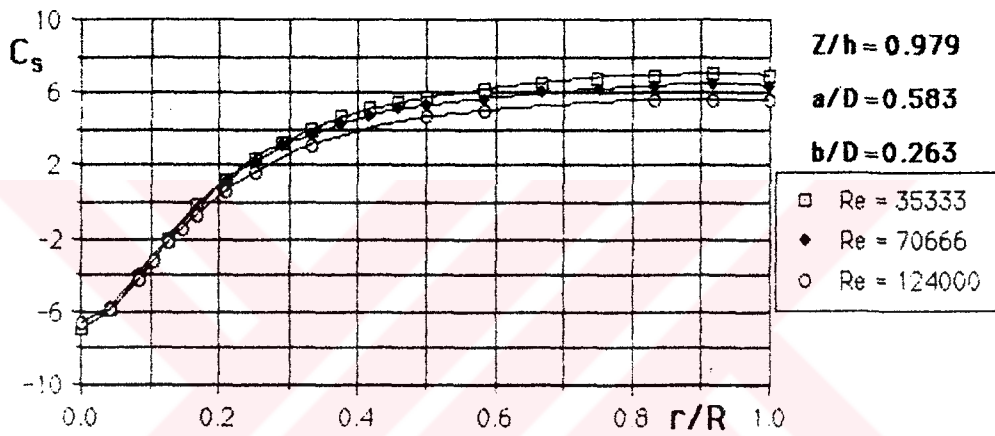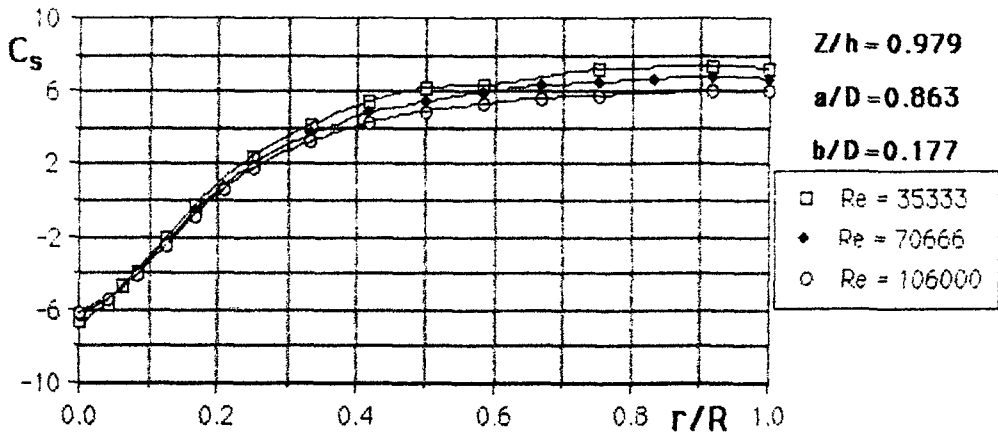0.708 and 1.500 at Z/h=0.979, respectively.

Figure 4.80 Radial distributions of static pressure coefficient on the cyclone having different a/D and b/D ratios for Re=70666 at Z/h= 0.412, Z/h=0.813 and Z/h=0.979, respectively.

(a)

(b)

(c)

Figure 4.81 Radial distributions of static pressure coefficient for different Re values on the cyclone having a/D ratios of 0.458, 0.583, 0.863 and b/D ratios of 0.367, 0.263, 0.177 at Z/h=0.979, respectively.